The tectonic evolution of the East Range of the Sudbury Basin, Ontario, Canada

Dissertation with the aim of achieving a doctoral degree

At the Faculty of Mathematics, Informatics and Natural Sciences

Institute of Geology

of Universität Hamburg

submitted by Martin David Clark

2016 in Hamburg

Date of the oral defense: January 25th 2017

The following evaluators are recommended for the admission of the dissertation:

Prof. Dr. Ulrich Riller – Universität Hamburg

Prof. Dr. Peter Lightfoot – Laurentian University

Eidesstattliche Versicherung

Declaration on oath

Hiermit erkläre ich an Eides statt, dass ich die vorliegende Dissertationsschriff selbst verfasst und keine anderen als die angegebenen Quellen und Hilfsmittel benutzt habe.

I hereby declare, on oath, that I have written the present dissertation on my own and have not used other than the acknowledged resources and aids.

Hamburg, den November 9, 2016 Unterschrift:

Summary

This thesis aims to understand how the eastern portion of the Sudbury Basin, the East Range, in Ontario, Canada, geometrically evolved since the emplacement of its defining lithology, the Sudbury Igneous Complex (SIC) at 1.85 Ga. The Sudbury Basin is an elliptical fold basin which due to variations in its surface expression can be subdivided into three ranges: The North Range, the South Range, and the East Range. The East Range is unique due to its inward curvature and steep dips of the SIC, where the mechanism by which the curvature and dips were generated remains unknown. Evidence of folding is apparent from tectonic foliations in sediments which have infilled the basin, and prominent folds have been constrained across the East Range, but the SIC can only be characterized by low levels of solid state strain. As the SIC and underlying rocks are petrographically distinct but mechanically isotropic, the mechanism by which the SIC folded still remains to be elucidated. Unique to the East Range are prominent, kilometer scale faults which mimic the curvature of the SIC, but their true geometry and kinematics and how they may relate to folding of the SIC remains unknown. Therefore, to better understand the effects of folding and faulting, a combination of methods including field work, computational spatial analysis, 3-D modeling, forward modeling, and kinematic restorations were conducted.

Combining high resolution digital elevation models derived from Light Detection and Ranging (LiDAR) data with surface fault traces yields non-uniform fault surface geometries characteristic for brittle deformation in the upper crust. The local heterogeneity of the strain field at surface together with fault surface geometries allows for the derivation of fault kinematics defining a new G.I.S.-based workflow. Fault kinematics of prominent faults across the East Range can be broadly classified as accomplishing reverse motion in the southern half and normal motion in the northern half of the East Range. This prompts the theory that these fault were the initial anisotropic element which allowed for folding to begin. As initially reverse faults are folded, they can be classified at surface as normal faults. To validate this theory from surface data, kinematic restorations were performed on an independent 3-D model of the SIC in the East Range. By using simple shear and flexural slip restoration algorithms, the importance of slip on faults for folding of the SIC is shown. This therefore advocates that slip on faults was an intrinsic component of folding, and therefore supports their temporal connection to folding of the SIC, and the generation of the curvature of the East Range of the Sudbury Basin.

Zussammenfassung

Mit dieser Arbeit ist beabsichtigt die geometrische Entwicklung des östlichen Bereichs des Sudbury Beckens, die East Range, in Ontario, Kanada, seit der Platznahme des Sudbury Igneous Complex (SIC) vor 1,85 Mrd. Jahren zu verstehen. Das Sudbury Becken ist ein elliptisches Faltenbecken, welches aufgrund von lokalen Variationen in drei Bereiche unterteilt wird: Die North Range, die South Range und die East Range. Die East Range hebt sich durch ihre einwärts gerichtete Krümmung und ein steiles Einfallen des SIC von den anderen Bereichen ab. Der Mechanismus, welcher die Bildung dieser Besonderheiten kontrollierte, ist bis heute unbekannt. Hinweise auf eine Faltung liefern tektonische Foliationen in Sedimenten, die das Becken verfüllten, sowie prominente Falten in der East Range, wobei die Deformation des SIC nur durch niedrige Festkörperverformung charakterisiert werden kann. Da der SIC und die ihn unterlagernden Gesteine trotz petrographischer Unterschiede mechanisch isotrop sind, ist der Mechanismus der Faltung des SIC bis heute unbekannt. Einzigartig sind in der East Range auftretende, kilometerlange Störungen, welche in ihrem Streichen der Krümmung des SIC folgen. Die wahre Geometrie und die Kinematik dieser Störungen und ihre mögliche Verbindung mit der Faltung des SIC bleiben unbekannt. Um die Effekte der Faltung und Störung besser zu verstehen wurde eine Kombination an Methoden, bestehend aus Feldarbeit, computergestützter räumlicher Analyse, 3-D Modellierung, Zukunftsmodellierung, und kinematischer Restauration angewendet.

Die Kombination aus hochauflösenden digitalen Höhenmodellen, erstellt aus Light Detection and Ranging (LiDAR) Daten, mit der Spur von Störungen an der Oberfläche ergibt nicht-uniforme Geometrien von Störungsflächen bei der bruchhaften Deformation in der oberen Erdkruste. Die Heterogenität des Spannungsfeldes an der Oberfläche zusammen mit der Geometrie der Störungsflächen erfordert die Entwicklung eines neuen G.I.S.-basierten Workflows zur Bestimmung der Kinematik. Die Kinematik prominenter Störungen in der East Range zeigt grob einen abschiebungsdominierten Charakter im südlichen Bereich und einen aufschiebungsdominierten Charakter im nördlichen Bereich der East Range. Dies legt die Hypothese nahe, dass die Störungen das initiale anisotrope Element darstellen, welches eine Faltung ermöglichte. Wenn initiale Aufschiebungen gefaltet werden, können sie an der Oberfläche als Abschiebungen klassifiziert werden. Um diese, auf Oberflächendaten basierende, Hypothese zu überprüfen wurden kinematische Restaurationen an einem

unabhängigen 3-D-Modell der East Range des SIC durchgeführt. Unter der Anwendung von Simple-shear- und Flexural-slip-Algorithmen wird die Bedeutung des Versatzes entlang der Störungsflächen verdeutlicht. Die Ergebnisse unterstützen die Hypothese, dass der Versatz entlang der Störungen eine wesentliche Komponente der Faltung war und damit mit der Faltung des SICs und der Krümmung der East Range in Verbindung steht.

Acknowledgements

Completing a doctoral thesis is rarely possible without the support, help, and guidance from others, and this thesis is no exception. As I completed this thesis at a university outside of my home country, I have an extensive list of people to thank for their help in this endeavor.

This work was funded by the Brownfield Exploration Group at Vale, and the Center for Excellence in Mining Innovation, Sudbury, under RA 1353-CA-030. The financial support and industry data provided by Vale were critical for the completion of this thesis. The 3-D models presented in this thesis were created using a program called Move by Midland Valley. An academic license agreement with Midland Valley made this work possible.

The working atmosphere at Universität Hamburg was one with many facets to both stimulate new ideas and to ensure a comfortable and enjoyable environment. Members of my research group made the work environment one of many laughs and I appreciate the discussions and help with the German university system. I particularly wish to thank Moritz Kirsch, Philipp Jansen, Paul Göllner, Lisa Bendschneider, Björn Bombach, Torben Wüstemann, and Pascal Asmussen. My first months in Hamburg were greatly supported by Torben and Pascal, but all have played important roles in the discussion of results or aided in the collection of data. In the final steps of preparing the thesis, Paul Göllner helped to translate the summary into German.

I was the only doctoral candidate in my research group during the majority of my time in Hamburg, and I thank members of the sedimentology group for their help and support, most notably, Marco Wunsch, Juliane Ludwig, Jesus Reolid, and Huaqing Bai. Juliane Ludwig helped to proof read parts of this thesis and Huaqing Bai helped to make weekends in the Geomatikum enjoyable.

Working with geologists at Vale's Brownfield Exploration group made my time in Sudbury enjoyable. The individual contribution from everyone there cannot be sufficiently acknowledged, but acknowledgement is made for help received from Peter Lightfoot and Lisa Gibson. Peter's focus on project deliverables and his lighthearted nature ensured a productive field season each year. Discussions with Lisa were always very helpful and enlightening and she is thanked for help in managing the logistics of working on company property in Sudbury. Editorial work provided on chapter 3 by Lisa Gibson and David Burrows was helpful. Dave Lotter is to be thanked for his time in training field crews.

Regardless of which continent I was on, I'm indebted to my friends for the role they played in balancing the stresses involved in completing the thesis. Dina Bolz helped me to integrate into Germany and develop my German.

The degree of support and guidance provided by my supervisor Ulrich Riller through the doctorate is one that cannot be understated. During all stages of the thesis, it was a pleasure to work under his supervision.

Lastly, without the unwavering support from my parents, David and Jitka, none of this would have been possible.

List of Derived Publications

Clark, M.D., Riller, U., 2017. Significance of first-order faults in folding mechanically isotropic layers: evidence from the Sudbury Basin, Canada. Journal of Structural Geology, 95, 113-126.

Clark, M.D., Riller, U., Gibson, L., 2017. Forward modeling and 3-D kinematic restoration of the Sudbury Igneous Complex of the eastern Sudbury Basin, Canada. Journal of Geology, in preparation.

Riller, U., Clark, M., Daxberger, H., Doman, D., Lenauer, I., Plath, S., Santimano, T., 2016. Fault-slip inversions: their importance in terms of strain of deducing the heterogeneity and kinematics of brittle deformation. Journal of Structural Geology, in review.

Table of Contents

1.0 Introduction

The Sudbury area in Ontario, Canada, is host to the 1.85 Ga Sudbury Igneous Complex (SIC; Krogh et al., 1984). The SIC is world renowned due to its association with Cu-Ni-PGE deposits whereby mineral extraction of SIC related deposits rivals Noril'sk as the world's largest Cu-Ni producer (Ames et al., 2008). From an academic perspective, the SIC itself is well known as it is the only multi-kilometer thick melt sheet exposed at surface which formed due to a meteorite impact (Dressler, 1984). As seen in its current geometry, the SIC was tectonically deformed whereby at surface it demarcates the extent of the Sudbury Basin, a NE-SW trending elliptical fold basin characterized by a synformal geometry (Fig. 1.1; Brocoum and Dalziel, 1974). Peculiarly, the SIC is characterized by low levels of solid state strain, bringing to question how did the SIC assume its elliptical shape (Fig. 1.1; Cowan, 1999).

At surface, the Sudbury Basin can be subdivided into three portions: the South Range, the North Range, and the East Range. The mechanism by which the South Range and North Range attained their current geometry has been largely constrained. The steep dips of the SIC in the South Range has been related to NW-directed thrusting associated to the South Range Shear Zone (e.g. Shanks and Schwerdtner, 1991a, b; Bailey et al., 2004; Riller, 2005; Mukwakwami et al., 2012), while the geometry of the SIC in the North Range is best described as the primary product of the emplacement of the SIC (Dreuse et al., 2010). In contrast to the North Range and South Range, the mechanism by which the SIC in the East Range has developed its geometry, specifically, its steeply dipping orientation with a unique inward curvature is unknown (Fig. 1.1). The proportion of the Sudbury Basin that the East Range spans is roughly one third of the other Ranges, and is characterized by a high density of prominent faults with an inward curvature mimicking the SIC itself (Fig. 1.1). Both the inward curvature of the faults and of the SIC are unique to the East Range. As the geometry of each Range has been the product of tectonic deformation, the question arises, how did the SIC in the East Range develop its unique curvature (Dence and Popelar, 1972; Klimczak et al., 2007)?

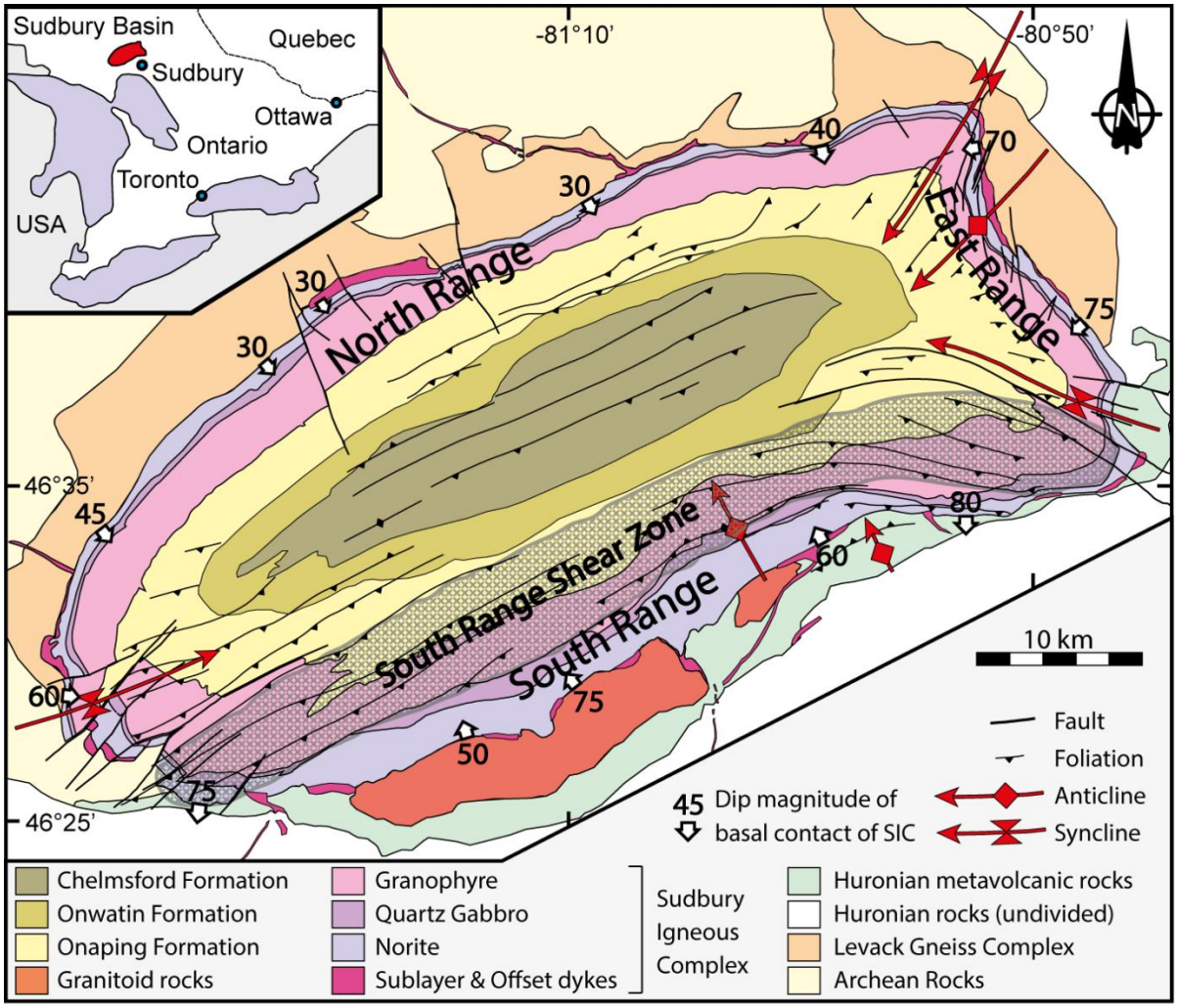

Figure 1.1: Simplified geological map of the Sudbury Basin in Ontario, Canada. Major lithological units defining the Sudbury Basin are after Ames et al., (2005). Faults, foliation trajectories modified after Cowan et al., (1999), anticlinal and synclinal fold-axial traces (red arrows) and dip magnitudes of the basal contact of the SIC after Rousell (1975) delineate the structure of the Sudbury Basin.

1.1 Purpose of this thesis

Due to the lack of previous structural studies in the East Range, this thesis aims to answer various questions which remain to constrain its structural evolution. Specifically, the mechanism by which the SIC in the East Range acquired its steep dip is unknown. The relative importance of slip on prominent curved faults should be recognized as large displacements of the SIC can be seen at surface (Fig. 1.1). In conjunction with relating slip on these faults to steepening of the SIC, the mechanism by which these faults acquired their curvature is also unknown. Due to similarities in the curvature of these faults and the curvature of the SIC in the East Range, folding is a likely mechanism although no other proof

has yet been identified. Therefore, identifying the relative importance of folding and faulting in the East Range are vital parameters to identify.

In addition, the orientations and kinematics of prominent East Range faults remains unknown. At surface, displaced SIC contacts provide a 2-D representation of the fault kinematics but there is no constraints for vertical slip components. Constraining the slip of these faults in 3-D has ramifications for not only constraining the broad scale structural evolution of the East Range but it is critical to understand how these faults have displaced ore bodies. Discerning the geometry of prominent East Range faults also provides insight into mineralization pathways from the SIC into the country rocks.

Furthermore, the primary "pre-deformational" geometry of the SIC is unknown. Although the primary geometry of the SIC has been estimated (Ivanov and Deutsch, 1999), it has never been imaged. The initial geometry of the SIC is thought to have been a planar isopotential sheet (Bowen, 1915; Grieve et al., 1991). This is contrasted by more recent studies whereby based on surface calculations aimed at deriving the basal contact geometry of the SIC, it has been suggested that this contact was not completely planar, and should contain primary embayment structures (Souch and Podolsky, 1969; Dreuse et al., 2010; Clark et al., 2012). Therefore, it is vital to better constrain whether the primary geometry of the SIC had primary embayment structures. From a mineral exploration perspective, this is vital to constrain as primary embayments or topographic undulations along the basal contact of the SIC are zones where Cu-Ni-PGE ores may have pooled during the gravitational stratification of the SIC (Keays and Lightfoot, 2004).

To solve these questions, this thesis aimed was to exploit older structural methodologies, within the framework of modern spatial analysis software packages to achieve highly detailed and precise results within a reasonable time frame. Specifically, chapter 2 focuses on harnessing LiDAR data to identify near surface planar geometries of fault surfaces to combine them with the orientation of field-measured outcrop-scale structures to derive the geometry and kinematics of prominent major faults. Aside from the field measurement of geological structures, this work was detailed and completed using ArcGIS. Moreover, this work was outlined as a Geographic Information System (G.I.S.) based workflow. Chapter 3 focused on testing a deformation hypothesis of the SIC in the East Range generated from surface data by performing forward modeling and kinematic restorations on a drill core constrained 3-D model of the SIC and faults. Using kinematic restoration techniques which

do and do not account for slip on faults, the importance of faults in folding of the SIC is highlighted. Therefore, together by analyzing surface and subsurface, I aim to provide a better understanding of the mechanism and path of deformation associated to the East Range of the Sudbury Basin, and of deformed mechanically isotropic igneous rocks in general.

1.2 References

Ames, D.E., Davidson, A., Wodicka, N., 2008. Geology of the Giant Sudbury Polymetallic Mining Camp, Ontario, Canada. Economic Geology 103, 1057-1077.

Bailey, J., Lafrance, B., McDonald, A.M., Fedorowich, J.S., Kamo, S., Archibald, D.A., 2004. Mazatzal-Labradorian-age (1.7-1.6 Ga) ductile deformation of the South Range Sudbury impact structure at the Thayer Lindsley mine, Ontario. Canadian Journal of Earth Sciences 41, 1491-1505.

Brocoum, S.J., Dalziel, I.W., 1974. The Sudbury Basin, the Southern Province, the Grenville Front, and the Penokean Orogeny. Geological Society of America Bulletin 85, 1571-1580.

Cowan, E.J., 1999. Magnetic fabric constraints on the initial geometry of the Sudbury Igneous Complex: a folded sheet or a basin-shaped igneous body? Tectonophysics 307, 135-162.

Dence, M.R., Popelar, J., 1972. Evidence for an Impact Origin for Lake Wanapitei, Ontario. *In* New Developments in Sudbury Geology, Geological Association of Canada, Special Paper Number 10, 7-18.

Dreuse, R., Doman, D., Santimano, T., Riller, U., 2010. Crater floor topography and impact melt sheet geometry of the Sudbury impact structure, Canada. Terra Nova 22(6), 463-469.

Dressler, B.O., 1984. General geology of the Sudbury area. *In* Pye, E.G., Naldrett, A.J., and Giblin, P.E., eds., The geology and ore deposits of the Sudbury Structure: Ontario Geological Survey Special Volume 1, 57-82.

Keays, R.R., Lightfoot, P.C., 2004. Formation of Ni-Cu-platinum group element sulphide mineralization in the Sudbury impact melt sheet. Mineralogy and Petrology 82, 217-258.

Klimczak, C., Wittek, A., Doman, D., Riller, U., 2007. Fold origin of the NE-lobe of the Sudbury Basin, Canada: Evidence from heterogenous fabric development in the Onaping Formation and the Sudbury Igneous Complex. Journal of Structural Geology 29, 1744-1756.

Krogh, T.E., Davis, D.W., Corfu, F., 1984. Precise U-Pb zircon and baddeleyite ages for the Sudbury area. *In* Pye, E.G., Naldrett, A.J., and Giblin, P.E., eds., The geology and ore deposits of the Sudbury Structure: Ontario Geological Survey Special Volume 1, 431-448.

Ivanov, B.A., Deutsch, A., 1999. Sudbury impact event: Cratering mechanics and thermal history. *In* Dressler, B.O., and Sharpton, V.L., eds., Large Meteorite Impacts and Planetary Evolution II, Geological Society of America Special Paper 399, 389-397.

Mukwakwami, J., Lafrance, B., Lesher, C.M., 2012. Back-thrusting and overturning of the southern margin of the 1.85 Ga Sudbury Igneous Complex at the Garson mine, Sudbury, Ontario. Precambrian Research 196, 81-105.

Riller, U., 2005. Structural characteristics of the Sudbury impact structure, Canada: Impact-induced versus orogenic deformation – A review. Meteoritics & Planetary Science 40, 1723-1740.

Rousell, D.H., 1975. The origin of foliation and lineation in the Onaping Formation and the deformation of the Sudbury Basin. Canadian Journal of Earth Sciences 12, 1379-1395.

Shanks, W.S., Schwerdtner, W.M., 1991a. Structural analysis of the central and southwestern Sudbury Structure, Southern Province, Canadian Shield. Canadian Journal of Earth Sciences 28, 411-430.

Shanks, W.S., Schwerdtner, W.M., 1991b. Crude quantitative estimates of the original northwest-southeast dimension of the Sudbury Structure, south-central Canadian Shield. Canadian Journal of Earth Sciences 28, 1677-1686.

Souch, B.E., Podolsky, T., geological staff, 1969. The sulfide ores of Sudbury: Their particular relationship to a distinctive inclusion-bearing facies of the nickel irruptive. Economic Geology Monograph 4, 252-261.

2.0 Significance of first-order faults in folding mechanically isotropic layers: evidence from the Sudbury Basin, Canada

2.1 Abstract

The Sudbury Basin is a non-cylindrical fold basin demarcated by the layered Sudbury Igneous Complex (SIC), the eastern part of which is transected by prominent curved faults. Folding of the SIC occurred in the brittle field and is peculiar due to its petrographically distinct, but initially mechanically similar layers. Overall, the layers are characterized by low levels of solid-state strain raising the question how layer contacts acquired their curvature. I addressed this question by developing a G.I.S.-based workflow to analyze the orientation and slip vectors of the faults. Slip vectors form clusters of normal and reverse slip along a given fault. The clustering is best interpreted in terms of successive slip events during folding of the SIC. As the faults formed most likely as planar reverse faults prior to folding of the SIC they subsequently served as mechanically anisotropic elements to fold the SIC. The results contribute to (1) better understand the folding mechanisms of thick melt sheets in the upper crust, (2) explain apparently incompatible principal strain axes during progressive deformation, and (3) efficiently analyze the orientation and kinematics of fault zones close to the Earth's surface.

2.2 Introduction

Knowledge of the geometry and kinematics of first-order faults is paramount for correlating displaced lithological contacts and quantifying displacement magnitudes in deformed crustal terrains. All too often, however, the lack of sufficient surface exposure and absence of structural information at depth, e.g., from seismic or drilling data, renders identification of fault surface geometries, kinematics associated with fault surfaces, and correlation of displaced markers across faults, impossible. One path to remedy this is to use topographic data, which can be used to infer the orientation of planar structures close to the Earth's surface (e.g., Burbank et al., 1999; Saleeby and Foster, 2004; Dreuse et al., 2010; García-Sellés et al., 2011), and thus may aid in identifying orientations of first-order faults at shallow crustal depths. The kinematics of such faults can be constrained using principal strain or

paleostress axis orientations inferred, for example, from higher-order (cm- to m-scale) structures at surface. This requires that orientations of first-order faults are known and that faults are cogenetic with nearby higher-order structures (Lisle, 1998; Schwerdtner, 1998; Schwerdtner et al., 2005). This approach may be a significant step forward in determining the kinematics of first-order faults.

The orientation of a surface is defined by the coordinates, e.g., cartesian or geographic, of any three points of this surface (Bennison et al., 2011). Therefore, one can obtain the orientation of a surface and its respective strike lines, also known as structure contours, from any three points of its intersecting trace with topography. Geological surfaces are, however, rarely perfectly planar (Ziesch et al., 2015), and may be rather curved, horizontally corrugated, or vertically corrugated (Fig. 2.1). Complex surface geometries can be manifested in multiple families of structure contours. With the availability of high-resolution digital elevation models (DEMs), structure contours of a geological surface can be identified accurately and efficiently. Nevertheless, an appropriate software framework to determine orientations and geometries of geological surfaces from DEMs remains to be developed. Geographic Information Systems (G.I.S.) software packages may lend themselves excellently for this task (Dadon et al., 2011). The availability of high-resolution topographic data and accuracy of GPS-assisted structural mapping prompts us to propose a G.I.S.-based workflow aimed to characterize non-planar surface geometries from high-resolution topography data.

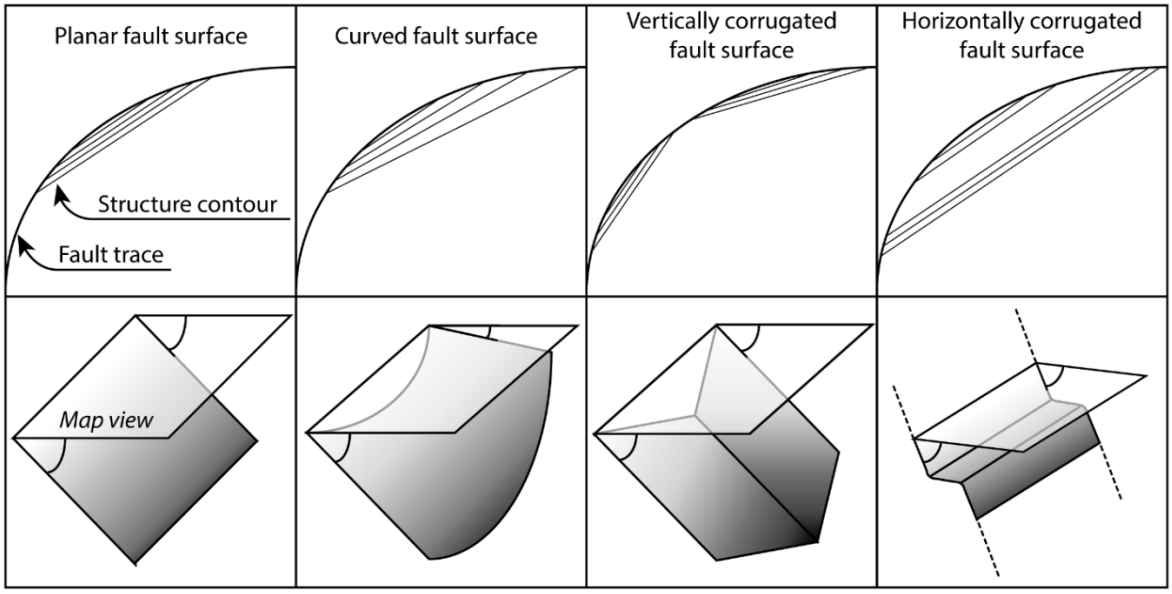

Figure 2.1: Conceptual representation of simple fault surfaces generated from the map pattern of structure contours. Top row contains four unique arrangements of structure contours from a curved fault trace as seen in map view. Bottom row contains the resultant geometry from the structure contours in the top row.

In brittlely deformed terrains, inversion of higher-order shear faults is now routinely applied to infer paleostress or strain (deformation) regimes (e.g., Gapais et al., 2000; Martínez-Díaz, 2002; Sperner et al., 2002; Beaudoin et al., 2012; Van Noten et al., 2013; Bartel et al., 2014). Lisle (1998) and Schwerdtner (1998) expanded the concept of shear fault inversion by using principal axis orientations of paleostress or ductile strain to identify the kinematics of nearby prominent faults. However, displacement on prominent brittle faults are rarely constrained to a single fault surface, but rather are accomplished by a fault core of pervasively fractured rock (gouge) and an enveloping fault damage zone of less fractured rock (Shipton and Cowie, 2001). The bulk of strain and displacement is accommodated within the fault core but to some extent also in the damage zone (Faulkner et al., 2006), in which higher-order brittle shear faults are generally well developed. Assuming that the states of strain are similar in fault cores and their damage zones (Shipton and Cowie, 2001), local principal strain directions inferred from inversion of higher-order shear faults in the damage zones allows one to determine the kinematics of lower-order faults. This concept was successfully applied to infer the kinematics of Neogene to active faults in the Eastern Cordillera of the Central Andes (Santimano and Riller, 2012a; Daxberger and Riller, 2015). Here, I test this concept in the eastern Sudbury Basin, a non-cylindrical fold basin located in the Paleoproterozoic Eastern Penokean Orogen of Ontario, Canada (Fig. 2.2a).

The perimeter of the Sudbury Basin (Fig. 2.2a) is made up by the Main Mass of the Sudbury Igneous Complex (SIC), an originally flat impact melt sheet that differentiated into petrographically distinct layers, known from bottom to top as the Norite, Quartz-Gabbro and Granophyre (Naldrett and Hewins, 1984; Pattison et al., 1979; Lightfoot et al., 1997a, b, c; Grieve et al., 1991). The Sublayer, a discontinuous layer of noritic composition containing massive sulfide deposits underlies the Norite of the Main Mass and is part of the SIC. Collectively, these units rest on Paleoproterozoic and Archean basement rocks and are overlain by the Whitewater Group which consists of the Onaping Formation and post-impact sedimentary rocks of the Chelmsford and Onwatin Formations (Dressler, 1984). Except where transected by a kilometer-scale ductile thrust, the South Range Shear Zone (Fig. 2.2a), the SIC and its underlying crystalline basement rocks are largely devoid of solid-state strain (Shanks and Schwerdtner, 1991a, b; Cowan and Schwerdtner, 1994; Klimczak et al., 2007; Lenauer and Riller, 2012a, b). This applies in particular for zones of maximal curvature of the SIC at surface, such as the synformal NE-lobe (Fig. 2.2b; Cowan and Schwerdtner, 1994; Cowan, 1999; Cowan et al., 1999; Klimczak et al., 2007) and begs the question of how the

contacts of the SIC and its underlying Archean basement rocks, mechanically acquired their curvature and steep dips (Fig. 2.2a) while maintaining overall structural continuity (Rousell, 1975; Dreuse et al., 2010). This problem is exacerbated by the fact that, although layers of the SIC are petrographically distinct, the layer interfaces do not show evidence for any concentration of contact-parallel planar strain fabrics. This observation renders folding of the SIC and its underlying basement rocks by flexural shear or flexural slip unlikely. Hence, SIC layers and underlying basement rocks seem to have behaved mechanically isotropic during the formation of the Sudbury Basin, which seems to defy an important mechanical prerequisite of folding.

Based on the observation that shortening directions inferred from inversion of brittle shear faults from the NE-lobe of the SIC are orthogonal to respective axial-planar foliation surfaces in the adjacent Onaping Formation, Klimczak et al. (2007) suggested that shape change, i.e., tilting, of the SIC was accomplished by brittle deformation. This opened up a new avenue in the understanding of how igneous layers of the SIC, which seem to be welded mechanically to the underlying basement rocks, collectively characterized by mechanical isotropy, were folded. To further explore the role of brittle deformation in large-scale folding of the SIC, I systematically analysed the kinematics of small-scale brittle shear faults and prominent, km-scale faults of the eastern Sudbury Basin. The latter requires knowledge of fault orientations. I address this issue by introducing a G.I.S.-based methodology for inferring the geometry of prominent faults from high-resolution topography and associated kinematics based on a comprehensive fault-slip analysis. Based on the results of our kinematic analysis of first-order faults I explore the role of faulting in the formation of the Sudbury Basin.

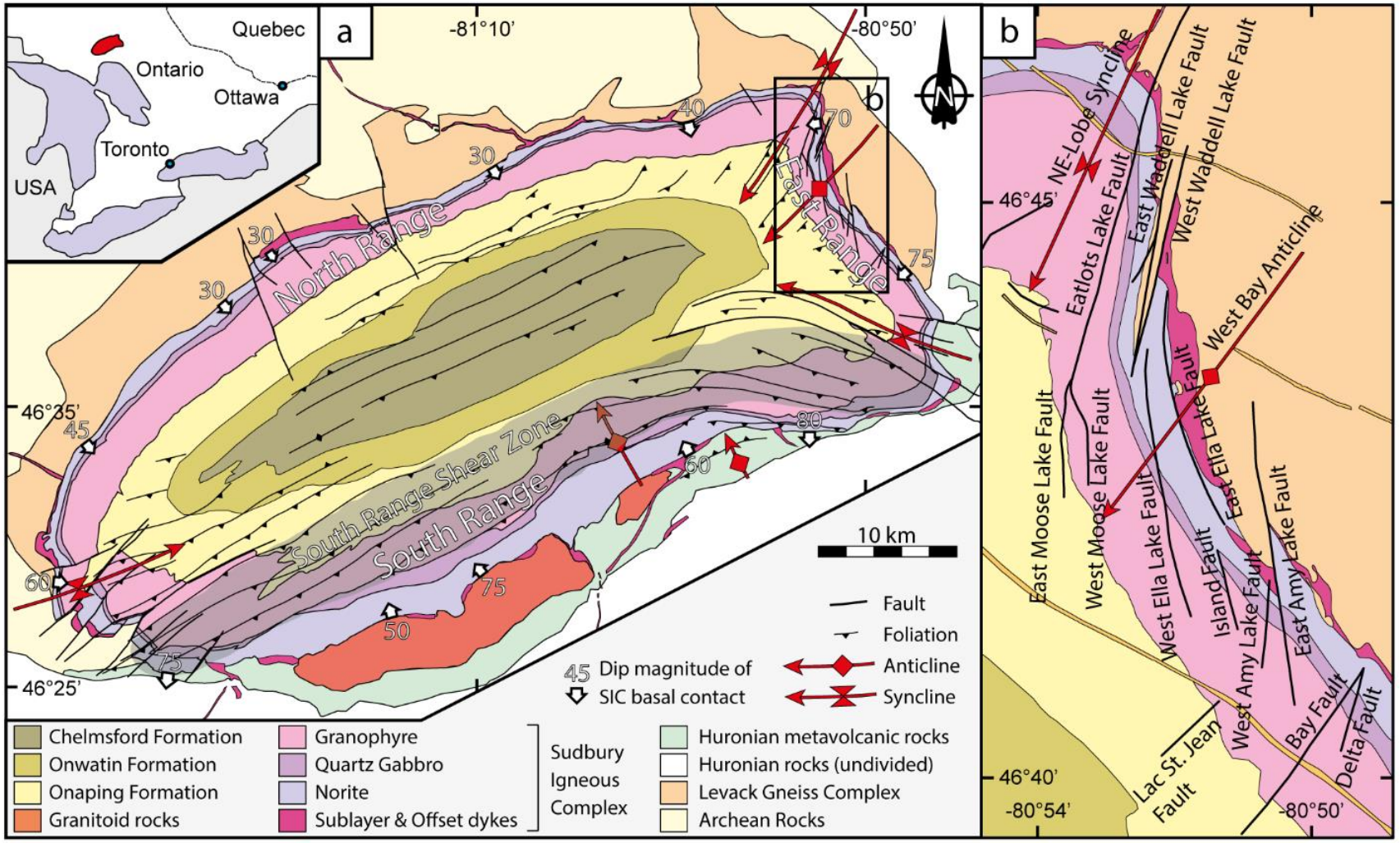

Figure 2.2: Map showing simplified geology of the Sudbury Basin in Ontario, Canada. (a) Major lithological units defining the Sudbury Basin. Prominent faults (black lines), foliation trajectories (black lines with barbs), fold axial traces (red arrows) and dips of the basal contact of the Norite (white arrows with numbers) delineate the structure of the Sudbury Basin. (b) Prominent structures of the East Range.

2.3 Geological background

The Sudbury Basin measures 65 km x 25 km at surface and straddles the interface between the igneous and high-grade metamorphic Archean rocks of the Levack Gneiss Complex (Krogh et al., 1984) to the north, and metasedimentary and metavolcanic rocks of the Paleoproterozoic Huronian Supergroup to the south (Fig. 2.2a). At surface, the Sudbury Basin forms three distinct morphological ranges; the South Range, the North Range, and the East Range (Fig. 2.2a). Contact orientations of the SIC vary greatly among the ranges. In the North Range and the East Range, contacts dip respectively at 30° to 40° and at ~70° towards the basin center. In the South Range contacts dip either 50° to 70° towards, or 80° away from, the basin center (Rousell, 1975; Dreuse et al., 2010). Zones of enhanced thickness of the Main Mass correspond spatially to local Sublayer accumulations and form embayments of the SIC in Archean and Paleoproterozoic host rocks (Keays and Lightfoot, 2004; Dreuse et al., 2010). The ranges are separated by 3 second-order synclines, the NE-lobe, the SE-lobe, and the western closure of the SIC (Fig. 2.2a). In between these synclines, the SIC forms anticlines, which, like the synclines, are disposed radially with respect to the center of the basin (Lenauer and Riller 2012a). The most prominent of these anticlines is the SW-plunging West Bay Anticline in the East Range (Clark et al., 2012), evident by the pronounced curvature of the SIC and steep dips towards the basin center (Fig. 2.2a, b).

A set of prominent, crudely N-S striking faults in the East Range, i.e., the Eatlots Lake fault, the East and West Waddell Lake faults, the East and West Ella Lake faults and the East and West Amy Lake faults, are spatially associated with the West Bay Anticline (Fig. 2.2b). The traces of these faults mimic the curvature of the Main Mass (Fig. 2.2b). Based on the notable strike separation of the Main Mass at the East Waddell Lake and East Amy Lake faults, these faults appear to be characterized by components of left-lateral slip (Fig. 2.2b). However, the actual kinematics of these faults and their possible kinematic relationship to the formation of the West Bay Anticline are unknown.

The SIC acquired its synformal geometry most likely during the 1.7-1.6 Ga Mazatzal orogeny (Bailey et al., 2004) and possibly during the 1.2-1.0 Ga Grenville orogeny (Card et al., 1984). The tectonic foliation imparted into the Whitewater Group and large parts of the SIC (Brocoum and Dalziel 1974; Rousell 1975; Everitt 1979), notably its fanning in the eastern part of the Basin and the axial-planar character in the NE- and SW-lobes (Fig. 2.2b), attests to folding strain in these units. The South Range Shear Zone, a prominent ductile deformation

zone characterized by NW-directed thrusting and transpressive deformation, transects the southern Sudbury Basin (Shanks and Schwerdtner, 1991a, b; Milkereit and Green, 1992; Boerner and Milkereit, 1999; Cowan and Schwerdtner, 1994; Cowan et al., 1999; Riller et al., 2010). Rotation of rocks affected by the Shear Zone accounts for the variable contact dips of the South Range SIC (Lenauer and Riller, 2012b; Santimano and Riller, 2012b).

2.4 Methodology

The proposed G.I.S.-workflow (Fig. 2.3) aimed to discern the geometry and kinematics of prominent faults in the East Range is divided into three parts: the analysis of orientation and geometry of prominent faults, the derivation of principal strain and paleostress directions from higher-order faults, and the identification of slip directions on prominent faults.

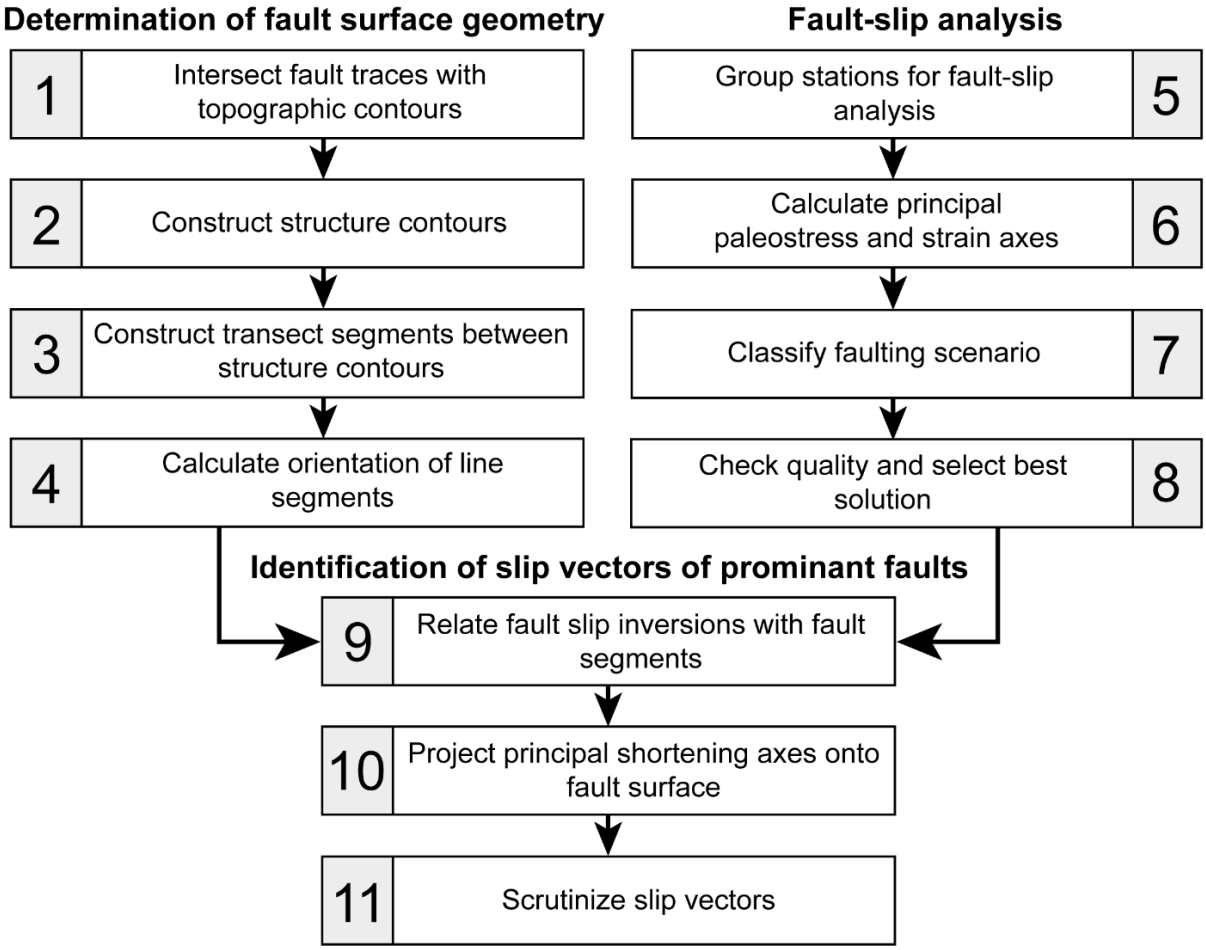

Figure 2.3: Workflow describing the analysis of fault surface geometry (steps 1 to 4), fault-slip analysis (steps 5 to 8) and identification of slip vectors (steps 9 to 11).

2.4.1 Analysis of geometry and orientation of fault surface

Structure contours of fault surface geometries were extracted from LiDAR (Light Detection and Ranging) bare-earth topography data with a horizontal resolution of one meter. The structure contours were generated with ArcGIS 10.1 (ESRI), which can facilitate the batch calculation of individual populations of spatial and tabular data, in this case, sets of matching elevation points along a fault trace. In addition, ArcGIS has built-in topology rules, which ensures computational accuracy on where known fault traces lie with respect to topography. However, functionality to combine points of equal elevation based on an attribute is not built into ArcGIS. To remedy this nonetheless, the third party toolset GeoWizards (ET Spatial Techniques) was harnessed to use the elevation attribute to create a set of structure contours for each prominent fault.

Once structure contours were generated, the fault geometry was classified as simple or complex, based on contour patterns (Fig. 2.1). Simple fault surface geometries are characterized by either uniform positive or negative slopes. Fault surface geometries may be planar, curved or corrugated (Fig. 2.1). More specifically, planar and horizontally corrugated fault surfaces are characterized by a variation in the horizontal spacing of structure contours, whereas curved and vertically corrugated fault surface geometries are evident by an azimuthal variation of structure contours (Fig. 2.1). Complex surfaces are characterized by combinations of the four end member geometries. In most cases, complex surfaces have repeating surfaces at the same (x, y) location but multiple depths (z). To generate a surface from complex assemblages of structure contours, the user must decide whether the structure contours are imaging repeating vertical segments or repeating shallow segments. These interpretations depend on the complexity of deformation, and on access to independent evidence of local shortening and extension orientations as well as strike separation of lithological units, to provide a degree of confidence in one interpretation over another. This allows for confidence when describing the variation of a fault surface, such as whether structure contours describe a shallowly dipping fault with subhorizontal secondary conjugate faults, or a subhorizontal fault with shallowly dipping secondary conjugate faults. In this study, I provide simplified fault orientations (Table 2.1). The geometry of a fault surface is visualized along a profile chosen to be perpendicular to the structure contours, spaced at a horizontal distance of 1m (Fig. 2.4a, b). The transecting lines, from which the fault surface

profile (Fig. 2.4b, c) was generated, was created using the freely available third-party script Transect Tool provided by Mateus Vidotti Ferreria (Personal Communication 2014).

Table 2.1: Average fault orientation (S: dip direction/dip), and slip direction (L: plunge direction/plunge), and number of associated normal slip (NF) and reverse slip (RF) vectors for each fault.

Fault Name	**S**	**L**	**NF**	**RF**
Delta Fault	288/85	004/70	7	9
Lac St. Jean Fault	321/90	No Shortening		
East Amy Lake Fault	260/88	172/40	6	5
West Amy Lake Fault	094/87	178/64	0	1
West Moose Lake Fault	268/82	327/74	1	2
East Moose Lake Fault	087/51	050/44	1	2
Bay Fault	126/82	040/25	8	5
East Ella Lake Fault	083/50	032/37	8	7
West Waddell Lake Fault	107/62	160/49	5	4
Minor Waddell Lake Fault	122/83	No Shortening		
Barnett Lake Fault	209/45	No Shortening		
Rocklin Fault	305/16	No Shortening		
Eatlots Lake Fault	108/84	024/42	1	1
East Waddell Lake Fault	294/18	269/16	4	4
West Ella Lake Fault	260/38	305/30	8	10
Island Fault	263/53	243/51	0	1

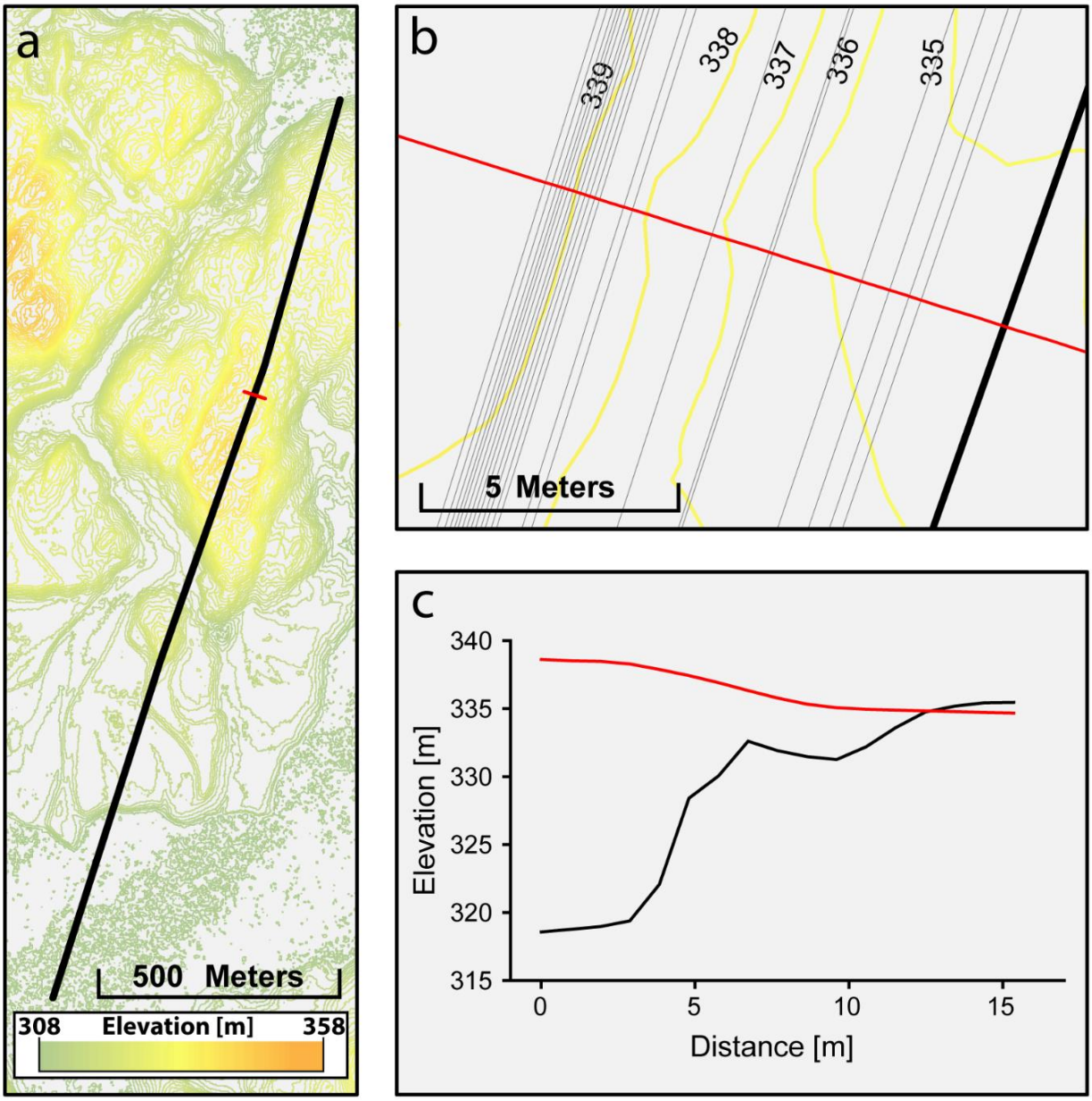

Figure 2.4: Application of the three-point technique. (a) Example fault (black line) overlain on topography. The red line shows the profile trace in (b) and (c). (b) A zoomed-in view of the fault trace and constructed structure contours (grey lines). Numbers correspond to the elevation of topographic contour lines in meters. Structure contours are used to segment the transect line concordant with the profile trace to be of finite length between strike lines. The azimuth and dip of these transect segments is extracted. (c) Resultant profile showing topography (red line) and orientation of fault segments (black line).

2.4.2 Derivation of principal strain and paleostress directions from higher-order faults

In order to use the orientation of principal strain or paleostress directions for deriving the kinematics of prominent faults, respective principal tensor axes were obtained from inversion

of higher-order brittle shear faults, also known as slickensides (Carey and Brunier, 1974). Higher-order fault were measured within the damage zone of a given prominent fault to ensure the cogenetic relationship between the two. For the inversion, the dip direction and dip of a brittle shear fault, the azimuth and plunge of the respective slip lineation, the sense-of-slip, a numerical value representing the reliability of slip data (certainty), and the mineral type of the lineation were recorded (Appendix: Table 1). The numerical value representing the reliability of slip data ranges from 1-4 where 1 represents certainty of the orientation of the slickenside with obvious slip sense, 2 represents a reliable orientation of the slickenside with a confident slip sense, 3 represents an unreliable orientation for the slickenside with a semi-confident slip sense, and 4 represents an unreliable orientation of slickenside or a slickenside with no recognizable slip sense. Fault data measured within an area of approximately 50 meters in diameter form a station of brittle fault measurement, the location of which is recorded in ArcGIS.

Fault-slip data was analyzed using the software package Tectonics FP v. 1.7.7 (Ortner et al., 2002). The data was corrected using a built-in checking algorithm. Specifically, this algorithm checks the angle between each fault and its respective lineation. In cases where the angle is larger than 10°, the respective fault is not considered for further analysis. For all other cases the measured slip lineations will be projected onto the respective faults, collectively forming a corrected dataset that will be used for the calculation of principal tensor axis orientations.

A common procedure in paleostress analysis is to separate a heterogenous data set into homogenous subsets (e.g., Fry, 1992; Nemcok and Lisle, 1995; Shan et al., 2006; Sperner and Zweigel, 2010), aimed to ensure a correct estimation of paleostress tensors from a series of events. Various authors have called this procedure to question, i.e., whether stress is truly homogeneous during an event (Pollard et al., 1993; Twiss and Unruh, 2007), and therefore advocate to interpret principal tensor axes in terms of deformation rate or incremental strain (Twiss and Unruh, 1998; Gapais et al., 2000). Following this concept, I refrain from subdividing a given fault data set into subsets and interpret our results in terms of strain, in variance to the primary intended use of inversion methods.

In the present study, the orientation of principal axes of paleostress and strain were calculated using the P-B-T method (Turner, 1953), the direct inversion method (Angelier and Goguel, 1979), the numerical dynamic analysis (Spang, 1972), and the right dihedra method (Angelier

and Mechler, 1977). The P-B-T method calculates the orientation of the P (principal shortening axis), B (principal intermediate axis), and T (principal extension axis). The direct inversion method computes the orientation of the rudimentary paleostress tensor with principal axes $\sigma_1 \geq \sigma_2 \geq \sigma_3$ and stress ratio $R_{stress} = (\sigma_2-\sigma_3) / (\sigma_1-\sigma_3)$. The numerical dynamic analysis (NDA) determines the reciprocal strain tensor with principal axes $\lambda_1 \geq \lambda_2 \geq \lambda_3$ and the strain ratio $R_{strain} = (\lambda_2- \lambda_3) / (\lambda_1- \lambda_3)$. The right dihedra method computes the compressive and tensile dihedra for each fault plane and identifies the orientation of the principal paleostress axes $\sigma_1 \geq \sigma_2 \geq \sigma_3$. For the P-B-T and NDA methods, the angle between the principal maximum strain axis and the fault (θ) must be chosen. For this study, I performed P-B-T and NDA calculations using the default angle θ of 30° approximating the fracture angle in undeformed rock. In addition, I performed these calculations with a best fit θ which varies between 10° and 85° defined by clustering between P- and T-axes against θ (Wallbrecher, 1986). By applying both angles of θ, both conditions of newly formed faults and reactivated ones can be accounted for.

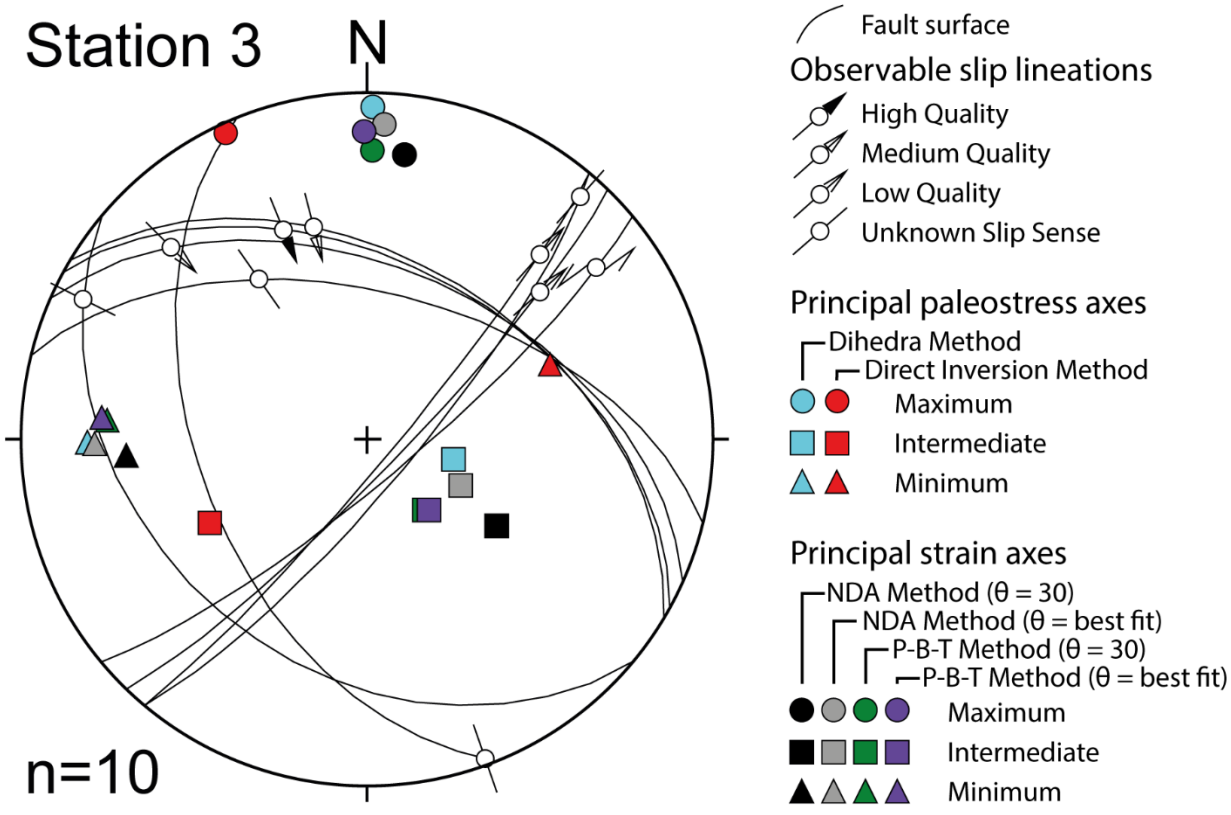

Figure 2.5: Variation in orientation of principal axes of paleostress and strain using multiple methods shown for slickensides of station 3 displayed in a lower-hemisphere equal-area projection.

To select the inversion, which best represents the fault population of a given station, various quality indicators suggested by Sperner and Zweigel (2010) are used (Appendix: Table 2). Depending on the diversity of fault surface orientations at a given station, certain fault-slip inversions may not generate plausible stress or strain tensors. An example displaying the diversity of solutions is given in Figure 2.5. For a more detailed description of fault-slip inversion methods the reader is referred to Sperner and Zweigel (2010). To eliminate potentially using a fault-slip inversion method which yields implausible results, individual fault planes and respective slip vectors are displayed and reviewed in lower-hemisphere equal-area projections (Fig. 2.6, Appendix: Figure 1). Accordingly, each inversion is classified as one of the following: dominance of a single fault-plane population, presence of conjugate fault sets, preference of axial contraction or axial extension, degree of tri-axial deformation, or evidence for non-coaxial deformation. Next, a quality matrix is constructed for each inversion (Appendix: Table 2). This matrix rates each method based on: the number of data (slickensides), the percentage of data used from the total collected dataset of a location, the average confidence number, the average misfit fluctuation, and the type of data used. The average confidence number is an average of the numerical value representing the reliability of slip data where the 1-4 classification is first modified to a 0-1 scale where; 1 : 1, 2 : 0.75, 3 : 0.5, 4 : 0.25, then these values are averaged. The average misfit fluctuation is an average of the arithmetic mean of the angles between the measured and theoretic slickensides for a calculated set of paleostress or strain axes. The type of data used represents the type of kinematic indicator, where a value of 1 represents a slickenside, 0.5 represents a tension/compression joint, 0.5 represents two conjugate planes, 0.5 represents a movement plane and a tension joint, and 0.25 represents a shear joint (Sperner and Zweigel, 2010). Furthermore, fluctuation histograms with each method are reviewed. These histograms show the count distribution of the dihedral angle between the measured lineation and stress vector for each slickenside. Solutions for rudimentary strain or stress tensors resulting in unimodal distributions of the dihedral angle are favored over bimodal distributions. Finally, for methods that assign negative expected values (NEV) which can be assigned to each slickenside when the slip sense is opposite to what is expected, a percentage of NEVs is taken. A higher percent indicates better agreement between the measured dataset and the calculated stress or strain tensor.

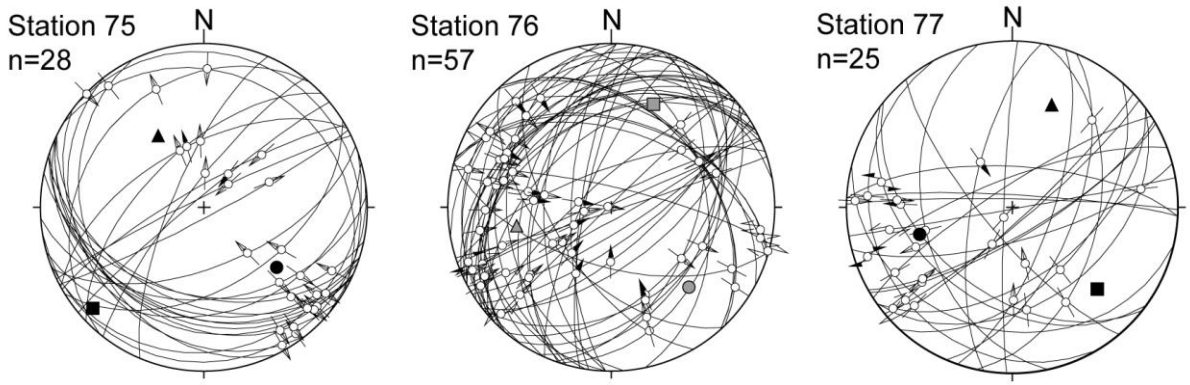

Figure 2.6: Lower hemisphere equal-area projections of selected slickenside populations and respective principal paleostress and strain axes. Circles, squares, and triangles represent respectively the maximum, intermediate, and minimum principal paleostress and principal strain axes. Grey shades of the symbols correspond to legend in Figure 2.5.

2.4.3 Identification of slip vectors of prominent faults

To identify the zone around a prominent fault where higher-order faults contribute to the slip on a larger fault, the width of a fault damage zone needs to be known (Shipton and Cowie, 2001). In case fault damage zones are not apparent in the field, empirical relationships are used for their identification. To derive the width of damage zones for prominent faults in the East Range, first, the length of a fault trace is used to estimate the maximum displacement on a fault surface (Scholz, 1990; Schlische et al., 1996; Davis et al., 2005; Burbank and Anderson, 2011). Next, the maximum displacement on a fault surface is used to calculate the width of a fault damage zone (Faulkner et al., 2011). Using the two empirical relationships, the damage zone width is calculated from the average of fault trace lengths, which amounts to ~650 m. This length is proportional to a maximum fault displacement of ~100 m (Burbank and Anderson, 2011). The maximum fault displacement of ~100 m is then proportional to a damage zone of 300 m (Faulkner et al., 2011). Fault-slip data measured within this 300 m wide zone are attributed to formation of the respective fault.

The direction and sense of slip on prominent faults in the East Range are identified using the software TectonicsFP (Ortner et al., 2002). Shortening directions obtained from the fault-slip analysis are plotted along with the orientation of the prominent fault surface, and the pole to this surface into lower-hemisphere equal-area projections (Fig. 2.7, Appendix: Figure 2). The average orientations of maximum shortening (λ_1) is projected through the pole of the fault

surface onto the fault surface (Lisle, 1998; Schwerdtner, 1998). This results in the slip direction on the fault surface. The angle between the average shortening direction and the slip vector on the fault defines the fault type.

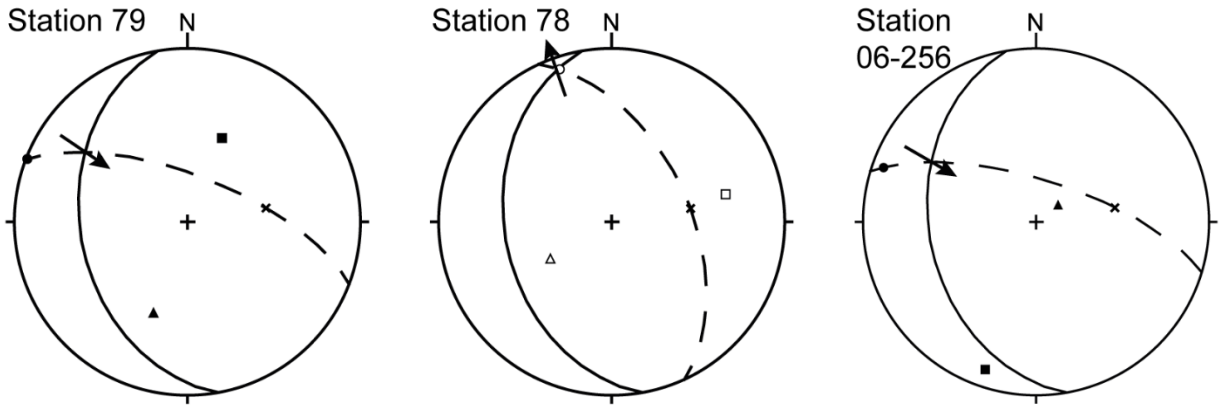

Figure 2.7: Lower-hemisphere equal-area projections of slip vectors on respective fault surfaces (solid great circles) through the pole of the fault surface (crosses) for selected stations of the West Ella Lake Fault. Open symbols indicate principal paleostress axes and solid symbols indicate principal strain axes.

2.5 Results

First-order faults in the East Range strike either N-S or NE-SW. N-S striking faults cut the SIC at low angles and are curved, whereas faults striking NE-SW are straight and cut the SIC at high angles (Fig. 2.2b). Strongly curved faults, such as the East and West Ella Lake faults, and the Barnett Lake fault, are spatially associated with the fold hinge zones of the West Bay Anticline and the NE-Lobe, respectively (Fig. 2.8). In order to explore the possible genetic relationship between faulting and folding of rocks in the East Range, the geometry, local strain axes and slip vectors of prominent faults are delineated.

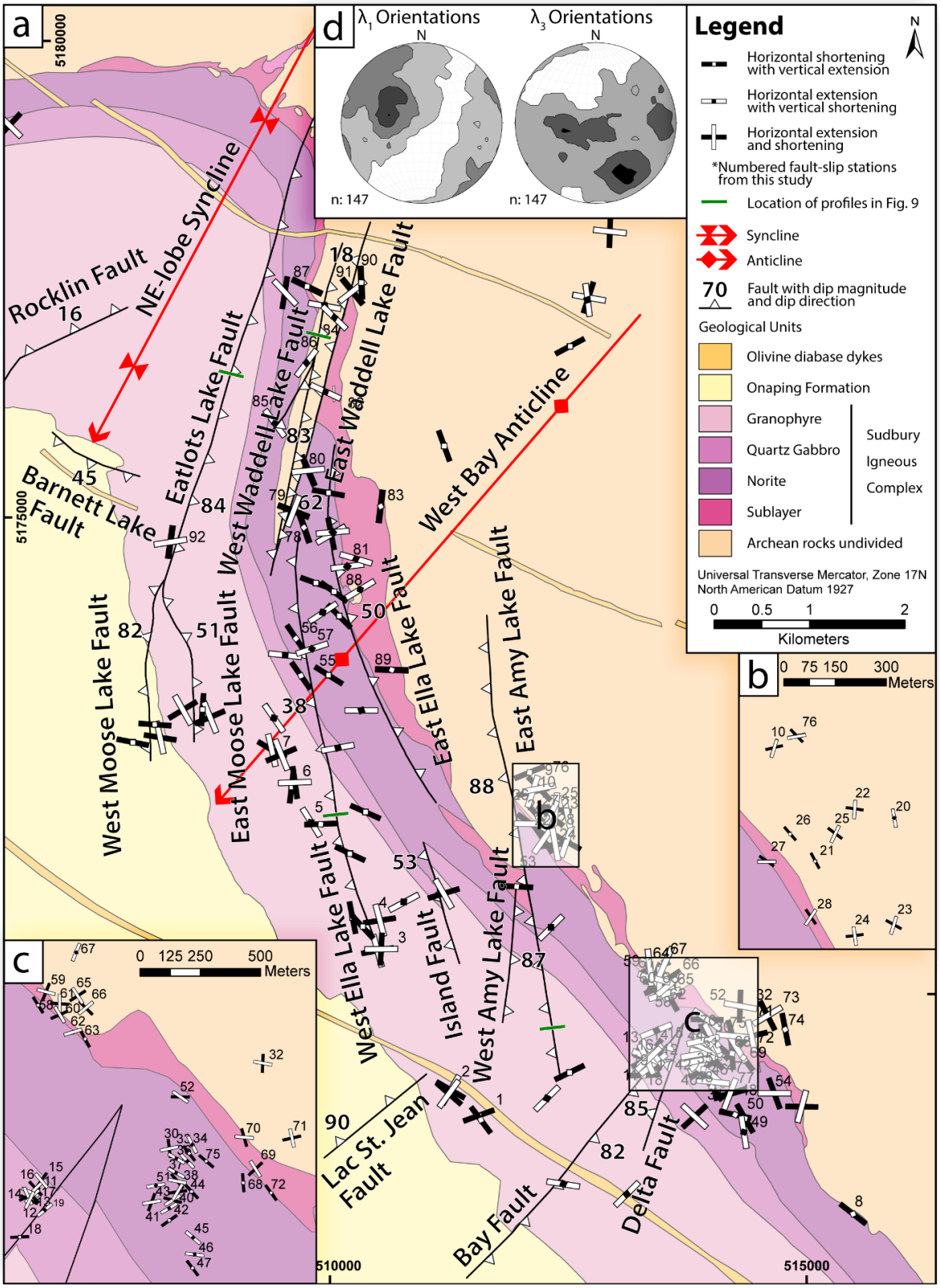

Figure 2.8: Principal strain directions in the East Range of the Sudbury Basin. (a) Geological map of the East Range displaying the orientation of local principal strain axes from this study (numbered stations) and from Riller et al. (in review) projected to map view. White triangles on faults show dip directions and numbers indicate average fault dips. (b) and (c) Close-ups of areas with a high spatial coverage of strain axis data. (d) Contour plots displaying the average orientations of shortening (λ_1) and extension (λ_3). Dark grey shades indicate strong clustering.

2.5.1 Fault surface geometries

Fault surface geometries were calculated to the range of elevations that the structure contours encompass delivering average fault orientations (Table 2.1) and fault geometries (Fig. 2.9). In terms of geometry, the faults can be classified as simple or complex (Fig. 2.1). Profiles displaying topography and geometry of fault segments surface were generated for four prominent faults and show variations in fault surface corrugation (Fig. 2.9). The East Amy Lake fault can be characterized by two segments, which steepen with depth (Fig. 2.9a). However, the method of creating a continuous surface from structure contours may generate artifacts such as oppositely dipping fault segments seen at a depth between 12 m and 16 m below surface. At a depth of 4 m to 8 m the fault is shallowing but this trend cannot be confirmed without the knowledge of more structure contours at depth. The West Waddell Lake fault can be characterized by a combination of two orientations of segments, a primary SE-dipping surface with smaller segments dipping in opposite directions (Fig. 2.9b). In effect these fault segments display a horizontally corrugated pattern (Fig. 2.1). The Eatlots Lake fault can be characterized by two segments, a steeply dipping fault segment and a segment, which shallows with increasing depth (Fig. 2.9c). The West Ella Lake fault is characterized by a fault surface profile which appears to be widely distributed across an elevation range of 309 m to 317 m (Fig. 2.9d). Overall this fault dips moderately to shallowly toward the west (Table 2.1) and consists of 3 shallowly west-dipping segments showing minor corrugations (Fig. 2.9d). The steeply dipping segments are interpreted to be artifacts. In summary, the fault profiles point to considerable geometric complexity of higher-order faults, collectively forming lower-order fault zones at shallow depth.

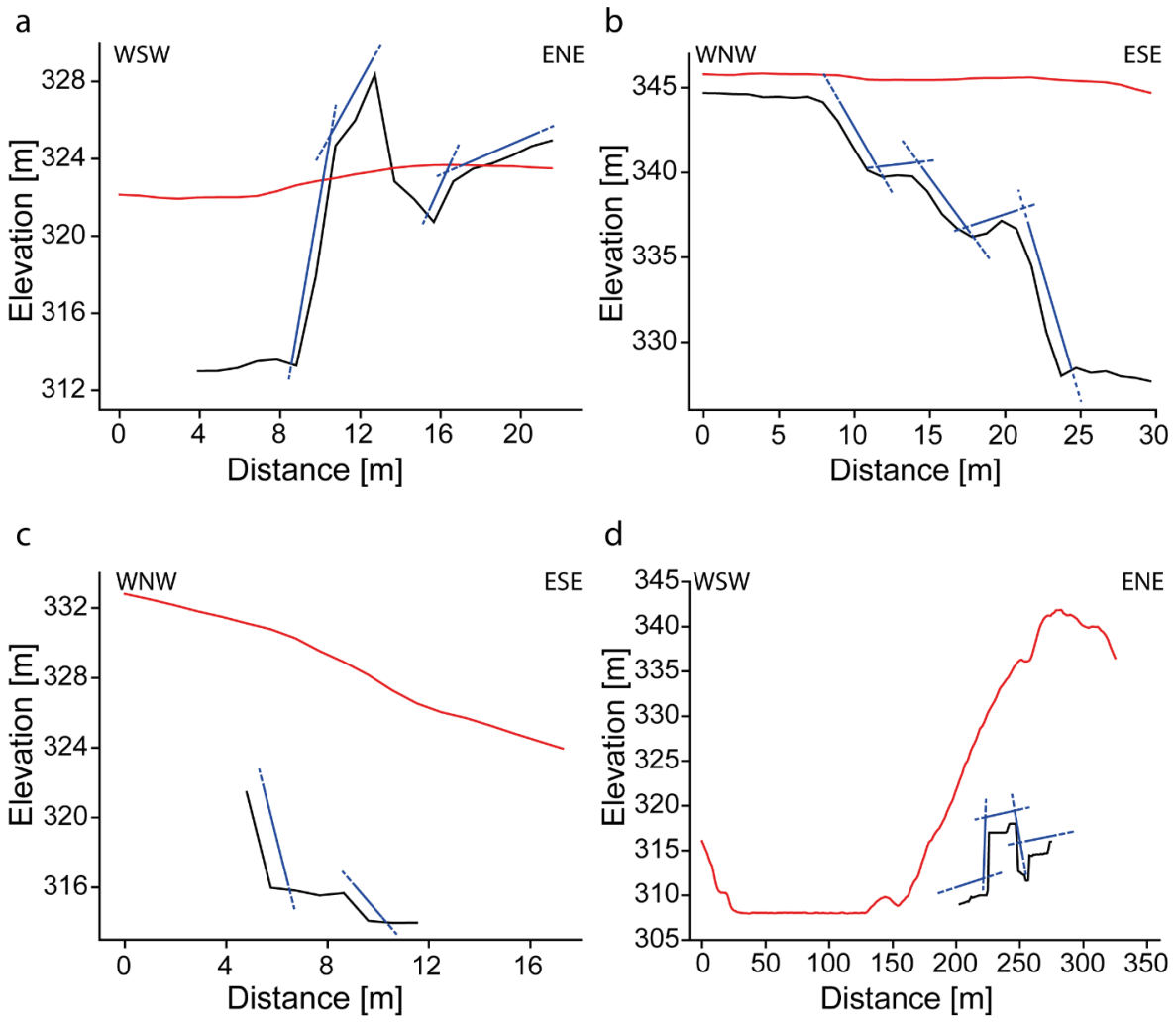

Figure 2.9: Selected profiles showing topography (red lines) and fault surface traces (black lines) calculated from the structure contours based on LiDAR images for (a) the East Amy Lake fault, (b) the West Waddell Lake fault, (c) the Eatlots Lake fault and (d) the West Ella Lake fault. For location of profiles see Figure 2.8.

2.5.2 Fault-slip analysis

Fault-slip data from the East Range were obtained and inverted in this study at a total of 91 stations (Fig. 2.8, Appendix: Table 3) and complemented by data from 56 stations reported in Riller et al. (in review). Of the 91 inversions from this study, 77 inversions were performed using strain inversion methods whereas 14 inversions were performed using paleostress inversion methods. Of the 56 stations reported in Riller et al. (in review), all 56 stations were performed using strain inversion methods. The variation in quality of fault-slip inversions is rather large and is primarily controlled by the number of brittle faults included in an inversion as well as the average misfit (error) of a particular method.

The majority of shortening axes are sub-horizontal to moderately NW-plunging, whereas maximum extension axes are more variable (Fig. 2.8d). These results are in agreement with previously acquired fault-slip data from the Sudbury area (Riller, 2005; Lenauer and Riller, 2012a, b). Locally however, strain axes differ in orientation from the regional average (Fig. 2.8a, d). In these areas, principal axes predominantly show horizontal shortening with vertical extension spatially intermingled with stations characterized by horizontal extension with either vertical or horizontal shortening. For example, north of the West Bay Anticline, horizontal shortening and vertical extension is more dominant than south of the anticline. Inversions spatially associated with the West Ella Lake fault in particular display a consistent pattern of NW-SE shortening with subvertical extension. However, there are also stations along the northern portion of the fault, displaying NE-SW directed extension with subvertical shortening. Along the southern half of this fault, W-E to NW-SE extension with N-S to NE-SW shortening prevails. Although based on somewhat fewer data, this presence of NE-SW extension and subvertical shortening as well as NW-SE shortening and subvertical extension is also seen along the northern half of the East Ella Lake fault. Overall, this change in orientation of principal strain axes occurs where the fault intersects the hinge zone, more specifically, the fold-axial trace, of the West Bay Anticline (Fig. 2.8a).

This change in principal strain axis orientations at the fold hinge zone is also evident from other faults in the East Range. In particular, NW-SE horizontal shortening and NE-SW to N-S extension prevails near the East and West Amy Lake faults, i.e., akin to the southern West Ella Lake fault. North of the fold hinge zone, W-E to NW-SE shortening and subvertical to N-S to NW-SE extension is evident at the West and East Moose lake faults, which merge into the Eatlots Lake fault (Fig. 2.8a). Similar to this fault, shortening at the East and West Waddell Lake faults is subvertical and extension ranges in direction from NW-SE to NE-SW. Near the northern termini of the faults shortening clusters in NW-SE directions, whereas extension is either subvertical or directed NE-SW. Despite the overall diversity in principal strain axis orientations observed for the East Range, there seems to be a pronounced change in strain axis orientations at the axial trace of the Wast Bay anticline, which has vital implications on the kinematics of first-order faults discussed next.

2.5.3 Slip vectors of faults

In this section, the significance of local slip vectors based on fault-slip inversion for unravelling the kinematics of first-order faults in the East Range is explored. Depending on the relative proportions of local thrust and normal slip vectors proximal to a given first-order fault, the overall kinematics of this fault can be assessed. Evidently, a number of first-order faults in the East Range, notably the Delta, Bay, Island, East and West Amy Lake, and the East Waddell Lake faults, transect and displace the Main Mass of the SIC (Figs. 2.2b, 2.10). The strike separation of SIC contacts points to a strong component of net sinistral displacement on these faults. In terms of fault-slip vectors, the Delta and Bay faults are characterized by highly variable local slip vectors, which are in agreement with the rather low magnitude of observed strike separation of SIC contacts on these faults (Fig. 2.10b). By contrast, slip vectors of the East and West Amy Lake faults, especially those located at displaced SIC contacts, indicate overall components of sinistral displacement in addition to reverse and normal slip on the faults (Fig. 2.10). The horizontal displacement components correlate well with the pronounced sinistral strike separations of displaced SIC contacts. This correlation corroborates the validity of using local principal strain axes inferred from fault-slip inversions for determining slip vectors and, thus, the kinematics of lower-order faults.

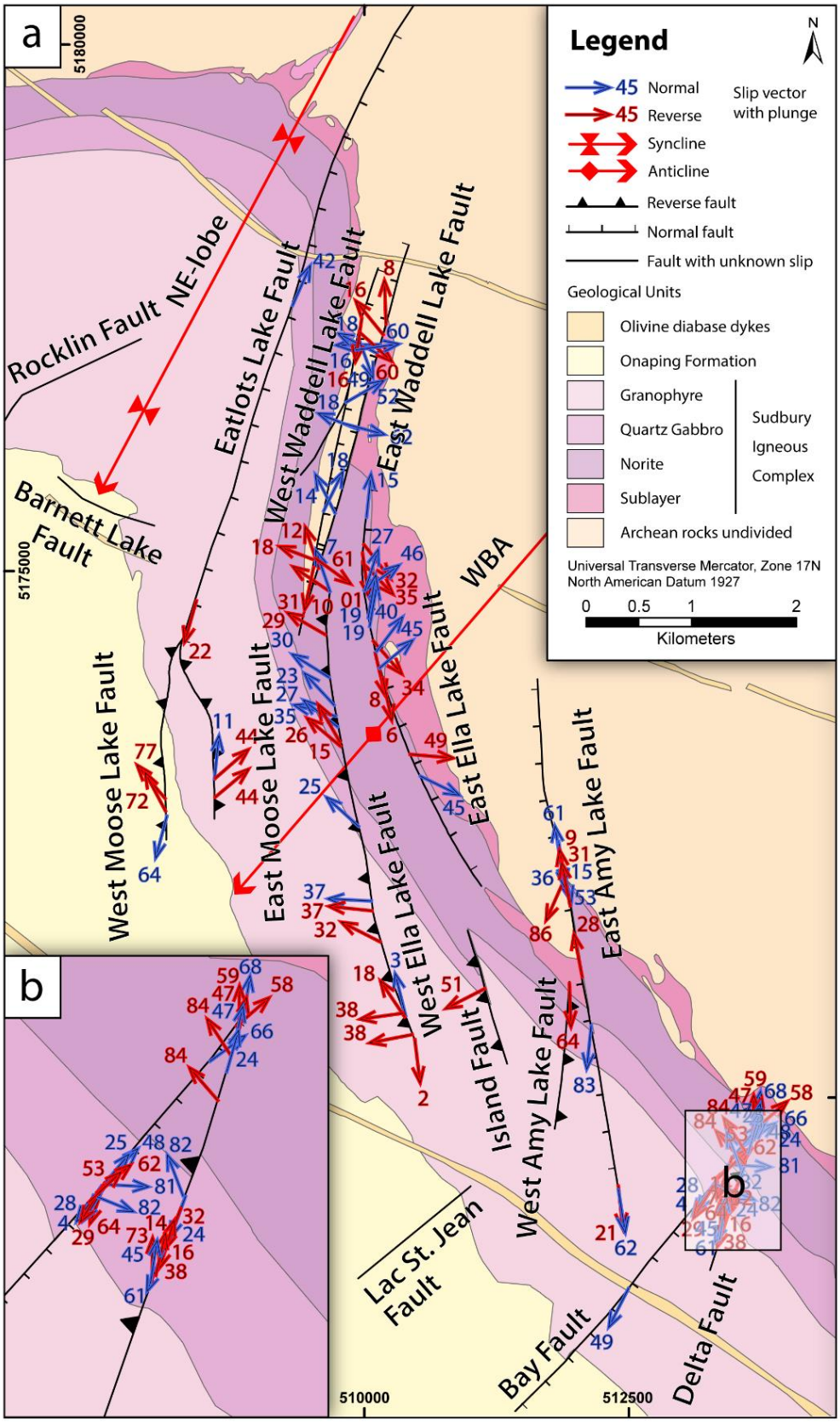

Figure 2.10: Slip vectors on prominent faults in the East Range of the Sudbury Basin. (a) Geological map of the East Range displaying fault types and their respective slip vectors (arrows). Each arrow represents the orientation of a slip vector calculated from the respective fault-slip inversion (Appendix: Figure 2, Table 3). (b) Close-up of area with a high spatial coverage of slip vectors.

Using local slip vectors as a proxy for identifying the kinematics of other prominent faults in the East Range reveals a spatial relationship between fault kinematics and the West Bay Anticline. Clustering of reverse and normal slip vectors along the East and West Ella Lake faults points to variable slip directions along these faults (Fig. 2.10). However, the southern portion of the West Ella Lake fault and the nearby Island fault, which are both located south of the axial trace of the West Bay Anticline, are characterized mostly by thrusting. By contrast, the portions of the West and East Ella Lake faults located north of the axial trace are better described as normal faults, although some stations do indicate reverse faulting. Similarly, the majority of slip vectors on the East and West Waddell Lake fault as well as the Eatlots Lake fault, collectively located north of the axial trace, indicate normal faulting, although some slip vectors on these faults suggest reverse sense-of-slip as well. Reverse faulting becomes also more important where the Eatlots Lake Fault branches into the conjugate West and East Moose Lake faults (Fig. 2.10).

Despite the overall variability of slip vectors on prominent faults in the East Range, there seems to be a systematic variation in fault kinematics with respect to the geometry of the West Bay Anticline. Normal slip vectors cluster particularly on faults north of the axial trace of the anticline, whereas reverse slip vectors are seen dominantly on faults south of the axial trace (Fig. 2.10, Table 2.1). Similar to the local variation in principal strain axes, there appears to be a major change in local slip vectors and, thus, fault kinematics at the axial trace of the West Bay Anticline.

2.6 Interpretation

By relating the fault kinematics to fault geometry, I attempt to shed light on the deformation mechanism by which the Main Mass of the SIC in the East Range acquired its curvature. This pertains to understanding folding mechanisms of initially mechanically isotropic rock units, such as layered magmatic complexes as well as thick sills and dikes. Specifically, it is unknown how the layers of the Main Mass and their underlying crystalline basement rocks, which lack layer-parallel structural anisotropy and, therefore, must be regarded as mechanically isotropic prior to deformation, transformed into a fold structure, the Sudbury Basin (Fig. 2.2).

Application of the G.I.S.-based workflow for fault characterization in the East Range shows that first-order faults have complex geometries (Fig. 2.9) and are associated with large variations in local strain axis orientations and resulting slip directions (Figs. 2.8, 2.10). This is a common characteristic in many terranes affected by brittle deformation (Peacock and Sanderson, 1991; Kim et al., 2004; Philippon et al., 2015). In general, the variability in the geometry and slip on prominent faults can be accounted for by: (1) successive deformation events characterized by the superposition of variable principal strain directions (Kim et al., 2001), (2) Progressive deformation involving a heterogeneous stress field near first-order faults (Homberg et al., 1997; de Joussineau et al., 2003; Twiss and Unruh, 2007), (3) variation of slip and geometry of fault segments along a given fault zone (Kim et al., 2004) or at fault tips (Philippon et al., 2015), (4) local kinematic partitioning of regional strain (Riller et al., 2010; Santimano and Riller, 2012a; Daxberger and Riller, 2015) and (5) progressive rotation of principal strains during a single deformation episode.

Successive deformation events are unlikely to have caused strain axis and slip vector variability as each station is characterized by a single homogeneous set of shear faults (Appendix: Figure 1), which do not feature multiple striations or mineral fibres. By contrast, paleostress heterogeneity is a common phenomenon associated with structural discontinuities and may well have contributed to the observed strain axis and slip vector variability on individual faults, as does the observed variation in fault segment geometry (Fig. 2.9). As strain axis and slip vector variability is larger between, than on individual faults, kinematic partitioning of regional strains on individual faults cannot be excluded either (Santimano and Riller, 2012a). However, none of the above mechanisms accounts for the presence of spatially intermingled horizontal and vertical shortening, amounting respectively to reverse and normal faulting, notably at fault segments north of the West Bay Anticline axial trace (Figs. 2.8, 2.10). In case the observed fault kinematics occurred indeed during a single pulse of progressive deformation, significant rotation must have affected the faults, which is explored next.

The N-striking faults cut the layers of the steeply westward dipping SIC at low angles and mimic the curvature of the SIC around the axial trace of the West Bay Anticline (Figs. 2.2, 2.8). The latter indicates that the faults were folded together with the SIC. Repetition of the SIC and adjacent Archean rocks at the East Waddell Lake and East Amy Lake faults (Fig. 2.2b) points to displacement of these rocks on normal faults dipping at shallower angles toward the West than the SIC in their current position. Back rotation of the normal faults by

about 80°, i.e., until the SIC and the fold axis of the West Bay Anticline become horizontal (Fig. 2.11), transforms the normal faults into SE-dipping thrust faults. The formation of such thrusts is typical for the Sudbury area, e.g., the South Range Shear Zone (Shanks and Schwerdtner, 1991a; Santimano and Riller, 2012b) and elsewhere in the Eastern Penokean Orogen (Riller et al., 1999; Schwerdtner et al., 2005).

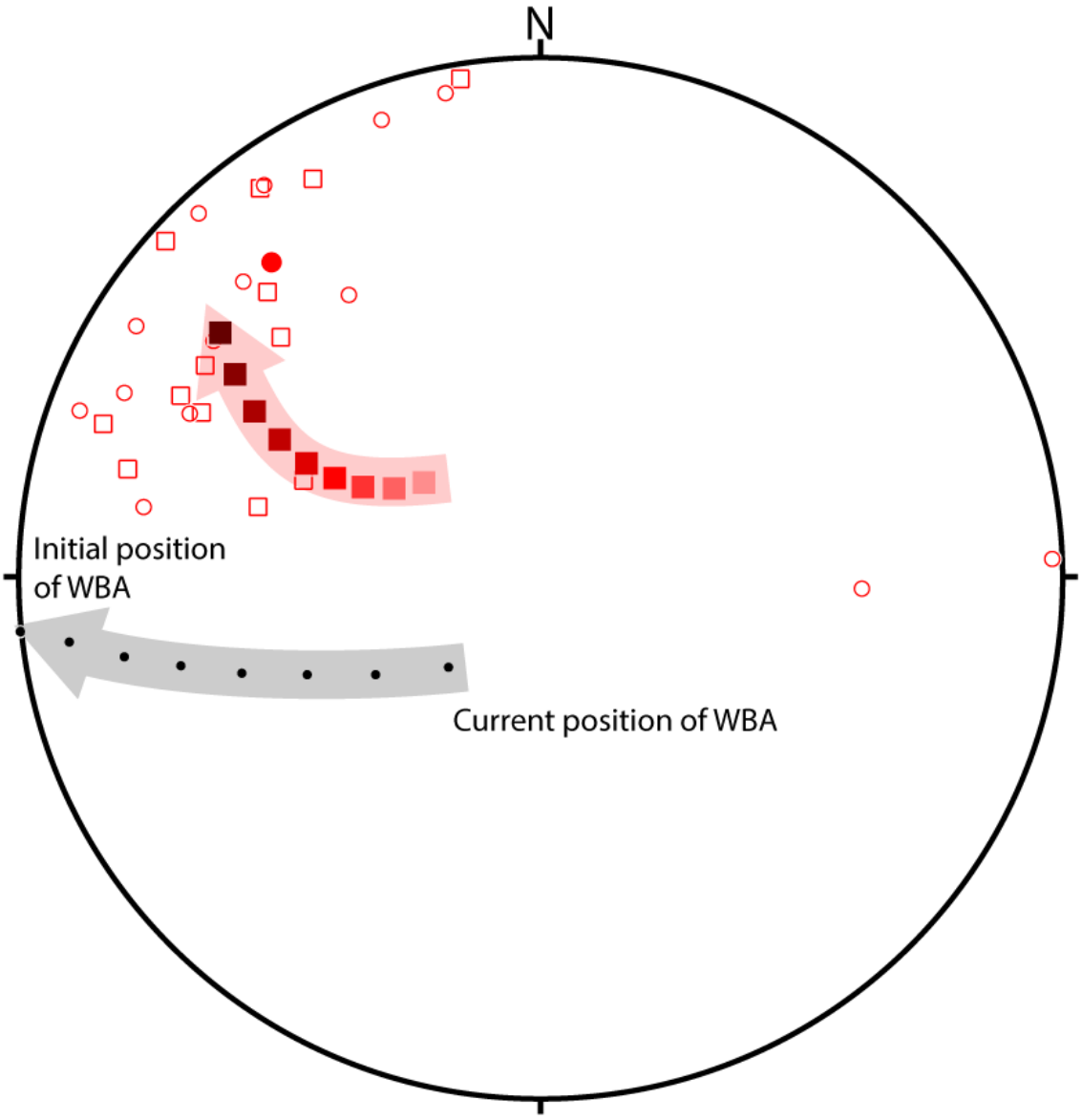

Figure 2.11: Lower-hemisphere equal-area projection displaying back rotation of the West Bay Anticline (WBA) fold axis to the horizontal (grey arrow) in 10° increments and respective back rotated set 2 principal shortening axes associated with the Ella Lake and Waddell Lake faults (squares). Red open circles are set 1 principal axes of shortening with their mean orientation (solid red circle). Red arrow shows progressive back rotation of mean set 2 shortening axis (solid squares) in 10° increments. Note the correspondence in orientation of set 1 and back rotated set 2 shortening axis orientations.

Progressive rotation of principal strain axes during a single deformation episode as cause for the observed variability of axes was tested for axes spatially associated with the Waddell - Ella lakes faults (Fig. 2.8). Inversion of brittle shear faults near these first-order faults resulted in two sets of strain axis configurations; (1) NW- to N-striking horizontal shortening and vertical extension and (2) vertical shortening associated with horizontal extension. Set 1 shortening directions are disposed mostly at small angles to the curved fault traces. Similarly, set 2 extension directions are consistently orthogonal to fault traces and, thus, vary in orientation with position along the curved faults. Set 2 strain axes are in agreement with normal faulting on the fault system in their current position. Applying the same magnitude of back rotation to set 2 principal strain axes transforms set 2 vertical shortening axes into subhorizontal NW-SE shortening axes, i.e., akin to set 1 shortening axes (Fig. 2.11). Thus, both strain axis populations can be attributed to the same progressive deformation characterized by reverse faulting followed by non-cylindrical folding of the Main Mass and prominent faults in the East Range under overall NW-SE shortening.

In summary, our analysis of fault segment geometry, fault-slip inversion and inference of slip vectors leads us to propose the following scenario for the evolution of curved first-order faults: NW-SE shortening led to the formation of multiple SE-dipping reverse fault segments (Fig. 2.12a). The segments coalesced to form coherent first-order thrust or reverse faults (Fig. 2.12b). Continued shortening led to folding of these faults (Fig. 2.12c, d) as the West Bay Anticline formed. Maintaining their overall sense of displacement, the northern fault segments assumed normal fault geometry while continued to be affected by NW-SE shortening. The first-order faults are, therefore, regarded as the planar mechanical anisotropies, which, upon folding, enabled the interfaces of the mechanically isotropic layers of the SIC to acquire their curvature evident in the West Bay Anticline (Clark et al., 2012).

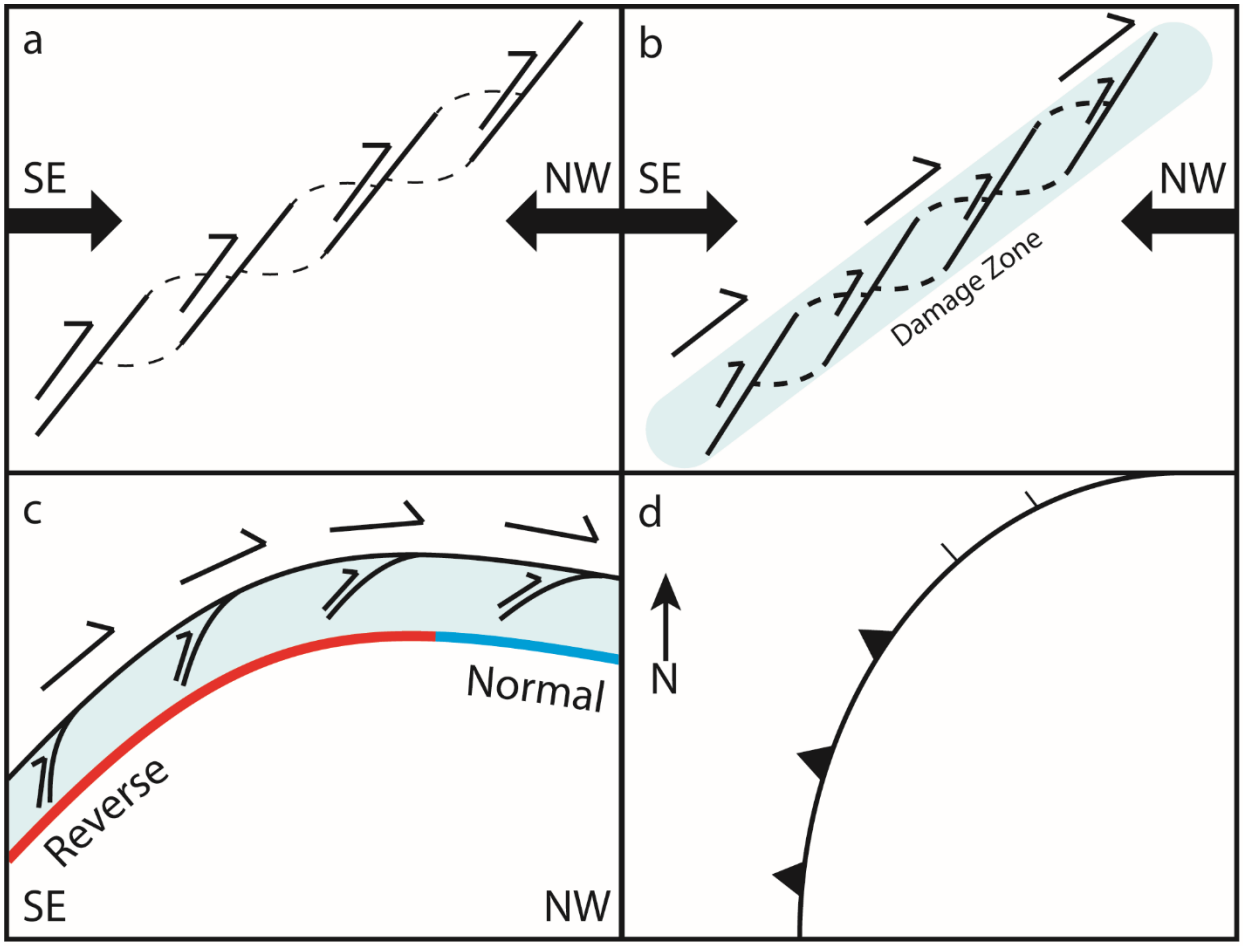

Figure 2.12: Schematic diagram displaying the evolution of first-order fault surfaces under NW-SE shortening indicated by black arrows. (a) Initial orientation of fault segments. (b) Fault segments coalesce to form coherent first-order thrust or reverse fault. (c) Folding of fault generates normal fault segment in the NW. (d) Map view of final fault trace.

2.7 Conclusion

A G.I.S.-based workflow was developed to construct near surface orientations of fault segments from surface fault traces. Application of the workflow for the East Range of the Sudbury Basin shows that fault segments are highly variable in geometry and form complex first-order faults. The fault segment geometries combined with local strain measurements allowed us to assess in detail the variability of kinematics along individual first-order faults. Principal strain axes inferred from the inversion of shear faults were used to construct slip vectors on the first-order faults. Both, strain axis and slip vector orientations are characterized by systematic variations that can be explained by heterogeneous stresses at the faults, variable orientation of fault segments and local partitioning of regional strains. Most importantly, however, progressive deformation involving large rotations of lithological contacts, first-

order faults and principal strain axes can account for the presence of horizontal and vertical shortening amounting respectively to reverse and normal slip vectors at a given fault. I conclude that progressive deformation under regional NW-SE shortening commenced with the formation of first-order faults as SE-dipping thrust faults. Continued shortening led to folding of these faults. While maintaining their overall sense of displacement, the northern fault segments assumed normal fault geometry. The first-order faults are regarded as the planar mechanical anisotropies, which, upon folding, enabled the interfaces of petrographically distinct, but mechanically isotropic, layers of the Main Mass of the SIC to acquire their curvature.

2.9 References

Angelier, J., Goguel, J., 1979. Sur une méthode simple de determination des axes principaux des contraintes pour une population de failles. Les Comptes Rendus de l'Académie des Sciences 288, 307-310.

Angelier, J., Mechler, P., 1977. Sur une méthode graphique de recherche des contraintes principales également utilisable en tectonique et en séismologie: la method des diédres droits. Bulletin de la Societe Geologique de France 7, 1309-1318.

Bailey, J., Lafrance, B., McDonald, A.M., Fedorowich, J.S., Kamo, S., Archibald, D.A., 2004. Mazatzal-Labradorian-age (1.7-1.6 Ga) ductile deformation of the South Range Sudbury impact structure at the Thayer Lindsley mine, Ontario. Canadian Journal of Earth Sciences 41, 1491-1505.

Bartel, E.M., Neubauer, F., Genser, J., Heberer, B., 2014. States of paleostress north and south of the Periadriatic fault: Comparison of the Drau Range and the Friuli Southalpine wedge. Tectonophysics 637, 305-327.

Beaudoin, N., Leprêtre, R., Bellahsen, N., Lacombe, O., Amrouch, K., Callot, J., Emmanuel, L., Daniel, J., 2012. Structural and microstructural evolution of the Rattlesnake Mountain Anticline (Wyoming, USA): New insights into the Sevier and Laramide orogenic stress build-up in the Bighorn Basin. Tectonophysics 576-577, 20-45.

Bennison, G.M., Olver, P.A., Moseley, K.A., 2011. Three-point problems. In: An Introduction to Geological Structures & Maps (8th Edition), Hodder Education, London, 23-27.

Boerner, D.E., Milkereit, B., 1999. Structural evolution of the Sudbury impact structure in the light of seismic reflection data. In Dressler, B.O., and Sharpton, V.L., eds., Large Meteorite Impacts and Planetary Evolution II: Boulder, Colorado, Geological Society of America Special Paper 339, 419-429.

Brocoum, S.J., Dalziel, J.W.D., 1974. The Sudbury Basin, the Southern Province, the Grenville Front, and the Penokean Orogeny. Geological Society of American Bulletin 85, 1571-1580.

Burbank, D.W., McLean, J.K., Bullen, M., Abdrakhmatov, K.Y., Miller, M.M., 1999. Partitioning of intermontane basins by thrust-related folding, Tien Shan, Kyrgyzstan. Basin Research 11, 75-92.

Burbank, D.W., Anderson, R.S., 2011. Tectonic Geomorphology. John Wiley & Sons, West Sussex.

Card, K.D., Gupta, V.K., McGrath, P.H., Grant, F.S., 1984. The Sudbury Structure: Its Regional Geological and Geophysical Setting. *In* Pye, E.G., Naldrett, A.J., and Giblin, P.E., eds., The geology and ore deposits of the Sudbury Structure: Ontario Geological Survey Special Volume 1, 25-43.

Carey, E., Brunier, B., 1974. Analyze théorique et numérique d'un modèle méchanique élémentaire appliqué à l'étude d'une population de failles. Comptes Rendus de l'Academie des Sciences (Paris) 279, 891-894.

Clark, M.D., Riller, U., Morris, W.A., 2012. Upper-crustal, basement-involved folding in the East Range of the Sudbury Basin, Ontario, inferred from paleomagnetic data and spatial analysis of mafic dykes. Canadian Journal of Earth Sciences 49, 1005-1017.

Cowan, E.J., Schwerdtner, W.M., 1994. Fold Origin of the Sudbury Basin. In: Lightfoot, P.C., Naldrett, A. (Eds.), Proceedings of the Sudbury - Noril'sk Symposium. Ontario Geological Survey, Special Volume 5, 45-55.

Cowan, E.J., 1999. Magnetic fabric constraints on the initial geometry of the Sudbury Igneous Complex: a folded sheet or a basin-shaped igneous body? Tectonophysics 307, 135-162.

Cowan, E.J., Riller, U., Schwerdtner, W.M., 1999. Emplacement geometry of the Sudbury Igneous Complex: Structural examination of a proposed impact melt-sheet. In Dressler, B.O., and Sharpton, V.L., eds., Large Meteorite Impacts and Planetary Evolution II: Boulder, Colorado, Geological Society of America Special Paper 339, 399-418.

Dadon, A., Peeters, A., Ben-Dor, E., Karnieli, A., 2011. A Semi-automated GIS model for extracting geological structural information from a spaceborne thematic image. GIScience & Remote Sensing 48, No. 2, 264-279.

Davis, K., Burbank, D.W., Fisher, D., Wallace, S., Nobes, D., 2005. Thrust-fault growth and segment linkage in the active Ostler fault zone, New Zealand. Journal of Structural Geology 27, 1528-1546.

Daxberger, H., Riller U., 2015. Kinematics of Neogene to Recent upper-crustal deformation in the southern Central Andes (23°–28°S) inferred from fault–slip analysis: Evidence for gravitational spreading of the Puna Plateau. Tectonophysics 642, 16-28.

de Joussineau, G., Petit, J.-P., Gauthier, B.D.M., 2003. Photoelastic and numerical investigation of stress distributions around fault models under biaxial compressive loading conditions. Tectonophysics 363, 19–43.

Dreuse, R., Doman, D., Santimano, T., Riller, U., 2010. Crater floor topography and impact melt sheet geometry of the Sudbury impact structure, Canada. Terra Nova 22(6), 463-469.

Dressler, B.O., 1984. General Geology of the Sudbury Area. *In* Pye, E.G., Naldrett, A.J., and Giblin, P.E., eds., The geology and ore deposits of the Sudbury Structure: Ontario Geological Survey Special Volume 1, 57-82.

Everitt, R.A., 1979. Jointing in the Sudbury Basin, Sudbury, Ontario. M.Sc. Thesis, Laurentian University.

Faulkner, D.R., Mitchell, T.M., Healy, D., Heap, M.J., 2006. Slip on 'weak' faults by the rotation of regional stress in the fracture damage zone. Nature 444, 922-925.

Faulkner, D.R., Mitchell, T.M., Jensen, E., Cembrano, J., 2011. Scaling of fault damage zones with displacement and the implications for fault growth processes. Journal of Geophysical Research 116, B5, B05403.

Fry, N., 1992. Stress ratio determinations from striated faults: a spherical plot for cases of near-vertical principal stress. Journal of Structural Geology 10, 1121-1131.

Gapais, D., Cobbold, P.R., Bourgeois, O., Rouby, D., de Urreiztieta, M., 2000. Tectonic significance of fault-slip data. Journal of Structural Geology 22, 881-888.

García-Sellés, D., Falivene, O., Arbués, P., Gratacos, O., Tavani, S., Muños, J.A., 2011. Supervised identification and reconstruction of near-planar geological surfaces from terrestrial laser scanning. Computers and Geosciences 37, 1584-1594.

Grieve, R.A.F., Stöffler, D., Deutsch, A., 1991. The Sudbury Structure – controversial or misunderstood. Journal of Geophysical Research 96, 22753-22764.

Homberg, C., Hu, J. C., Angelier, J., Bergerat, F., Lacombe, O., 1997. Characterization of stress perturbations near major fault zones: Insights from 2-D distinct-element numerical modelling and field studies (Jura Mountains). Journal of Structural Geology 19, 703–718.

Keays, R.R., Lightfoot, P.C., 2004. Formation of Ni-Cu-Platinum group element sulfide mineralization in the Sudbury impact melt sheet. Mineralogy and Petrology 82, 217–258.

Kim, Y.S., Andrews, J.R., Sanderson, D.J., 2001. Reactivated strike-slip faults: examples from north Cornwall, UK. Tectonophysics 340, 173-194.

Kim, Y.S., Peacock, D.C.P., Sanderson, D.J., 2004. Fault damage zones. Journal of Structural Geology 26, 503-517.

Klimczak, C., Wittek, A., Doman, D., Riller, U., 2007. Fold origin of the NE-lobe of the Sudbury Basin, Canada: Evidence from heterogenous fabric development in the Onaping Formation and the Sudbury Igneous Complex. Journal of Structural Geology 29, 1744-1756.

Krogh, T.E., Davis, D.W., Corfu, F., 1984. Precise U-Pb zircon and baddeleyite ages for the Sudbury area. *In* Pye, E.G., Naldrett, A.J., and Giblin, P.E., eds., The geology and ore deposits of the Sudbury Structure: Ontario Geological Survey Special Volume 1, 431-448.

Lenauer, I., Riller, U., 2012a. Strain fabric evolution within and near deformed igneous sheets: The Sudbury Igneous Complex, Canada. Tectonophysics 558-559, 45-57.

Lenauer, I., Riller, U., 2012b. Geometric consequences of ductile fabric development from brittle shear faults in mafic melt sheets: Evidence from the Sudbury Igneous Complex, Canada. Journal of Structural Geology 35, 40-50.

Lightfoot, P.C., Doherty, W., Farrell, K.P., Keays, R.R., Pekeski, D., Moore, M., 1997a. Geochemistry of the main mass, sublayer, offsets, and inclusions from the Sudbury Igneous Complex, Ontario. Mineral Deposit Study: Ontario Geological Survey Open File Report 5959.

Lightfoot, P.C., Keays, R.R., Morrison, G.G., Bite, A., Farrell, K., 1997b. Geochemical relationships in the Sudbury Igneous Complex: Origin of the main mass and offset dikes. Economic Geology 92, 289-307.

Lightfoot, P.C., Keays, R.R., Morrison, G.G., Bite, A., Farrell, K., 1997c. Geologic and geochemical relationships between the contact sublayer, inclusions, and the main mass of the Sudbury Igneous Complex : A case study of the Whistle mine embayment. Economic Geology 92, 647-673.

Lisle, R.J., 1998. Simple graphical constructions for the direction of shear. Journal of Structural Geology 20, 969-973.

Martínez-Díaz, J.J., 2002. Stress field variation related to fault interaction in a reverse oblique-slip fault: the Alhama de Murcia fault, Betic Cordillera, Spain. Tectonophysics 356, 291-305.

Milkereit, B., Green, A., 1992. Deep geometry of the Sudbury structure from seismic reflection profiling. Geology 20, 807-811.

Naldrett, A.J., Hewins, R.H., 1984. The main mass of the Sudbury Igneous Complex. Ontario Geological Survey Special Volume 1, 235-251.

Nemcok, M., Lisle, R.J., 1995. A stress inversion procedure for polyphase fault/slip data sets. Journal of Structural Geology 17, 1445-1453.

Ortner, H., Reiter, F., Acs, P., 2002. Easy handling of tectonic data: The programs Tectonics VB for Mac and Tectonics FP for Windows™. Computers & Geosciences 28, 1193-1200.

Pattison, E.F. 1979. The Sudbury Sublayer. Canadian Mineralogist 17: 257-274.

Peacock, D.C.P., Sanderson, D.J., 1991. Displacements, segment linkage and relay ramps in normal fault zones. Journal of Structural Geology 13, 721-733.

Philippon, M., Willingshofer, E., Sokoutis, D., Corti, G., Sani, F., Bonini, M., Cloetingh, S., 2015. Slip re-orientation in oblique rifts. Geology 43, 147-150.

Pollard, D.D., Saltzer, S.D., Rubin, A.M., 1993. Stress inversion methods: are they based on faulty assumptions? Journal of Structural Geology 15, 1045-1054.

Riller, U., Schwerdtner, W.M., Halls, H.C., Card, K.D., 1999. Transpressive tectonism in the eastern Penokean orogen, Canada: Consequences for Proterozoic crustal kinematics and continental fragmentation. Precambrian Research 93, 51-70.

Riller, U., 2005. Structural characteristics of the Sudbury impact structure, Canada: Impact-induced versus orogenic deformation – A review. Meteoritics & Planetary Science 40, 1723-1740.

Riller, U., Boutelier, D., Schrank, C., Cruden, A.R., 2010. Role of kilometer-scale weak circular heterogeneities on upper crustal deformation patterns: Evidence from scaled analogue modeling and the Sudbury Basin, Canada. Earth and Planetary Science Letters 297, 587-597.

Rousell, D.H., 1975. Origin of foliation and lineation in Onaping Formation and the deformation of the Sudbury Basin. Canadian Journal of Earth Sciences 12(8), 1379-1395.

Saleeby, J., Foster, Z., 2004. Topographic response to mantle lithosphere removal in the southern Sierra Nevada region, California. Geology 32, 245-248.

Santimano, T., Riller, U., 2012a. Kinematics of Tertiary to Quaternary intracontinental deformation of upper crust in the Eastern Cordillera, southern Central Andes, NW Argentina. Tectonics 31(4), 1-15.

Santimano, T., Riller, U., 2012b. Revisiting thrusting, reverse faulting and transpression in the southern Sudbury Basin, Ontario. Precambrian Research 200-203, 74-81.

Schlische, R.W., Young, S.S., Ackermann, R.V., Gupta, A., 1996. Geometry and scaling relations of a population of very small rift-related normal faults. Geology 24, 683-686.

Scholz, C.H., 1990. The Mechanics of Earthquakes and Faulting (2nd Ed). Cambridge University Press, Cambridge.

Schwerdtner, W.M., 1998. Graphic derivation of the local sense of shear strain components in stretched walls of lithotectonic boundaries. Journal of Structural Geology 20, 957-967.

Schwerdtner, W.M., Riller, U.P., Borowik, A., 2005. Structural testing of tectonic hypotheses by field-based analysis of distributed tangential shear: examples from major high-strain zones in the Grenville Province and other parts of the southern Canadian Shield. Canadian Journal of Earth Sciences 42, 1927-1947.

Shan, Y., Lin, G., Li, Z., Zhao, C., 2006. Influence of measurement errors on stress estimated from single-phase fault/slip data. Journal of Structural Geology 28, 943-951.

Shanks, W.S., Schwerdtner, W.M., 1991a. Structural analysis of the central and southwestern Sudbury Structure, Southern Province, Canadian Shield. Canadian Journal of Earth Sciences 28, 411-430.

Shanks, W.S., Schwerdtner, W.M., 1991b. Crude quantitative estimates of the original northwest-southeast dimension of the Sudbury Structure, south-central Canadian Shield. Canadian Journal of Earth Sciences 28, 1677-1686.

Shipton, Z.K., Cowie, P.A., 2001. Damage zone and slip-surface evolution over μm to km scales in high-porosity Navajo sandstone, Utah. Journal of Structural Geology 23, 1825-1844.

Spang, J.H., 1972. Numerical method for dynamic analysis of calcite twin lamellae. Geological Society of America Bulletin 83, 467-472.

Sperner, B., Ratschbacher, L., Nemčok, M., 2002. Interplay between subduction retreat and lateral extrusion: Tectonics of the Western Carpathians. Tectonics 21(6), 1-24.

Sperner, B., Zweigel, P., 2010. A plea for more caution in fault-slip analysis. Tectonophysics 482, 29-41.

Turner, F.J., 1953. Nature and dynamic interpretation of deformation lamellae in calcite of three marbles. American Journal of Science 251, 276-298.

Twiss, R.J., Unruh, J.R., 1998. Analysis of fault slip inversion: Do they constrain stress or strain rate? Journal of Geophysical Research 103, 12205-12222.

Twiss, R.J., Unruh, J.R., 2007. Structure, deformation, and strength of the Loma Prieta fault, northern California, USA, as inferred from the 1989-1990 Loma Prieta aftershock sequence. Geological Society of America Bulletin 119, 1079-1106.

Van Noten, K., Claes, H., Soete, J., Foubert, A., Özkul, M., Swennen, R., 2013. Fracture networks and strike-slip deformation along reactivated normal faults in Quaternary travertine deposits, Denizli Basin, western Turkey. Tectonophysics 588, 154-170.

Wallbrecher, E., 1986. Tektonische und gefügeanalytische Arbeitsweisen. Enke-Verlag, Stuttgart.

Ziesch, J., Aruffo, C.M., Tanner, D.C., Beilecke, T., Dance, T., Henk, A., Weber, B., Tenthorey, E., Lippmann, A., Krawczyk, C.M., 2015. Geological structure and kinematics of

normal faults in the Otway Basin, Australia, based on quantitative analysis of 3-D seismic reflection data. Basin Research, 1-20.

3.0 Forward modeling and 3-D kinematic restoration of igneous rocks from the East Range of the Sudbury Basin, Canada

3.1 Abstract

Conducting kinematic restorations of deformed igneous terranes in the upper crust have been rarely attempted due to the (1) non-planarity of lithologies, (2) often poorly constrained fault kinematics, and (3) overall lack of geometrical constraints for lithologies and structures at depth. Because of a vast array of drill holes, the Sudbury Basin in Ontario, Canada, is constrained with respect to points (1) and (3) above. The tectonic evolution in the eastern portion of the Sudbury Basin, referred to as the East Range, is still unknown and only now being addressed with recent advances in the characterization of local folding and faulting. Here, I use the known subsurface geometry of the Sudbury Igneous Complex (SIC) and faults extracted from drill core to attempt a restoration of the East Range to its pre-deformational geometry. Through forward modeling I identify rotation magnitudes of a prominent local kilometer-scale fold, the West Bay Anticline, and of a newly defined tilt axis. I combine a 3-D model of the faults and lithological boundaries of the SIC with fault kinematics calculated from the inversion of brittle structures at surface, and rotation magnitudes about the fold axis of the West Bay Anticline to kinematically restore the SIC using both simple shear and flexural slip restoration algorithms. I show that restorations accomplished by both algorithms highlight the importance of slip on faults in facilitating folding of the igneous rock units of the SIC. Moreover, I provide the magnitude of shortening between pre- and post- deformation for two members of the SIC; the Granophyre and Quartz Gabbro. These results highlight not only flexural slip as the most likely deformation mechanism for the East Range but also show the presence of local thickening of the SIC interpreted as a primary embayment to the initial geometry of the SIC.

3.2 Introduction

3-D kinematic restorations are powerful tools to understand the geometrical evolution of deformed geological terranes (e.g. Rouby et al., 2002; Moretti et al., 2006; Ziesch et al., 2015; Li et al., 2016). More often than not, restorations rely on geophysical observations, such as seismic data, validated by a finite number of control drill holes to constrain the

geometry of deformed lithologies. In some geological environments, seismic data can provide a high quality dataset for model creation and subsequent 3-D restoration, however, this methodology is significantly limited when there are no, or poorly identifiable reflections in seismic profiles, or when there is a poor control on imaged lithologies between control drill holes. These limitations are particularly evident in igneous complexes and igneous-dominated terranes. Igneous rocks, unlike sedimentary ones, often have complex geometries even before deformation occurs. Unfortunately, these geometries are poorly constrained using seismic imagery, due to the lack of reflections at igneous lithological contacts. Therefore, deriving the 3-D geometry of deformed igneous rocks requires harnessing other data sources. The Sudbury Basin in Ontario, Canada is a product of tectonic deformation with a plethora of research into the geometry of its defining lithological suite, the Sudbury Igneous Complex (SIC) (Fig. 3.1a; Brocoum and Dalziel, 1974). Due to the extensive collection of drill core from exploration and mining activities and a long history of research, the geometry of the SIC is broadly constrained to a depth of about 1.5 kilometers, and locally constrained to depths of up to 3km. This geometry of the SIC allows for an attempt at kinematically restoring large portions of the Sudbury Basin.

Kinematically restoring the Sudbury Basin offers the opportunity to address longstanding questions about the structural history of this fold basin. The pre-folding geometry of the units which compose the SIC has never been constrained. The currently accepted theory is that the SIC was a ponded impact melt sheet, which differentiated into horizontal layers, known from top to bottom as the Granophyre, Quartz Gabbro, Norite, and Sublayer (Bowen, 1915; Grieve et al., 1991). In this model, the planarity of contacts both within the melt sheet and between the melt sheet and underlying country rocks is an issue as there is evidence for the presence of embayment geometries along the base of the melt sheet in its present and pre-deformation states (e.g. Clark et al., 2012; Dreuse et al., 2010). Primary SIC embayments, however, have never been quantitatively proven through a restoration to their pre-deformation geometry. This is an important issue for mineral exploration at Sudbury, as pre-deformation embayments have been suggested to correlate with areas of increased melt sheet thickness and associated generation of Cu-Ni-PGE ore deposits (Keays and Lightfoot, 2004).

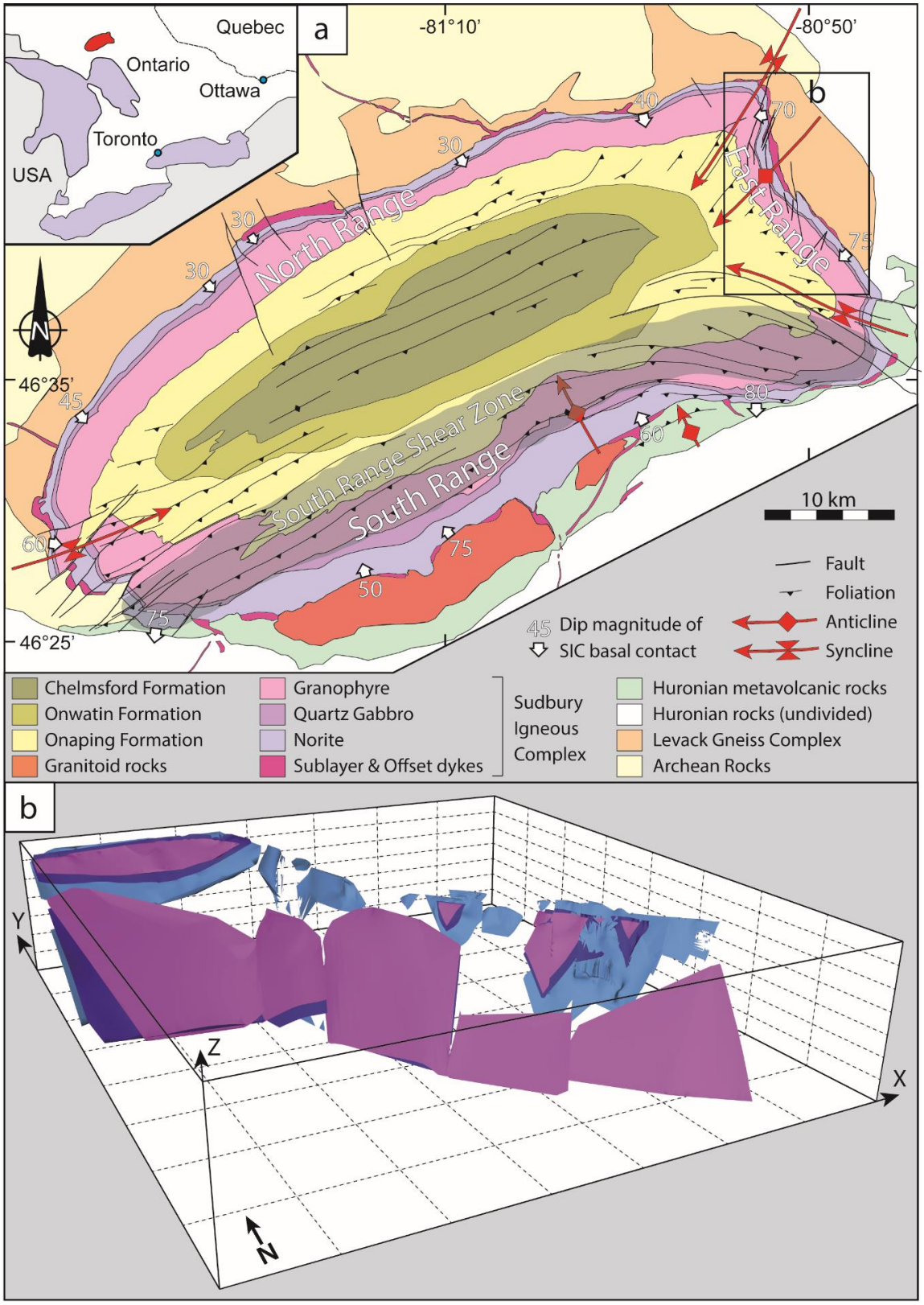

Figure 3.1: Map showing simplified geology of the Sudbury Basin in Ontario, Canada. (a) Major lithological units defining the Sudbury Basin. Prominent faults (black lines), foliation trajectories (black lines with barbs), fold-axial traces (red arrows) and dips of the basal contact of the Norite (white arrows with numbers) delineate the structure of the Sudbury Basin. (b) 3-D model of the East Range showing the basal contacts of the SIC layers, namely the Granophyre (pink), the Quartz Gabbro (purple), and the Felsic Norite (blue).

In addition to issues with constraining the pre-deformed melt sheet geometry, the path by which the SIC deformed into its current non-cylindrical basin geometry is not fully understood. The Sudbury Basin has three morphological ranges; the South Range, the North Range, and the East Range, each with notably different geometries (Fig. 3.1a). In comparison to the other ranges, the SIC in the East Range dips towards the center of the basin at a notably steep angle, and has a unique inward curvature with a much shorter length in plan view than the other ranges (Fig. 3.1a). The mechanism by which the SIC in the East Range attained its curvature has recently been proposed to be accomplished by folding using prominent faults as slip surfaces, but this remains to be verified (Clark and Riller, 2016). Moreover at surface, the principal shortening orientations inferred from the inversion of mesoscopic brittle shear faults are well known, but the magnitude of shortening has not been constrained (Riller et al., 1999; Clark and Riller, 2016). Due to the availability of an extensive industry-collected drill-core database and building on the foundation of an industry 3-D model, here I show the first 3-D kinematic restoration of deformed igneous rocks, in an attempt to answer longstanding questions surrounding the initial geometry and structural evolution of the East Range of the Sudbury Basin.

3.3 Geological Background

The Sudbury Basin is characterized by a broadly elliptical outline at surface which measures 65 km x 25 km (Fig. 3.1a). The Basin straddles the interface between the igneous and high-grade metamorphic Archean rocks of the Levack Gneiss Complex (Krogh et al., 1984) to the north, and the metasedimentary and metavolcanic rocks of the Paleoproterozoic Huronian Supergroup to the south (Fig. 3.1a). The Basin contains top to bottom, a central sedimentary sequence called the Whitewater Group composed of the Chelmsford Formation and Onwatin Formation, underlain by the Onaping Formation, a brecciated igneous unit related to the emplacement of the SIC (Fig. 3.1a; Avermann and Brockmeyer, 1992). The Basin itself is defined by the Main Mass of the Sudbury Igneous Complex (SIC) which is composed of the Granophyre, the Quartz Gabbro, and the Norite (Naldrett and Hewins, 1984). Zones of enhanced thickness of the Main Mass, the layered portion of the SIC, correspond spatially to local accumulations of ore-bearing and footwall inclusion-bearing Norite, known as the

Sublayer, in places forming embayments in Archean and Paleoproterozoic host rocks (Fig. 3.1a; Keays and Lightfoot, 2004; Dreuse et al., 2010).

Contact orientations of the SIC vary greatly among the ranges. In the North Range and the East Range, contacts dip respectively at 30° to 40° and at ~70° towards the basin center. In the South Range contacts dip either 50° to 70° towards, or 80° away from, the basin center (Rousell, 1975; Dreuse et al., 2010). The surface length of the SIC in each range is not uniform, whereby the East Range contains the shortest proportion of the SIC (Fig. 3.1a). The ranges are separated by three second-order synclines; the NE-lobe, the SE-lobe, and the western closure of the SIC (Fig. 3.1a). Between these synclines, the SIC forms anticlines, which, similar to the synclines, are disposed radially with respect to the center of the basin (Lenauer and Riller, 2012a). The most prominent of these anticlines is the SW-plunging West Bay Anticline in the East Range (Clark et al., 2012), evident at surface from the pronounced inward curvature of the SIC (Fig. 3.1a, b).

A set of prominent, crudely N-S striking faults in the East Range, i.e., the Eatlots Lake fault, the East and West Waddell Lake faults, the East and West Ella Lake faults and the East and West Amy Lake faults, are spatially associated with the West Bay Anticline (Fig. 3.1a). The traces of these faults mimic the curvature of the Main Mass at surface (Fig. 3.1a). Based on the notable displacement of the Main Mass along the East Waddell Lake and East Amy Lake faults, these faults at surface show left-lateral slip (Fig. 3.1a). These faults are characterized kinematically by normal slip north of the intersection with the West Bay Anticline and reverse slip to the south of the West Bay Anticline, which can be accounted for by folding of these faults following an initial phase of faulting (Clark and Riller, 2016).

The SIC acquired its synformal geometry most likely during the 1.7-1.6 Ga Mazatzal Orogeny (Bailey et al., 2004) and to some extent during the 1.2-1.0 Ga Grenville Orogeny (Card et al., 1984; Tschirhart and Morris, 2012). The tectonic foliation imparted into post-impact rocks of the Whitewater Group, the Onaping Formation, and large parts of the SIC (Brocoum and Dalziel 1974; Rousell 1975; Everitt 1979), notably the fanning in the eastern part of the Basin and the axial-planar character in the NE- and SE-lobes (Fig. 3.1a), attests to folding strain in these units. Folding strain is also evident further into the Levack Gneiss Complex, associated with the strike variation of 2.45 Ga Matachewan dykes across the East Range (Ernst and Halls 1984; Heaman, 1997; Phinney and Halls, 2001; Clark et al., 2012).

The South Range Shear Zone (Fig. 3.1a), a prominent ductile deformation zone characterized by NW-directed thrusting and transpressive deformation, transects the southern Sudbury Basin (Shanks and Schwerdtner, 1991a, b; Milkereit and Green, 1992; Boerner and Milkereit, 1999; Cowan and Schwerdtner, 1994; Cowan et al., 1999; Riller et al., 2010). Rotation of rocks affected by the shear zone accounts for the variable contact dips of the South Range SIC (Lenauer and Riller, 2012b; Santimano and Riller, 2012a).

3.4 Methodology

Our kinematic restorations are performed using the software Move v.2016.2 from Midland Valley. This software allows restorations to be performed by unfolding, and by restoring displacements on faults. As documented by Clark and Riller (2016), prominent curved faults in the East Range formed prior to folding. Therefore, the kinematic restoration must be conducted by first unfolding the SIC contacts and faults, and second by restoring displacements on faults. To define the particular unfolding algorithm, Move can facilitate unfolding by either vertical shear/simple shear, or flexural slip algorithms. I opted to perform restorations using both the simple shear and the flexural slip algorithms to be able to assess and compare the results from both.

Performing an accurate kinematic restoration to restore the SIC to its pre-deformed geometry requires a strong understanding of the current 3-D geometry of the SIC, as well as careful attention to defining the appropriate restoration parameters. The 3-D model used for the restoration is well constrained by surface mapping and diamond drill hole data on Vale property, and includes surfaces for the Granophyre, the Quartz Gabbro and the Felsic Norite layers (Fig. 3.1b). The 3-D model was imported into Move as a point dataset and interpolated into the surfaces presented here. The surfaces are not continuous, in areas cut by faults that are poorly constrained and therefore not shown, and in other areas discontinuous due to property boundaries of other mining companies. The clipping of surfaces due to property boundaries is particularly evident in the Felsic Norite at its NE extent where the modelled surfaces occur in small discontinuous patches (Fig. 3.1b). Each of the surfaces in this 3-D model are considered to have been isopotential when they solidified making them appropriate to be kinematically restored. The geometry of associated units such as the Sublayer are much more irregular, exhibited by their surface geometry and distribution (Fig.

3.1a). Therefore due to these irregularities the Sublayer was not considered for the restoration.

Defining restoration parameters to apply to the model, specifically, (1) defining the particular restoration algorithm to employ, (2) setting the parameters associated with that specific restoration algorithm, and (3) defining the target orientations for the kinematic restoration are of the highest importance to ensure its successful application. Simple shear and flexural slip algorithms have unique parameters which must be carefully specified. Parameters associated to the simple shear algorithm include defining: the target geometry to unfold to, and the unfolding direction (shear direction). The parameters of the flexural slip algorithm include defining; the target geometry to unfold to, the objects to be unfolded, the pin plane, the fold-axial plane, the unfolding plane, and the profile plane. To kinematically restore the East Range, displacements of the SIC along the prominent curved faults, such as the East and West Ella Lake faults and the East and West Amy Lake faults and the effect of folding by the West Bay Anticline, must be accounted for. Defining the target geometry to unfold to is a primary consideration, as folding about the steeply inclined fold axis of the West Bay Anticline cannot explain how the East Range SIC acquired its steep dip, but explains only the inward curvature visible in plan view (Fig. 3.1a, b). Therefore, in addition to rotation about the fold axis of the West Bay Anticline, the West Bay Anticline itself, folded lithologies of the SIC, and Archean country rocks, have all been tilted around an associated tilt axis, which remains unconstrained. To remedy this unconstrained variable along with the constraining the target geometry for the kinematic restoration, forward modeling of the orientation of the SIC when it was emplaced at 1.85 Ga to its current orientation was conducted.

Forward modeling aims to model the progressive rotation of the SIC in the East Range and the progressive tilting of the fold axis of the West Bay Anticline. Assumptions of the forward model include: the melt sheet was characterized by initially isopotential, i.e. horizontal, layers, and the fold axis of the West Bay Anticline was initially horizontal trending and oriented orthogonally to regional NW-SE directed shortening (Riller et al., 1999). Since the contacts of the Granophyre, Quartz Gabbro, and Felsic Norite formed prior to any significant geometric modification of the SIC, the rotation of a single horizontal sheet is sufficient to represent each of these layers. The orientation of the West Bay Anticline was approximated by 8 increments of fold axis orientations (Fig. 3.2a, b), ranging from its initial horizontal orientation to its present orientation at 225/70 (Clark et al., 2012). The orientations of the fold axis of the West Bay Anticline are tilted around an axis oriented at

330/05, defined as the pole to the migration path for West Bay Anticline increments, collectively defining a great circle in Figure 3.2b. Rotation magnitudes applied to each fold limb around the fold axis of the West Bay Anticline were varied between 20-30° in a clockwise sense to the northern limb and 20-30° in a counter clock wise sense to the southern limb. These rotation magnitudes were inferred from the strike variation of Matachewan dykes in the East Range (Clark et al., 2012). For each forward model iteration, the discrepancy between the modelled limb orientations and the actual orientation of SIC segments are compared to ensure a best estimate.

Constraining the target geometries of the north and south fold limbs, the orientation of the fold axis of the West Bay Anticline, and the secondary tilt axis for each iteration of folding defines the orientation of the two remaining required parameters for the kinematic restoration: the fold-axial plane, and the profile plane. The orientation of the fold-axial plane is taken to be the bisector plane of the fold, as thickness ratios of displaced layers cannot be calculated (Groshong, 2006). The thicknesses of the folded medium do not apply here as the "layered" SIC and its underlying host rocks are mechanically isotropic. Therefore mechanically, the boundary of one layer to an adjacent layer is constrained by faulting. Once the orientation of the fold-axial plane is constrained, the profile plane can be calculated.

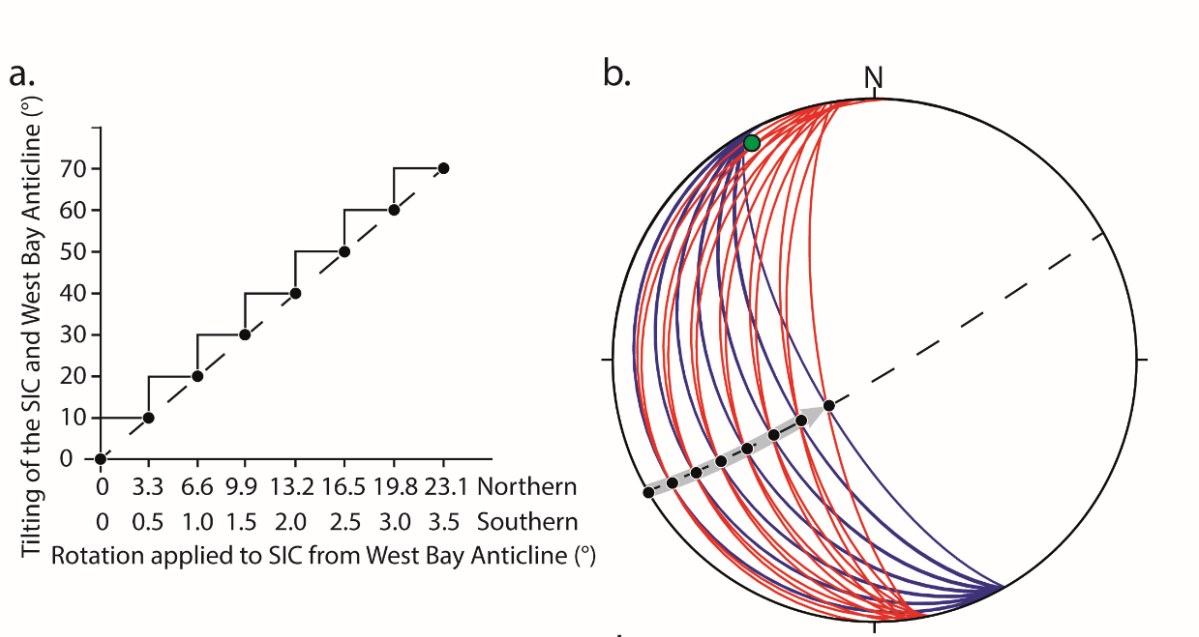

c.

Timeline	Fold and tilt axes orientations	Calculated SIC segments
Present day	FA: 225/70 TA: 330/05	N: 260.7/72.8 S: 240.2/70
	FA: 230.5/60.3 TA: 330/05	N: 259.5/62.8 S: 240.6/60
	FA: 233.4/50.4 TA: 330/05	N: 258.6/52.5 S: 240.9/50
	FA: 235.2/40.5 TA: 330/05	N: 258.1/42.1 S: 241.3/40
	FA: 236.6/30.5 TA: 330/05	N: 257.8/31.6 S: 241.7/30
	FA: 237.7/20.6 TA: 330/05	N: 257.7/21.1 S: 242/20
	FA: 238.7/10.6 TA: 330/05	N: 257.9/10.5 S: 242.4/10
Onset of folding	FA: 239.6/00 TA: 330/05	N: 270/00 S: 270/00

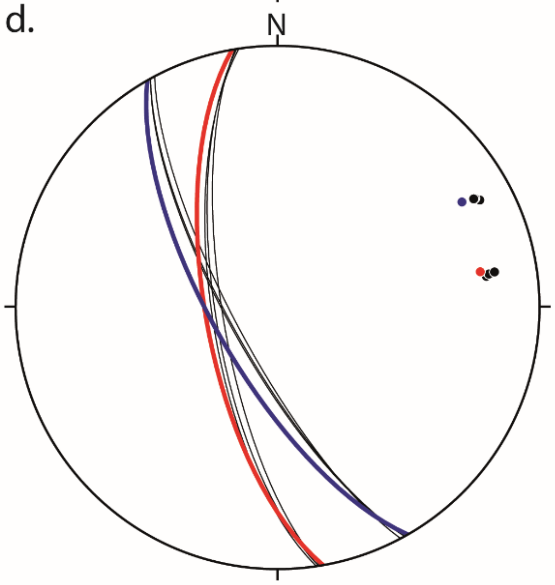

Figure 3.2: Forward modeling of the basal contacts of the SIC. (a) Graphical representation of the magnitude of the rotation component about the West Bay Anticline and the tilt component applied to the basal contacts of the SIC. The straight dashed line displays the hypothetical progressive rotation of the SIC and the country rocks of the East Range. The stepped line displays the rotations applied in the forward modeling of the SIC basal contact to the northern and southern SIC fold limbs respectively. The two labels of the X-axis correspond to the rotations applied to the northern and southern SIC segments. (b) Lower-hemisphere equal-area projection showing the effect of rotation applied about the fold axis of the West Bay Anticline and the tilt axis in (a). The tilt axis (green point) and its associated rotation path (dashed line) shows the rotation trajectory applied to the West Bay Anticline and the SIC's northern and southern fold limbs. The grey arrow displays the path of the West Bay Anticline from an initially horizontal fold axis to its current orientation at 225/70. (c) Table displaying the orientation of fold and tilt axes, as well as the orientation of modelled SIC segments for each step. The orientations of the northern and southern SIC basal contacts in red and blue respectively, correlate to the similarly coloured great circles in (d). (d) Comparison of the forward modelled northern and southern SIC basal contacts as great circles in red and blue respectively, to the current orientation of basal SIC contacts of the Granophyre, Quartz Gabbro, and Felsic Norite as great circles in black. The points are the poles to these surfaces.

3.5 Results

3.5.1 Forward modeling to derive folding and tilting axes and rotation magnitudes associated to the evolution of basal SIC contacts and prominent faults

Forward modeling of the SIC basal contacts is conducted with the goal of yielding the closest fit between the forward modelled and the current orientation of SIC layers derived from the industry 3-D model based on surface mapping and industry drill hole data. The most accurate forward model (Fig. 3.2) was accomplished by performing a clockwise rotation to the northern and southern SIC fold limb of 23.1° and 3.5° respectively about the fold axis of the West Bay Anticline with 70° clockwise rotation about the newly calculated tilt axis oriented at 330/05 (Fig. 3.2b, d). The migration path of the fold axis of the West Bay Anticline was approximated as the most direct path between the current orientation of the fold axis (Clark et al., 2012) and the assumed starting orientation at the onset of deformation. The tilt axis was constrained by fitting a great circle to the migration path of the fold axis of the West Bay Anticline, and recording its pole. Incremental clockwise rotations of 3.3° and 0.5° were performed to the northern and southern limbs about the fold axis of the West Bay Anticline respectively in combination with a 10° rotation about the tilt axis. Together these incremental rotations attempt to model the progressive deformation of the SIC and of the West Bay Anticline (Fig. 3.2a). To check the accuracy of the forward model, the angular departure between the forward modelled orientation of the SIC contacts and the current orientation of SIC contacts is measured using their poles (Fig. 3.2d). The measurement of the angular departure yielded a discrepancy of 2.2° for the northern fold limb and 4.6° for the southern fold limb, and is therefore considered to be the best estimate to constrain the orientation of the target SIC in the kinematic restoration (Fig. 3.2d).

3.5.2 3-D kinematic restoration applying the simple shear algorithm

Two kinematic restorations were accomplished using the simple shear algorithm. One attempts to bring the Granophyre to a horizontal target orientation (Fig. 3.3a, b), and the other attempts to bring the Quartz Gabbro to a horizontal target orientation (Fig. 3.3c, d). Both used an unfolding direction oriented at 045/20 with an up dip shear direction, which is calculated as the normal to the West Bay Anticline (oriented at 225/70). This stage of simple shearing on the kinematic restoration can be described by the magnitude of shear strain, whereby it is calculated by $\gamma = \tan \psi$ where γ is the shear strain and ψ is the angle of rotation.

The resulting magnitude of shear strain associated with the simple shear restoration of the Granophyre and of the Quartz Gabbro is 0.4 and 0.1 for the northern and southern SIC limbs respectively. Subsequently, a second simple shear restoration was performed to the restoration of both the Granophyre and the Quartz Gabbro, whereby each used an unfolding direction oriented at 150/85 with an up dip shear direction. This unfolding direction is oriented normal to the tilt axis (oriented at 330/05) in order to bring the restored layer to the horizontal, i.e., its theoretical orientation prior to deformation (Fig. 3.3). The magnitude of shear strain associated with the removal of the tilt component is 2.7.

From these restorations it is apparent that regardless of whether the Granophyre or the Quartz Gabbro was restored to a horizontal orientation, this did not also result in restored horizontal orientations for the contacts of the other passively restored layers (Fig. 3.3a, c). As a result there were portions of the Quartz Gabbro with variable thicknesses and non-horizontal contacts (Fig. 3.3a, c).

As the simple shear restorations are aimed to restore the folding associated with the West Bay Anticline, both restorations resulted in a subhorizontal orientation of the responding passively restored layer close to where the fold axis of the West Bay Anticline intersects the profile (Fig. 3.3a, c). At this location, the lithological contacts define a Quartz Gabbro thickness of ~300m. In both NW and SE directions away from where the fold axis of the West Bay Anticline intersects the profile, the thickness of the Quartz Gabbro increases to a maximum of 1487m in the NW, where the NE-lobe syncline is located and it also thickens up to 763m in the SE approaching the SE-lobe syncline (Fig. 3.1a, 3.3a, c). In addition to the variability in thickness of the Quartz Gabbro, there are breaks in the continuity of the upper or lower contact characterized by strong thickness variations of the Quartz Gabbro. These breaks are coincident with the locations of prominent curved faults in the East Range. The effects of applying the simple shear algorithm to the Granophyre and Quartz Gabbro had a pronounced effect on the Felsic Norite which became highly distorted beyond the range of the profiles (Fig. 3.3b, d).

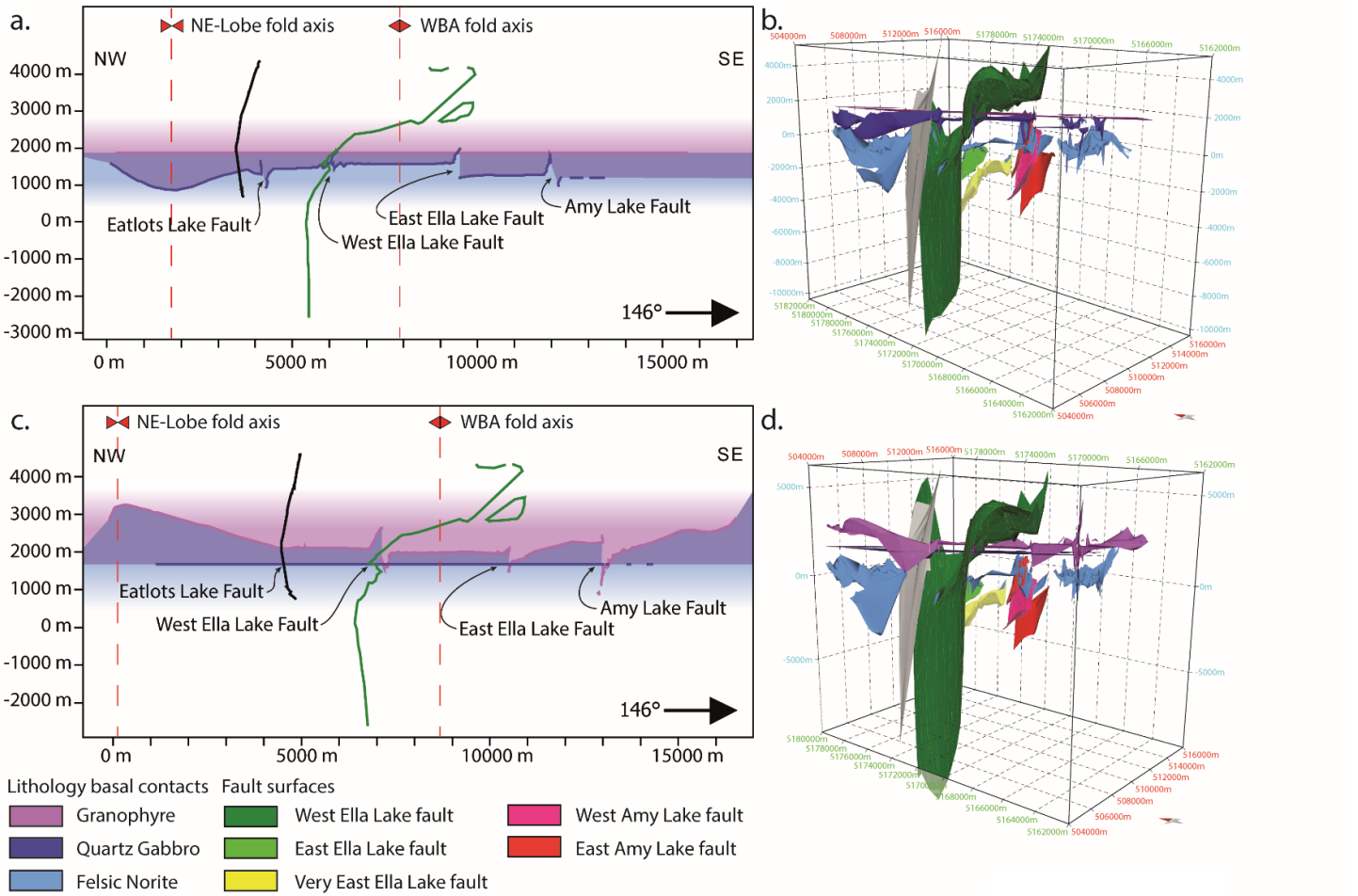

Figure 3.3: Kinematic restoration of the SIC to a horizontal target surface using the simple shear algorithm. (a) Vertical profile showing the intersection of the fault surfaces and lithological basal contacts after applying the simple shear algorithm to bring the Granophyre into a flat plane. (b) 3-D model of the fault surfaces and lithological basal contacts after applying simple shear to bring the Granophyre to a horizontal target orientation. (c) Vertical profile showing the intersection of the fault surfaces and lithological basal contacts after applying the simple shear algorithm to bring the Quartz Gabbro into a flat plane. (d) 3-D model of the fault surfaces and lithological basal contacts after applying simple shear to bring the Quartz Gabbro to a horizontal target orientation.

3.5.3 3-D kinematic restoration applying flexural slip and simple shear

One kinematic restoration was accomplished using the flexural-slip algorithm, in an attempt to bring the most prominent of the curved East Range faults, the West Ella Lake fault, into a flat plane (Fig. 3.4). Given the hypothesis that slip on prominent curved faults has helped to accomplish the folding of the SIC in the East Range, the most realistic way to unfold the SIC is to restore the faults to their pre-deformed orientations and unfold the SIC contacts as passive geometrical elements (Clark and Riller, 2016). Therefore, I unfolded the SIC by using the most prominent of the curved faults in the East Range, the West Ella Lake fault, to perform the flexural slip unfolding algorithm. The target orientation of the West Ella Lake fault was identified by using the rotation magnitudes that were isolated in the forward modeling of the orientation of SIC contacts. More specifically, the West Ella Lake fault was unfolded by a counter clockwise rotation of 3.5° south and 23.1° north of the intersection of the fault with the fold axis of the West Bay Anticline resulting in a target orientation of 250/70 for the unfolded West Ella Lake fault.

Unfolding the West Ella Lake fault resulted in the removal of the plan view curvature of the SIC contacts as well as of the other curved prominent faults in the East Range (Fig. 3.4c, d). Horizontal profiles through the model are provided to highlight the key geometrical differences before and after the kinematic restoration is performed (Fig. 3.4a, c). After unfolding, two anomalies remained which deviated away from the planarity of the SIC contacts (Fig. 3.4). The first anomaly is the sharp concave curvature in the Granophyre and Quartz Gabbro contacts located at the NW corner of the profile, where the fold axis of the NE-lobe syncline transects the SIC (Fig. 3.4c). The second anomaly is visible in the local outward curvature of the basal contact of the Felsic Norite, near the SE corner of the profile (Fig. 3.4c).

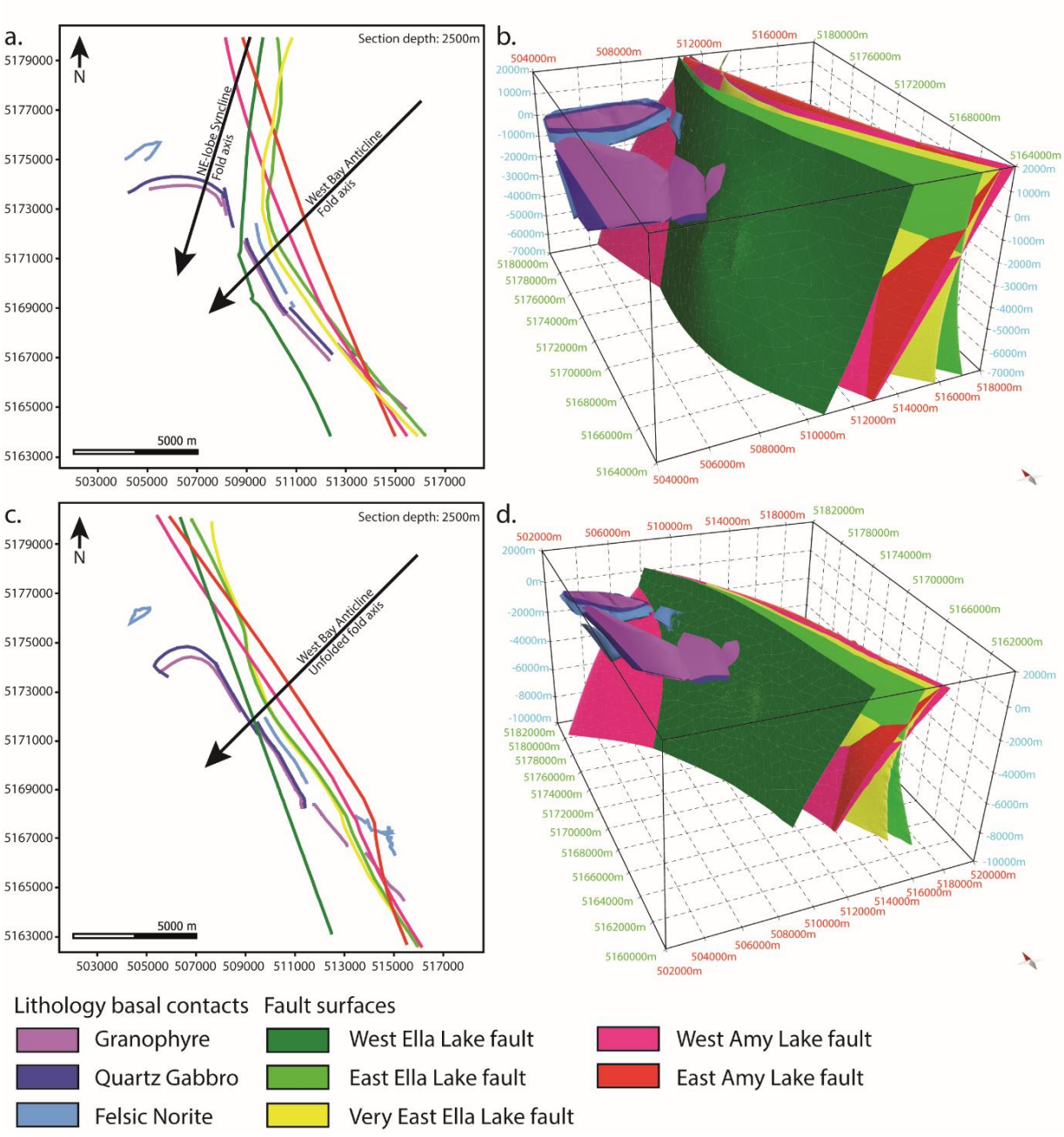

Figure 3.4: Kinematic restoration of the West Ella Lake fault using the flexural slip algorithm. (a) Horizontal cross section showing the trace of the fault surfaces and lithological basal contacts prior to applying the flexural slip algorithm. (b) 3-D model of the fault surfaces and lithological basal contacts prior to applying the flexural slip algorithm. (c) Horizontal cross section showing the trace of the fault surfaces and lithological basal contacts after applying the flexural slip algorithm. (d) 3-D model of the fault surfaces and lithological basal contacts after applying the flexural slip algorithm.

Once the folding-related curvature of the West Ella Lake fault was removed, the Granophyre and Quartz Gabbro were restored to a horizontal target geometry using the simple shear algorithm (Fig. 3.5). This restoration has a magnitude of shear strain of 2.7. This step resulted in overall flat surfaces for the Granophyre and Quartz Gabbro, and a Felsic Norite

basal surface which deepened towards the SE, indicating a thickening of the Felsic Norite in that direction. All prominent faults could then be characterized by an average NW dip.

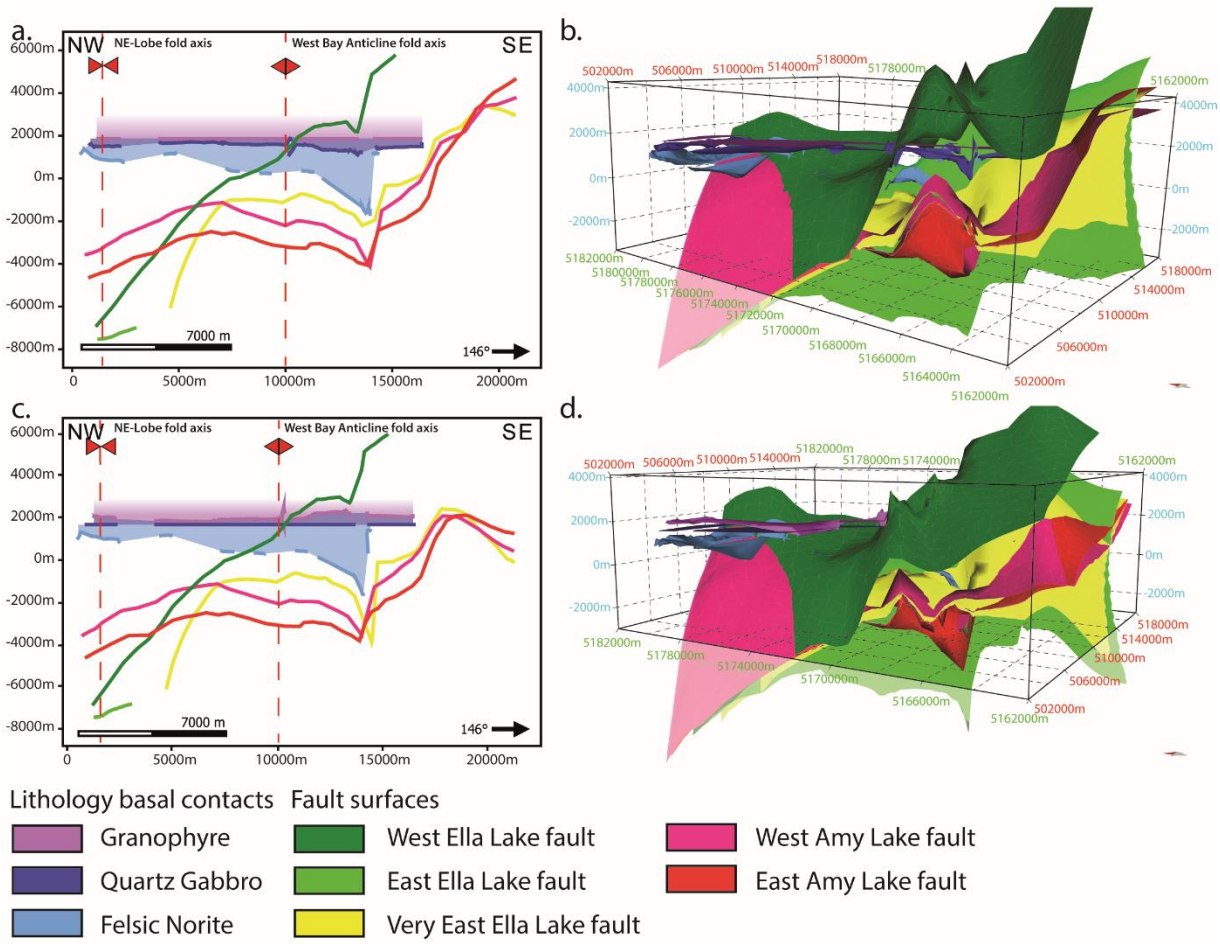

Figure 3.5: Kinematic restoration of the SIC after applying flexural slip to restore the West Ella Lake fault, using the simple shear algorithm. (a) Vertical profile showing the intersection of the fault surfaces and lithological basal contacts after applying the simple shear algorithm to bring the Granophyre into a flat plane. (b) 3-D model of the fault surfaces and lithological basal contacts prior after applying the simple shear algorithm to bring the Granophyre into a flat plane. (c) Vertical profile showing the trace of the fault surfaces and lithological basal contacts after applying the simple shear algorithm to bring the Quartz Gabbro into a flat plane. (d) 3-D model of the fault surfaces and lithological basal contacts after applying the simple shear algorithm to bring the Quartz Gabbro into a flat plane.

To visualize the length change of the East Range in plan view, I generated horizontal sectional strain ellipses by measuring the contact length and azimuth of the present day geometry of the Granophyre and Quartz Gabbro and compared it to the contact length and azimuth of the restored products (Fig. 3.6). The magnitude of shortening for the East Range is given for each restoration with a contact lengths of 1.3 km for the Granophyre and 0.9 km for the Quartz Gabbro. For the restoration of the Granophyre, the small magnitude of

shortening is accompanied by a minor plan view counter clockwise rotation of 5° of the Granophyre basal contact. This contrasts with the magnitude of shortening of the Quartz Gabbro and clockwise rotation of 3° of the Quartz Gabbro basal contact.

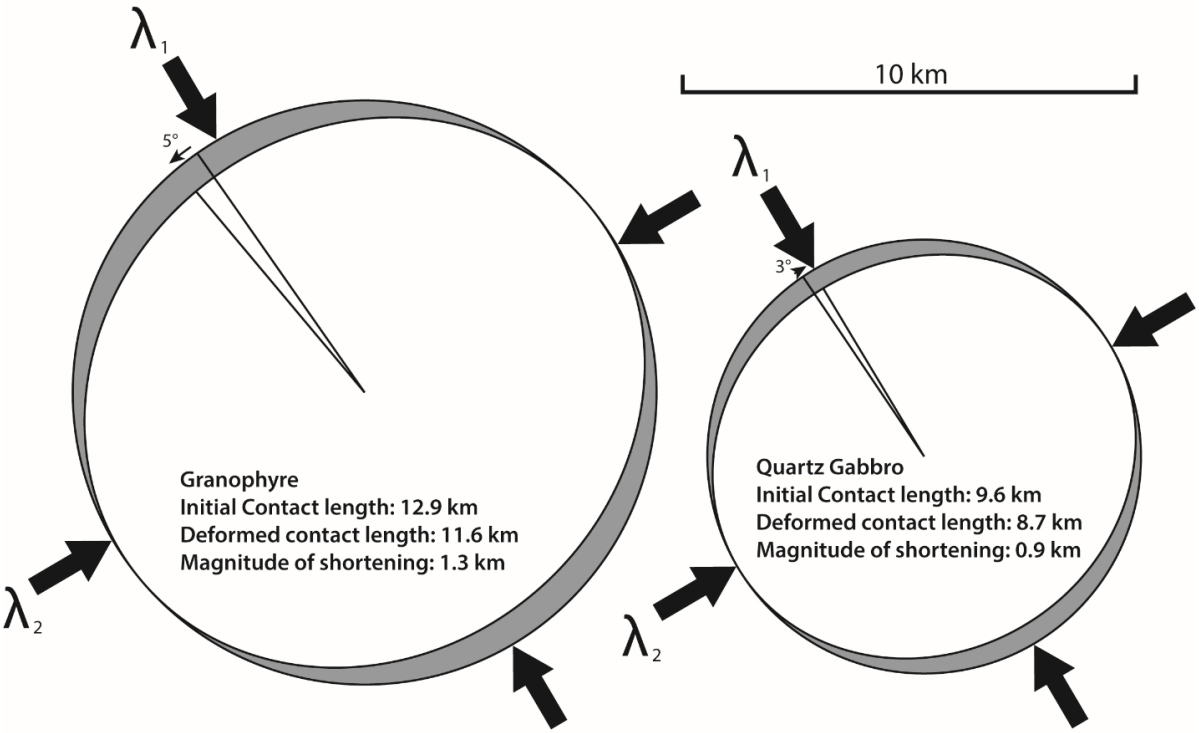

Figure 3.6: Sectional strain ellipses showing the change from the undeformed length (grey circle) to the deformed length (white ellipse) for the Granophyre (left) and Quartz Gabbro (right). Principal orientations of shortening (λ_1) and extension (λ_2) are shown by the black arrows.

3.6 Interpretation

3.6.1 Forward modeling

The interplay between folding and tilting of the East Range has previously neither been recognized nor quantified, but is a result that has been highlighted by forward modeling the SIC contacts. Rotations about both, the fold axis of the West Bay Anticline, and about a tilt axis are necessary to generate the current orientation of SIC contact from an initial horizontal orientation. The effects of these two rotations are already hinted at by the geometry of the SIC in the East Range (Fig. 3.1a, b). Firstly, the dips of the East Range SIC are distinctively steeper than of the SIC in the North Range, suggesting a unique tilt component that has locally steepened the contacts. Secondly, the dip direction of the SIC across the East Range

is radially displaced in a counter clockwise manner from NW to SE which, along with the similar curvature of prominent faults, illustrates well the effect of folding about the West Bay Anticline.

The assumption built into the forward model that the West Bay Anticline was originally manifested as an anticline with a horizontal fold axis oriented orthogonally to the regional NW-SE shortening can be questioned. There is no previous assessment of the initial orientation of the fold axis of the West Bay Anticline. Its initial orientation was most likely orthogonal to both the regional compression orientation and the strike of the folded unit. Due to the initial mechanically isotropic nature of the SIC, the orientation of the lithological contacts of the SIC prior to folding cannot be used to constrain the primary orientation of the fold axis of the West Bay Anticline. Rather, folding of the SIC in the East Range was rather completed using mechanical contacts, defined as the prominent curved faults (Clark and Riller, 2016). Therefore, the assumption that the initial azimuth of the fold axis of the West Bay Anticline is oriented to the NE-SW remains justified by the fact that regional shortening was directed NW-SE during formation of the Sudbury Basin (Riller et al., 1999, Clark and Riller, 2016). The assumption that the fold axis of the West Bay Anticline had an initial horizontal plunge, however, was based on the assumption that the fold axis was originally parallel to the SIC layering at 1.85 Ga. This assumption is potentially invalid as the lithological contacts between layers of the SIC were most likely not used to accomplish folding, but rather accomplished using mechanical contacts (Clark and Riller, 2016). Therefore, the horizontal orientation of West Bay Anticline should then lie on the initial orientation of prominent curved fault surface, most likely on the initial orientation of the West Ella Lake fault at the onset of faulting, which is not constrained.

The clockwise rotations of 23.1° and 3.5° about the fold axis of the West Bay Anticline to the northern and southern SIC fold limbs, respectively, is more accurate than the estimates previous made (Clark et al., 2012). This rotation was estimated by using surface strike deviations of Matachewan dyke segments across the East Range. Their work proposed that the cumulative rotation about the fold axis of the West Bay Anticline was in the range of 20-30° clockwise applied to the northern limb and 20-30° counter clockwise to the southern limb (Clark et al., 2012). The 23.1° clockwise rotation calculated for the northern limb during the forward modeling of the current study is therefore consistent with the previous estimate using Matachewan dykes (Fig. 3.2a). In contrast, the clockwise rotation calculated for the southern limb of 3.5° is not consistent with the previous study. The clockwise 3.5° rotation for the

southern limb, calculated through the current forward modeling study considered superior to the previous 20-30° estimate, because the forward modeling exercise is constrained by a drill hole supported 3-D model of the SIC contacts. This information was not available or considered in estimates previously made based on the Matachewan dyke segments (Clark et al., 2012).

The clockwise rotation estimates here of 23.1° to the northern limb and 3.5° to the southern limb provide insight to the character of the West Bay Anticline. By comparing the rotations applied about the West Bay Anticline for the northern and southern fold limbs and assuming that the fold axial plane mirrors the fold's bisector plane, which equally divides the cumulative rotation, I can make first estimates of the symmetry of the West Bay Anticline. The clockwise direction of rotation for both fold limbs suggests that the West Bay Anticline is not an upright fold. The rotation magnitudes of 23.1° and 3.5° furthermore indicate that the northern limb was rotated by a much larger degree than the southern limb. Therefore, together, the same clockwise rotation direction and the strong variance between rotation magnitudes suggests that the West Bay Anticline is best classified as a steeply-plunging, and most likely moderately-inclined anticlinal fold with a fold axial plane dipping to the SE.

3.6.2 3-D kinematic restorations – Which restoration better approximates the folding and faulting in the East Range

The two sets of kinematic restorations performed here were done to compare restored surfaces from both simple shear and flexural slip assumptions, and to accentuate the effect of unfolding via flexural slip, which acts on discrete slip planes (Fig. 3.3, 3.5). For the East Range, the restorations accomplished using flexural slip are more reasonable than those using simple shear, due to the way the flexural slip algorithm accounts for slip on prominent surfaces. The importance of these prominent surfaces in the folding of the SIC has been outlined (Clark and Riller, 2016). In both simple shear kinematic restorations, the thickness of the subhorizontal restored Quartz Gabbro is not consistent through the profile (Fig. 3.3a, c). Other than gradual thickness variations at the NW and SE ends of the profile that are interpreted to be associated with folding at the NE-lobe and the SE-lobe, thickness variations of the Quartz Gabbro occur as abrupt breaks and correlate with the presence of prominent curved faults. These abrupt thickness changes in the Quartz Gabbro were not present in the kinematic restoration accomplished using flexural slip where the thickness of the Quartz

Gabbro is mostly uniform (Fig. 3.5a, c). The lack of abrupt thickness variations of the Quartz Gabbro for the restoration using the flexural slip algorithm suggest that vertical components of fault displacements of this unit were better restored when the prominent curved faults were accounted for in the flexural slip restoration.

In contrast to the simple shear restorations, the flexural slip algorithm results display only two deviations away from a constant thickness Quartz Gabbro: a localized tear where the fold axis of the West Bay Anticline transects the contact, and a gradual thickening of the Quartz Gabbro on the profile at the 12,000m mark (Fig. 3.5a, c). Unfortunately, comparisons of the Felsic Norite between the simple shear and the flexural slip restorations are not possible because the profiles of the simple shear restorations do not contain the basal contact of the Felsic Norite. This is due to the strong tearing effect simple shear caused to the discontinuous surface of the Felsic Norite, which translated most of the Felsic Norite outwards from the Basin and from where the profile is taken (Fig. 3.3b, d).

In the flexural slip restoration the Felsic Norite did not share the consistent thickness imaged for the Quartz Gabbro (Fig. 3.5a, c). At the NW end of the profile the basal contact of the Felsic Norite has a similar curvature to that of the Granophyre and Quartz Gabbro in all restorations, as a result of the unrestored NE-lobe syncline (Fig. 3.5a, c). Uniquely, in the flexural slip restoration, the Felsic Norite thickens towards the SE to a maximum thickness at 14000m along the profile (Fig. 3.5a, c). Although there is a small basal contact segment of the Felsic Norite at 15000m along the profile which suggests that the drastic thickening does not continue to the SE, this trend cannot be confirmed further to the SE due to a lack of data (Fig. 3.5a, c).

The thickening of the Felsic Norite southeast of the intersection of the West Ella Lake fault and West Bay Anticline (Fig. 3.5a, c), can be interpreted in three ways. Firstly, prominent embayments in the underlying country rocks (Dreuse et al., 2010) could result in localized thickening of the entire SIC stratigraphy, and not just the lower main mass layers of the mafic norite and sublayer. The origin of embayments could be linked to pre-existing discontinuities that were subsequently excavated during the initial emplacement of the SIC. Secondly, impact-related processes such as cratering and isostatic readjustment of the crater floor prior to tectonic deformation could result in localized thickening of the SIC (Clark et al., 2012; Dreuse et al., 2010). Thirdly, the thickening may be related to the South Range Shear Zone. The northeastward extent of shearing associated with the South Range Shear Zone is poorly

constrained in the East Range (Lenauer and Riller, 2012a). At surface, the northeastward extent of the South Range Shear Zone terminates at the trace of the fold axis of the SE-lobe syncline, but at depth its extent is even more poorly constrained (Fig. 3.1a). It is possible that the thickening of the Felsic Norite towards the SE is a relic from shearing associated with the South Range Shear Zone. In all three scenarios, the geometry of the embayment would be evident from the geometry of the melt sheet, but without more information of the thickness of the Felsic Norite towards the SE, it is difficult to make a definitive statement as to which scenario is most accurate. Therefore, I favor the first scenario of pre-deformation embayments. What makes the first scenario more plausible is the spatial relationship between large sulphide accumulations and the thickening of the Felsic Norite. In the East Range, there are prominent ore deposits known as the Capre Cu-Ni-PGE zone located between 14000-19000m along the profile (Fig. 3.5a, c; Ames et al., 2008). The relationship between thickening of the Felsic Norite and emplacement of ore deposits is highlighted by Keays and Lightfoot (2004). In essence, thickened Felsic Norite overlays thickened Sublayer and accumulations of Cu-Ni mineralization gravitationally flowed into embayments prior to the solidification of the SIC, and any post-emplacement deformation of the SIC. Therefore, on these grounds, pre-deformation embayment structures are the most plausible explanation for the drastic thickening of the Felsic Norite.

3.6.3 3-D kinematic restorations – interplay between faulting and folding

To better understand how faulting relates to folding, it's important to first understand how active faults were prior to the onset of folding. Clark and Riller (2016) proposed that faults were the required precursor for folding to begin in the East Range, although the pre-folding displacement magnitude on faults was not constrained. By looking at the unfolded products from the restorations if faults were active prior to the onset of folding, then displacements of the contacts of the Granophyre and Quartz Gabbro should not be visible in the profiles in the restoration accomplished using the flexural slip (Fig. 3.3a, c, 3.5a, c). In the horizontal section associated with the first restoration step of flexural slip, there are minor fault-associated discontinuities visible in the SIC, interpreted here to be at an intermediate stage of deformation of the SIC (Fig. 3.4c). Once the SIC is brought to the horizontal, accounting for the tilt component, there are no longer sharp changes in the thickness of the units of the SIC and this is interpreted to signal the complete restoration of the East Range (Fig. 3.5a, c). In

all restorations, where the West Ella Lake fault transects the Quartz Gabbro and Granophyre, there are always residual local tearing effects in the responding surface (Fig. 3.5a, c). Since this tearing does not cause a change in thickness of the Quartz Gabbro, I view this to be largely an artifact-driven geometry most likely related to the global application of the simple shear algorithm.

3.6.4 Shortening of the East Range – Restoration vs. regional and local strain estimates

Averaged NW-SE shortening in the East Range has been found to match the regional average of NW-SE shortening for the whole basin as calculated from fault inversions and inferred by the general orientation and shape of the basin (Riller et al., 1999; Clark and Riller, 2016). In the current study, the sectional strain ellipses estimate for the first time in research on the Sudbury Basin, the magnitude of shortening and the horizontal rotation component associated with shortening of the East Range. The counter clockwise and clockwise plan view rotation of 5° and 3° for the strike of the Granophyre and Quartz Gabbro, respectively, suggests that there was no significant plan view rotation for the East Range SIC. The magnitude of shortening is equivalent to a 10% change in length of the East Range SIC in both restorations of the Quartz Gabbro and Granophyre. This percentage of horizontal shortening is much less than expected, considering the length disparity between the East Range SIC and other Ranges. One explanation for the lower than expected degree of shortening is the exclusion of the NE-lobe and SE-lobe synclines in this restoration. The magnitude of folding about the fold axis of the NE-lobe syncline has been constrained to about 36° by paleomagnetic data (Clark et al., 2012) which is larger than the rotations calculated here about the West Bay Anticline, suggesting that the folding about other structures such as the NE-lobe syncline may have accomplished a significant amount of plan view shortening. Therefore, to develop an understanding of how much shortening the entire East Range underwent, restoring the NE-lobe and SE-lobe synclines is required to provide a more complete estimate.

Another explanation for the magnitude of shortening is that much of the deformation was accomplished by vertical extension. Considering the plan-view thickness of the SIC, there is no sign of changes in thickness in the NE-SW orientation deemed to be the intermediate principal strain axis (Fig. 3.1a). Therefore the shortening of the East Range should have translated to vertically-oriented extension.

3.7 Conclusion

In this study I have kinematically restored the 3-D geometry of SIC in the East Range of the Sudbury Basin by using a combination of flexural slip and simple shear algorithms. Forward modeling provided constraints on the rotation direction and magnitude associated with the West Bay Anticline and tilt magnitudes around a newly constrained tilt axis which affected the East Range SIC and adjacent rocks. By taking into account slip on prominent curved faults in the flexural slip algorithm, I are able to account for displacement of the SIC along these faults, and show that fault displacement was an intrinsic component to folding. The kinematic restoration revealed that the initial solidified SIC was non-planar, characterized by undulations in the thickness of the Quartz Gabbro and Felsic Norite. Moreover, the location of drastic thickening of the restored Felsic Norite correlates to a known ore deposit, which may have significant implications for ongoing mineral exploration. Lastly, I advocate that restoring deformed igneous terranes is achievable, as long as there are sufficient constraints on the geometry of deformed igneous units.

3.9 References

Ames, D.E., Davidson, A., Wodicka, N., 2008. Geology of the Giant Sudbury Polymetallic Mining Camp, Ontario, Canada. Economic Geology 103, 1057-1077.

Boerner, D.E., Milkereit, B., 1999. Structural evolution of the Sudbury impact structure in the light of seismic reflection data. In Dressler, B.O., and Sharpton, V.L., eds., Large Meteorite Impacts and Planetary Evolution II: Boulder, Colorado, Geological Society of America Special Paper 339, 419-429.

Bowan, N.L., 1915. The Later Stages of the Evolution of the Igneous Rocks. The Journal of Geology 23, 8, 1-91.

Brocoum, S.J., Dalziel, J.W.D., 1974. The Sudbury Basin, the Southern Province, the Grenville Front, and the Penokean Orogeny. Geological Society of American Bulletin 85, 1571-1580.

Card, K.D., Gupta, V.K., McGrath, P.H., Grant, F.S., 1984. The Sudbury Structure: Its Regional Geological and Geophysical Setting. *In* Pye, E.G., Naldrett, A.J., and Giblin, P.E., eds., The geology and ore deposits of the Sudbury Structure: Ontario Geological Survey Special Volume 1, 25-43.

Clark, M.D., Riller, U., Morris, W.A., 2012. Upper-crustal, basement-involved folding in the East Range of the Sudbury Basin, Ontario, inferred from paleomagnetic data and spatial analysis of mafic dykes. Canadian Journal of Earth Sciences 49, 1005-1017.

Clark, M.D., Riller, U., 2016. Significance of first-order faults in folding mechanically isotropic layers: evidence from the Sudbury Basin, Canada. Manuscript submitted for publication.

Cowan, E.J., Schwerdtner, W.M., 1994. Fold Origin of the Sudbury Basin. In: Lightfoot, P.C., Naldrett, A. (Eds.), Proceedings of the Sudbury - Noril'sk Symposium. Ontario Geological Survey, Special Volume 5, 45-55.

Cowan, E.J., 1999. Magnetic fabric constraints on the initial geometry of the Sudbury Igneous Complex: a folded sheet or a basin-shaped igneous body? Tectonophysics 307, 135-162.

Dreuse, R., Doman, D., Santimano, T., Riller, U., 2010. Crater floor topography and impact melt sheet geometry of the Sudbury impact structure, Canada. Terra Nova 22(6), 463-469.

Ernst, R.E., Halls, H.C., 1984. Paleomagnetism of the Hearst dike swarm and implications for the tectonic history of the Kapuskasing Structural Zone, northern Ontario. Canadian Journal of Earth Sciences 21(12), 1499-1506.

Everitt, R.A., 1979. Jointing in the Sudbury Basin, Sudbury, Ontario. M.Sc. Thesis, Laurentian University.

Groshong Jr, R.H., 2006. 3-D Structural Geology. Springer-Verlag Berlin, Heidelberg.

Grieve, R.A.F., Stöffler, D., Deutsch, A., 1991. The Sudbury Structure: Controversial or Misunderstood? Journal of Geophysical Research 96, E5, 22753-22764.

Heaman, L.M., 1997. Global mafic magmatism at 2.45 Ga: Remnants of an ancient large igneous province? Geology 25(4), 299-302.

Keays, R.R., Lightfoot, P.C., 2004. Formation of Ni-Cu-PGE sulphide mineralization in the Sudbury Impact Melt Sheet. Mineral. Petrol. 82, 217-258.

Krogh, T.E., Davis, D.W., Corfu, F., 1984. Precise U-Pb zircon and baddeleyite ages for the Sudbury area. *In* Pye, E.G., Naldrett, A.J., and Giblin, P.E., eds., The geology and ore deposits of the Sudbury Structure: Ontario Geological Survey Special Volume 1, 431-448.

Lenauer, I., Riller, U., 2012a. Strain fabric evolution within and near deformed igneous sheets: The Sudbury Igneous Complex, Canada. Tectonophysics 558-559, 45-57.

Lenauer, I., Riller, U., 2012b. Geometric consequences of ductile fabric development from brittle shear faults in mafic melt sheets: Evidence from the Sudbury Igneous Complex, Canada. Journal of Structural Geology 35, 40-50.

Li, Y., Wei, D., Chen, Z., Jia, D., Ma, D., Wang, Y., Cui, J., Shen, S., 2016. Multiphase deformation deduced from 3D construction and restoration: Implication for the hydrocarbon exploration in the mountain front of the Northern Tianshan. Marine and Petroleum Geology 77, 916-930.

Milkereit, B., Green, A., 1992. Deep geometry of the Sudbury structure from seismic reflection profiling. Geology 20, 807-811.

Moretti, I., Lepage, F., Guiton, M., 2006. KINE3D: a New 3D Restoration Method Based on a Mixed Approach Linking Geometry and Geomechanics. Oil & Gas Science and Technology 61(2), 277-289.

Phinny, W.C., Halls, H.C., 2001. Petrogenesis of the Early Proterozoic Matachewan dyke swarm, Canada, and implications for magma emplacement and subsequent deformation. Canadian Journal of Earth Sciences 38(11), 1541-1563.

Riller, U., Boutelier, D., Schrank, C., Cruden, A.R., 2010. Role of kilometer-scale weak circular heterogeneities on upper crustal deformation patterns: Evidence from scaled analogue modeling and the Sudbury Basin, Canada. Earth and Planetary Science Letters 297, 587-597.

Riller, U., Schwerdtner, W.M., Halls, H.C., Card, K.D., 1999. Transpressive tectonism in the eastern Penokean orogen, Canada Consequences for Proterozoic crustal kinematics and continental fragmentation, Precambrian Research 93, 51-70.

Rouby, D., Raillard, S., Guillocheau, F., Bouroullec, R., Nalpas, T., 2002. Kinematics of a growth fault/raft system on the West African margin using 3-D restoration. Journal of Structural Geology 24, 783-796.

Rousell, D.H., 1975. Origin of foliation and lineation in Onaping Formation and the deformation of the Sudbury Basin. Canadian Journal of Earth Sciences 12(8), 1379-1395.

Santimano, T., Riller, U., 2012a. Revisiting thrusting, reverse faulting and transpression in the southern Sudbury Basin, Ontario. Precambrian Research 200-203, 74-81.

Shanks, W.S., Schwerdtner, W.M., 1991a. Structural analysis of the central and southwestern Sudbury Structure, Southern Province, Canadian Shield. Canadian Journal of Earth Sciences 28, 411-430.

Shanks, W.S., Schwerdtner, W.M., 1991b. Crude quantitative estimates of the original northwest-southeast dimension of the Sudbury Structure, south-central Canadian Shield. Canadian Journal of Earth Sciences 28, 1677-1686.

Tschirhart, P., Morris, B., 2012. Grenville age deformation of the Sudbury impact structure: evidence from magnetic modelling of the Sudbury diabase dyke swarm. Terra Nova 24, 213-220.

Ziesch, J., Aruffo, C.M., Tanner, D.C., Beilecke, T., Dance, T., Henk, A., Weber, B., Tenthorey, E., Lippmann, A., Krawczyk, C.M., 2015. Geological structure and kinematics of normal faults in the Otway Basin, Australia, based on quantitative analysis of 3-D seismic reflection data. Basin Research, 1-20.

4.0 Conclusions

This work aims to better understand the tectonic deformation of the East Range of the Sudbury Basin. The mechanism by which the East Range of the Sudbury Basin was folded is identified to have used slip on prominent curved faults. As the rocks of the SIC and underlying country rocks are mechanically isotropic, folding required the introduction of a mechanically anisotropic element to begin. Proposed here, NE-SW shortening most likely related to the 1.7-1.6 Mazatzal Orogeny resulted in the formation of first-order thrust faults. As shortening continued through younger tectonic events such as the 1.2-1.0 Ga Grenville Orogeny, these thrust faults, along with the SIC were folded. Folding of prominent faults resulted in the northern fault segments assuming a normal fault geometry.

To validate this hypothesis sourced from surface data, two kinematic restorations were performed using simple shear and flexural slip algorithms on an independent dataset of the subsurface geometry of the SIC. By harnessing the flexural slip restoration algorithm which accounts for the displacement on prominent slip surfaces together with the forward modelled targets of the SIC contacts, the effect of slip on prominent curved faults such as the West and East Ella Lake faults and West and East Amy Lake faults were shown to be removed in the restored products. This illustrates that their slip was accumulated during folding of the SIC. In addition, removing the effect of folding associated to the West Bay Anticline resulted in straightening of the plan view curvature of the prominent faults further reinforcing their genetic relationship to folding of the SIC.

Forward modeling of the SIC contacts and the fold axis to the West Bay Anticline showed that tilting of these elements was an intrinsic component of progressive deformation of the East Range. This work proposes the orientation of the axis associated to tilting to be 330/05 with a previously unconstrained tilting magnitude of 70°. This tilting was derived in conjunction with folding associated to the West Bay Anticline. The rotation magnitudes associated to folding about the West Bay Anticline were constrained, whereby the northern and southern SIC fold limbs were folded by 23.1° and 3.5°, respectively. These rotation magnitudes suggest that the West Bay Anticline is best characterized as a steeply plunging moderately inclined anticlinal fold with a SE dipping fold axial plane. This characterization of the amount folding and of the type of fold is the most accurate to date.

In addition to highlighting the mechanism by which the East Range deformed, the restored geometry of the SIC illustrates that there was a prominent embayment in the initial geometry of the SIC in the East Range. Coincident with the location of the Capre Cu-Ni-PGE deposit in the East Range gives support for the genetic link between drastic thickening of the SIC and the formation of ore deposits (Keays and Lightfoot, 2004). The idea that prominent embayments to the initial geometry of the SIC is not a new concept (e.g. Dreuse et al., 2010, Clark et al., 2012), but here is the first time they are imaged in 3-D as a source from a kinematic restoration of their current geometry.

This work further advances how various structural methodologies can be applied more efficiently using computational advancements. A G.I.S. based workflow was developed for the analysis of the geometry and kinematics of faults. By harnessing older techniques, within a G.I.S. based framework, here I show how they constrain deformed surfaces in a heavily deformed igneous terranes. Moreover, this work also shows that with the proper constraints (i.e. drill-core lithological geometries) performing the kinematic restoration of deformed igneous terranes are possible. Together, this work aims to highlight the possibility of unravelling structural questions in areas previously left unstudied.

4.1 Outlook for future research

The work presented here helps to set the foundation for studies aimed to develop a better understanding of deformation associated to the Sudbury Basin and deformed igneous terranes in general.

The kinematic restoration illustrates that it is possible to accomplish kinematic restorations of the igneous rocks of the SIC and structures of the Sudbury Basin, and due to the extensive mineral exploration history of the whole Basin, this should also be possible for the other Ranges. If the SIC can be restored to its predeformational geometry for the South Range and the North Range, basin-scale restorations could be conducted which could better relate deformation mechanisms of each Range. In this work, the SIC and structures of the East Range was found to be best restored using a flexural slip restoration algorithm. How the folded and faulted SIC in the East Range geometrically transitions to the sheared geometry of the SIC in the South Range would be of interest to discern.

While a restoration of the whole Basin would aid to unravel the deformation on a large scale, local studies of the fault geometry and kinematics would help to better understand how a single fault segments, how slip accumulates along the fault, and how this controls the distribution of fault-related ore deposits. The East Range is pervasively faulted and in many cases, this faulting segments Cu-Ni-PGE mineralization. Slip on individual fault segments can be drastically different than the overall slip of a fault (Fig. 4.1). A study conducted on a 10m to 100m scale with G.I.S.-based workflow applied here could better image and understand structural evolution on a scale relatable to the size of ore deposits.

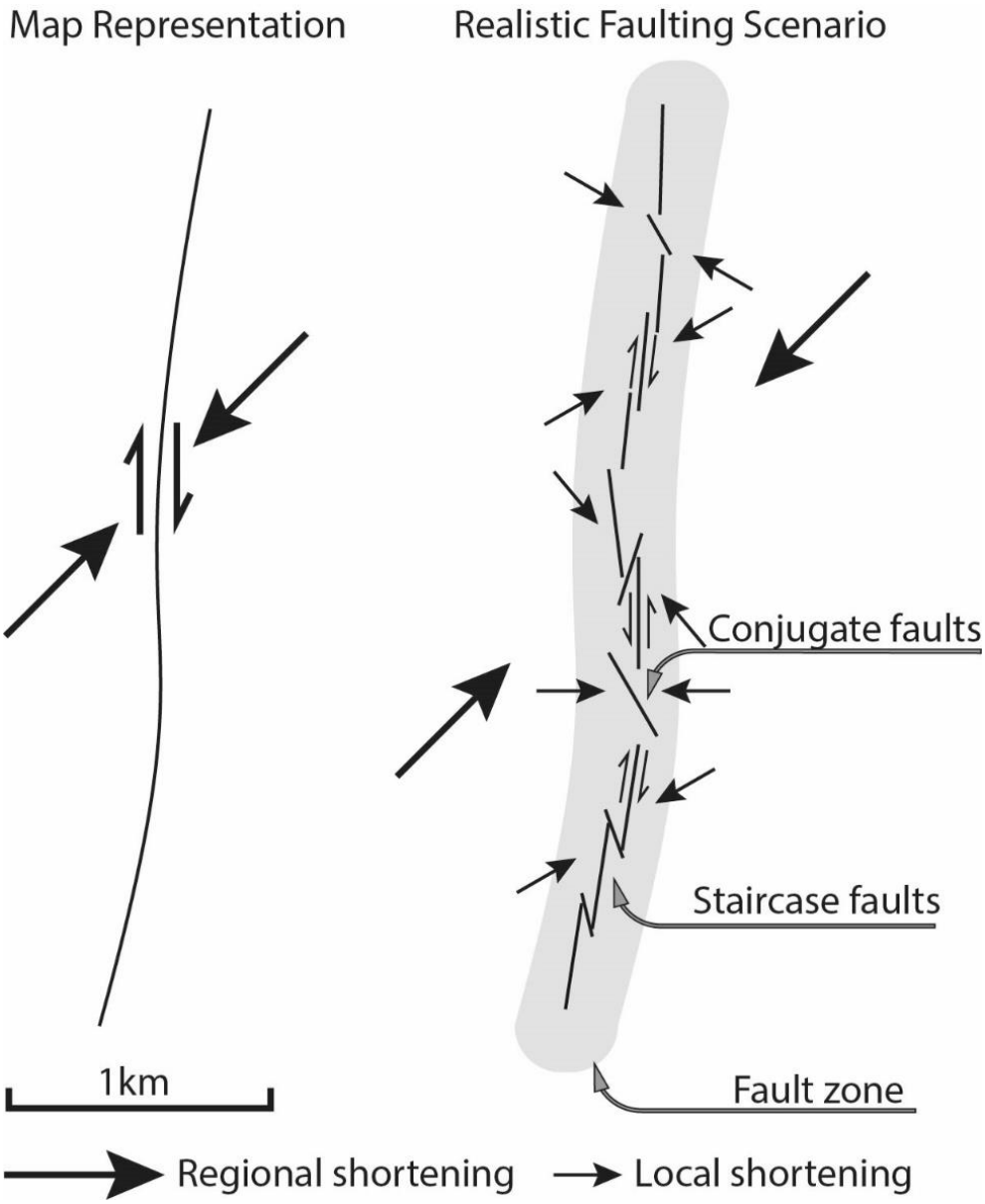

Figure 4.1: Schematic diagram showing map representation of faults (left) and a more realistic faulting scenario (right) with their associated regional and local plan view slip vectors, and associated principal axes of shortening (λ_1).

As the new G.I.S.-based workflow proposed here to calculate both the geometry of planar surfaces and in the case of faults, their kinematics, its application to a variety of study areas is possible and encouraged. The benefit to this methodology is the ability to harness high resolution datasets and maintain the high resolution when calculating planar surfaces. With the data here, fault surface geometries with a resolution of 1 m could be generated with ranges up to roughly 50 m. This methodology can be harnessed to achieve a much stronger result in areas that may either have millimeter or centimeter high resolution topography datasets, or where the range of elevations is much higher (i.e. mountainous regions). In either case, planar surfaces can be much more quantitatively described.

4.2 References

Clark, M.D., Riller, U., Morris, W.A., 2012. Upper-crustal, basement-involved folding in the East Range of the Sudbury Basin, Ontario, inferred from paleomagnetic data and spatial analysis of mafic dykes. Canadian Journal of Earth Sciences 49, 1005-1017.

Dreuse, R., Doman, D., Santimano, T., Riller, U., 2010. Crater floor topography and impact melt sheet geometry of the Sudbury impact structure, Canada. Terra Nova 22(6), 463-469.

Keays, R.R., Lightfoot, P.C., 2004. Formation of Ni-Cu-platinum group element sulphide mineralization in the Sudbury impact melt sheet. Mineralogy and Petrology 82, 217-258.

Appendix

Appendix Figure 1: Results from fault-slip analysis displayed on lower-hemisphere equal-area projections

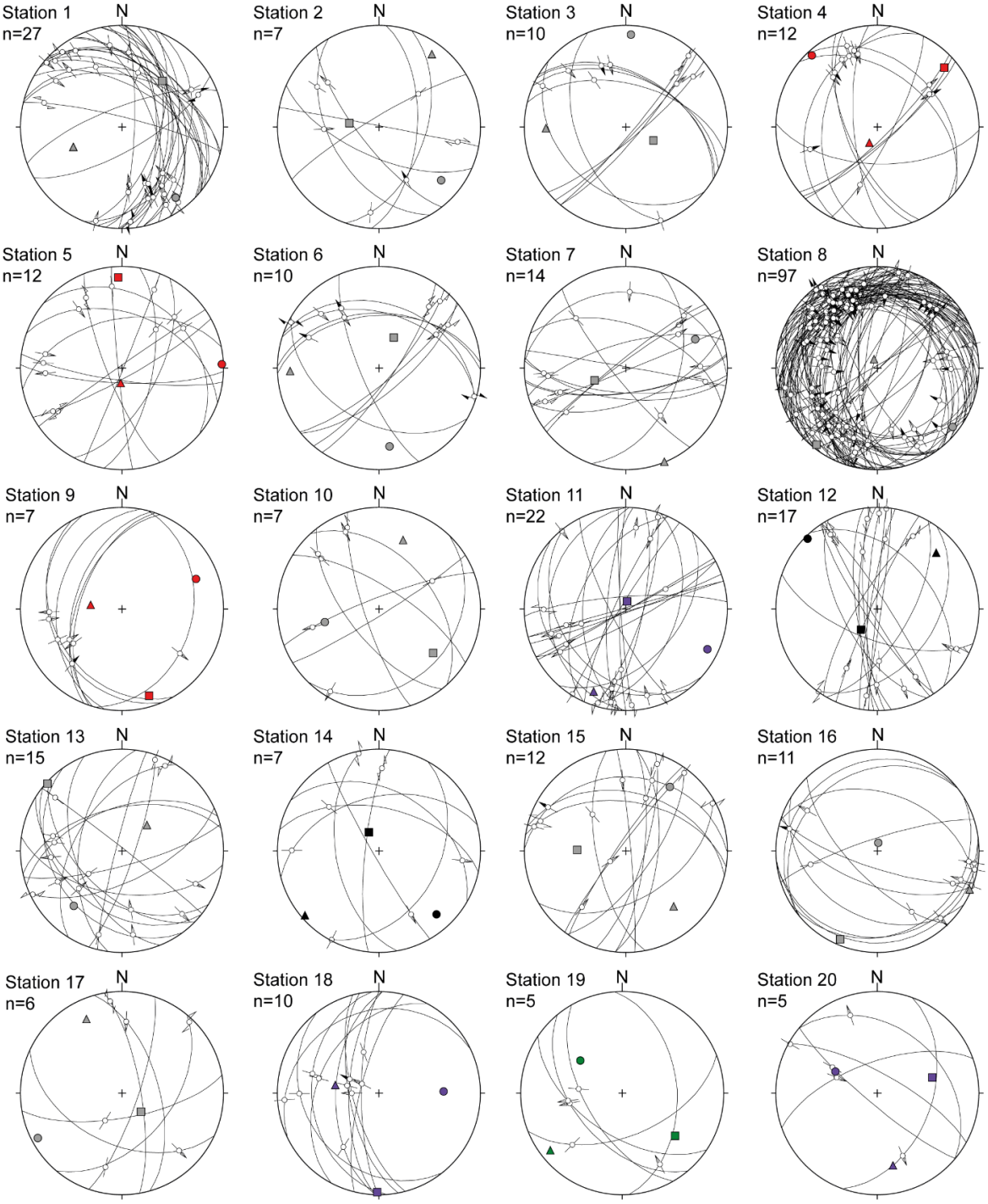

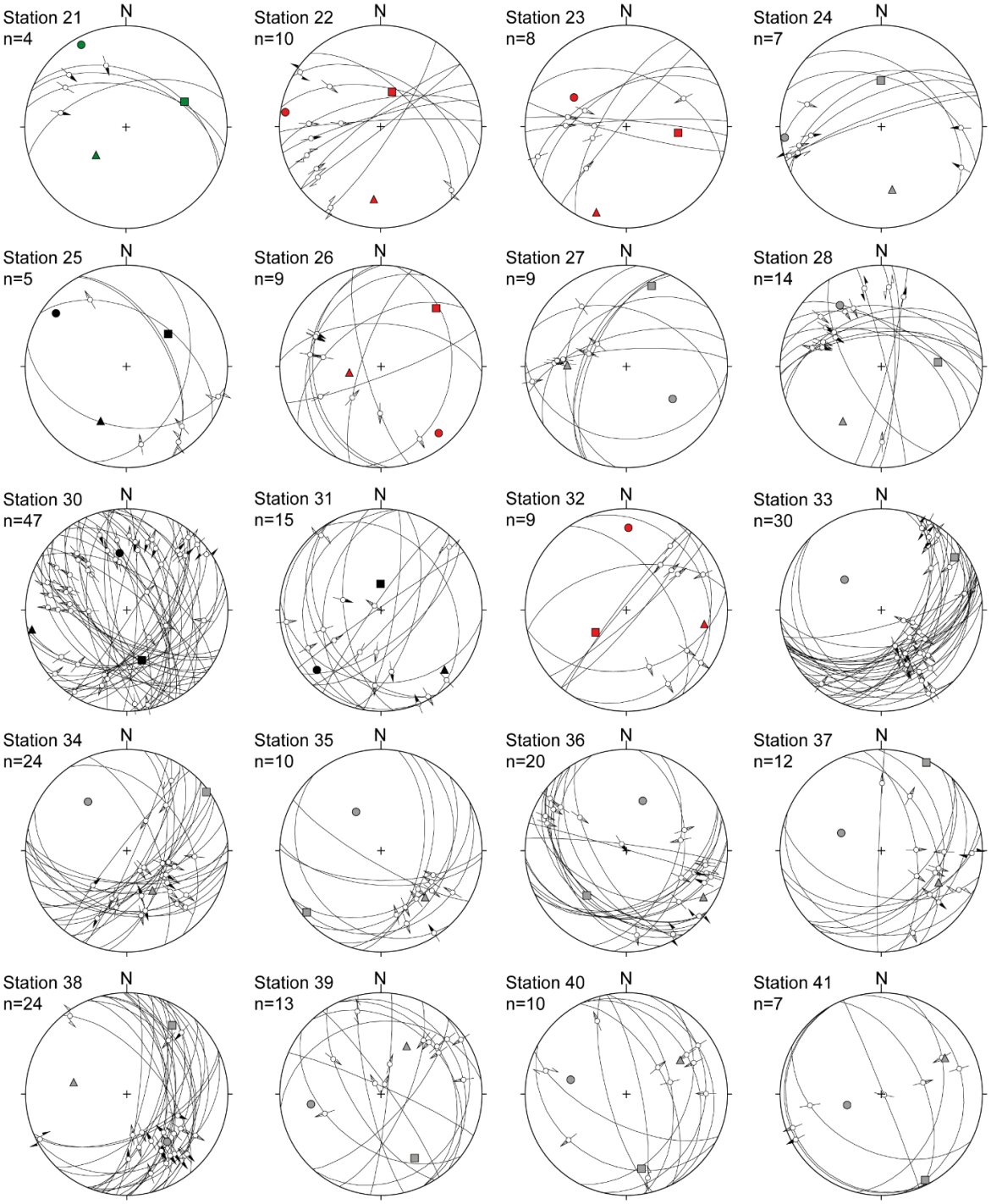
Station 21
n=4
N
Station 22
n=10
N
Station 23
n=8
N
Station 24
n=7
N
Station 25
n=5
N
Station 26
n=9
N
Station 27
n=9
N
Station 28
n=14
N
Station 30
n=47
N
Station 31
n=15
N
Station 32
n=9
N
Station 33
n=30
N
Station 34
n=24
N
Station 35
n=10
N
Station 36
n=20
N
Station 37
n=12
N
Station 38
n=24
N
Station 39
n=13
N
Station 40
n=10
N
Station 41
n=7
N

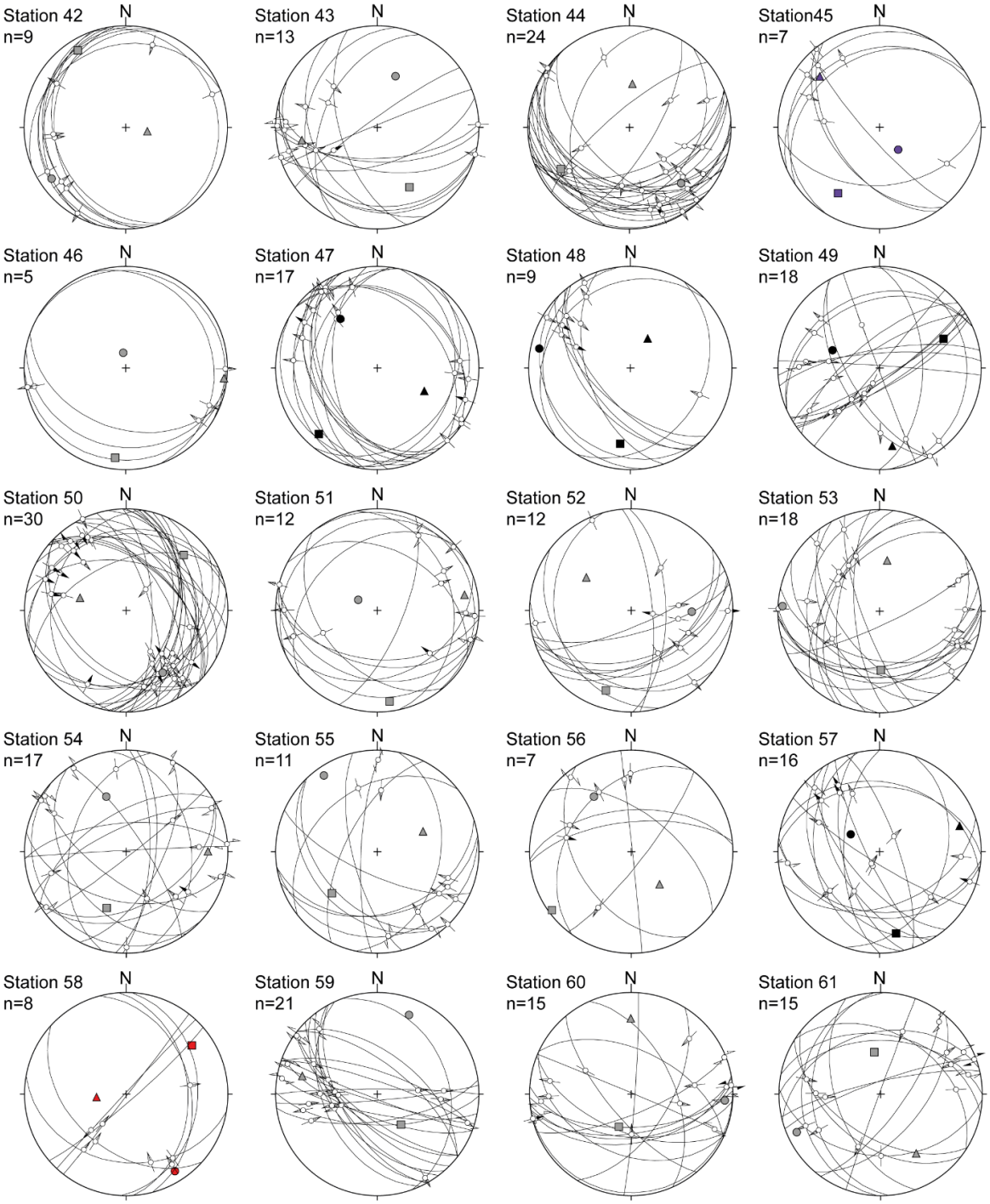
Station 42
n=9
N
Station 43
n=13
N
Station 44
n=24
N
Station45
n=7
N
Station 46
n=5
N
Station 47
n=17
N
Station 48
n=9
N
Station 49
n=18
N
Station 50
n=30
N
Station 51
n=12
N
Station 52
n=12
N
Station 53
n=18
N
Station 54
n=17
N
Station 55
n=11
N
Station 56
n=7
N
Station 57
n=16
N
Station 58
n=8
N
Station 59
n=21
N
Station 60
n=15
N
Station 61
n=15
N

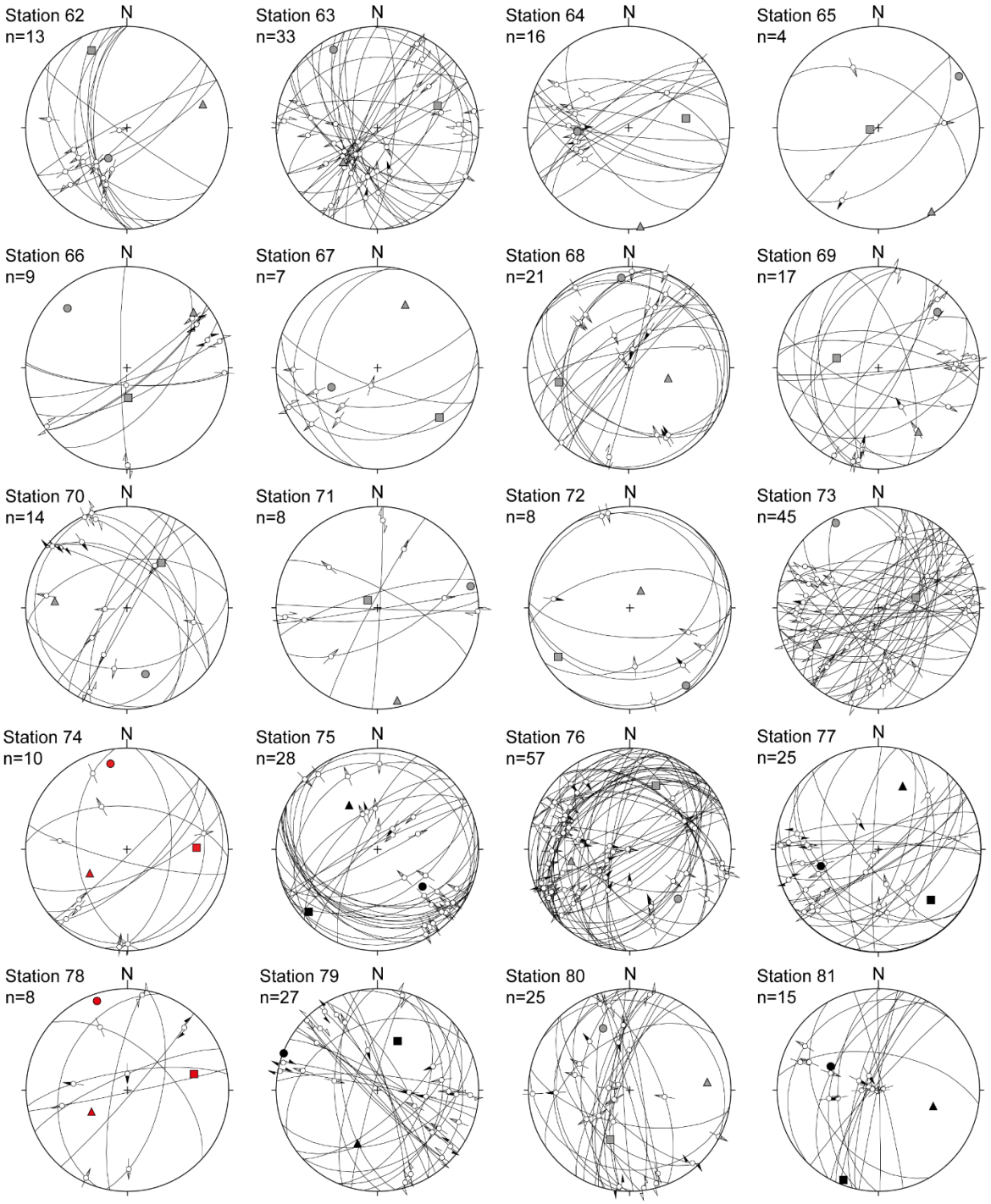
Station 62
n=13
N
Station 63
n=33
N
Station 64
n=16
N
Station 65
n=4
N
Station 66
n=9
N
Station 67
n=7
N
Station 68
n=21
N
Station 69
n=17
N
Station 70
n=14
N
Station 71
n=8
N
Station 72
n=8
N
Station 73
n=45
N
Station 74
n=10
N
Station 75
n=28
N
Station 76
n=57
N
Station 77
n=25
N
Station 78
n=8
N
Station 79
n=27
N
Station 80
n=25
N
Station 81
n=15
N

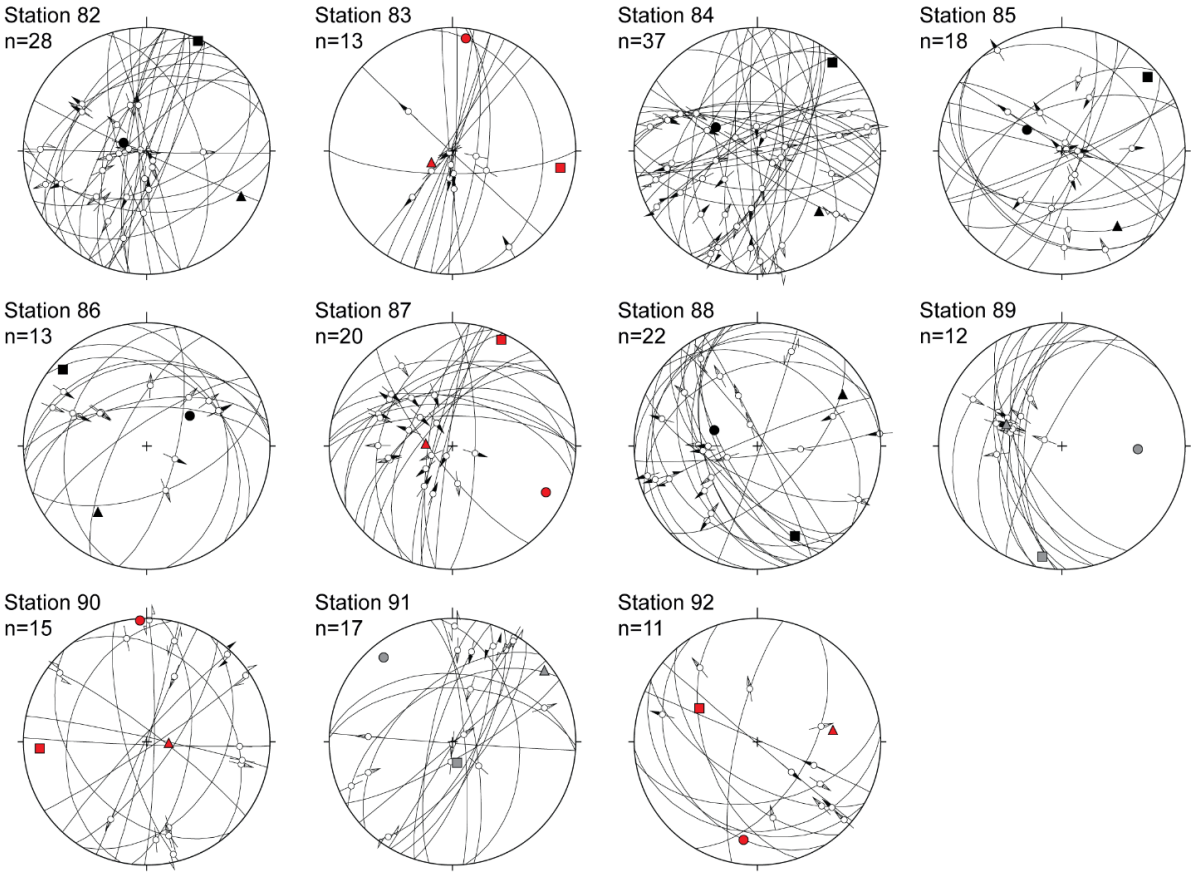

*Legend for stereonet symbology is shown in Chapter 2: Figure 5.

Appendix Figure 2: Calculation of slip vectors of prominent faults displayed on lower-hemisphere equal-area projections

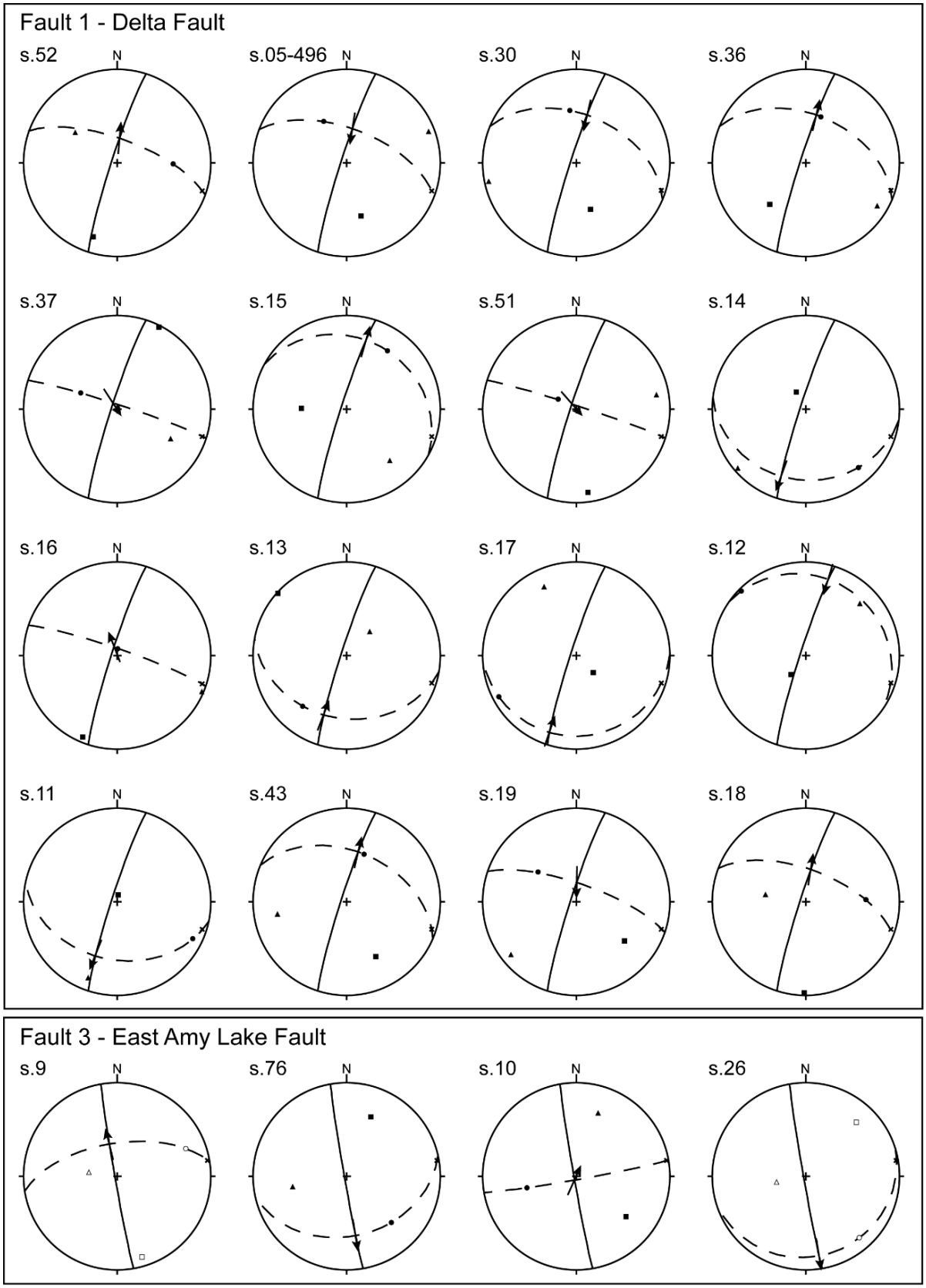

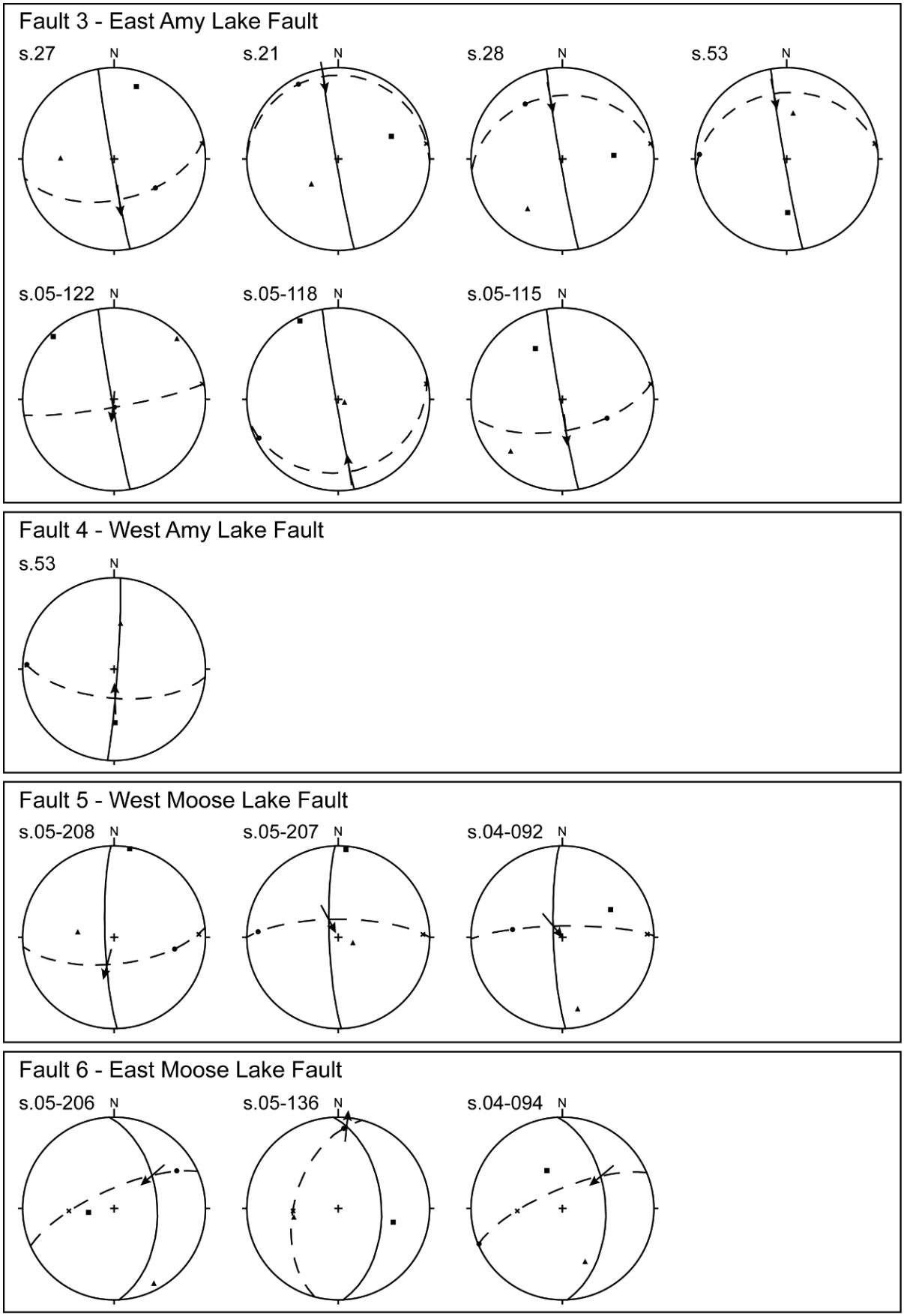
Fault 3 - East Amy Lake Fault
s.27
N
s.21
N
s.28
N
s.53
N
s.05-122
N
s.05-118
N
s.05-115
N
Fault 4 - West Amy Lake Fault
s.53
N
Fault 5 - West Moose Lake Fault
s.05-208
N
s.05-207
N
s.04-092
N
Fault 6 - East Moose Lake Fault
s.05-206
N
s.05-136
N
s.04-094
N

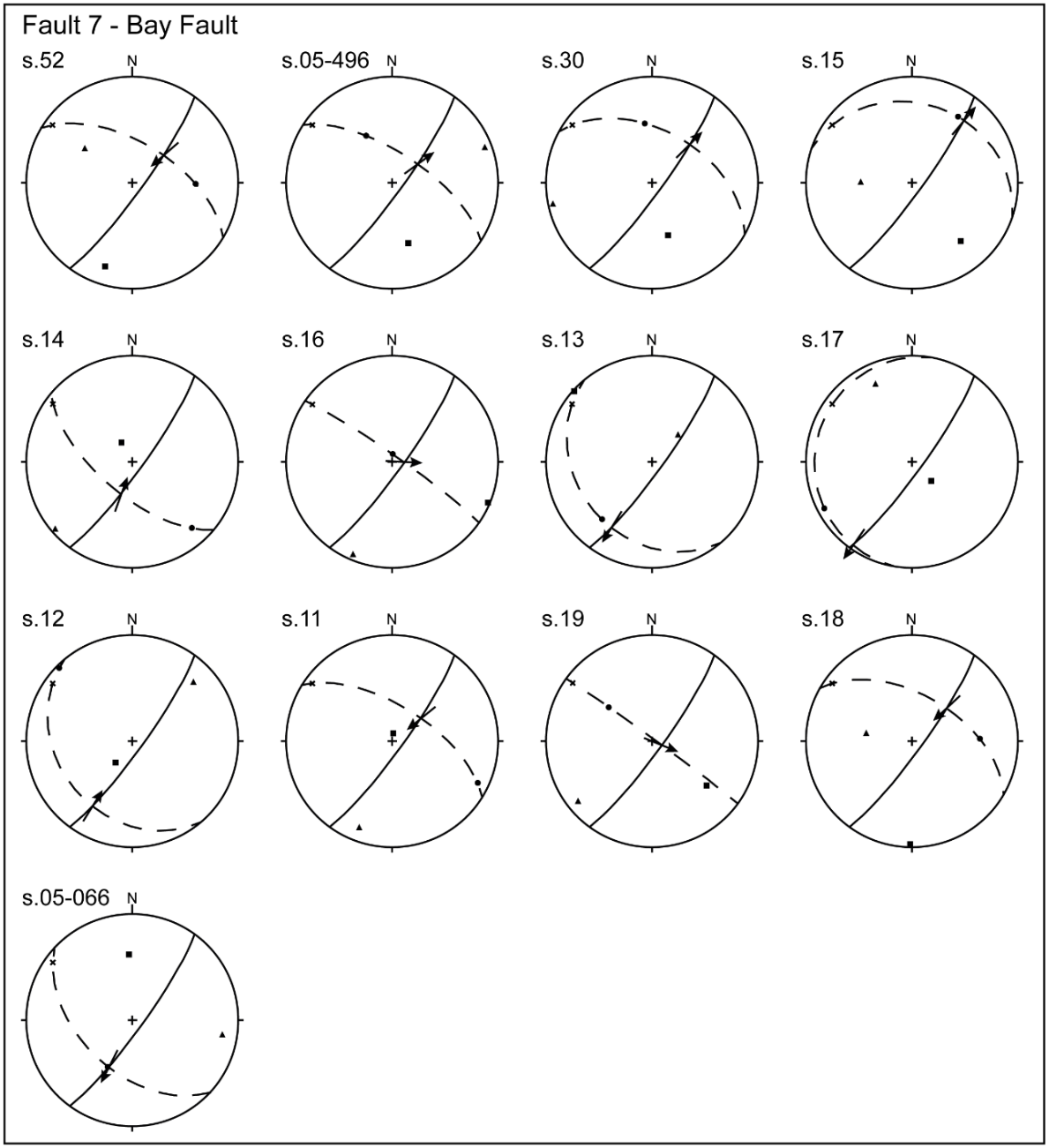
Fault 7 - Bay Fault
s.52
N
s.05-496
N
s.30
N
s.15
N
s.14
N
s.16
N
s.13
N
s.17
N
s.12
N
s.11
N
s.19
N
s.18
N
s.05-066
N

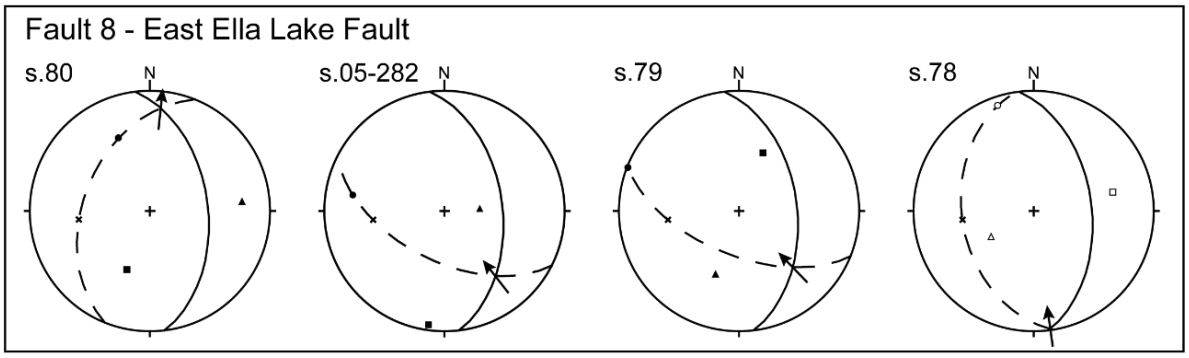
Fault 8 - East Ella Lake Fault
s.80
N
s.05-282
N
s.79
N
s.78
N

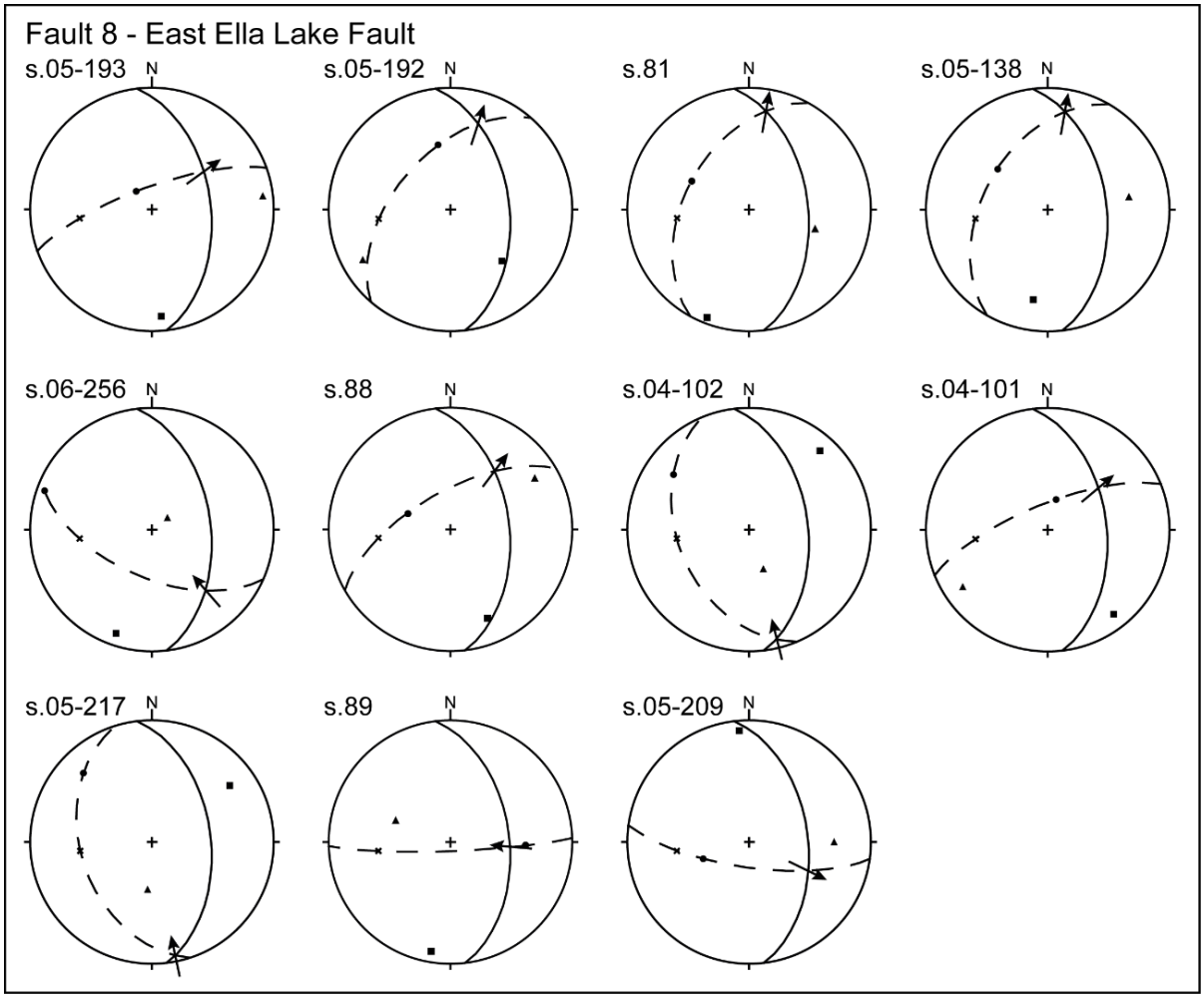
Fault 8 - East Ella Lake Fault
s.05-193
s.05-192
s.81
s.05-138
s.06-256
s.88
s.04-102
s.04-101
s.05-217
s.89
s.05-209
N

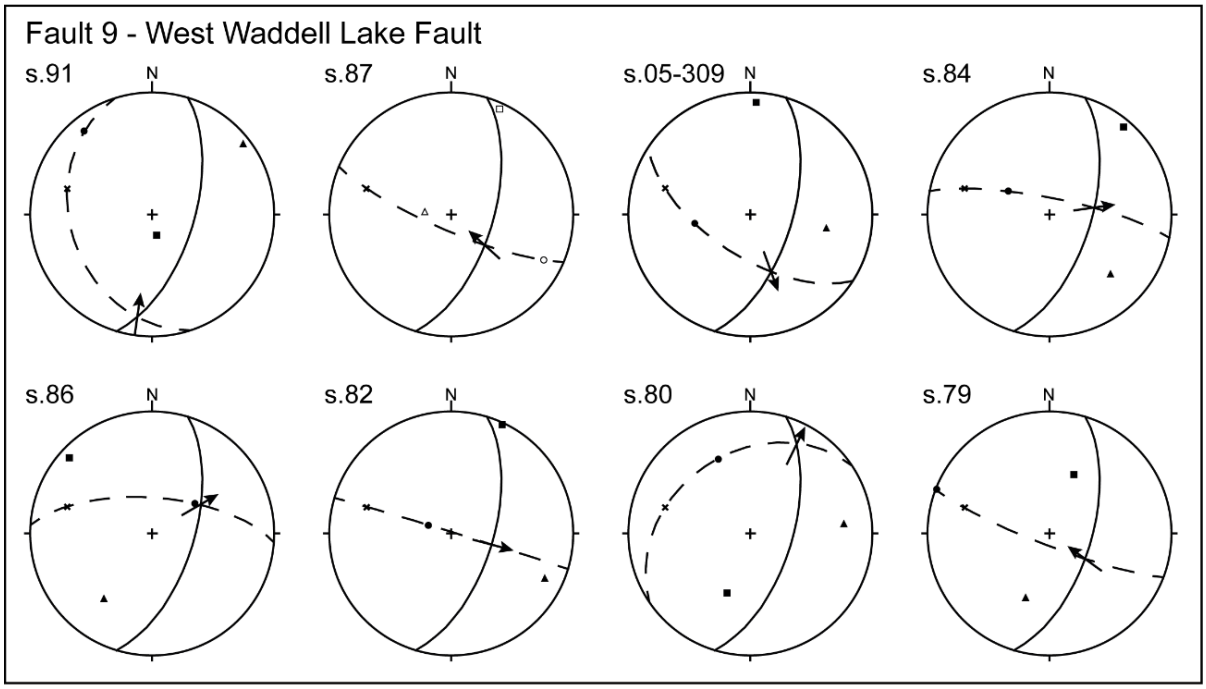
Fault 9 - West Waddell Lake Fault
s.91
s.87
s.05-309
s.84
s.86
s.82
s.80
s.79
N

Fault 9 - West Waddell Lake Fault

s.78

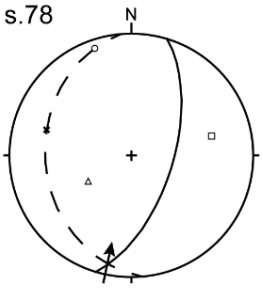

Fault 13 - Eatlots Lake Fault

s.05-385

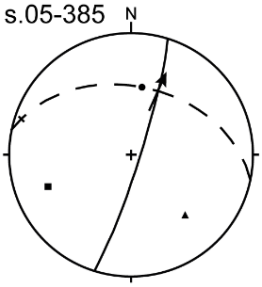

s.92

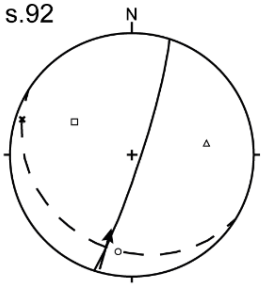

Fault 14 - East Waddell Lake Fault

s.90

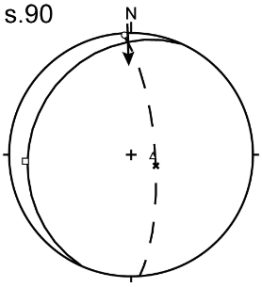

s.91

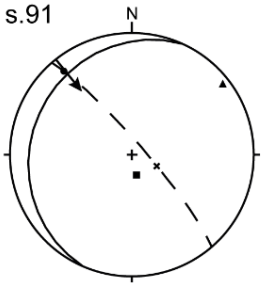

s.05-309

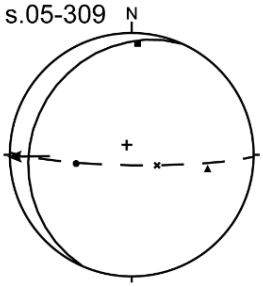

s.84

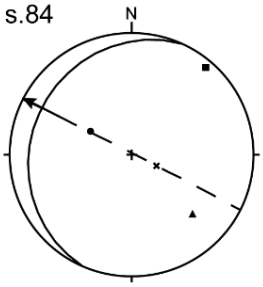

s.82

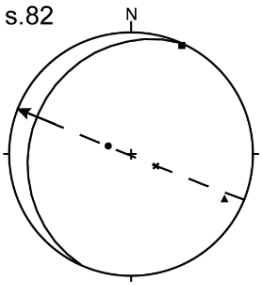

s.80

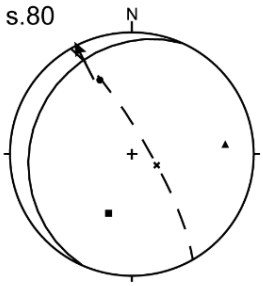

s.79

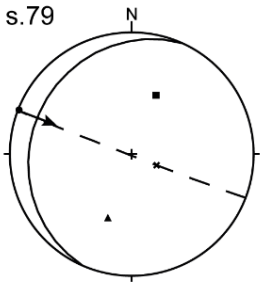

s.78

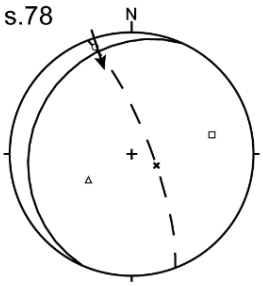

Fault 15 - West Ella Lake Fault

s.79

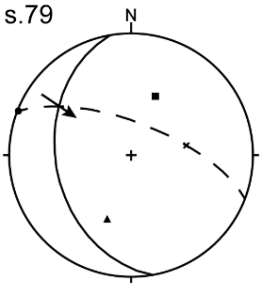

s.78

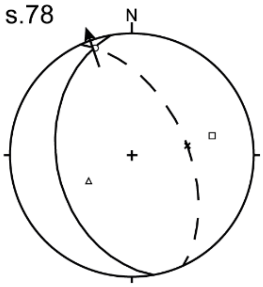

s.06-256

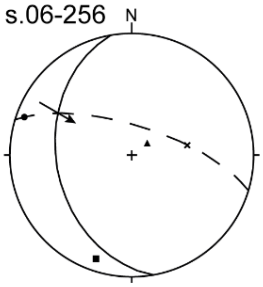

s.04-101

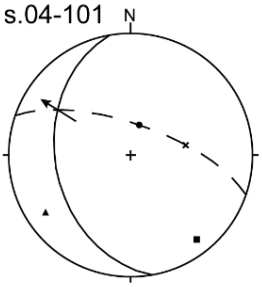

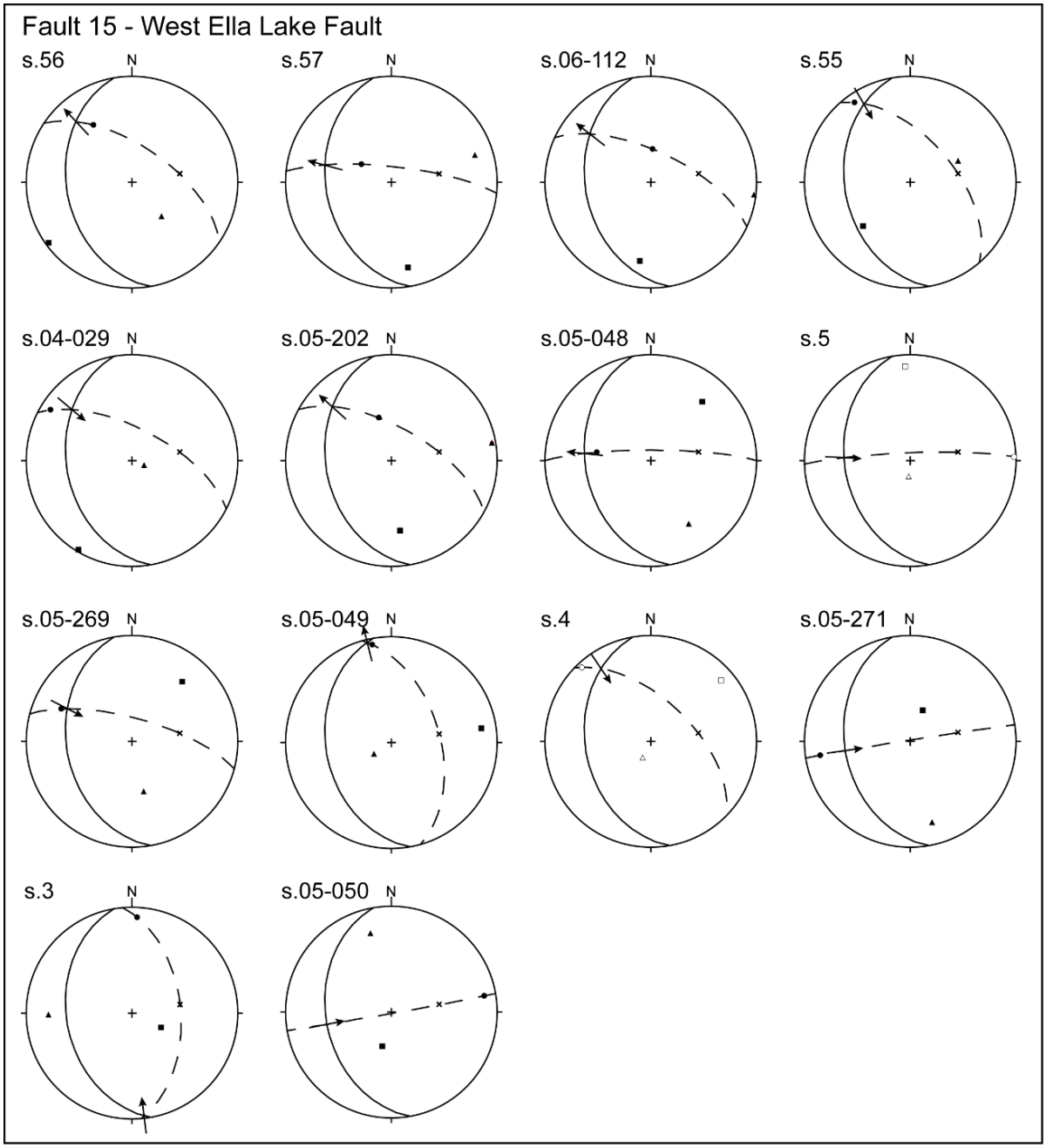

*Displayed are slip vectors on all fault surfaces (solid great circles) calculated using the projection path (dashed great circles) through the shortening direction (point) pole of the fault surface (crosses). Open symbols indicate principal paleostress axes and solid symbols indicate principal strain axes.

Appendix Table 1: Field collected brittle faults for fault-slip analysis.

Abbreviation of slip sense are: 0: unknown, 1: reverse, 2: normal. Abbreviation for certainty are: 1: obvious, 2: confident, 3: semi-confident, 4: unreliable or unknown. Abbreviations of mineralizations are: Epid: Epidote, FeO: Iron Oxide, FeEpid: Iron coated epidote, FeMin: Iron coated unknown mineral, Chl: Chlorite, FeChl: Iron coated Chlorite, Qz: Quartz.

Station ID	Easting NAD27	Northing NAD27	Accuracy (+/-m)	Datum	Fault Dip Direction	Fault Dip	Lineation Azimuth	Lineation Plunge	Sense	Certainty	Mineral
1a	511586	5168667	5	NAD27	030	57	310	29	2	2	No data
1a	511586	5168667	5	NAD27	044	40	150	04	2	2	No data
1a	511586	5168667	5	NAD27	038	52	306	15	0	4	No data
1a	511586	5168667	5	NAD27	078	38	152	15	1	3	No data
1a	511586	5168667	5	NAD27	099	58	158	40	1	1	No data
1a	511586	5168667	5	NAD27	112	35	196	05	1	3	No data
1a	511586	5168667	5	NAD27	104	45	141	43	1	2	No data
1a	511586	5168667	5	NAD27	040	32	010	12	2	3	No data
1a	511586	5168667	5	NAD27	062	47	346	25	1	3	No data
1a	511586	5168667	5	NAD27	016	43	342	25	0	4	No data
1a	511586	5168667	5	NAD27	091	49	194	22	1	1	No data
1b	511577	5168672	9	NAD27	082	60	171	33	1	1	No data
1b	511577	5168672	9	NAD27	092	80	189	44	1	3	No data
1b	511577	5168672	9	NAD27	088	48	159	42	1	3	No data
1b	511577	5168672	9	NAD27	061	47	158	21	1	3	No data
1b	511577	5168672	9	NAD27	109	60	173	35	1	2	No data
1b	511577	5168672	9	NAD27	339	74	064	24	1	2	No data
1b	511577	5168672	9	NAD27	150	71	063	21	1	1	No data
1b	511577	5168672	9	NAD27	078	45	152	43	1	3	No data
1b	511577	5168672	9	NAD27	036	32	306	10	1	2	No data
1c	511567	5168674	9	NAD27	042	39	327	15	0	4	No data
1c	511567	5168674	9	NAD27	092	52	184	41	1	2	No data
1c	511567	5168674	9	NAD27	014	48	280	40	1	3	No data
1c	511567	5168674	9	NAD27	090	62	148	34	2	1	No data
1c	511567	5168674	9	NAD27	014	82	278	22	2	2	No data
1c	511567	5168674	9	NAD27	069	65	148	23	1	3	No data
1c	511567	5168674	9	NAD27	039	46	024	18	0	4	No data
2a	511253	5169001	5	NAD27	011	89	109	22	2	3	No data
2a	511253	5169001	5	NAD27	204	66	284	51	1	2	No data
2a	511253	5169001	5	NAD27	094	59	141	31	1	1	No data
2a	511253	5169001	5	NAD27	240	50	328	45	0	4	No data
2a	511253	5169001	5	NAD27	329	82	050	48	0	4	No data
2a	511253	5169001	5	NAD27	232	74	284	22	2	3	No data
2b	511226	5168886	4	NAD27	109	52	206	30	0	4	No data
3a	510561	5170441	6	NAD27	248	50	150	10	0	4	No data
3a	510561	5170441	6	NAD27	140	80	055	18	2	3	No data
3a	510561	5170441	6	NAD27	130	84	041	28	2	3	No data
3a	510561	5170441	6	NAD27	220	35	328	43	0	4	No data
3a	510561	5170441	6	NAD27	130	79	044	07	0	4	No data

Station ID	Easting NAD27	Northing NAD27	Accuracy (+/-m)	Datum	Fault Dip Direction	Fault Dip	Lineation Azimuth	Lineation Plunge	Sense	Certainty	Mineral
3a	510561	5170441	6	NAD27	031	47	346	37	1	2	No data
3a	510561	5170441	6	NAD27	029	48	339	34	1	1	No data
3a	510561	5170441	6	NAD27	024	49	303	31	1	3	No data
3b	510504	5170483	4	NAD27	014	55	323	46	0	4	No data
3b	510504	5170483	4	NAD27	134	82	049	35	2	3	No data
4a	510342	5170678	5	NAD27	140	78	050	39	2	1	No data
4a	510342	5170678	5	NAD27	135	81	055	34	2	2	No data
4a	510342	5170678	5	NAD27	117	78	208	42	2	3	No data
4a	510342	5170678	5	NAD27	278	45	348	28	1	2	No data
4a	510342	5170678	5	NAD27	182	60	250	30	1	1	FeEpid
4a	510342	5170678	5	NAD27	250	64	332	37	1	1	No data
4a	510342	5170678	5	NAD27	046	36	340	15	0	4	No data
4a	510342	5170678	5	NAD27	040	46	338	26	0	4	No data
4a	510342	5170678	5	NAD27	265	71	352	29	1	2	No data
4a	510342	5170678	5	NAD27	246	66	332	40	1	3	No data
4b	510325	5170723	5	NAD27	294	32	333	28	1	2	No data
4b	510325	5170723	5	NAD27	137	77	060	39	1	2	FeEpid
5a	509964	5171714	10	NAD27	248	78	342	25	1	2	No data
5a	509964	5171714	10	NAD27	100	65	016	57	0	4	No data
5b	509871	5171801	6	NAD27	325	88	222	25	1	2	No data
5b	509871	5171801	6	NAD27	151	82	232	20	1	3	No data
5b	509871	5171801	6	NAD27	182	78	260	24	2	3	No data
5b	509871	5171801	6	NAD27	348	50	265	36	1	3	No data
5b	509871	5171801	6	NAD27	188	80	276	24	0	4	No data
5c	509858	5171808	8	NAD27	020	45	309	43	1	3	No data
5c	509858	5171808	8	NAD27	118	61	050	26	0	4	No data
5c	509858	5171808	8	NAD27	264	87	352	20	0	4	No data
5c	509858	5171808	8	NAD27	112	89	016	18	0	4	No data
5c	509858	5171808	8	NAD27	040	30	057	28	0	4	No data
6	509625	5172212	7	NAD27	020	37	107	03	2	1	No data
6	509625	5172212	7	NAD27	357	47	282	36	2	1	No data
6	509625	5172212	7	NAD27	140	70	060	20	2	2	No data
6	509625	5172212	7	NAD27	001	45	328	35	1	3	No data
6	509625	5172212	7	NAD27	018	45	304	32	1	3	No data
6	509625	5172212	7	NAD27	210	45	330	30	2	1	No data
6	509625	5172212	7	NAD27	141	78	060	35	1	2	No data
6	509625	5172212	7	NAD27	130	79	052	10	2	2	No data
6	509625	5172212	7	NAD27	247	75	336	33	2	1	No data
6	509625	5172212	7	NAD27	124	78	040	23	1	2	No data
7a	509527	5172417	4	NAD27	160	62	234	28	0	4	No data
7a	509527	5172417	4	NAD27	172	70	248	28	0	4	No data
7a	509527	5172417	4	NAD27	184	70	266	20	0	4	No data
7a	509527	5172417	4	NAD27	186	65	264	24	0	4	No data

Station ID	Easting NAD27	Northing NAD27	Accuracy (+/-m)	Datum	Fault Dip Direction	Fault Dip	Lineation Azimuth	Lineation Plunge	Sense	Certainty	Mineral
7a	509527	5172417	4	NAD27	173	70	245	30	0	4	No data
7b	509475	5172508	6	NAD27	020	55	111	40	1	3	No data
7b	509475	5172508	6	NAD27	324	85	048	33	2	2	No data
7b	509475	5172508	6	NAD27	010	89	088	21	1	3	No data
7b	509475	5172508	6	NAD27	231	80	309	30	0	4	No data
7c	509438	5172577	6	NAD27	004	26	003	26	1	3	No data
7c	509438	5172577	6	NAD27	158	88	246	15	1	2	No data
7c	509438	5172577	6	NAD27	321	83	069	25	2	3	No data
7c	509438	5172577	6	NAD27	344	70	101	45	2	3	No data
7c	509438	5172577	6	NAD27	110	47	140	35	2	3	No data
8a	515481	5167699	5	NAD27	116	55	048	25	2	1	Epid
8a	515481	5167699	5	NAD27	128	70	050	17	2	1	Epid
8a	515481	5167699	5	NAD27	254	55	265	55	1	1	Epid
8a	515481	5167699	5	NAD27	256	08	258	04	2	2	No data
8b	515479	5167696	5	NAD27	255	55	168	40	2	3	Epid
8b	515479	5167696	5	NAD27	254	62	344	35	1	2	Epid
8b	515479	5167696	5	NAD27	240	76	337	25	1	3	Epid
8b	515479	5167696	5	NAD27	300	80	213	20	1	2	Epid
8b	515479	5167696	5	NAD27	209	26	151	20	1	2	FeO
8b	515479	5167696	5	NAD27	283	70	208	35	1	2	Epid
8b	515479	5167696	5	NAD27	293	66	203	62	1	2	FeO Epid
8b	515479	5167696	5	NAD27	236	38	134	10	1	1	Chl
8b	515479	5167696	5	NAD27	266	75	178	72	1	2	Epid
8b	515479	5167696	5	NAD27	271	60	356	20	1	2	Epid
8b	515479	5167696	5	NAD27	282	60	197	28	1	3	Epid
8b	515479	5167696	5	NAD27	044	35	082	29	1	2	Epid
8b	515479	5167696	5	NAD27	112	54	165	36	2	3	FeEpid
8b	515479	5167696	5	NAD27	183	24	148	20	1	2	FeEpid
8b	515479	5167696	5	NAD27	138	89	228	30	0	4	Epid
8b	515479	5167696	5	NAD27	134	89	228	40	2	3	Epid
8b	515479	5167696	5	NAD27	049	49	078	36	1	2	Epid
8b	515479	5167696	5	NAD27	063	39	090	34	0	4	Epid
8b	515479	5167696	5	NAD27	288	36	296	36	1	3	Epid
8b	515479	5167696	5	NAD27	288	70	013	32	1	1	Epid
8b	515479	5167696	5	NAD27	107	76	016	05	0	4	Epid
8b	515479	5167696	5	NAD27	284	62	206	36	0	4	Epid
8b	515479	5167696	5	NAD27	287	86	192	52	2	1	Epid
8b	515479	5167696	5	NAD27	161	31	150	20	1	3	Epid
not used	512142	5172217	6	NAD27	004	72	286	31	1	2	No data
9	512087	5172317	4	NAD27	247	29	262	28	1	2	Epid
9	512087	5172317	4	NAD27	105	31	128	31	2	2	Epid
9	512087	5172317	4	NAD27	280	36	244	32	0	4	Epid
9	512087	5172317	4	NAD27	287	51	220	30	1	1	Epid

Station ID	Easting NAD27	Northing NAD27	Accuracy (+/-m)	Datum	Fault Dip Direction	Fault Dip	Lineation Azimuth	Lineation Plunge	Sense	Certainty	Mineral
9	512087	5172317	4	NAD27	292	54	245	35	1	3	Epid
9	512087	5172317	4	NAD27	289	56	236	40	2	2	Epid
9	512087	5172317	4	NAD27	240	32	268	30	2	2	Epid
not used	512150	5171999	6	NAD27	326	89	230	07	1	3	Epid
10a	512126	5172104	8	NAD27	339	81	241	34	2	3	No data
10a	512126	5172104	8	NAD27	032	72	310	26	0	4	No data
10a	512126	5172104	8	NAD27	252	78	326	12	1	3	Epid
10a	512126	5172104	8	NAD27	148	85	052	41	0	4	No data
10a	512126	5172104	8	NAD27	134	25	210	05	2	3	No data
10a	512126	5172104	8	NAD27	232	65	332	28	0	4	No data
10b	512121	5172120	7	NAD27	048	46	321	32	2	3	Qz
not used	512147	5172239	5	NAD27	292	41	270	38	2	2	Epid
not used	512208	5172252	5	NAD27	040	40	087	28	0	4	No data
11	513324	5169294	7	NAD27	272	55	176	15	1	2	FeO
11	513324	5169294	7	NAD27	344	89	248	39	1	3	Epid
11	513324	5169294	7	NAD27	160	87	248	30	2	3	Epid
11	513324	5169294	7	NAD27	294	81	010	26	1	2	FeGouge
11	513324	5169294	7	NAD27	270	85	164	40	0	4	Gouge
11	513324	5169294	7	NAD27	222	23	166	14	1	2	FeEpid
11	513324	5169294	7	NAD27	295	51	001	15	2	2	FeEpid
11	513324	5169294	7	NAD27	266	86	173	06	1	3	FeGouge
11	513324	5169294	7	NAD27	131	46	190	30	2	2	FeMin
11	513324	5169294	7	NAD27	108	76	015	06	1	3	FeMin
11	513324	5169294	7	NAD27	164	88	184	22	0	4	FeO
11	513324	5169294	7	NAD27	270	25	252	22	2	3	FeEpid
11	513324	5169294	7	NAD27	150	89	231	32	1	3	Epid
11	513324	5169294	7	NAD27	302	86	205	02	0	4	FeGouge
11	513324	5169294	7	NAD27	152	79	242	25	2	3	Epid
11	513324	5169294	7	NAD27	232	35	334	19	1	3	Epid
11	513324	5169294	7	NAD27	243	78	161	10	2	3	Epid
11	513324	5169294	7	NAD27	101	76	198	10	2	3	Epid
11	513324	5169294	7	NAD27	152	89	066	54	0	4	Epid
11	513324	5169294	7	NAD27	356	80	258	22	2	3	Epid
11	513324	5169294	7	NAD27	274	75	198	19	0	4	FeO
11	513324	5169294	7	NAD27	110	48	198	05	1	3	FeO
12	513337	5169310	5	NAD27	049	44	118	19	1	3	FeMin
12	513337	5169310	5	NAD27	262	73	185	25	2	3	FeGouge
12	513337	5169310	5	NAD27	275	89	012	01	0	4	FeEpid
12	513337	5169310	5	NAD27	057	82	326	16	2	2	FeMin
12	513337	5169310	5	NAD27	302	75	021	20	1	2	FeMin
12	513337	5169310	5	NAD27	266	79	355	12	1	3	FeEpid
12	513337	5169310	5	NAD27	200	65	116	14	1	3	FeEpid
12	513337	5169310	5	NAD27	294	85	201	35	1	3	FeMin

Station ID	Easting NAD27	Northing NAD27	Accuracy (+/-m)	Datum	Fault Dip Direction	Fault Dip	Lineation Azimuth	Lineation Plunge	Sense	Certainty	Mineral
12	513337	5169310	5	NAD27	280	84	019	32	0	4	Epid
12	513337	5169310	5	NAD27	120	64	162	35	0	4	Epid
12	513337	5169310	5	NAD27	236	80	149	25	2	3	FeMin
12	513337	5169310	5	NAD27	241	62	148	25	2	3	FeMin
12	513337	5169310	5	NAD27	269	75	020	45	0	4	FeO
12	513337	5169310	5	NAD27	098	87	190	15	0	4	FeO Gouge
12	513337	5169310	5	NAD27	272	82	004	07	0	4	FeO Epid Gouge
12	513337	5169310	5	NAD27	239	85	334	15	2	3	FeMin
12	513337	5169310	5	NAD27	126	42	026	10	1	3	FeEpid
13	513342	5169316	5	NAD27	165	78	230	56	0	4	FeO
13	513342	5169316	5	NAD27	302	52	196	02	2	2	FeO
13	513342	5169316	5	NAD27	155	65	243	02	1	2	Epid
13	513342	5169316	5	NAD27	234	31	244	28	1	3	FeO
13	513342	5169316	5	NAD27	212	48	140	12	2	3	FeO
13	513342	5169316	5	NAD27	224	55	169	43	1	3	Epid
13	513342	5169316	5	NAD27	038	88	306	17	0	4	FeO Gouge
13	513342	5169316	5	NAD27	188	55	112	23	2	2	FeO
13	513342	5169316	5	NAD27	219	40	262	25	2	3	Epid
13	513342	5169316	5	NAD27	284	85	200	15	0	4	FeMin
13	513342	5169316	5	NAD27	278	55	230	42	1	3	FeO
13	513342	5169316	5	NAD27	109	80	022	05	0	4	FeO Gouge
13	513342	5169316	5	NAD27	340	55	257	45	0	4	FeO Min
13	513342	5169316	5	NAD27	347	55	257	45	0	4	FeO Min
13	513342	5169316	5	NAD27	248	52	170	20	1	3	FeO Epid
14a	513357	5169338	4	NAD27	030	40	092	12	2	3	FeO Epid
14a	513357	5169338	4	NAD27	119	40	209	02	0	4	FeMin
15a	513366	5169367	4	NAD27	085	86	354	31	1	3	FeO Gouge
15a	513366	5169367	4	NAD27	149	50	050	12	2	3	FeMin
15a	513366	5169367	4	NAD27	107	75	020	10	2	3	FeEpid
15a	513366	5169367	4	NAD27	304	83	208	31	1	3	FeO
15a	513366	5169367	4	NAD27	307	85	198	75	1	3	FeO
15a	513366	5169367	4	NAD27	096	75	027	42	0	4	FeMin
15a	513366	5169367	4	NAD27	096	64	024	25	0	4	FeMin
15a	513366	5169367	4	NAD27	001	28	110	03	0	4	FeMin
14b	513344	5169343	3	NAD27	345	46	264	21	0	4	Epid
14b	513344	5169343	3	NAD27	260	55	352	05	1	3	FeO
14b	513344	5169343	3	NAD27	276	79	002	20	1	2	FeO
14b	513344	5169343	3	NAD27	012	55	317	30	0	4	Epid
14b	513344	5169343	3	NAD27	240	85	118	29	2	3	FeMin
16	513328	5169326	3	NAD27	198	76	119	19	0	4	FeGouge
16	513328	5169326	3	NAD27	226	68	139	36	0	4	FeGouge
16	513328	5169326	3	NAD27	172	16	098	01	1	3	Epid
16	513328	5169326	3	NAD27	175	10	100	08	0	4	Epid

Station ID	Easting NAD27	Northing NAD27	Accuracy (+/-m)	Datum	Fault Dip Direction	Fault Dip	Lineation Azimuth	Lineation Plunge	Sense	Certainty	Mineral
16	513328	5169326	3	NAD27	148	18	109	14	1	3	Epid
16	513328	5169326	3	NAD27	320	14	285	05	2	1	FeEpid
16	513328	5169326	3	NAD27	322	23	300	20	2	3	Epid
16	513328	5169326	3	NAD27	018	42	092	05	0	4	Epid
16	513328	5169326	3	NAD27	342	80	240	35	0	4	Epid Gouge
16	513328	5169326	3	NAD27	212	35	137	10	2	2	FeO
16	513328	5169326	3	NAD27	200	62	316	12	0	4	FeMin
17	513317	5169310	4	NAD27	205	48	132	24	2	2	Epid
17	513317	5169310	4	NAD27	074	60	230	11	2	2	FeEpid
17	513317	5169310	4	NAD27	080	75	330	15	1	3	FeEpid
17	513317	5169310	4	NAD27	109	77	187	25	0	4	FeEpid Gouge
17	513317	5169310	4	NAD27	170	70	202	57	0	4	FeEpid
17	513317	5169310	4	NAD27	130	50	284	35	2	3	FeEpid
18	513284	5169140	6	NAD27	266	34	286	31	0	4	Epid
18	513284	5169140	6	NAD27	298	40	284	38	0	4	Epid
18	513284	5169140	6	NAD27	232	28	270	24	0	4	FeGouge
18	513284	5169140	6	NAD27	270	76	338	54	0	4	Epid
18	513284	5169140	6	NAD27	284	75	298	74	2	2	Epid
18	513284	5169140	6	NAD27	255	69	269	66	2	3	Epid
18	513284	5169140	6	NAD27	272	66	296	64	2	1	Epid
18	513284	5169140	6	NAD27	334	20	266	07	0	4	Epid
18	513284	5169140	6	NAD27	259	66	284	64	0	4	Epid
18	513284	5169140	6	NAD27	272	55	184	52	0	4	Epid
not used	513507	5169124	8	NAD27	331	46	262	26	0	4	Epid
not used	513507	5169124	8	NAD27	339	50	271	30	2	3	FeEpid
not used	513507	5169124	8	NAD27	075	40	318	20	0	4	FeEpid
not used	513449	5169151	8	NAD27	150	25	190	19	1	1	Chl
19	513388	5169252	3	NAD27	214	56	256	43	2	2	Gouge
19	513388	5169252	3	NAD27	240	60	276	55	0	4	FeEpid Gouge
19	513388	5169252	3	NAD27	230	50	259	40	2	3	Epid
19	513388	5169252	3	NAD27	158	55	227	32	0	4	Epid
19	513388	5169252	3	NAD27	086	45	160	30	1	3	FeO
15b	513381	5169382	4	NAD27	014	42	294	19	2	1	Epid
15b	513381	5169382	4	NAD27	259	66	278	07	0	4	FeO
15b	513381	5169382	4	NAD27	009	50	290	11	2	3	FeO
15b	513381	5169382	4	NAD27	125	69	041	03	0	4	Gouge
20a	512424	5171918	8	NAD27	220	81	303	48	0	4	Epid
20a	512424	5171918	8	NAD27	029	74	302	01	0	4	FeO Gouge
20a	512424	5171918	8	NAD27	340	65	262	65	1	3	Epid
20b	512527	5171895	5	NAD27	110	45	159	35	2	3	FeO
20b	512527	5171895	5	NAD27	040	35	348	07	2	3	Epid
21	512244	5171780	4	NAD27	025	45	350	23	1	1	FeMin
21	512244	5171780	4	NAD27	344	55	279	37	1	1	FeMin

Station ID	Easting NAD27	Northing NAD27	Accuracy (+/-m)	Datum	Fault Dip Direction	Fault Dip	Lineation Azimuth	Lineation Plunge	Sense	Certainty	Mineral
21	512244	5171780	4	NAD27	021	51	312	25	1	1	Chl
21	512244	5171780	4	NAD27	011	56	294	35	0	4	FeGouge
22a	512362	5171920	9	NAD27	030	49	308	01	2	1	No data
22a	512362	5171920	9	NAD27	046	59	126	03	1	3	Epid
22a	512362	5171920	9	NAD27	322	80	238	25	1	2	Epid
22a	512362	5171920	9	NAD27	142	88	224	21	2	3	No data
22a	512362	5171920	9	NAD27	349	68	274	29	1	2	Epid
22a	512362	5171920	9	NAD27	345	81	265	30	1	1	FeMin
22b	512355	5171931	10	NAD27	335	81	258	21	1	2	FeMin
22b	512355	5171931	10	NAD27	123	80	221	08	2	2	FeMin
22b	512355	5171931	10	NAD27	011	58	294	44	1	3	FeMin
22c	512362	5171947	10	NAD27	357	85	269	58	1	3	Epid
23a	512474	5171616	5	NAD27	310	86	228	42	1	2	Epid
23a	512474	5171616	5	NAD27	336	58	240	15	0	4	Epid
23a	512474	5171616	5	NAD27	326	59	291	54	1	3	Epid
23a	512474	5171616	5	NAD27	300	70	242	65	0	4	Epid
not used	515124	5171594	4	NAD27	155	85	250	25	1	3	Epid
not used	515124	5171594	4	NAD27	221	72	301	60	2	2	Epid Chl
not used	515124	5171594	4	NAD27	250	62	157	11	2	2	Epid Chl
not used	515124	5171594	4	NAD27	004	89	282	40	1	2	FeEpid
23b	512496	5171583	7	NAD27	194	84	226	46	0	4	FeChl
23b	512496	5171583	7	NAD27	005	85	287	40	1	2	FeEpid
23b	512496	5171583	7	NAD27	357	85	267	40	1	3	FeEpid
not used	512591	5171459	4	NAD27	039	34	350	33	2	3	FeEpid
not used	512591	5171459	4	NAD27	032	87	302	44	1	3	FeEpid
23c	512456	5171579	7	NAD27	020	46	063	36	1	3	Epid
24a	512393	5171569	5	NAD27	340	80	250	15	2	3	FeChl
24a	512393	5171569	5	NAD27	342	84	255	05	2	1	FeChl
24b	512327	5171552	12	NAD27	336	64	250	36	1	1	FeMin
24b	512327	5171552	12	NAD27	021	50	105	33	1	1	FeMin
24b	512327	5171552	12	NAD27	350	45	266	42	1	3	FeMin
24b	512327	5171552	12	NAD27	042	40	116	11	1	1	FeMin
24b	512327	5171552	12	NAD27	333	53	250	23	1	2	FeMin
25	512303	5171861	6	NAD27	192	40	104	10	1	2	Epid
25	512303	5171861	6	NAD27	032	45	312	43	2	3	FeMin
25	512303	5171861	6	NAD27	063	53	161	21	1	2	Qz
25	512303	5171861	6	NAD27	062	55	130	15	1	3	No data
25	512303	5171861	6	NAD27	109	40	180	35	1	2	Qz
not used	512193	5171737	6	NAD27	019	86	110	26	0	4	Epid
not used	512193	5171737	6	NAD27	259	66	168	05	0	4	FeGouge
26	512171	5171860	8	NAD27	099	31	149	14	2	3	FeMin Epid
26	512171	5171860	8	NAD27	003	55	276	42	1	1	FeMin
26	512171	5171860	8	NAD27	296	30	294	25	1	1	FeMin

Station ID	Easting NAD27	Northing NAD27	Accuracy (+/-m)	Datum	Fault Dip Direction	Fault Dip	Lineation Azimuth	Lineation Plunge	Sense	Certainty	Mineral
26	512171	5171860	8	NAD27	270	30	279	26	1	2	FeMin
26	512171	5171860	8	NAD27	266	33	295	31	1	1	FeMin
26	512171	5171860	8	NAD27	325	52	274	47	2	2	FeMin
26	512171	5171860	8	NAD27	254	77	155	55	2	2	FeMin
26	512171	5171860	8	NAD27	288	74	200	60	1	3	Epid
26	512171	5171860	8	NAD27	159	82	255	35	0	4	Epid
27a	512104	5171799	4	NAD27	183	29	260	05	1	3	FeEpid
27a	512104	5171799	4	NAD27	293	61	307	59	2	3	FeMin
27a	512104	5171799	4	NAD27	325	43	279	20	1	2	FeMin
27a	512104	5171799	4	NAD27	021	44	330	18	0	4	FeMin
27a	512104	5171799	4	NAD27	356	76	258	35	1	2	FeEpid
27a	512104	5171799	4	NAD27	294	55	290	53	1	3	FeMin
27a	512104	5171799	4	NAD27	276	40	273	30	2	3	FeMin
27a	512104	5171799	4	NAD27	296	58	289	54	2	3	FeMin
27b	512099	5171758	6	NAD27	345	64	282	34	0	4	FeMin
28	512232	5171616	5	NAD27	039	60	317	45	1	2	FeMin
28	512232	5171616	5	NAD27	341	46	271	43	2	2	FeMin
28	512232	5171616	5	NAD27	027	55	327	35	1	2	FeMin
28	512232	5171616	5	NAD27	008	40	296	39	1	3	FeEpid
28	512232	5171616	5	NAD27	016	64	300	36	1	1	FeEpid
28	512232	5171616	5	NAD27	239	66	302	45	1	1	FeMin
28	512232	5171616	5	NAD27	003	59	296	48	2	2	FeMin
28	512232	5171616	5	NAD27	355	62	284	41	1	2	FeMin
28	512232	5171616	5	NAD27	356	65	285	40	1	1	FeMin
28	512232	5171616	5	NAD27	346	52	284	45	1	3	FeMin
28	512232	5171616	5	NAD27	091	79	019	19	2	2	FeMin
28	512232	5171616	5	NAD27	105	85	023	28	2	1	FeMin
28	512232	5171616	5	NAD27	076	86	352	22	2	1	FeMin
28	512232	5171616	5	NAD27	096	77	178	26	1	2	FeMin
29a	513808	5169570	5	NAD27	111	21	092	20	0	4	FeEpid
30a	513894	5169503	4	NAD27	167	46	233	20	0	4	FeEpid
30a	513894	5169503	4	NAD27	247	61	265	54	0	4	FeEpid
30a	513894	5169503	4	NAD27	242	76	314	49	0	4	Epid
30a	513894	5169503	4	NAD27	218	64	277	32	2	2	FeMin
30a	513894	5169503	4	NAD27	233	62	288	25	2	2	FeMin
30a	513894	5169503	4	NAD27	207	69	285	46	2	2	FeEpid
30a	513894	5169503	4	NAD27	203	65	290	28	2	2	FeMin
30a	513894	5169503	4	NAD27	236	55	281	31	2	2	FeMin
30a	513894	5169503	4	NAD27	242	66	319	33	2	2	Epid
30a	513894	5169503	4	NAD27	208	65	291	19	2	2	FeEpid
30a	513894	5169503	4	NAD27	222	63	302	21	2	2	FeMin
30a	513894	5169503	4	NAD27	214	59	268	43	2	2	FeEpid
30a	513894	5169503	4	NAD27	215	38	275	28	2	2	FeMin

Station ID	Easting NAD27	Northing NAD27	Accuracy (+/-m)	Datum	Fault Dip Direction	Fault Dip	Lineation Azimuth	Lineation Plunge	Sense	Certainty	Mineral
30a	513894	5169503	4	NAD27	224	43	275	39	2	2	FeEpid
30a	513894	5169503	4	NAD27	131	44	047	06	0	4	FeMin
30a	513894	5169503	4	NAD27	092	82	358	34	1	1	FeEpid
30a	513894	5169503	4	NAD27	080	46	024	22	2	3	Epid
30b	513908	5169502	3	NAD27	077	29	044	24	0	4	Epid
30b	513908	5169502	3	NAD27	123	85	216	05	0	4	No data
30b	513908	5169502	3	NAD27	073	61	349	49	2	3	FeEpid
30b	513908	5169502	3	NAD27	053	44	039	35	0	4	Epid
30b	513908	5169502	3	NAD27	058	72	337	54	0	4	Epid
30b	513908	5169502	3	NAD27	128	62	138	54	2	3	FeMin
30b	513908	5169502	3	NAD27	136	58	112	55	2	3	FeMin
30b	513908	5169502	3	NAD27	260	80	359	40	2	2	FeMin
30b	513908	5169502	3	NAD27	162	46	092	30	1	2	FeEpid
30b	513908	5169502	3	NAD27	142	54	057	03	2	1	FeMin
30b	513908	5169502	3	NAD27	113	55	040	24	2	1	FeMin
30b	513908	5169502	3	NAD27	120	54	047	22	2	1	FeMin
30c	513915	5169519	3	NAD27	076	62	001	28	2	3	FeMin
30c	513915	5169519	3	NAD27	084	35	167	04	1	2	Epid
30c	513915	5169519	3	NAD27	066	69	055	54	2	3	FeMin
30c	513915	5169519	3	NAD27	076	80	352	31	0	4	Epid
30c	513915	5169519	3	NAD27	263	58	313	42	0	4	Epid
30c	513915	5169519	3	NAD27	281	82	189	31	0	4	FeEpid
30c	513915	5169519	3	NAD27	263	74	170	09	0	4	No data
30c	513915	5169519	3	NAD27	038	76	322	40	2	3	FeMin
30c	513915	5169519	3	NAD27	048	66	350	46	1	2	FeMin Epid
30c	513915	5169519	3	NAD27	127	64	204	35	0	4	Epid
30c	513915	5169519	3	NAD27	032	60	314	29	1	2	FeMin
30c	513915	5169519	3	NAD27	088	55	024	34	1	1	Epid
30c	513915	5169519	3	NAD27	082	55	017	31	1	1	Epid
30c	513915	5169519	3	NAD27	117	70	192	20	2	2	FeEpid
30c	513915	5169519	3	NAD27	171	41	215	17	1	2	FeMin
30c	513915	5169519	3	NAD27	126	57	038	08	2	2	FeMin
30c	513915	5169519	3	NAD27	150	28	040	10	2	2	FeMin
30c	513915	5169519	3	NAD27	061	69	341	22	1	1	FeMin
31a	513809	5168688	3	NAD27	100	79	198	28	2	2	FeEpid
31a	513809	5168688	3	NAD27	325	88	236	44	1	2	FeEpid
31a	513809	5168688	3	NAD27	237	34	334	01	1	3	FeEpid
31a	513809	5168688	3	NAD27	245	05	158	01	1	1	FeChl
31a	513809	5168688	3	NAD27	141	64	192	59	2	3	FeChl
31b	513812	5168735	4	NAD27	278	24	243	18	1	2	Epid
31b	513812	5168735	4	NAD27	185	29	262	05	1	3	FeEpid
31c	513827	5168704	5	NAD27	105	62	167	36	2	1	No data
31c	513827	5168704	5	NAD27	056	31	140	11	0	4	No data

Station ID	Easting NAD27	Northing NAD27	Accuracy (+/-m)	Datum	Fault Dip Direction	Fault Dip	Lineation Azimuth	Lineation Plunge	Sense	Certainty	Mineral
31c	513827	5168704	5	NAD27	132	78	194	48	0	4	No data
31d	513822	5168702	4	NAD27	238	41	324	09	2	2	No data
31d	513822	5168702	4	NAD27	263	60	278	43	1	1	No data
31d	513822	5168702	4	NAD27	279	43	255	30	0	4	No data
31d	513822	5168702	4	NAD27	305	84	125	48	1	2	No data
31d	513822	5168702	4	NAD27	132	60	026	20	2	3	No data
32	514295	5169862	n/a coordinates extracted from airphoto	NAD27	307	84	043	25	0	4	FeMin
32	514295	5169862	n/a coordinates extracted from airphoto	NAD27	130	80	051	40	2	2	FeMin
32	514295	5169862	n/a coordinates extracted from airphoto	NAD27	310	87	056	43	1	2	FeMin
32	514295	5169862	n/a coordinates extracted from airphoto	NAD27	139	82	070	35	2	2	FeEpid
32	514295	5169862	n/a coordinates extracted from airphoto	NAD27	169	40	160	25	2	3	FeO
32	514295	5169862	n/a coordinates extracted from airphoto	NAD27	348	55	062	15	1	3	Epid
32	514295	5169862	n/a coordinates extracted from airphoto	NAD27	066	20	125	10	2	2	FeEpid
32	514295	5169862	n/a coordinates extracted from airphoto	NAD27	056	55	117	23	2	2	FeMin
32	514295	5169862	n/a coordinates extracted from airphoto	NAD27	120	20	150	15	2	3	FeMin
8c	515496	5167684	4	NAD27	031	40	326	20	1	1	FeChl
8c	515496	5167684	4	NAD27	009	27	340	17	1	1	FeEpid
8c	515496	5167684	4	NAD27	349	35	314	33	1	2	FeMin
8c	515496	5167684	4	NAD27	342	30	317	29	1	3	FeEpid Gouge
8c	515496	5167684	4	NAD27	310	10	312	09	1	2	FeEpid
8c	515496	5167684	4	NAD27	348	40	308	29	0	4	FeMin
8c	515496	5167684	4	NAD27	010	25	312	15	1	1	FeEpid
8c	515496	5167684	4	NAD27	001	28	308	15	1	2	FeMin
8c	515496	5167684	4	NAD27	032	25	322	14	1	2	FeEpid
8c	515496	5167684	4	NAD27	051	39	327	01	1	1	FeEpid
8c	515496	5167684	4	NAD27	304	19	328	14	1	1	Epid
8c	515496	5167684	4	NAD27	307	27	327	25	1	2	FeEpid
8c	515496	5167684	4	NAD27	274	35	253	34	1	2	FeEpid
8c	515496	5167684	4	NAD27	347	32	335	30	1	1	FeMin
8c	515496	5167684	4	NAD27	354	29	330	28	1	3	FeMin
8c	515496	5167684	4	NAD27	024	35	323	22	1	1	FeMin
8c	515496	5167684	4	NAD27	033	30	340	22	1	1	FeMin
8c	515496	5167684	4	NAD27	108	07	076	05	1	2	FeMin Gouge
8c	515496	5167684	4	NAD27	012	20	337	11	1	1	FeEpid
8c	515496	5167684	4	NAD27	270	16	253	12	0	4	FeMin
8c	515496	5167684	4	NAD27	234	40	243	38	1	1	FeMin

Station ID	Easting NAD27	Northing NAD27	Accuracy (+/-m)	Datum	Fault Dip Direction	Fault Dip	Lineation Azimuth	Lineation Plunge	Sense	Certainty	Mineral
8c	515496	5167684	4	NAD27	045	21	040	19	1	1	FeMin
8c	515496	5167684	4	NAD27	019	19	064	15	0	4	FeEpid
8c	515496	5167684	4	NAD27	025	22	035	19	1	1	Chl
8c	515496	5167684	4	NAD27	333	22	345	22	1	1	FeChl
8c	515496	5167684	4	NAD27	294	25	289	23	2	3	FeMin
8c	515496	5167684	4	NAD27	334	37	333	36	1	2	FeChl
8c	515496	5167684	4	NAD27	317	25	250	18	1	2	FeEpid
8d	515485	5167672	9	NAD27	326	37	320	34	1	1	FeChl
8d	515485	5167672	9	NAD27	235	35	344	30	1	2	FeEpid
8d	515485	5167672	9	NAD27	345	24	326	22	1	1	FeChl
8d	515485	5167672	9	NAD27	270	75	174	28	0	4	Epid Gouge
8d	515485	5167672	9	NAD27	090	35	117	30	1	1	Epid
8d	515485	5167672	9	NAD27	281	41	280	39	1	1	Epid
8d	515485	5167672	9	NAD27	326	26	318	25	1	2	FeChl
8d	515485	5167672	9	NAD27	144	65	217	25	2	1	Epid
8d	515485	5167672	9	NAD27	116	55	196	16	2	1	Epid
8d	515485	5167672	9	NAD27	330	88	240	09	1	2	Epid
8d	515485	5167672	9	NAD27	335	35	312	31	1	3	FeEpid
8d	515485	5167672	9	NAD27	261	30	291	27	1	1	FeChl
8d	515485	5167672	9	NAD27	054	34	084	09	1	1	FeEpid
8d	515485	5167672	9	NAD27	232	30	230	25	1	2	FeMin
8d	515485	5167672	9	NAD27	328	35	338	30	1	1	Epid
8d	515485	5167672	9	NAD27	031	40	075	28	1	2	Epid
8d	515485	5167672	9	NAD27	136	85	220	10	1	2	FeMin
8d	515485	5167672	9	NAD27	320	34	332	28	1	3	Epid
8d	515485	5167672	9	NAD27	243	32	237	27	1	2	FeMin
8d	515485	5167672	9	NAD27	286	48	018	09	2	2	Epid
8d	515485	5167672	9	NAD27	292	60	354	38	2	2	FeMin
8d	515485	5167672	9	NAD27	288	50	306	40	1	3	FeEpid
8d	515485	5167672	9	NAD27	305	45	345	40	1	3	FeEpid
8d	515485	5167672	9	NAD27	199	34	135	15	1	1	FeEpid
8d	515485	5167672	9	NAD27	272	65	212	55	1	2	FeMin
8d	515485	5167672	9	NAD27	309	35	318	29	1	1	Epid
8d	515485	5167672	9	NAD27	260	32	236	30	1	1	FeChl
8d	515485	5167672	9	NAD27	276	34	247	30	1	1	FeChl
8d	515485	5167672	9	NAD27	338	30	340	28	1	1	FeMin
8d	515485	5167672	9	NAD27	206	38	160	25	1	1	FeEpid
8d	515485	5167672	9	NAD27	236	34	198	30	1	2	FeEpid
8d	515485	5167672	9	NAD27	276	80	190	44	1	2	Epid
8d	515485	5167672	9	NAD27	014	43	338	34	1	1	FeEpid
8d	515485	5167672	9	NAD27	345	30	307	25	1	3	Epid
33	514001	5169523	6	NAD27	113	16	028	03	1	3	Epid
33	514001	5169523	6	NAD27	134	59	055	23	1	3	Epid

Station ID	Easting NAD27	Northing NAD27	Accuracy (+/-m)	Datum	Fault Dip Direction	Fault Dip	Lineation Azimuth	Lineation Plunge	Sense	Certainty	Mineral
33	514001	5169523	6	NAD27	120	48	040	05	1	2	FeMin
33	514001	5169523	6	NAD27	104	42	026	11	1	1	FeMin
33	514001	5169523	6	NAD27	110	56	035	23	1	2	FeMin
33	514001	5169523	6	NAD27	146	26	140	21	1	3	Epid
33	514001	5169523	6	NAD27	131	64	116	56	1	3	Epid
33	514001	5169523	6	NAD27	156	60	123	51	1	3	FeMin
33	514001	5169523	6	NAD27	139	34	030	07	2	2	FeMin
33	514001	5169523	6	NAD27	164	40	132	40	2	2	FeMin
33	514001	5169523	6	NAD27	113	57	036	13	1	1	FeMin
33	514001	5169523	6	NAD27	165	77	086	75	1	2	FeO Epid
33	514001	5169523	6	NAD27	158	55	160	46	2	3	FeMin
33	514001	5169523	6	NAD27	138	21	150	20	1	2	FeEpid
33	514001	5169523	6	NAD27	160	46	155	31	1	3	FeEpid
33	514001	5169523	6	NAD27	160	37	158	37	2	3	FeMin
33	514001	5169523	6	NAD27	158	44	139	39	1	2	FeMin
33	514001	5169523	6	NAD27	162	49	162	47	2	3	FeMin
33	514001	5169523	6	NAD27	170	49	156	41	2	1	FeEpid
33	514001	5169523	6	NAD27	153	36	156	21	2	1	FeEpid
33	514001	5169523	6	NAD27	161	50	154	30	2	1	FeEpid
33	514001	5169523	6	NAD27	176	60	158	60	2	1	FeMin
33	514001	5169523	6	NAD27	123	45	155	41	2	3	FeMin
33	514001	5169523	6	NAD27	141	58	135	51	2	3	FeMin
33	514001	5169523	6	NAD27	153	48	071	24	2	2	FeMin
33	514001	5169523	6	NAD27	121	66	048	37	1	3	FeEpid
33	514001	5169523	6	NAD27	226	30	142	15	1	3	FeEpid
33	514001	5169523	6	NAD27	224	19	149	10	1	3	FeEpid
33	514001	5169523	6	NAD27	160	53	127	42	2	3	FeEpid
33	514001	5169523	6	NAD27	174	32	148	31	2	2	FeEpid
34	513989	5169488	4	NAD27	148	65	112	57	2	3	FeMin
34	513989	5169488	4	NAD27	116	72	036	18	2	3	FeMin
34	513989	5169488	4	NAD27	308	85	216	51	1	1	FeEpid
34	513989	5169488	4	NAD27	186	40	135	31	1	2	FeMin
34	513989	5169488	4	NAD27	204	41	167	36	2	2	FeMin
34	513989	5169488	4	NAD27	133	60	191	43	1	3	FeEpid
34	513989	5169488	4	NAD27	186	64	120	52	2	1	FeMin
34	513989	5169488	4	NAD27	146	71	135	70	2	2	FeMin
34	513989	5169488	4	NAD27	100	59	040	41	1	2	FeEpid
34	513989	5169488	4	NAD27	137	71	145	67	2	2	FeEpid
34	513989	5169488	4	NAD27	068	66	037	57	1	2	Epid
34	513989	5169488	4	NAD27	186	55	135	39	2	3	FeEpid
34	513989	5169488	4	NAD27	114	84	195	49	2	2	Epid
34	513989	5169488	4	NAD27	122	75	212	30	2	1	FeEpid
34	513989	5169488	4	NAD27	193	36	133	22	1	2	FeMin

Station ID	Easting NAD27	Northing NAD27	Accuracy (+/-m)	Datum	Fault Dip Direction	Fault Dip	Lineation Azimuth	Lineation Plunge	Sense	Certainty	Mineral
34	513989	5169488	4	NAD27	056	40	096	35	1	2	FeMin
34	513989	5169488	4	NAD27	163	63	114	45	2	3	FeEpid
34	513989	5169488	4	NAD27	180	64	137	36	2	3	FeMin
34	513989	5169488	4	NAD27	177	56	166	44	2	3	FeMin
34	513989	5169488	4	NAD27	175	38	122	35	2	3	FeMin
34	513989	5169488	4	NAD27	123	58	159	48	1	1	FeMin
34	513989	5169488	4	NAD27	106	55	156	32	2	1	FeMin
34	513989	5169488	4	NAD27	150	56	122	52	2	1	FeMin
34	513989	5169488	4	NAD27	137	59	108	51	2	2	FeMin
35	513981	5169455	4	NAD27	133	40	165	32	1	2	Epid
35	513981	5169455	4	NAD27	210	79	137	34	2	3	Epid
35	513981	5169455	4	NAD27	107	50	136	46	2	2	Epid
35	513981	5169455	4	NAD27	152	41	146	17	1	3	FeMin
35	513981	5169455	4	NAD27	228	23	147	04	1	1	FeMin
35	513981	5169455	4	NAD27	100	56	154	37	2	2	FeEpid
35	513981	5169455	4	NAD27	184	62	120	42	1	2	FeEpid
35	513981	5169455	4	NAD27	115	33	159	21	2	3	FeMin
35	513981	5169455	4	NAD27	181	66	120	40	1	2	FeMin/Epid
35	513981	5169455	4	NAD27	151	22	120	20	1	3	FeMin
36	513936	5169466	6	NAD27	162	43	101	19	0	4	FeMin
36	513936	5169466	6	NAD27	201	54	138	25	0	4	FeMin
36	513936	5169466	6	NAD27	155	41	113	21	2	1	FeEpid
36	513926	5169435	5	NAD27	236	34	008	10	1	3	FeMin
36	513926	5169435	5	NAD27	007	85	004	32	1	1	FeMin
36	513926	5169435	5	NAD27	250	36	302	21	2	2	Epid
36	513926	5169435	5	NAD27	160	38	112	02	1	3	FeMin
36	513926	5169435	5	NAD27	016	89	109	19	2	3	FeMin
36	513926	5169435	5	NAD27	217	36	133	02	1	1	FeEpid
36	513926	5169435	5	NAD27	218	44	294	15	1	3	FeEpid
36	513926	5169435	5	NAD27	226	39	305	10	0	4	FeEpid
36	513926	5169435	5	NAD27	219	44	290	19	1	3	FeMin
36	513926	5169435	5	NAD27	231	42	297	15	1	2	FeMin
36	513926	5169435	5	NAD27	174	34	111	20	1	1	FeMin
36	513926	5169435	5	NAD27	236	53	147	09	2	1	FeMin
36	513926	5169435	5	NAD27	176	33	108	12	1	3	FeMin
36	513926	5169435	5	NAD27	240	66	294	36	1	3	FeEpid
36	513926	5169435	5	NAD27	154	46	117	38	2	3	FeMin
36	513926	5169435	5	NAD27	110	49	084	35	1	2	FeMin
36	513926	5169435	5	NAD27	097	42	072	35	2	2	FeEpid
37	513934	5169406	4	NAD27	127	42	108	38	2	3	FeMin
37	513934	5169406	4	NAD27	134	25	132	21	2	1	FeMin
37	513934	5169406	4	NAD27	164	40	134	31	1	3	FeMin
37	513934	5169406	4	NAD27	195	53	113	18	1	2	FeEpid

Station ID	Easting NAD27	Northing NAD27	Accuracy (+/-m)	Datum	Fault Dip Direction	Fault Dip	Lineation Azimuth	Lineation Plunge	Sense	Certainty	Mineral
37	513934	5169406	4	NAD27	202	19	160	09	2	2	FeMin
37	513934	5169406	4	NAD27	170	45	088	15	1	1	FeEpid
37	513934	5169406	4	NAD27	134	44	112	42	2	2	FeEpid
37	513934	5169406	4	NAD27	068	47	028	39	2	2	FeMin
37	513934	5169406	4	NAD27	088	38	091	34	1	3	FeEpid
37	513934	5169406	4	NAD27	272	88	004	34	2	2	FeEpid
37	513934	5169406	4	NAD27	080	62	086	50	2	2	FeMin
37	513934	5169406	4	NAD27	136	55	128	42	2	2	FeMin
38	513939	5169372	3	NAD27	134	59	152	44	2	3	FeMin
38	513939	5169372	3	NAD27	108	29	151	25	1	2	Epid
38	513939	5169372	3	NAD27	051	61	324	05	2	2	Epid
38	513939	5169372	3	NAD27	088	58	137	32	2	1	FeMin
38	513939	5169372	3	NAD27	094	50	150	36	2	1	FeEpid
38	513939	5169372	3	NAD27	069	59	125	35	1	3	FeMin
38	513939	5169372	3	NAD27	089	57	136	46	1	1	FeMin
38	513939	5169372	3	NAD27	113	22	121	19	2	2	FeMin
38	513939	5169372	3	NAD27	105	38	122	34	2	2	FeMin
38	513939	5169372	3	NAD27	132	36	139	34	1	3	FeEpid
38	513939	5169372	3	NAD27	111	61	165	44	2	2	FeMin
38	513939	5169372	3	NAD27	075	35	138	12	2	1	FeEpid
38	513939	5169372	3	NAD27	155	56	240	02	2	1	FeEpid
38	513939	5169372	3	NAD27	157	54	108	49	2	1	FeEpid
38	513939	5169372	3	NAD27	113	48	040	21	1	1	FeEpid
38	513939	5169372	3	NAD27	076	33	143	28	1	2	FeMin
38	513939	5169372	3	NAD27	102	59	146	41	1	1	FeEpid
38	513939	5169372	3	NAD27	067	39	141	25	2	1	FeMin
38	513939	5169372	3	NAD27	090	50	169	24	1	2	FeMin
38	513939	5169372	3	NAD27	104	76	167	55	1	2	FeO
38	513939	5169372	3	NAD27	154	26	142	19	2	1	FeMin
38	513939	5169372	3	NAD27	077	53	144	26	2	1	FeEpid
38	513939	5169372	3	NAD27	096	80	178	36	1	1	Epid
38	513939	5169372	3	NAD27	109	64	044	30	1	3	FeEpid
39	513941	5169328	9	NAD27	352	29	050	15	0	4	FeMin
39	513941	5169328	9	NAD27	024	84	344	78	2	3	FeEpid
39	513941	5169328	9	NAD27	055	83	028	80	2	3	Epid
39	513941	5169328	9	NAD27	132	70	044	34	1	2	Epid
39	513941	5169328	9	NAD27	114	69	053	26	1	2	FeMin
39	513941	5169328	9	NAD27	048	31	043	29	1	2	FeEpid
39	513941	5169328	9	NAD27	065	29	050	25	0	4	FeMin
39	513941	5169328	9	NAD27	065	19	080	17	1	2	FeMin
39	513941	5169328	9	NAD27	096	85	030	63	2	3	Epid
39	513941	5169328	9	NAD27	257	80	342	16	1	3	Epid
39	513941	5169328	9	NAD27	218	46	252	43	2	3	FeMin

Station ID	Easting NAD27	Northing NAD27	Accuracy (+/-m)	Datum	Fault Dip Direction	Fault Dip	Lineation Azimuth	Lineation Plunge	Sense	Certainty	Mineral
39	513941	5169328	9	NAD27	130	18	053	14	1	2	FeEpid
39	513941	5169328	9	NAD27	238	67	295	35	1	3	FeMin
40a	513914	5169306	5	NAD27	205	65	292	21	2	3	Epid
40b	513926	5169280	4	NAD27	080	53	076	40	0	4	Epid
40b	513926	5169280	4	NAD27	103	23	090	20	1	3	FeEpid
40b	513926	5169280	4	NAD27	255	75	336	23	2	2	Epid
40b	513926	5169280	4	NAD27	067	30	057	29	1	3	FeEpid
40b	513926	5169280	4	NAD27	064	16	056	15	0	4	FeGouge
40b	513926	5169280	4	NAD27	117	40	066	26	1	2	FeEpid
40b	513926	5169280	4	NAD27	079	78	164	15	1	2	Epid
40b	513926	5169280	4	NAD27	209	30	230	21	2	2	FeEpid
40b	513926	5169280	4	NAD27	063	57	054	40	2	3	FeEpid
41a	513898	5169270	4	NAD27	240	07	249	01	2	2	FeMin
41a	513898	5169270	4	NAD27	239	05	242	01	2	1	FeEpid
41a	513898	5169270	4	NAD27	104	40	059	31	1	3	Epid
41a	513898	5169270	4	NAD27	077	20	072	18	0	4	FeMin
41b	513915	5169247	4	NAD27	066	55	072	38	2	2	FeEpid
41b	513915	5169247	4	NAD27	068	88	084	85	0	4	Epid
41b	513915	5169247	4	NAD27	208	43	259	27	0	4	FeEpid
42a	513906	5169203	3	NAD27	338	20	018	16	1	2	Epid
42a	513906	5169203	3	NAD27	290	21	302	15	2	2	FeEpid
42a	513906	5169203	3	NAD27	253	20	230	18	1	3	FeEpid
42a	513906	5169203	3	NAD27	260	21	224	18	1	3	FeEpid
42b	513858	5169154	4	NAD27	070	10	069	09	0	4	Epid
42b	513858	5169154	4	NAD27	264	30	262	25	1	2	FeEpid
42b	513858	5169154	4	NAD27	286	15	032	07	1	3	FeO
42b	513858	5169154	4	NAD27	250	30	264	25	1	2	FeEpid
42c	513863	5169212	3	NAD27	274	15	241	10	0	4	FeEpid
43a	513840	5169270	9	NAD27	195	24	286	01	2	3	FeEpid
43a	513840	5169270	9	NAD27	182	62	277	05	1	2	FeEpid
43a	513840	5169270	9	NAD27	163	60	260	05	1	3	FeEpid
43a	513840	5169270	9	NAD27	178	65	086	02	0	4	Epid
43a	513840	5169270	9	NAD27	191	55	280	15	1	3	FeEpid
43a	513840	5169270	9	NAD27	280	30	258	20	1	2	Epid
43b	513825	5169298	6	NAD27	324	83	241	50	1	1	FeEpid
43b	513825	5169298	6	NAD27	338	88	224	34	1	3	Epid
43b	513825	5169298	6	NAD27	241	36	285	25	2	3	Epid
43b	513825	5169298	6	NAD27	207	19	267	05	0	4	FeEpid
43b	513825	5169298	6	NAD27	294	45	296	36	0	4	Epid
43b	513825	5169298	6	NAD27	196	20	255	11	1	3	FeEpid
43b	513825	5169298	6	NAD27	253	60	312	40	1	3	Epid
44a	513985	5169364	5	NAD27	121	70	080	35	1	3	FeMin
44a	513985	5169364	5	NAD27	159	40	131	35	1	2	Epid

Station ID	Easting NAD27	Northing NAD27	Accuracy (+/-m)	Datum	Fault Dip Direction	Fault Dip	Lineation Azimuth	Lineation Plunge	Sense	Certainty	Mineral
44a	513985	5169364	5	NAD27	195	43	113	25	1	2	FeEpid
44a	513985	5169364	5	NAD27	230	02	306	02	2	3	FeEpid
44a	513985	5169364	5	NAD27	218	33	300	01	0	4	FeEpid
44a	513985	5169364	5	NAD27	320	75	265	40	2	3	Epid
44a	513985	5169364	5	NAD27	129	35	076	11	1	2	FeMin
44a	513985	5169364	5	NAD27	164	44	106	26	1	3	FeMin
44a	513985	5169364	5	NAD27	182	24	152	22	0	4	FeMin
44a	513985	5169364	5	NAD27	164	33	137	15	2	3.5	FeMin
44a	513985	5169364	5	NAD27	204	40	139	15	2	3	FeMin
44a	513985	5169364	5	NAD27	159	55	113	38	0	4	FeEpid
44a	513985	5169364	5	NAD27	158	44	142	38	1	3	FeEpid
44a	513985	5169364	5	NAD27	198	22	159	22	2	1	FeEpid
44a	513985	5169364	5	NAD27	222	20	159	10	0	4	FeEpid
44a	513985	5169364	5	NAD27	228	14	148	02	2	3	FeMin
44a	513985	5169364	5	NAD27	159	55	136	46	1	3	FeMin
44a	513985	5169364	5	NAD27	177	18	166	17	0	4	FeMin
44a	513985	5169364	5	NAD27	224	28	233	15	2	3	FeMin
44a	513985	5169364	5	NAD27	205	43	188	40	2	3	FeMin Gouge
44a	513985	5169364	5	NAD27	186	38	170	32	0	4	FeMin
44a	513985	5169364	5	NAD27	176	20	159	18	1	3	FeMin
44b	514012	5169293	4	NAD27	284	43	336	22	0	4	FeEpid
44b	514012	5169293	4	NAD27	225	55	135	05	2	3	Epid
45a	514006	5169152	3	NAD27	232	50	322	02	0	4	Chl/Epid/ Qz
45a	514006	5169152	3	NAD27	236	52	273	40	0	4	Epid
45a	514006	5169152	3	NAD27	228	80	307	14	0	4	Chl/Epid
46a	514029	5169053	4	NAD27	191	23	259	10	2	3.5	Epid
46a	514029	5169053	4	NAD27	179	10	259	01	2	3.5	Epid
45b	514005	5169122	4	NAD27	336	24	332	18	2	3	Epid
45b	514005	5169122	4	NAD27	176	42	124	18	0	4	Epid
45b	514005	5169122	4	NAD27	326	30	296	16	1	3	Chl/Epid
45b	514005	5169122	4	NAD27	302	13	306	11	1	3	Chl/Epid
46b	514003	5169092	3	NAD27	200	40	124	15	1	3	FeEpid
46c	514005	5169059	3	NAD27	030	05	270	03	1	3	FeEpid
46c	514005	5169059	3	NAD27	070	15	114	11	2	3	FeEpid
47a	514013	5169001	3	NAD27	236	36	300	13	2	1	FeEpid
47a	514013	5169001	3	NAD27	232	38	292	22	2	3	FeEpid
47a	514013	5169001	3	NAD27	210	10	123	03	0	4	FeEpid
47a	514013	5169001	3	NAD27	103	25	094	23	2	3	Epid
47a	514013	5169001	3	NAD27	128	26	085	20	1	2	Epid
47a	514013	5169001	3	NAD27	250	20	275	17	2	2	Epid
47a	514013	5169001	3	NAD27	277	45	326	35	2	2	Epid
47a	514013	5169001	3	NAD27	110	11	097	09	1	3	FeMin
47b	513990	5168970	4	NAD27	037	28	108	05	1	1	FeMin

Station ID	Easting NAD27	Northing NAD27	Accuracy (+/-m)	Datum	Fault Dip Direction	Fault Dip	Lineation Azimuth	Lineation Plunge	Sense	Certainty	Mineral
47b	513990	5168970	4	NAD27	264	54	318	35	0	4	FeEpid
47b	513990	5168970	4	NAD27	048	35	313	03	2	3	FeChl
47b	513990	5168970	4	NAD27	038	26	123	07	0	4	FeMin
47b	513990	5168970	4	NAD27	244	46	336	15	2	2	FeMin
47b	513990	5168970	4	NAD27	248	38	325	08	2	2	FeMin
47b	513990	5168970	4	NAD27	282	19	312	16	2	2	FeMin
47b	513990	5168970	4	NAD27	280	35	341	15	2	2	Epid
47b	513990	5168970	4	NAD27	242	43	324	08	2	2	Epid
48	514245	5168723	4	NAD27	230	62	288	40	1	1	Epid
48	514245	5168723	4	NAD27	251	55	312	35	1	3	FeMin
48	514245	5168723	4	NAD27	317	19	328	15	2	3	FeMin
48	514245	5168723	4	NAD27	122	28	111	27	1	3	Epid
48	514245	5168723	4	NAD27	263	15	332	06	2	3	Epid
48	514245	5168723	4	NAD27	222	60	295	25	1	2	Epid
48	514245	5168723	4	NAD27	234	55	309	20	1	2	Epid
48	514245	5168723	4	NAD27	226	17	303	11	1	3	FeEpid
48	514245	5168723	4	NAD27	232	50	300	20	1	1	FeMin
not used	514259	5168582	3	NAD27	274	40	291	34	0	4	Epid
not used	514252	5168536	4	NAD27	191	35	206	33	1	3	FeEpid
not used	514252	5168536	4	NAD27	224	77	242	74	2	3	FeEpid
8e	515472	5167673	9	NAD27	320	40	297	35	1	2	Epid
8e	515472	5167673	9	NAD27	332	30	323	27	1	3	FeEpid
8e	515472	5167673	9	NAD27	321	25	301	23	1	2	Epid
8e	515472	5167673	9	NAD27	288	51	305	50	1	3	Epid
8e	515472	5167673	9	NAD27	284	45	272	43	1	3	Epid
8e	515472	5167673	9	NAD27	297	46	290	45	1	1	Epid
8e	515472	5167673	9	NAD27	282	44	298	38	1	1	Epid
49a	514319	5168553	6	NAD27	240	65	140	05	1	3	FeMin
49a	514319	5168553	6	NAD27	336	34	300	24	2	3	FeMin
49a	514319	5168553	6	NAD27	241	57	178	37	2	3	FeEpid
49a	514319	5168553	6	NAD27	336	28	310	26	2	2	FeEpid
49a	514319	5168553	6	NAD27	084	15	140	05	0	4	Epid Gouge
49a	514319	5168553	6	NAD27	320	68	237	21	1	3	Epid
49b	514337	5168544	4	NAD27	150	82	190	73	2	2	FeEpid
49b	514337	5168544	4	NAD27	151	74	204	62	2	3	Epid
49b	514337	5168544	4	NAD27	144	80	224	68	2	3	FeEpid
49b	514337	5168544	4	NAD27	147	75	250	45	2	3	FeMin
49b	514337	5168544	4	NAD27	145	80	240	37	2	3	Epid
49b	514337	5168544	4	NAD27	350	75	270	50	1	3	Epid
49c	514353	5168529	4	NAD27	004	88	272	28	1	3	FeEpid
49c	514353	5168529	4	NAD27	356	78	250	25	1	3	FeMin
49c	514353	5168529	4	NAD27	310	89	222	56	1	3	Epid
49c	514353	5168529	4	NAD27	249	89	332	52	0	4	FeMin

Station ID	Easting NAD27	Northing NAD27	Accuracy (+/-m)	Datum	Fault Dip Direction	Fault Dip	Lineation Azimuth	Lineation Plunge	Sense	Certainty	Mineral
49c	514353	5168529	4	NAD27	090	55	158	25	0	4	FeMin
49c	514353	5168529	4	NAD27	328	75	240	55	1	3	FeMin
50a	514363	5168655	5	NAD27	040	51	319	15	1	1	Chl/Epid
50a	514363	5168655	5	NAD27	042	50	332	25	0	4	Chl
50a	514363	5168655	5	NAD27	010	50	320	35	1	2	FeChl
50a	514363	5168655	5	NAD27	090	41	148	40	2	2	FeChl
50a	514363	5168655	5	NAD27	064	35	334	01	1	2	FeChl
50a	514363	5168655	5	NAD27	040	40	330	15	1	1	FeChl
50a	514363	5168655	5	NAD27	080	30	142	15	2	3	FeChl
50a	514363	5168655	5	NAD27	114	29	160	20	2	3	FeChl
50a	514363	5168655	5	NAD27	088	69	145	49	2	3	FeChl
50a	514363	5168655	5	NAD27	097	52	172	28	0	4	FeChl
50a	514363	5168655	5	NAD27	094	45	131	35	2	2	FeChl
50a	514363	5168655	5	NAD27	060	57	141	15	2	2	FeChl
50a	514363	5168655	5	NAD27	100	45	157	35	2	1	FeChl
50b	514328	5168713	4	NAD27	044	49	331	21	0	4	Chl
50b	514328	5168713	4	NAD27	155	30	012	18	2	1	Epid
50b	514328	5168713	4	NAD27	028	34	315	11	0	4	FeEpid
50b	514328	5168713	4	NAD27	110	51	153	40	2	3	FeEpid/ Chl
50b	514328	5168713	4	NAD27	088	32	146	21	2	3	Epid
50b	514328	5168713	4	NAD27	170	25	128	20	2	1	FeChl
50b	514328	5168713	4	NAD27	335	50	278	42	2	2	FeEpid
50b	514328	5168713	4	NAD27	143	32	146	30	2	2	FeEpid
50b	514328	5168713	4	NAD27	279	27	299	22	1	1	Chl
50b	514328	5168713	4	NAD27	348	26	320	17	1	1	Chl
50b	514328	5168713	4	NAD27	224	42	282	25	1	1	Chl
50b	514328	5168713	4	NAD27	225	35	290	14	1	1	Chl
50b	514328	5168713	4	NAD27	342	22	300	16	1	1	FeChl
50b	514328	5168713	4	NAD27	099	45	140	35	1	2	Chl
50b	514328	5168713	4	NAD27	105	50	139	42	1	1	Chl
50b	514328	5168713	4	NAD27	060	45	104	35	2	3	Epid
50b	514328	5168713	4	NAD27	073	70	050	60	1	3	Chl
51a	513842	5169329	4	NAD27	196	16	285	01	2	2	Epid
51a	513842	5169329	4	NAD27	112	69	038	13	1	3	FeEpid
51a	513842	5169329	4	NAD27	195	32	268	05	2	3	FeMin
51a	513842	5169329	4	NAD27	193	45	106	06	1	2	FeEpid
51a	513842	5169329	4	NAD27	185	50	131	32	1	1	FeEpid
51a	513842	5169329	4	NAD27	160	34	094	10	1	3	FeEpid
51a	513842	5169329	4	NAD27	053	06	093	02	1	3	FeEpid
51a	513842	5169329	4	NAD27	320	34	255	11	2	2	FeEpid
51b	513858	5169378	4	NAD27	230	43	247	40	0	4	Epid
51b	513858	5169378	4	NAD27	078	26	060	20	2	3	FeMin
51b	513858	5169378	4	NAD27	028	39	067	32	2	2	FeEpid

Station ID	Easting NAD27	Northing NAD27	Accuracy (+/-m)	Datum	Fault Dip Direction	Fault Dip	Lineation Azimuth	Lineation Plunge	Sense	Certainty	Mineral
51b	513858	5169378	4	NAD27	334	12	229	03	2	3	FeEpid
not used	513943	5169602	4	NAD27	082	78	000	31	0	4	FeEpid
not used	513991	5169600	4	NAD27	067	58	094	53	2	2	FeMin
not used	513991	5169600	4	NAD27	131	68	074	54	2	3	FeEpid
52	513952	5169722	4	NAD27	163	50	151	38	0	4	FeMin
52	513952	5169722	4	NAD27	217	29	138	08	2	3	Epid
52	513952	5169722	4	NAD27	165	71	081	56	0	4	Epid
52	513952	5169722	4	NAD27	143	45	125	48	0	4	FeMin
52	513952	5169722	4	NAD27	151	47	108	44	2	3	FeMin
52	513952	5169722	4	NAD27	161	44	129	36	1	3.5	FeO
52	513952	5169722	4	NAD27	085	73	098	71	1	1	FeO
52	513952	5169722	4	NAD27	254	26	154	02	0	4	Epid
52	513952	5169722	4	NAD27	157	77	049	54	2	2	Epid
52	513952	5169722	4	NAD27	185	24	263	07	0	4	Epid
52	513952	5169722	4	NAD27	172	35	092	03	2	1	FeO
52	513952	5169722	4	NAD27	089	62	037	46	1	3.5	FeMin
29b	513824	5169650	3	NAD27	080	67	009	31	0	4	FeEpid
29b	513824	5169650	3	NAD27	069	89	343	30	1	2	FeEpid
29b	513824	5169650	3	NAD27	248	82	327	45	2	3	Epid
29b	513824	5169650	3	NAD27	248	78	317	30	2	2	Epid
29b	513824	5169650	3	NAD27	243	81	326	42	0	4	FeEpid
29b	513824	5169650	3	NAD27	246	84	330	35	2	3	FeEpid
29b	513824	5169650	3	NAD27	077	84	353	39	1	3	FeEpid
53a	511964	5171136	5	NAD27	265	70	351	45	1	3	Epid
53a	511964	5171136	5	NAD27	234	57	320	12	0	4	Epid
53a	511964	5171136	5	NAD27	250	76	324	10	0	4	Epid
53a	511964	5171136	5	NAD27	147	30	088	19	2	3	FeEpid
53a	511964	5171136	5	NAD27	193	50	108	16	0	4	FeEpid
53a	511964	5171136	5	NAD27	176	35	108	18	2	3	FeEpid
53a	511964	5171136	5	NAD27	166	45	104	25	2	3	FeEpid
53a	511964	5171136	5	NAD27	176	42	118	17	2	3	FeEpid
53a	511964	5171136	5	NAD27	210	41	124	15	2	2	FeEpid
53a	511964	5171136	5	NAD27	292	50	302	44	0	4	FeEpid
53a	511964	5171136	5	NAD27	278	56	326	45	0	4	FeEpid
53a	511964	5171136	5	NAD27	182	30	089	04	0	4	FeEpid
53a	511964	5171136	5	NAD27	178	35	114	17	0	4	Epid
53b	511938	5171098	9	NAD27	310	49	255	38	1	2	FeEpid
53b	511938	5171098	9	NAD27	296	45	313	40	1	2	FeMin
53b	511938	5171098	9	NAD27	155	79	073	17	1	2	FeEpid
53b	511938	5171098	9	NAD27	242	45	240	40	2	3.5	FeEpid
53b	511938	5171098	9	NAD27	271	29	278	28	1	3	FeMin
54a	514652	5168954	7	NAD27	151	36	132	35	1	2	FeEpid
54a	514652	5168954	7	NAD27	357	89	086	29	1	2	Epid

Station ID	Easting NAD27	Northing NAD27	Accuracy (+/-m)	Datum	Fault Dip Direction	Fault Dip	Lineation Azimuth	Lineation Plunge	Sense	Certainty	Mineral
54a	514652	5168954	7	NAD27	096	66	160	50	1	3	Epid
54a	514652	5168954	7	NAD27	335	71	066	07	2	3	Epid
54a	514652	5168954	7	NAD27	081	36	132	43	1	1	Epid
54a	514652	5168954	7	NAD27	117	61	028	01	1	2	FeChl
54a	514652	5168954	7	NAD27	191	49	103	06	1	2	FeEpid
54a	514652	5168954	7	NAD27	216	66	307	05	2	2	Epid
54a	514652	5168954	7	NAD27	234	41	298	21	2	3	FeEpid
54a	514652	5168954	7	NAD27	223	11	301	02	2	2	FeEpid
54a	514652	5168954	7	NAD27	328	59	251	26	1	3	FeEpid
54a	514652	5168954	7	NAD27	092	71	178	06	0	4	Epid
54b	514658	5168945	7	NAD27	356	67	086	01	2	2	Epid
54b	514658	5168945	7	NAD27	142	86	056	44	2	3	Epid
54b	514658	5168945	7	NAD27	150	45	303	44	1	3	FeEpid
54b	514658	5168945	7	NAD27	284	44	352	18	0	4	FeEpid
54b	514658	5168945	7	NAD27	057	76	322	05	2	3	FeEpid
55a	509705	5173294	5	NAD27	297	64	024	47	1	3	FeEpid
55a	509705	5173294	5	NAD27	225	34	135	02	1	3	FeMin
55a	509705	5173294	5	NAD27	171	37	117	23	1	2	FeEpid
55a	509705	5173294	5	NAD27	162	39	110	27	1	3	FeEpid
55a	509705	5173294	5	NAD27	172	17	123	03	1	3	FeEpid
55a	509705	5173294	5	NAD27	322	37	342	30	0	4	FeGouge
55b	509677	5173371	10	NAD27	273	77	355	09	1	3	FeGouge
55b	509677	5173371	10	NAD27	226	43	143	10	1	3	FeEpid
55b	509677	5173371	10	NAD27	204	71	122	28	1	3	FeMin
55b	509677	5173371	10	NAD27	256	70	179	15	2	3	FeMin
55b	509677	5173371	10	NAD27	102	38	138	12	1	3	FeEpid
not used	50983	5173557	5	NAD27	120	85	046	64	2	3.5	Epid
56a	509640	5173588	4	NAD27	084	89	350	29	1	3	FeEpid
56a	509640	5173588	4	NAD27	354	66	284	34	1	1	FeO
56a	509640	5173588	4	NAD27	356	56	293	35	1	2	FeO
56b	509637	5173858	4	NAD27	128	80	210	36	2	2	FeMin
56b	509637	5173858	4	NAD27	037	58	331	34	2	3	FeEpid
56b	509637	5173858	4	NAD27	306	37	004	31	1	2	FeEpid
56b	509637	5173858	4	NAD27	237	45	322	07	2	3	FeMin
57	509807	5173617	4	NAD27	240	55	212	53	2	3	FeEpid
57	509807	5173617	4	NAD27	258	36	233	28	0	4	FeEpid
57	509807	5173617	4	NAD27	256	60	322	28	2	1	FeEpid
57	509807	5173617	4	NAD27	236	38	232	37	2	3	FeMin
57	509807	5173617	4	NAD27	212	81	294	34	2	2	FeMin
57	509807	5173617	4	NAD27	244	80	202	78	0	4	Epid
57	509807	5173617	4	NAD27	244	80	212	79	1	3	FeMin
57	509807	5173617	4	NAD27	071	75	040	75	2	3	FeMin
57	509807	5173617	4	NAD27	012	32	332	15	2	1	FeMin

Station ID	Easting NAD27	Northing NAD27	Accuracy (+/-m)	Datum	Fault Dip Direction	Fault Dip	Lineation Azimuth	Lineation Plunge	Sense	Certainty	Mineral
57	509807	5173617	4	NAD27	002	36	318	12	2	1	FeMin
57	509807	5173617	4	NAD27	188	35	296	04	2	1	FeMin
57	509807	5173617	4	NAD27	110	35	131	31	2	2	Epid
57	509807	5173617	4	NAD27	161	45	294	04	2	3	FeEpid
57	509807	5173617	4	NAD27	185	40	263	10	1	3	FeMin
57	509807	5173617	4	NAD27	270	61	338	39	2	3	FeMin
57	509807	5173617	4	NAD27	230	65	316	12	2	3	FeMin
58a	513357	5170102	5	NAD27	086	39	155	37	0	4	No data
58a	513357	5170102	5	NAD27	128	89	220	32	1	3	No data
58a	513357	5170102	5	NAD27	139	84	224	60	1	3	No data
58a	513357	5170102	5	NAD27	222	44	214	39	1	3	No data
58a	513357	5170102	5	NAD27	075	37	082	35	2	3	No data
58b	513363	5170106	6	NAD27	190	33	160	30	1	3	No data
58b	513363	5170106	6	NAD27	313	89	221	49	2	3	No data
58b	513363	5170106	6	NAD27	093	30	157	37	1	3	No data
59a	513396	5170152	8	NAD27	181	65	287	36	2	2	No data
59a	513396	5170152	8	NAD27	175	85	287	32	1	2	No data
59a	513396	5170152	8	NAD27	172	68	254	33	1	3	No data
59a	513396	5170152	8	NAD27	191	74	271	03	1	2	Epid
59a	513396	5170152	8	NAD27	019	80	292	32	1	3	Epid
59a	513396	5170152	8	NAD27	070	30	149	03	2	2	No data
59a	513396	5170152	8	NAD27	019	72	116	42	2	2	Epid
59a	513396	5170152	8	NAD27	241	60	273	56	2	2	No data
59a	513396	5170152	8	NAD27	197	84	113	07	2	3	No data
59b	513409	5170161	7	NAD27	217	71	306	05	2	2	No data
59b	513409	5170161	7	NAD27	201	71	290	08	2	2	No data
59b	513409	5170161	7	NAD27	217	66	109	05	2	3	No data
59b	513409	5170161	7	NAD27	038	66	078	52	2	2	No data
59b	513409	5170161	7	NAD27	240	54	252	55	2	3	No data
59b	513409	5170161	7	NAD27	225	66	265	56	2	2	No data
59c	513393	5170160	8	NAD27	233	61	250	54	2	3	No data
59c	513393	5170160	8	NAD27	229	55	258	55	2	2	No data
59c	513393	5170160	8	NAD27	245	46	276	53	2	2	No data
59d	513379	5170161	6	NAD27	038	57	266	36	2	2	No data
59d	513379	5170161	6	NAD27	201	86	282	48	2	3	No data
59d	513379	5170161	6	NAD27	000	86	104	35	2	2	No data
60a	513455	5170108	4	NAD27	122	59	038	27	1	3	No data
60a	513455	5170108	4	NAD27	171	58	252	06	2	2	No data
60a	513455	5170108	4	NAD27	178	63	092	09	1	3	No data
60a	513455	5170108	4	NAD27	023	89	114	12	1	3	No data
60a	513455	5170108	4	NAD27	170	50	082	10	0	4	No data
60a	513455	5170108	4	NAD27	230	71	290	45	0	4	No data
61a	513452	5170066	4	NAD27	266	33	240	29	2	2	No data

Station ID	Easting NAD27	Northing NAD27	Accuracy (+/-m)	Datum	Fault Dip Direction	Fault Dip	Lineation Azimuth	Lineation Plunge	Sense	Certainty	Mineral
61a	513452	5170066	4	NAD27	272	23	248	15	2	2	No data
61a	513452	5170066	4	NAD27	290	90	336	26	1	2	No data
61a	513452	5170066	4	NAD27	250	54	206	40	2	2	No data
61a	513452	5170066	4	NAD27	183	39	180	30	0	4	No data
62a	513507	5169992	4	NAD27	270	63	224	51	0	4	No data
62a	513507	5169992	4	NAD27	142	69	209	58	2	3	No data
62a	513507	5169992	4	NAD27	261	60	204	37	2	2	No data
62a	513507	5169992	4	NAD27	270	58	198	26	0	4	No data
62a	513507	5169992	4	NAD27	254	56	206	44	2	2	No data
63a	513553	5169976	4	NAD27	251	69	205	69	2	2	No data
63a	513553	5169976	4	NAD27	225	84	166	71	2	2	No data
63a	513553	5169976	4	NAD27	296	78	203	50	1	2	No data
63a	513553	5169976	4	NAD27	318	87	062	66	0	4	No data
64a	513342	5170281	5	NAD27	330	87	247	46	1	3	No data
64a	513342	5170281	5	NAD27	347	53	312	42	2	4	No data
64a	513342	5170281	5	NAD27	017	54	306	14	2	3	No data
64a	513342	5170281	5	NAD27	348	65	049	48	0	4	No data
64a	513342	5170281	5	NAD27	206	72	290	57	1	1	No data
64a	513342	5170281	5	NAD27	200	51	230	39	1	4	No data
64a	513342	5170281	5	NAD27	202	68	285	45	0	4	No data
64b	513350	5170295	7	NAD27	201	78	290	26	0	4	No data
64b	513350	5170295	7	NAD27	234	57	284	44	2	3	No data
64b	513350	5170295	7	NAD27	011	80	299	36	2	2	No data
64b	513350	5170295	7	NAD27	186	83	274	48	1	2	No data
64b	513350	5170295	7	NAD27	328	75	263	44	2	1	No data
64b	513350	5170295	7	NAD27	319	66	255	45	0	4	No data
64b	513350	5170295	7	NAD27	326	66	255	47	2	3	No data
64b	513350	5170295	7	NAD27	333	85	242	44	0	4	No data
64b	513350	5170295	7	NAD27	136	80	045	04	0	4	No data
not used	513585	5170268	4	NAD27	278	76	157	14	0	4	No data
not used	513585	5170268	4	NAD27	314	68	054	27	0	4	No data
not used	513585	5170268	4	NAD27	273	75	008	09	0	4	No data
not used	513585	5170268	4	NAD27	312	85	203	48	1	3	No data
not used	513585	5170268	4	NAD27	308	71	056	03	0	4	No data
not used	513585	5170268	4	NAD27	276	86	268	20	0	4	No data
not used	513633	5170196	4	NAD27	226	75	115	10	0	4	No data
not used	513633	5170196	4	NAD27	302	67	215	12	0	4	No data
not used	513633	5170196	4	NAD27	176	50	230	30	0	4	No data
not used	513699	5170156	3	NAD27	179	39	083	21	0	4	No data
not used	513699	5170156	3	NAD27	184	47	280	02	0	4	No data
not used	513699	5170156	3	NAD27	212	38	300	01	0	4	No data
not used	513699	5170156	3	NAD27	175	60	084	16	2	2	No data
63b	513569	5169953	4	NAD27	153	80	222	35	2	2	FeEp

Station ID	Easting NAD27	Northing NAD27	Accuracy (+/-m)	Datum	Fault Dip Direction	Fault Dip	Lineation Azimuth	Lineation Plunge	Sense	Certainty	Mineral
63b	513569	5169953	4	NAD27	212	59	252	10	0	4	Epid
63b	513569	5169953	4	NAD27	141	59	084	30	1	3	Epid
63c	513570	5169960	6	NAD27	139	87	039	35	1	3	FeEpid
63c	513570	5169960	6	NAD27	186	78	276	09	2	2	Epid
63c	513570	5169960	6	NAD27	210	59	286	19	2	2	Epid
63d	513567	5169957	3	NAD27	230	65	180	55	1	2	Epid
63d	513567	5169957	3	NAD27	299	81	250	03	2	2	Epid
63d	513567	5169957	3	NAD27	087	16	094	05	0	4	Epid
63d	513567	5169957	3	NAD27	296	85	025	09	1	2	Epid
63d	513567	5169957	3	NAD27	118	76	002	25	2	3	Chl
63d	513567	5169957	3	NAD27	032	14	120	05	2	2	Epid
63e	513562	5169945	4	NAD27	194	84	233	41	2	2	FeEp
63e	513562	5169945	4	NAD27	332	59	245	41	2	3	FeO
63e	513562	5169945	4	NAD27	153	87	199	64	2	3	FeO
63f	513556	5169952	7	NAD27	251	59	233	55	2	3	FeO
63f	513556	5169952	7	NAD27	246	65	222	59	0	4	FeO
63g	513554	5169953	6	NAD27	133	89	049	45	2	3	FeO
63h	513543	5169958	7	NAD27	270	70	210	35	0	4	FeO
63h	513543	5169958	7	NAD27	006	69	069	12	2	2	Epid
63h	513543	5169958	7	NAD27	218	54	230	53	1	2	FeO
63h	513543	5169958	7	NAD27	237	59	204	35	1	3	Epid
63i	513541	5169969	4	NAD27	094	76	180	56	1	1	Epid
63i	513541	5169969	4	NAD27	261	60	236	55	0	4	Epid
63i	513541	5169969	4	NAD27	255	71	138	42	0	4	Epid
63i	513541	5169969	4	NAD27	125	54	202	39	1	1	FeO
63i	513541	5169969	4	NAD27	288	79	214	46	1	3	Epid
63j	513542	5169983	7	NAD27	212	59	248	50	2	3	FeO
62b	513514	5169987	8	NAD27	137	84	218	21	1	2	FeEpid
62b	513514	5169987	8	NAD27	152	75	234	26	0	4	FeO
62b	513514	5169987	8	NAD27	216	85	254	84	1	3	Epid
62c	513502	5169986	7	NAD27	220	45	232	44	2	3	Epid
62c	513502	5169986	7	NAD27	268	47	240	40	2	2	FeEpid
62c	513502	5169986	7	NAD27	244	27	274	15	2	3	Epid
62d	513503	5169998	6	NAD27	332	84	227	43	2	2	No data
62e	513506	5169993	4	NAD27	267	61	221	48	2	3	No data
66a	513545	5170090	4	NAD27	142	75	058	19	1	1	Epid
66a	513545	5170090	4	NAD27	153	66	064	20	1	1	Epid
66a	513545	5170090	4	NAD27	144	85	234	02	2	2	No data
66a	513545	5170090	4	NAD27	163	80	064	07	1	3	Epid
66b	513555	5170102	5	NAD27	142	74	062	19	1	2	No data
66b	513555	5170102	5	NAD27	182	76	094	04	0	4	No data
66b	513555	5170102	5	NAD27	183	76	183	01	0	4	No data
66b	513555	5170102	5	NAD27	128	55	052	21	1	2	No data

Station ID	Easting NAD27	Northing NAD27	Accuracy (+/-m)	Datum	Fault Dip Direction	Fault Dip	Lineation Azimuth	Lineation Plunge	Sense	Certainty	Mineral
63k	513563	5170001	5	NAD27	356	31	080	03	1	2	No data
61b	513446	5170050	4	NAD27	218	48	280	25	1	2	FeEpid
61c	513455	5170063	3	NAD27	345	39	060	05	2	3	Epid
61c	513455	5170063	3	NAD27	000	46	080	15	1	3	Epid
61c	513455	5170063	3	NAD27	011	41	066	24	1	2	Epid
61c	513455	5170063	3	NAD27	130	56	061	22	2	2	Epid
61c	513455	5170063	3	NAD27	033	40	080	16	0	4	No data
61d	513445	5170078	4	NAD27	347	80	255	46	1	2	Epid
61d	513445	5170078	4	NAD27	212	55	274	39	0	4	No data
61d	513445	5170078	4	NAD27	340	80	070	02	2	1	No data
61d	513445	5170078	4	NAD27	126	72	046	07	1	2	Epid
60b	513451	5170102	6	NAD27	184	55	268	14	2	3	Epid
60b	513451	5170102	6	NAD27	204	40	270	22	2	3	No data
60b	513451	5170102	6	NAD27	025	54	082	37	1	3	No data
60c	513457	5170106	4	NAD27	066	55	096	43	2	2	Epid
60c	513457	5170106	4	NAD27	094	87	114	26	1	2	FeO
60c	513457	5170106	4	NAD27	202	59	279	20	2	3	Epid
65a	513509	5170148	6	NAD27	168	79	046	36	2	2	No data
65a	513509	5170148	6	NAD27	315	89	201	29	1	3	No data
65a	513509	5170148	6	NAD27	134	52	204	19	2	1	No data
65b	513543	5170137	7	NAD27	030	50	338	35	1	3	No data
66c	513581	5170085	7	NAD27	269	85	172	05	1	2	Epid
60d	513441	5170121	6	NAD27	158	74	070	01	1	2	No data
60d	513441	5170121	6	NAD27	174	54	080	05	2	1	No data
60d	513441	5170121	6	NAD27	178	03	256	02	1	1	No data
67a	513539	5170313	5	NAD27	157	80	242	04	2	2	Epid
67b	513529	5170324	4	NAD27	177	58	220	45	2	3	FeEpid
67b	513529	5170324	4	NAD27	169	30	224	04	2	3	Epid
67c	513526	5170315	4	NAD27	278	39	248	38	2	3	Epid
67d	513510	5170331	5	NAD27	198	37	217	36	2	3	FeEpid
67d	513510	5170331	5	NAD27	200	75	200	74	1	3	Epid
67e	513491	5170332	4	NAD27	284	19	269	16	2	2	FeEpid
not used	513654	5169763	4	NAD27	250	44	296	32	1	3	Epid
68	514214	5169366	No data	NAD27	103	86	192	11	2	3	No data
68	514214	5169366	No data	NAD27	290	37	314	37	1	3	No data
68	514214	5169366	No data	NAD27	111	06	202	06	2	3	No data
68	514214	5169366	No data	NAD27	282	40	320	31	1	3	No data
68	514214	5169366	No data	NAD27	132	88	222	01	0	4	No data
68	514214	5169366	No data	NAD27	113	89	030	35	2	2	Epid
68	514214	5169366	No data	NAD27	331	48	048	59	1	3	No data
68	514214	5169366	No data	NAD27	306	80	125	24	2	3	No data
68	514214	5169366	No data	NAD27	351	77	092	29	0	4	No data
68	514214	5169366	No data	NAD27	042	21	327	04	0	4	Epid

Station ID	Easting NAD27	Northing NAD27	Accuracy (+/-m)	Datum	Fault Dip Direction	Fault Dip	Lineation Azimuth	Lineation Plunge	Sense	Certainty	Mineral
68	514214	5169366	No data	NAD27	217	45	155	19	1	1	FeMin
68	514214	5169366	No data	NAD27	212	44	161	24	1	3	Epid
68	514214	5169366	No data	NAD27	198	34	148	27	1	1	Epid
68	514214	5169366	No data	NAD27	339	67	057	65	1	1	FeEpid
68	514214	5169366	No data	NAD27	328	79	050	80	1	1	FeEpid
68	514214	5169366	No data	NAD27	322	62	064	84	1	2	FeMin
68	514214	5169366	No data	NAD27	314	82	046	77	1	2	FeEpid
68	514214	5169366	No data	NAD27	284	37	312	36	1	2	FeMin
68	514214	5169366	No data	NAD27	308	86	037	05	0	4	FeO
68	514214	5169366	No data	NAD27	029	20	027	17	1	3	FeO
68	514214	5169366	No data	NAD27	022	06	002	04	1	3	FeO
69a	514261	5169437	No data	NAD27	254	43	195	19	1	1	Epid
69a	514261	5169437	No data	NAD27	178	57	150	53	1	1	Chl
69a	514261	5169437	No data	NAD27	231	24	192	16	2	2	FeO
69a	514261	5169437	No data	NAD27	278	34	195	05	1	2	FeO
69a	514261	5169437	No data	NAD27	285	39	188	01	1	3	FeO
70a	514206	5169494	No data	NAD27	291	73	216	06	2	2	Epid
70a	514206	5169494	No data	NAD27	305	76	293	41	2	2	No data
70a	514206	5169494	No data	NAD27	295	89	220	46	2	2	No data
70a	514206	5169494	No data	NAD27	036	51	321	26	1	1	Epid
70a	514206	5169494	No data	NAD27	313	85	223	53	2	3	No data
70a	514206	5169494	No data	NAD27	038	72	304	15	1	1	FeMin
70a	514206	5169494	No data	NAD27	065	55	339	09	1	3	FeMin
70a	514206	5169494	No data	NAD27	036	55	308	06	1	1	FeMin
70a	514206	5169494	No data	NAD27	119	86	029	49	1	2	FeMin
70a	514206	5169494	No data	NAD27	254	10	154	05	0	4	FeMin
70a	514206	5169494	No data	NAD27	174	40	192	40	2	3	FeO
70b	514227	5169612	No data	NAD27	351	51	277	22	2	2	Epid
70b	514227	5169612	No data	NAD27	069	44	336	04	2	2	No data
70b	514227	5169612	No data	NAD27	101	33	102	35	1	3	No data
70b	514227	5169612	No data	NAD27	254	41	n/a	n/a	2	4	No data
69b	514266	5169409	No data	NAD27	173	85	081	06	2	2	Epid
69b	514266	5169409	No data	NAD27	150	38	093	20	2	3	No data
69b	514266	5169409	No data	NAD27	073	66	158	33	1	3	No data
69b	514266	5169409	No data	NAD27	201	71	110	25	2	2	No data
69b	514266	5169409	No data	NAD27	312	85	044	12	1	2	No data
69b	514266	5169409	No data	NAD27	125	76	044	01	0	4	No data
69b	514266	5169409	No data	NAD27	280	75	178	11	2	3	No data
69b	514266	5169409	No data	NAD27	176	87	100	23	2	3	No data
69b	514266	5169409	No data	NAD27	010	71	108	31	1	3	No data
69b	514266	5169409	No data	NAD27	118	72	212	05	0	4	No data
69b	514266	5169409	No data	NAD27	007	61	095	40	1	3	No data
69b	514266	5169409	No data	NAD27	331	66	060	30	2	1	Epid

Station ID	Easting NAD27	Northing NAD27	Accuracy (+/-m)	Datum	Fault Dip Direction	Fault Dip	Lineation Azimuth	Lineation Plunge	Sense	Certainty	Mineral
71a	514430	5169555	No data	NAD27	028	75	298	40	2	3	No data
71a	514430	5169555	No data	NAD27	182	90	088	01	1	3	No data
71a	514430	5169555	No data	NAD27	171	89	089	33	2	3	No data
71a	514430	5169555	No data	NAD27	298	85	355	30	2	2	No data
71a	514430	5169555	No data	NAD27	153	64	218	31	1	3	No data
71a	514430	5169555	No data	NAD27	176	80	268	10	2	3	No data
71a	514430	5169555	No data	NAD27	093	88	355	15	1	2	No data
72a	514321	5169315	No data	NAD27	351	60	268	30	1	1	FeEpid
72a	514321	5169315	No data	NAD27	178	30	137	24	1	1	FeMin
72a	514321	5169315	No data	NAD27	180	36	121	15	1	2	FeEpid
72a	514321	5169315	No data	NAD27	183	66	119	34	1	3	FeEpid
72b	514336	5169332	No data	NAD27	147	45	174	39	1	3	FeMin
72b	514336	5169332	No data	NAD27	129	06	166	05	0	4	FeMin
72b	514336	5169332	No data	NAD27	352	06	343	05	0	4	FeMin
72b	514336	5169332	No data	NAD27	058	14	347	04	1	3	FeMin
not used	514384	5169329	No data	NAD27	168	56	177	49	1	2	Epid
not used	514384	5169329	No data	NAD27	158	48	121	43	1	3	No data
not used	514393	5169337	No data	NAD27	125	79	069	50	1	3	No data
71b	514400	5169547	No data	NAD27	344	78	255	29	1	3	No data
73a	514549	5169796	No data	NAD27	087	49	171	46	1	3	No data
73a	514549	5169796	No data	NAD27	103	59	172	33	1	2	No data
73a	514549	5169796	No data	NAD27	111	46	166	11	0	4	No data
73a	514549	5169796	No data	NAD27	115	63	185	27	0	4	No data
73a	514549	5169796	No data	NAD27	103	74	187	22	0	4	No data
73a	514549	5169796	No data	NAD27	107	85	012	25	0	4	No data
73a	514549	5169796	No data	NAD27	122	65	034	50	0	4	No data
73a	514549	5169796	No data	NAD27	081	51	356	39	0	4	No data
73a	514549	5169796	No data	NAD27	127	56	210	64	1	3	No data
74a	514804	5169661	No data	NAD27	263	49	338	21	0	4	FeO
74a	514804	5169661	No data	NAD27	095	54	344	04	0	4	FeMin
74a	514804	5169661	No data	NAD27	142	66	225	28	2	3	FeEpid
74a	514804	5169661	No data	NAD27	135	68	222	10	0	4	Epid
74a	514804	5169661	No data	NAD27	136	86	162	12	1	3	Epid
74a	514804	5169661	No data	NAD27	004	55	329	50	2	3	FeEpid
73b	514615	5169716	No data	NAD27	160	78	257	04	2	2	Epid
73b	514615	5169716	No data	NAD27	150	68	066	01	0	4	Epid
73b	514615	5169716	No data	NAD27	024	74	291	20	1	3	FeMin
73b	514615	5169716	No data	NAD27	015	79	285	37	1	3	FeMin
73b	514615	5169716	No data	NAD27	207	61	283	30	0	4	Epid
73b	514615	5169716	No data	NAD27	168	80	079	04	0	4	Epid
73b	514615	5169716	No data	NAD27	183	89	080	15	0	4	Epid
73b	514615	5169716	No data	NAD27	170	73	248	26	0	4	Epid
73b	514615	5169716	No data	NAD27	310	86	222	27	1	3	FeEpid

Station ID	Easting NAD27	Northing NAD27	Accuracy (+/-m)	Datum	Fault Dip Direction	Fault Dip	Lineation Azimuth	Lineation Plunge	Sense	Certainty	Mineral
73c	514590	5169728	No data	NAD27	178	85	265	19	0	4	FeEpid
73c	514590	5169728	No data	NAD27	183	64	254	20	2	3	FeMin
73c	514590	5169728	No data	NAD27	156	87	069	09	1	3	FeEpid
73c	514590	5169728	No data	NAD27	182	83	268	21	0	4	FeEpid
73c	514590	5169728	No data	NAD27	012	62	281	21	2	2	FeEpid
73d	514602	5169754	No data	NAD27	244	62	332	57	2	3	FeEpid
73e	514580	5169764	No data	NAD27	134	69	044	19	0	4	FeEpid
73e	514580	5169764	No data	NAD27	168	52	073	10	1	3	FeMin
73e	514580	5169764	No data	NAD27	168	47	088	12	1	2	FeEpid
73e	514580	5169764	No data	NAD27	222	66	290	31	0	4	Epid
73e	514580	5169764	No data	NAD27	142	79	047	29	0	4	Epid
73e	514580	5169764	No data	NAD27	326	43	265	18	0	4	FeEpid
73e	514580	5169764	No data	NAD27	154	87	063	31	1	3	Epid
73f	514570	5169772	No data	NAD27	135	79	188	68	1	3	FeEpid
73f	514570	5169772	No data	NAD27	121	84	092	80	1	3	FeEpid
73f	514570	5169772	No data	NAD27	132	87	219	49	2	3	FeMin
73f	514570	5169772	No data	NAD27	119	51	158	29	2	3	FeMin
73g	514575	5169830	No data	NAD27	340	83	252	29	2	3	FeEpid
73g	514575	5169830	No data	NAD27	286	87	195	03	1	3	FeMin
73g	514575	5169830	No data	NAD27	309	55	240	39	0	4	Epid
73g	514575	5169830	No data	NAD27	318	70	223	25	1	2	FeEpid
73g	514575	5169830	No data	NAD27	308	83	216	24	1	3	FeEpid
73g	514575	5169830	No data	NAD27	309	76	228	11	1	2	FeEpid
73g	514575	5169830	No data	NAD27	009	53	104	40	1	3	FeMin
73g	514575	5169830	No data	NAD27	352	67	282	23	2	1	FeEpid
73g	514575	5169830	No data	NAD27	206	77	294	29	1	2	FeMin
73g	514575	5169830	No data	NAD27	329	65	266	45	2	3	FeEpid
75a	514054	5169419	No data	NAD27	293	74	350	54	2	3	FeEpid
75a	514054	5169419	No data	NAD27	192	45	318	10	2	2	FeEpid
75a	514054	5169419	No data	NAD27	232	24	148	09	2	3	FeEpid
75a	514054	5169419	No data	NAD27	164	35	124	31	2	3	FeEpid
75a	514054	5169419	No data	NAD27	148	49	124	34	1	2	FeMin
75a	514054	5169419	No data	NAD27	334	85	024	69	1	3	FeEpid
75a	514054	5169419	No data	NAD27	206	41	134	15	2	1	FeEpid
75a	514054	5169419	No data	NAD27	244	28	321	05	0	4	FeMin
75a	514054	5169419	No data	NAD27	206	31	130	11	1	3	FeEpid
75a	514054	5169419	No data	NAD27	198	36	126	16	1	3	Epid
75a	514054	5169419	No data	NAD27	040	07	314	01	1	2	FeMin
75a	514054	5169419	No data	NAD27	171	06	144	04	1	3	FeEpid
75a	514054	5169419	No data	NAD27	204	26	134	06	2	3	FeEpid
75a	514054	5169419	No data	NAD27	200	33	125	10	2	2	FeO
75a	514054	5169419	No data	NAD27	216	30	140	15	2	3	FeEpid
75a	514054	5169419	No data	NAD27	158	60	141	49	1	2	FeEpid

Station ID	Easting NAD27	Northing NAD27	Accuracy (+/-m)	Datum	Fault Dip Direction	Fault Dip	Lineation Azimuth	Lineation Plunge	Sense	Certainty	Mineral
75a	514054	5169419	No data	NAD27	205	34	136	10	1	2	FeMin
75a	514054	5169419	No data	NAD27	176	43	136	33	2	3	FeMin
75b	514051	5169437	No data	NAD27	316	61	338	60	2	2	FeMin
75b	514051	5169437	No data	NAD27	331	59	344	58	2	1	FeEpid
75b	514051	5169437	No data	NAD27	330	80	052	51	1	3	FeEpid
75b	514051	5169437	No data	NAD27	320	85	033	69	1	1	FeEpid
75b	514051	5169437	No data	NAD27	310	26	338	24	2	3	FeMin
75b	514051	5169437	No data	NAD27	152	85	062	55	2	3	FeEpid
75b	514051	5169437	No data	NAD27	198	45	139	21	0	4	FeEpid
75b	514051	5169437	No data	NAD27	308	80	354	71	2	3	FeMin
75b	514051	5169437	No data	NAD27	160	13	148	12	2	2	FeEpid
75c	514075	5169506	No data	NAD27	031	19	002	14	1	3	Epid
74b	514755	5169619	No data	NAD27	142	10	184	07	1	3	Chl
74b	514755	5169619	No data	NAD27	103	25	184	03	1	2	Chl
74b	514755	5169619	No data	NAD27	158	68	075	25	2	3	Chl
74c	514754	5169580	No data	NAD27	194	80	273	33	0	4	FeMin
76a	512198	5172145	No data	NAD27	016	46	108	03	2	3	Epid
76a	512198	5172145	No data	NAD27	125	40	112	45	2	2	Epid
76a	512198	5172147	No data	NAD27	108	35	164	24	0	4	Epid
76a	512198	5172147	No data	NAD27	110	47	124	39	2	2	Epid
76a	512198	5172147	No data	NAD27	048	39	062	35	2	3	FeEpid
76b	512201	5172150	No data	NAD27	340	71	051	44	0	4	Epid
76c	512207	5172153	No data	NAD27	028	39	328	20	1	1	FeMin
76c	512207	5172153	No data	NAD27	326	45	244	11	2	3	Epid
76d	512213	5172153	No data	NAD27	332	44	251	05	1	1	FeO
76d	512213	5172153	No data	NAD27	318	35	240	06	1	2	FeMin
76e	512209	5172146	No data	NAD27	046	40	123	11	0	4	Epid
76f	512200	5172143	No data	NAD27	018	51	298	14	1	3	Epid
76g	512202	5172143	No data	NAD27	196	60	112	21	0	4	Epid
76g	512202	5172143	No data	NAD27	017	45	100	10	1	3	FeO
76h	512209	5172142	No data	NAD27	289	54	230	36	1	2	FeMin
76i	512194	5172156	No data	NAD27	151	84	231	24	1	2	Epid
76i	512194	5172156	No data	NAD27	144	73	235	26	1	2	FeEpid
76i	512194	5172156	No data	NAD27	162	88	249	30	1	3	Epid
76j	512189	5172160	No data	NAD27	148	78	234	35	0	4	Epid
76k	512187	5172156	No data	NAD27	316	89	228	07	2	2	Epid
76l	512185	5172158	No data	NAD27	139	69	168	52	1	1	Chl
76l	512185	5172158	No data	NAD27	142	62	072	33	1	3	Epid
76m	512179	5172150	No data	NAD27	278	75	195	55	1	1	Epid
76m	512179	5172150	No data	NAD27	294	76	196	75	1	1	Epid
76m	512179	5172150	No data	NAD27	272	70	184	68	1	1	Epid
76n	512182	5172158	No data	NAD27	078	41	042	31	0	4	FeEpid
76n	512182	5172158	No data	NAD27	335	85	248	15	1	3	Epid

Station ID	Easting NAD27	Northing NAD27	Accuracy (+/-m)	Datum	Fault Dip Direction	Fault Dip	Lineation Azimuth	Lineation Plunge	Sense	Certainty	Mineral
76o	512184	5172148	No data	NAD27	288	46	278	45	1	3	FeEpid
76p	512182	5172148	No data	NAD27	130	46	160	45	1	1	FeEpid
76p	512182	5172148	No data	NAD27	141	41	160	40	1	1	FeEpid
76q	512178	5172148	No data	NAD27	350	20	302	14	2	2	FeMin
76q	512178	5172148	No data	NAD27	315	14	318	11	1	1	Epid
76q	512178	5172148	No data	NAD27	048	40	060	25	2	2	FeO
76r	512190	5172143	No data	NAD27	318	35	282	26	1	2	Epid
76s	512185	5172144	No data	NAD27	322	29	246	07	1	3	FeMin
76t	512184	5172144	No data	NAD27	272	20	260	19	1	2	FeEpid
76t	512184	5172144	No data	NAD27	279	30	297	25	1	1	FeO
76u	512187	5172141	No data	NAD27	013	80	099	07	1	3	Epid
76u	512187	5172141	No data	NAD27	266	36	320	30	1	3	Epid
76v	512188	5172141	No data	NAD27	319	54	275	53	1	1	FeEpid
76w	512185	5172143	No data	NAD27	312	36	285	29	1	2	FeMin
76x	512183	5172144	No data	NAD27	281	77	268	69	1	2	FeEpid
76x	512183	5172144	No data	NAD27	295	29	305	25	1	2	Epid
76y	512181	5172143	No data	NAD27	304	11	285	10	1	2	Epid
76z	512180	5172142	No data	NAD27	240	60	235	56	1	2	Epid
76za	512178	5172143	No data	NAD27	286	51	275	50	1	1	Epid
76za	512178	5172143	No data	NAD27	116	40	163	32	1	3	FeEpid
76zb	512180	5172142	No data	NAD27	227	56	238	55	1	3	Epid
76zc	512185	5172139	No data	NAD27	318	77	285	71	1	1	FeEpid
76zc	512185	5172139	No data	NAD27	272	56	280	55	1	3	FeEpid
76zd	512187	5172146	No data	NAD27	311	31	268	26	1	3	Epid
76zd	512187	5172146	No data	NAD27	336	89	285	88	1	2	Epid
76ze	512186	5172142	No data	NAD27	334	36	277	31	0	4	Epid
76ze	512186	5172139	No data	NAD27	337	35	294	25	1	2	FeEpid
76ze	512186	5172139	No data	NAD27	320	40	290	35	1	2	FeEpid
76ze	512186	5172139	No data	NAD27	332	35	294	30	1	2	FeEpid
76zf	512192	5172147	No data	NAD27	313	36	240	15	1	2	FeEpid
77a	514086	5168877	5	NAD27	132	51	140	37	0	4	No data
77a	514086	5168877	5	NAD27	194	26	273	07	1	3	No data
77a	514086	5168877	5	NAD27	230	76	165	62	1	2	No data
77a	514086	5168877	5	NAD27	140	82	193	66	0	4	No data
77a	514086	5168877	5	NAD27	280	70	318	59	1	1	No data
77a	514086	5168877	5	NAD27	272	86	251	76	0	4	No data
77a	514086	5168877	5	NAD27	144	41	176	46	0	4	No data
77a	514086	5168877	5	NAD27	219	47	274	36	2	1	Epid
77a	514086	5168877	5	NAD27	109	70	196	48	1	3	No data
77a	514086	5168877	5	NAD27	258	45	255	44	0	4	Epid
77a	514086	5168877	5	NAD27	241	16	229	14	2	3	Epid
77a	514086	5168877	5	NAD27	217	41	247	36	2	3	No data
77b	514037	5168837	7	NAD27	001	86	272	31	1	3	No data

Station ID	Easting NAD27	Northing NAD27	Accuracy (+/-m)	Datum	Fault Dip Direction	Fault Dip	Lineation Azimuth	Lineation Plunge	Sense	Certainty	Mineral
77b	514037	5168837	7	NAD27	003	84	278	13	0	4	No data
77b	514037	5168837	7	NAD27	137	83	232	18	0	4	No data
77b	514037	5168837	7	NAD27	102	46	151	35	0	4	No data
77b	514037	5168837	7	NAD27	149	75	214	24	2	3	No data
77b	514037	5168837	7	NAD27	144	54	231	07	2	3	Epid
77b	514037	5168837	7	NAD27	113	59	040	31	0	4	Epid
77b	514037	5168837	7	NAD27	150	76	223	29	1	2	No data
77b	514037	5168837	7	NAD27	003	70	282	20	2	1	Epid
77b	514037	5168837	7	NAD27	170	89	273	25	1	3	Epid
77b	514037	5168837	7	NAD27	327	80	262	15	0	4	Epid
77b	514037	5168837	7	NAD27	339	76	253	08	1	1	Epid
77b	514037	5168837	7	NAD27	165	73	083	22	0	4	Epid
78a	509762	5174845	9	NAD27	102	62	181	24	2	3	Chl/Epid
78a	509762	5174845	9	NAD27	168	88	257	34	2	3	Chl
78a	509762	5174845	9	NAD27	042	57	305	47	0	4	No data
78a	509762	5174845	9	NAD27	351	75	278	45	2	1	FeO
78b	509800	5174924	8	NAD27	336	78	352	71	1	1	Chl/Epid
78b	509800	5174924	8	NAD27	288	34	201	11	1	3	Chl
78c	509774	5174962	13	NAD27	131	86	032	18	1	1	Chl/Epid
78c	509774	5174962	13	NAD27	280	78	006	05	1	2	Epid
79a	509704	5175045	5	NAD27	333	35	288	18	2	2	Epid
79a	509704	5175045	5	NAD27	098	36	125	24	1	2	FeO
79a	509704	5175045	5	NAD27	137	68	067	40	1	1	FeEpid
79a	509704	5175045	5	NAD27	055	82	320	08	2	1	FeO
79a	509704	5175045	5	NAD27	228	87	326	18	2	2	Epid
79a	509704	5175045	5	NAD27	290	70	340	54	1	1	FeO
79a	509704	5175045	5	NAD27	138	30	122	28	1	2	FeEpid
79a	509704	5175045	5	NAD27	011	87	284	02	1	1	FeEpid
79a	509704	5175045	5	NAD27	225	84	311	02	1	3	FeEpid
79a	509704	5175045	5	NAD27	005	78	088	08	1	2	FeO
79a	509704	5175045	5	NAD27	160	47	094	22	1	1	FeEpid
79a	509704	5175045	5	NAD27	143	57	075	40	1	2	Epid
79a	509704	5175045	5	NAD27	260	62	331	25	2	2	FeO
79a	509704	5175045	5	NAD27	285	86	030	05	2	3	FeO
79a	509704	5175045	5	NAD27	080	17	112	17	1	2	Epid
79a	509704	5175045	5	NAD27	225	82	146	07	2	3	FeEpid
79a	509704	5175045	5	NAD27	016	84	283	04	1	1	Epid
79a	509704	5175045	5	NAD27	030	78	083	61	1	1	Epid
79a	509704	5175045	5	NAD27	060	69	142	65	1	2	Epid
79a	509704	5175045	5	NAD27	074	82	142	02	1	2	Epid
79a	509704	5175045	5	NAD27	070	82	152	11	1	2	Epid
79a	509704	5175045	5	NAD27	112	51	098	48	1	1	Chl
79a	509704	5175045	5	NAD27	060	85	317	17	0	4	Chl-FeO

Station ID	Easting NAD27	Northing NAD27	Accuracy (+/-m)	Datum	Fault Dip Direction	Fault Dip	Lineation Azimuth	Lineation Plunge	Sense	Certainty	Mineral
79a	509704	5175045	5	NAD27	038	88	128	10	1	1	Chl-Epid
79a	509704	5175045	5	NAD27	036	86	305	25	0	4	Epid
79b	509679	5175130	6	NAD27	268	55	282	53	1	3	Epid
79b	509679	5175130	6	NAD27	113	32	090	34	1	3	Epid
80a	509792	5175399	4	NAD27	268	28	268	28	2	1	FeO
80a	509792	5175399	4	NAD27	326	47	301	36	2	2	Epid
80a	509792	5175399	4	NAD27	275	26	338	04	2	3	FeEpid
80a	509792	5175399	4	NAD27	271	50	319	36	2	1	FeEpid
80a	509792	5175399	4	NAD27	285	68	006	56	1	1	FeEpid
80a	509792	5175399	4	NAD27	302	71	001	58	0	4	Epid
80a	509792	5175399	4	NAD27	280	73	276	72	1	2	FeEpid
80a	509792	5175399	4	NAD27	189	22	084	05	0	4	FeO
80a	509792	5175399	4	NAD27	297	76	217	60	1	3	Epid
80a	509792	5175399	4	NAD27	226	48	236	48	2	3	FeEpid
80a	509792	5175399	4	NAD27	247	50	284	41	2	2	FeO
80a	509792	5175399	4	NAD27	192	62	206	58	0	4	Epid
80a	509792	5175399	4	NAD27	290	82	244	74	0	4	Epid
80a	509792	5175399	4	NAD27	288	80	294	78	0	4	Epid
80a	509792	5175399	4	NAD27	275	78	230	78	2	2	Epid
80b	509742	5175486	7	NAD27	268	85	348	35	2	2	FeO
80b	509742	5175486	7	NAD27	227	66	131	09	1	1	FeO
80b	509742	5175486	7	NAD27	068	65	106	65	1	3	No data
80b	509742	5175486	7	NAD27	073	83	163	14	0	4	Epid
80b	509742	5175486	7	NAD27	264	64	348	16	2	3	No data
80b	509742	5175486	7	NAD27	284	64	016	06	1	2	Epid
80b	509742	5175486	7	NAD27	275	75	184	05	2	1	Epid
80b	509742	5175486	7	NAD27	031	14	295	09	1	2	Epid
80c	509715	5175516	6	NAD27	254	89	164	05	2	3	Epid
80c	509715	5175516	6	NAD27	082	80	168	02	1	2	Epid
81	510239	5174572	11	NAD27	315	17	301	16	2	3	FeO
81	510239	5174572	11	NAD27	240	40	301	39	2	2	Epid
81	510239	5174572	11	NAD27	292	82	294	72	1	3	Epid
81	510239	5174572	11	NAD27	271	57	259	55	2	1	Epid
81	510239	5174572	11	NAD27	295	78	271	75	0	4	Epid
81	510239	5174572	11	NAD27	283	80	320	74	1	1	Epid
81	510239	5174572	11	NAD27	285	73	293	66	1	1	Epid
81	510239	5174572	11	NAD27	089	89	088	88	0	4	Epid
81	510239	5174572	11	NAD27	282	51	260	50	1	2	Epid
81	510239	5174572	11	NAD27	298	82	286	82	1	2	Epid
81	510239	5174572	11	NAD27	300	49	290	47	1	2	Epid
81	510239	5174572	11	NAD27	008	60	292	18	0	4	FeO
81	510239	5174572	11	NAD27	312	86	284	84	0	4	Epid
81	510239	5174572	11	NAD27	076	86	074	86	0	4	Epid

Station ID	Easting NAD27	Northing NAD27	Accuracy (+/-m)	Datum	Fault Dip Direction	Fault Dip	Lineation Azimuth	Lineation Plunge	Sense	Certainty	Mineral
81	510239	5174572	11	NAD27	281	89	269	85	0	4	Epid
not used	510393	5175300	7	NAD27	029	49	098	34	0	4	Epid
not used	510572	5175299	9	NAD27	160	76	227	48	2	2	Chl/Epid
not used	510572	5175299	9	NAD27	256	89	073	82	2	3	No data
82a	510049	5176326	8	NAD27	110	75	210	52	0	4	Epid
82a	510049	5176326	8	NAD27	278	76	268	72	1	3	Epid
82a	510049	5176326	8	NAD27	108	89	290	86	1	3	Epid
82a	510049	5176326	8	NAD27	268	85	332	56	2	1	FeO
82a	510049	5176326	8	NAD27	156	66	203	56	2	1	FeO
82a	510049	5176326	8	NAD27	318	79	254	56	1	3	Epid
82a	510049	5176326	8	NAD27	279	86	279	79	0	4	Epid
82a	510049	5176326	8	NAD27	108	83	224	80	2	2	FeO
82a	510049	5176326	8	NAD27	280	62	205	52	1	2	FeEpid
82a	510049	5176326	8	NAD27	074	88	213	79	1	1	Epid
82a	510049	5176326	8	NAD27	298	89	223	34	2	3	Epid
82a	510049	5176326	8	NAD27	118	76	212	69	1	1	FeEpid
82a	510049	5176326	8	NAD27	302	64	311	64	2	2	Chl/Epid
82a	510049	5176326	8	NAD27	328	58	339	54	1	3	Epid
82a	510049	5176326	8	NAD27	262	86	198	70	0	4	Epid
82a	510049	5176326	8	NAD27	071	54	092	54	2	2	Chl/Epid
82b	509936	5176300	6	NAD27	254	72	265	72	0	4	Epid
82b	509936	5176300	6	NAD27	291	68	273	47	2	3	FeO
82b	509936	5176300	6	NAD27	343	42	302	42	2	1	FeEpid
82b	509936	5176300	6	NAD27	181	89	275	15	2	3	FeO
82b	509936	5176300	6	NAD27	185	49	250	28	2	1	Epid
82b	509936	5176300	6	NAD27	145	39	194	26	0	4	Epid
82c	509894	5176384	6	NAD27	175	58	229	45	2	2	FeO
82c	509894	5176384	6	NAD27	278	78	277	74	2	2	FeEpid
82c	509894	5176384	6	NAD27	324	41	236	31	2	3	FeO
82c	509894	5176384	6	NAD27	294	36	302	36	2	2	FeO
82c	509894	5176384	6	NAD27	311	39	301	39	2	1	FeO
82c	509894	5176384	6	NAD27	204	88	335	70	0	4	FeO
not used	510013	5176660	7	NAD27	084	30	086	30	2	1	Chl/Epid
not used	510013	5176660	7	NAD27	064	32	152	08	2	3	FeO
not used	510013	5176660	7	NAD27	118	53	070	44	1	3	Epid
not used	510013	5176660	7	NAD27	116	54	108	54	1	3	Epid
not used	510013	5176660	7	NAD27	113	20	113	20	2	3	Epid
not used	510013	5176660	7	NAD27	118	48	119	35	0	4	Epid
not used	510013	5176660	7	NAD27	218	23	147	23	1	2	FeO
not used	510013	5176660	7	NAD27	242	32	093	26	0	4	FeEpid
83	510562	5175024	9	NAD27	098	74	102	72	0	4	FeEpid
83	510562	5175024	9	NAD27	180	75	177	74	2	1	FeEpid
83	510562	5175024	9	NAD27	302	85	186	70	0	4	FeEpid

Station ID	Easting NAD27	Northing NAD27	Accuracy (+/-m)	Datum	Fault Dip Direction	Fault Dip	Lineation Azimuth	Lineation Plunge	Sense	Certainty	Mineral
83	510562	5175024	9	NAD27	080	28	324	01	2	1	FeO
83	510562	5175024	9	NAD27	288	89	285	75	2	2	Chl
83	510562	5175024	9	NAD27	100	89	189	72	2	1	FeEpid
83	510562	5175024	9	NAD27	108	88	204	81	2	2	FeEpid
83	510562	5175024	9	NAD27	223	89	308	50	2	1	FeEpid
83	510562	5175024	9	NAD27	295	89	275	85	2	1	Epid
83	510562	5175024	9	NAD27	310	89	219	49	2	1	Epid
83	510562	5175024	9	NAD27	092	88	198	64	1	1	Chl/Epid
83	510562	5175024	9	NAD27	096	66	118	62	0	4	Epid
83	510562	5175024	9	NAD27	265	88	245	88	0	4	Epid
not used	510180	5176853	7	NAD27	160	84	250	50	1	2	FeEpid
not used	510180	5176853	7	NAD27	151	70	248	40	2	2	FeEpid
not used	510180	5176853	7	NAD27	329	84	272	75	2	3	FeO
not used	510180	5176853	7	NAD27	325	82	247	37	1	1	Epid
not used	510180	5176853	7	NAD27	247	76	280	40	1	2	FeO
84a	510065	5177148	9	NAD27	021	79	021	79	1	1	Epid
84a	510065	5177148	9	NAD27	004	59	299	29	1	3	Epid
84a	510065	5177148	9	NAD27	120	66	197	14	2	1	Epid
84a	510065	5177148	9	NAD27	120	72	188	52	2	1	FeO
84a	510065	5177148	9	NAD27	108	59	187	24	1	1	Epid
84a	510065	5177148	9	NAD27	210	88	166	72	2	2	FeO
84a	510065	5177148	9	NAD27	095	50	160	17	2	3	Epid
84a	510065	5177148	9	NAD27	055	51	120	48	2	2	Epid
84a	510065	5177148	9	NAD27	123	68	196	37	2	2	Epid
84a	510065	5177148	9	NAD27	257	64	235	54	2	1	Epid
84a	510065	5177148	9	NAD27	105	80	156	60	2	2	Epid
84a	510065	5177148	9	NAD27	215	79	117	21	1	2	FeO
84a	510065	5177148	9	NAD27	170	83	077	05	1	2	FeO
84a	510065	5177148	9	NAD27	348	88	084	10	0	4	FeO
84a	510065	5177148	9	NAD27	095	74	105	72	2	3	Epid
84a	510065	5177148	9	NAD27	168	88	068	33	2	2	FeO
84a	510065	5177148	9	NAD27	309	41	260	33	2	3	FeEpid
84a	510065	5177148	9	NAD27	085	72	081	72	2	2	Epid
84b	510021	5177026	10	NAD27	176	54	242	30	2	1	FeChl
84b	510021	5177026	10	NAD27	007	65	284	11	0	4	FeO
84b	510021	5177026	10	NAD27	183	64	263	28	2	1	Epid
84b	510021	5177026	10	NAD27	012	71	294	20	1	1	Epid
84b	510021	5177026	10	NAD27	018	75	295	43	1	2	FeO
84b	510021	5177026	10	NAD27	302	54	292	53	1	1	Epid
84b	510021	5177026	10	NAD27	275	46	214	40	1	1	Epid
84b	510021	5177026	10	NAD27	310	71	211	55	0	4	Epid
84b	510021	5177026	10	NAD27	117	74	207	10	2	2	FeEpid
84b	510021	5177026	10	NAD27	326	79	226	64	1	2	Epid

Station ID	Easting NAD27	Northing NAD27	Accuracy (+/-m)	Datum	Fault Dip Direction	Fault Dip	Lineation Azimuth	Lineation Plunge	Sense	Certainty	Mineral
84b	510021	5177026	10	NAD27	002	57	260	38	1	1	FeO
84c	510088	5177107	9	NAD27	279	71	221	35	1	2	FeEpid
84c	510088	5177107	9	NAD27	347	67	065	20	1	3	Epid
84c	510088	5177107	9	NAD27	330	82	243	07	1	1	FeEpid
84c	510088	5177107	9	NAD27	341	79	261	14	1	2	FeEpid
84c	510088	5177107	9	NAD27	260	89	157	02	1	3	Epid
84c	510088	5177107	9	NAD27	268	86	213	07	1	3	Epid
84c	510088	5177107	9	NAD27	335	75	359	75	1	1	Epid
84c	510088	5177107	9	NAD27	266	76	310	76	1	3	Epid
85	509335	5175959	5	NAD27	023	84	022	84	1	3	FeEpid
85	509335	5175959	5	NAD27	050	25	323	13	2	1	FeEpid
85	509335	5175959	5	NAD27	117	76	167	73	2	1	FeEpid
85	509335	5175959	5	NAD27	178	55	218	45	2	1	Epid
85	509335	5175959	5	NAD27	186	51	190	50	0	4	Epid
85	509335	5175959	5	NAD27	123	88	104	82	2	1	FeEpid
85	509335	5175959	5	NAD27	106	77	148	71	0	4	Epid
85	509335	5175959	5	NAD27	340	60	028	50	1	1	FeEpid
85	509335	5175959	5	NAD27	155	82	126	69	2	3	FeEpid
85	509335	5175959	5	NAD27	204	40	176	34	2	3	FeO
85	509335	5175959	5	NAD27	143	58	083	46	2	1	Epid
85	509335	5175959	5	NAD27	223	32	153	19	1	2	FeO
85	509335	5175959	5	NAD27	034	76	322	63	2	1	Epid
85	509335	5175959	5	NAD27	034	88	306	45	2	1	Epid
85	509335	5175959	5	NAD27	319	55	008	35	1	2	Epid
85	509335	5175959	5	NAD27	222	30	179	21	0	4	FeO
85	509335	5175959	5	NAD27	014	89	216	86	1	1	Epid
85	509335	5175959	5	NAD27	157	86	049	80	2	1	Epid
86a	509753	5176525	8	NAD27	103	70	114	68	2	1	Epid
86a	509753	5176525	8	NAD27	036	39	054	37	2	3	FeO
86a	509753	5176525	8	NAD27	081	35	064	34	2	1	FeO
86a	509753	5176525	8	NAD27	051	36	064	36	2	1	FeO
86a	509753	5176525	8	NAD27	158	58	157	56	2	2	Epid
86a	509753	5176525	8	NAD27	326	76	032	44	2	3	FeEpid
86b	509726	5176722	7	NAD27	352	34	295	14	1	3	FeO
86b	509726	5176722	7	NAD27	297	71	030	55	2	3	Epid
86b	509726	5176722	7	NAD27	355	31	303	21	1	1	FeO
86b	509726	5176722	7	NAD27	337	49	297	36	1	1	Epid
86b	509726	5176722	7	NAD27	358	64	265	64	1	2	Epid
86b	509726	5176722	7	NAD27	348	60	302	54	1	2	Epid
86b	509726	5176722	7	NAD27	285	35	294	34	1	3	Felds
87	509765	5177319	7	NAD27	330	39	307	35	2	1	Epid
87	509765	5177319	7	NAD27	289	41	271	38	2	2	FeEpid
87	509765	5177319	7	NAD27	002	62	295	34	1	1	FeEpid

Station ID	Easting NAD27	Northing NAD27	Accuracy (+/-m)	Datum	Fault Dip Direction	Fault Dip	Lineation Azimuth	Lineation Plunge	Sense	Certainty	Mineral
87	509765	5177319	7	NAD27	316	64	273	35	2	2	Epid
87	509765	5177319	7	NAD27	330	44	290	39	1	3	FeEpid
87	509765	5177319	7	NAD27	294	59	290	59	2	1	FeEpid
87	509765	5177319	7	NAD27	284	78	243	76	2	2	Epid
87	509765	5177319	7	NAD27	285	85	186	56	1	1	Epid
87	509765	5177319	7	NAD27	289	80	201	59	1	1	Epid
87	509765	5177319	7	NAD27	003	56	342	51	1	1	FeEpid
87	509765	5177319	7	NAD27	352	52	320	47	1	1	FeEpid
87	509765	5177319	7	NAD27	232	77	172	65	2	3	FeEpid
87	509765	5177319	7	NAD27	322	66	250	50	1	1	FeEpid
87	509765	5177319	7	NAD27	014	58	306	38	1	1	Epid
87	509765	5177319	7	NAD27	012	32	329	21	1	3	FeEpid
87	509765	5177319	7	NAD27	000	70	294	67	1	1	FeEpid
87	509765	5177319	7	NAD27	278	87	158	82	2	1	Epid
87	509765	5177319	7	NAD27	278	74	223	69	2	1	Epid
87	509765	5177319	7	NAD27	310	72	325	71	1	1	FeEpid
87	509765	5177319	7	NAD27	091	75	106	73	2	1	Epid
87b	509709	5177080	10	NAD27	279	65	348	35	2	1	Epid
87b	509709	5177080	10	NAD27	156	40	073	10	2	3	Epid
87b	509709	5177080	10	NAD27	020	48	337	32	2	2	Chl/Epid
87b	509709	5177080	10	NAD27	063	66	131	25	1	3	Epid
87b	509709	5177080	10	NAD27	295	64	322	46	2	2	FeEpid
88a	510256	5174403	5	NAD27	255	54	264	49	2	1	FeEpid
88a	510256	5174403	5	NAD27	273	15	252	14	2	1	FeO
88a	510256	5174403	5	NAD27	259	47	230	43	2	1	FeO
88a	510256	5174403	5	NAD27	254	54	235	54	2	2	FeEpid
88a	510256	5174403	5	NAD27	308	14	255	08	2	1	FeEpid
88a	510256	5174403	5	NAD27	356	14	086	07	1	1	Epid
88a	510256	5174403	5	NAD27	337	84	242	25	1	1	FeEpid
88a	510256	5174403	5	NAD27	220	28	214	25	2	1	FeEpid
88a	510256	5174403	5	NAD27	248	39	214	35	1	2	FeEpid
88a	510256	5174403	5	NAD27	237	56	310	30	2	2	Epid
88a	510256	5174403	5	NAD27	173	84	086	62	0	04	Chl
88b	510264	5174269	9	NAD27	205	67	319	30	2	1	FeEpid
88b	510264	5174269	9	NAD27	040	33	120	11	2	2	Epid
88b	510264	5174269	9	NAD27	109	88	030	19	2	3	FeEpid
88b	510264	5174269	9	NAD27	135	60	069	34	1	1	Chl
88b	510264	5174269	9	NAD27	337	36	332	35	2	3	FeEpid
88c	510259	5174122	8	NAD27	064	86	340	54	2	2	Epid
88c	510259	5174122	8	NAD27	052	85	341	75	2	3	Epid
88c	510259	5174122	8	NAD27	225	60	273	52	2	3	Epid
88c	510259	5174122	8	NAD27	232	63	271	58	2	1	Epid
88c	510259	5174122	8	NAD27	240	69	250	69	2	2	Epid

Station ID	Easting NAD27	Northing NAD27	Accuracy (+/-m)	Datum	Fault Dip Direction	Fault Dip	Lineation Azimuth	Lineation Plunge	Sense	Certainty	Mineral
88c	510259	5174122	8	NAD27	245	65	322	14	1	2	FeEpid
not used	510868	5173967	30	NAD27	148	84	242	17	1	2	Kflz/Qrz
not used	510766	5173605	8	NAD27	076	27	106	26	2	2	Epid
89	510617	5173415	5	NAD27	226	73	269	36	2	3	Epid
89	510617	5173415	5	NAD27	273	65	328	53	1	3	FeO
89	510617	5173415	5	NAD27	301	41	298	41	1	1	FeO
89	510617	5173415	5	NAD27	321	21	298	18	1	3	FeEpid
89	510617	5173415	5	NAD27	297	78	290	78	2	3	Epid
89	510617	5173415	5	NAD27	256	46	263	46	2	2	FeEpid
89	510617	5173415	5	NAD27	268	55	286	40	2	1	FeEpid
89	510617	5173415	5	NAD27	272	61	312	61	2	2	FeEpid
89	510617	5173415	5	NAD27	282	50	296	44	2	3	FeEpid
89	510617	5173415	5	NAD27	246	52	293	47	1	1	Chl/Epid
89	510617	5173415	5	NAD27	238	64	284	54	2	2	FeO
89	510617	5173415	5	NAD27	283	56	292	54	1	3	FeO
89	510617	5173415	5	NAD27	255	60	292	58	2	3	FeEpid
90a	510399	5177466	4	NAD27	037	83	322	09	2	2	Felds
90a	510399	5177466	4	NAD27	054	32	107	29	2	2	Felds
90a	510399	5177466	4	NAD27	282	36	348	14	0	4	Felds
90a	510399	5177466	4	NAD27	255	76	166	07	2	3	Epid
90a	510399	5177466	4	NAD27	146	86	062	03	1	3	FeEpid
90b	510362	5177509	7	NAD27	105	89	060	11	2	3	FeEpid
90b	510362	5177509	7	NAD27	294	89	000	39	1	2	Epid
90b	510362	5177509	7	NAD27	182	88	098	25	0	04	Epid
90b	510362	5177509	7	NAD27	012	87	064	16	0	04	Epid
90b	510362	5177509	7	NAD27	091	85	355	02	2	2	Epid
90b	510362	5177509	7	NAD27	313	86	039	04	2	1	Chl/Epid
90c	510298	5177521	8	NAD27	097	61	171	19	0	04	Epid
90c	510298	5177521	8	NAD27	125	74	207	32	2	3	Epid
90c	510298	5177521	8	NAD27	121	38	164	26	2	2	FeEpid
90c	510298	5177521	8	NAD27	228	41	180	03	1	3	FeO
91a	510170	5177452	7	NAD27	084	45	002	06	2	3	FeO
91a	510170	5177452	7	NAD27	281	75	008	28	1	2	FeEpid
91a	510170	5177452	7	NAD27	004	44	070	22	2	3	FeEpid
91a	510170	5177452	7	NAD27	108	74	026	16	2	1	FeFelds
91a	510170	5177452	7	NAD27	115	71	038	12	2	2	FeO
91a	510170	5177452	7	NAD27	127	70	220	10	1	2	FeO
91a	510170	5177452	7	NAD27	120	75	230	03	0	04	FeO
91a	510170	5177452	7	NAD27	080	75	126	64	0	04	Epid
91a	510170	5177452	7	NAD27	150	79	185	77	0	04	Epid
91a	510170	5177452	7	NAD27	288	78	356	22	1	01	FeEpid
91a	510170	5177452	7	NAD27	002	54	018	50	1	03	FeEpid
91a	510170	5177452	7	NAD27	085	82	061	80	2	03	Epid

Station ID	Easting NAD27	Northing NAD27	Accuracy (+/-m)	Datum	Fault Dip Direction	Fault Dip	Lineation Azimuth	Lineation Plunge	Sense	Certainty	Mineral
91a	510170	5177452	7	NAD27	139	89	160	87	2	02	Epid
91b	510181	5177303	6	NAD27	121	89	040	05	2	02	FeEpid
91b	510181	5177303	6	NAD27	184	89	281	32	2	02	FeO
91b	510181	5177303	6	NAD27	328	54	252	07	0	04	FeEpid
91b	510181	5177303	6	NAD27	315	52	245	32	1	03	FeEpid
92a	508307	5174745	4	NAD27	120	55	080	42	2	03	FeO
92a	508307	5174745	4	NAD27	210	63	144	22	1	02	FeO
92a	508307	5174745	4	NAD27	251	55	322	25	2	02	FeO
92a	508307	5174745	4	NAD27	282	76	350	54	2	02	FeEpid
92b	508388	5174840	8	NAD27	170	49	123	40	2	02	FeO
92c	508273	5174755	6	NAD27	024	89	116	49	1	01	FeEpid
92c	508273	5174755	6	NAD27	220	89	130	60	2	01	FeEpid
92c	508273	5174755	6	NAD27	177	28	133	16	1	01	FeEpid
92c	508273	5174755	6	NAD27	237	30	280	06	2	01	FeEpid
92c	508273	5174755	6	NAD27	211	29	125	18	1	02	FeEpid
92c	508273	5174755	6	NAD27	229	57	158	44	1	02	FeEpid

Appendix Table 2: Fault-slip quality matrix.

Column headings abbreviations are: n: number of brittle surfaces, %Data: percent data used in calculation, NEV: negative expected value, %NEV: number of brittle surfaces divided by the number of negative expected values. Entries of 1 for data type represent slickenside/brittle structures. Abbreviation for tested fault-slip methods are: DI: Direct Inversion, NDAt30: Numerical Dynamic Analysis method using a theta angle of 30°, NDAtbf: Numerical Dynamic Analysis method using a best fit theta angle, PTt30: P-T-B method using a theta angle of 30°, PTtbf: P-T-B method using a best fit theta value. Quality measures for individual methods are: a: Excellent, b: Good, c: Fair, d: Acceptable, e: Poor.

Station	n	%Data	Confidence Number Average	Correction Error Average	Data Type	Tested fault-slip methods	DI			NDA t30			NDA tbf			PBT t30			PBT tbf			DI	NDA t30	NDA tbs	Estimated Faulting Scenario	Applied Fault-sip Method
							NEV	Average Misfit	Quality	NEV	Average Misfit	Quality	NEV	Average Misfit	Quality	P-Rpercent	B-Rpercent	T-Rpercent	P-Rpercent	B-Rpercent	T-Rpercent	%NEV	%NEV	%NEV		
1	27	100	0.63	10.86	1	Inversion/NDAt30/ NDAtbf/PTt30/PTtbf	12	17.3	d	6	11.7	b	6	10.8	b	61	73	62	63	73	70	44	22	22	Conjugate fault sets	NDAtbf - Strain
2	7	100	0.50	15.60	1	Inversion/NDAt30/ NDAtbf/PTt30/PTtbf	2	17.3	d	2	19.8	e	2	18.3	e	44	44	46	50	44	60	29	29	29	Triaxial Deformation?	NADtbf - Strain
3	10	100	0.48	8.08	1	Inversion/NDAt30/ NDAtbf/PTt30/PTtbf	3	4.4	c	0	16.5	d	0	20.7	e	90	49	62	91	49	63	30	0	0	Conjugate fault sets	NDAtbf - Strain
4	12	100	0.69	5.09	1	Inversion/NDAt30/ NDAtbf/PTt30/PTtbf	4	16.6	d	3	21.7	e	3	15.2	d	26	51	25	54	51	45	33	25	25	Axial Contraction	INV - Stress
5	12	100	0.42	8.40	1	Inversion/NDAt30/ NDAtbf/PTt30/PTtbf	3	13.8	c	2	6.0	c	1	28.2	e	55	61	38	67	61	53	25	17	8	Axial Contraction	INV - Stress
6	10	100	0.80	9.30	1	Inversion/NDAt30/ NDAtbf/PTt30/PTtbf	5	6.2	c	3	23.8	e	3	27.4	e	21	47	9	42	47	45	50	30	30	Conjugate fault sets	NDAtbf - Strain
7	14	100	0.43	7.78	1	Inversion/NDAt30/ NDAtbf/PTt30/PTtbf	5	16.8	d	1	22.5	e	1	12.6	d	51	49	55	63	49	62	36	7	7	Non-Coaxial Deformation?	NADtbf - Strain
8	97	100	0.76	4.30	1	Inversion/NDAt30/ NDAtbf/PTt30/PTtbf	31	21.4	e	13	23.6	e	13	24.1	e	17	36	59	36	36	48	32	13	13	Conjugate fault sets	NDAtbf - Strain
9	7	100	0.68	2.24	1	Inversion/NDAt30/ NDAtbf/PTt30/PTtbf	3	6.4	d	3	18.8	e	3	25.2	e	37	83	37	72	83	67	43	43	43	unknown	INV - Stress
10	7	100	0.39	10.51	1	Inversion/NDAt30/ NDAtbf/PTt30/PTtbf	4	26.3	e	1	31.3	e	1	27.8	e	54	64	51	58	64	58	57	14	14	unknown	NDAtbf - Strain
11	22	100	0.50	9.09	1	Inversion/NDAt30/ NDAtbf/PTt30/PTtbf	6	9.0	c	7	27.6	e	10	15.0	c	-6	53	40	37	53	56	27	32	45	unknown	PTtbf - Strain
12	17	100	0.56	7.12	1	Inversion/NDAt30/ NDAtbf/PTt30/PTtbf	9	15.8	d	3	24.4	e	5	16.5	d	49	69	46	57	69	60	53	18	29	Axial Extension	NDAt30 - Strain
13	15	100	0.45	6.25	1	Inversion/NDAt30/ NDAtbf/PTt30/PTtbf	8	24.9	e	3	35.4	e	4	31.0	e	43	-1	37	41	-1	49	53	20	27	Axial Contraction	NDAtbf - Strain
14	7	100	0.43	8.49	1	Inversion/NDAt30/ NDAtbf/PTt30/PTtbf	0	36.7	e	0	15.8	d	0	17.5	d	83	50	78	84	50	78	0	0	0	unknown	NDAt30 - Strain
15	12	100	0.44	10.28	1	Inversion/NDAt30/ NDAtbf/PTt30/PTtbf	7	7.3	c	1	32.9	e	1	32.4	e	12	49	60	41	49	61	58	8	8	unknown	NDAtbf - Strain
16	11	100	0.43	7.61	1	Inversion/NDAt30/ NDAtbf/PTt30/PTtbf	7	8.1	c	1	14.0	c	3	14.2	c	74	42	70	87	42	88	64	9	27	Conjugate fault sets	NDAtbf - Strain
17	6	100	0.50	28.35	1	Inversion/NDAt30/ NDAtbf/PTt30/PTtbf	2	8.5	e	0	21.8	e	0	15.5	e	59	57	76	66	57	82	33	0	0	unknown	NDAtbf - Strain
18	10	100	0.40	3.41	1	Inversion/NDAt30/ NDAtbf/PTt30/PTtbf	2	9.6	c	Insufficient data to calculate			Insufficient data to calculate			99	86	96	97	86	98	20	Not appli-cable	Not appli-cable	unknown	PTtbf - Strain
19	5	100	0.55	4.78	1	Inversion/NDAt30/ NDAtbf/PTt30/PTtbf	3	0.8	e	Insufficient data to calculate			Insufficient data to calculate			71	61	73	76	61	78	60	Not appli-cable	Not appli-cable	unknown	PTt30 - Strain

Station	n	%Data	Confidence Number Average	Correction Error Average	Data Type	Tested fault-slip methods	DI			NDA t30			NDA tbf			PBT t30			PBT tbf			DI	NDA t30	NDA tbs	Estimated Faulting Scenario	Applied Fault-slip Method
							NEV	Average Misfit	Quality	NEV	Average Misfit	Quality	NEV	Average Misfit	Quality	P-Rpercent	B-Rpercent	T-Rpercent	P-Rpercent	B-Rpercent	T-Rpercent	%NEV	%NEV	%NEV		
20	5	100	0.40	7.66	1	Inversion/NDAt30/ NDAtbf/PTt30/PTtbf	3	12.0	e	Insufficient data to calculate			Insufficient data to calculate			60	71	56	66	71	62	60	Not appli-cable	Not appli-cable	unknown	PTtbf - Strain
21	4	100	0.94	7.33	1	Inversion/NDAt30/ NDAtbf/PTt30/PTtbf	1	0.0	e	Insufficient data to calculate			Insufficient data to calculate			86	92	94	91	92	90	25	Not appli-cable	Not appli-cable	unknown	PTt30 - Strain
22	10	100	0.70	6.02	1	Inversion/NDAt30/ NDAtbf/PTt30/PTtbf	1	2.4	c	1	7.0	c	1	6.5	c	82	91	86	82	91	86	10	10	10	Axial Contraction	INV - Stress
23	8	100	0.47	7.85	1	Inversion/NDAt30/ NDAtbf/PTt30/PTtbf	2	16.4	d	0	24.8	e	0	26.6	e	66	56	80	65	56	80	25	0	0	Axial Contraction	INV - Stress
24	7	100	0.82	9.71	1	Inversion/NDAt30/ NDAtbf/PTt30/PTtbf	2	6.1	d	2	16.9	d	3	11.1	d	72	87	71	85	87	83	29	29	43	Axial Contraction?	NDAtbf - Strain
25	5	100	0.65	14.42	1	Inversion/NDAt30/ NDAtbf/PTt30/PTtbf	1	9.4	e	0	7.4	e	1	23.4	e	86	56	56	72	56	73	20	0	20	Axial Contraction?	NDAt30 - Strain
26	9	100	0.72	9.08	1	Inversion/NDAt30/ NDAtbf/PTt30/PTtbf	3	9.2	d	3	25.5	e	2	20.8	e	44	69	33	63	69	64	33	33	22	Axial Contraction?	INV - Stress
27	9	100	0.50	6.77	1	Inversion/NDAt30/ NDAtbf/PTt30/PTtbf	4	2.8	d	4	33.1	e	2	15.0	d	20	66	22	70	66	90	44	44	22	unknown	NDAtbf - Strain
28	14	100	0.80	7.65	1	Inversion/NDAt30/ NDAtbf/PTt30/PTtbf	3	16.9	d	3	11.0	c	4	8.7	c	73	68	45	78	68	55	21	21	29	Conjugate fault sets	NDAtbf - Strain
30	47	100	0.61	5.38	1	Inversion/NDAt30/ NDAtbf/PTt30/PTtbf	14	18.8	e	6	18.3	e	6	18.4	e	59	69	56	61	69	56	30	13	13	Conjugate fault sets	NDAt30 - Strain
31	15	100	0.63	9.78	1	Inversion/NDAt30/ NDAtbf/PTt30/PTtbf	7	19.4	e	5	34.3	e	6	19.3	e	17	43	32	29	43	36	47	33	40	Conjugate fault sets?	NDAt30 - Strain
32	9	100	0.61	7.29	1	Inversion/NDAt30/ NDAtbf/PTt30/PTtbf	3	3.1	d	0	34.5	e	2	41.9	e	35	42	60	46	42	51	33	0	22	Axial Extension	INV - Stress
33	30	100	0.68	5.78	1	Inversion/NDAt30/ NDAtbf/PTt30/PTtbf	14	25.3	d	9	13.1	c	17	21.7	e	26	49	67	73	49	37	47	30	57	Conjugate fault sets	NDAtbf - Strain
34	24	100	0.73	4.38	1	Inversion/NDAt30/ NDAtbf/PTt30/PTtbf	11	12.6	c	7	17.2	d	8	23.8	e	31	53	47	67	53	68	46	29	33	Conjugate fault sets	NDAtbf - Strain
35	10	100	0.68	4.85	1	Inversion/NDAt30/ NDAtbf/PTt30/PTtbf	5	9.5	c	4	20.4	e	5	17.5	d	63	68	31	67	68	89	50	40	50	unknown	NDAtbf - Strain
36	20	100	0.64	8.85	1	Inversion/NDAt30/ NDAtbf/PTt30/PTtbf	8	13.2	c	6	20.0	e	11	17.2	d	42	74	39	63	74	57	40	30	55	Conjugate fault sets	NDAtbf - Strain
37	12	100	0.73	4.82	1	Inversion/NDAt30/ NDAtbf/PTt30/PTtbf	5	18.6	e	4	20.2	e	4	24.2	e	46	66	32	68	66	60	42	33	33	Conjugate fault sets?	NDAtbf - Strain
38	24	100	0.83	4.72	1	Inversion/NDAt30/ NDAtbf/PTt30/PTtbf	10	12.4	c	11	16.3	d	13	16.9	d	-9	64	9	68	64	79	42	46	54	Conjugate fault sets?	NDAtbf - Strain
39	13	100	0.56	5.16	1	Inversion/NDAt30/ NDAtbf/PTt30/PTtbf	4	17.6	d	1	18.8	e	1	17.3	d	54	69	64	66	69	78	31	8	8	Axial Contraction?	NDAtbf - Strain
40	10	100	0.55	5.22	1	Inversion/NDAt30/ NDAtbf/PTt30/PTtbf	4	13.2	c	1	35.6	e	1	25.5	e	36	63	44	45	63	51	40	10	10	unknown	NDAtbf - Strain
41	7	100	0.54	4.94	1	Inversion/NDAt30/ NDAtbf/PTt30/PTtbf	4	0.6	d	0	14.8	d	1	9.0	d	64	95	64	90	95	92	57	0	14	Conjugate fault sets?	NDAtbf - Strain
42	9	100	0.55	1.96	1	Inversion/NDAt30/ NDAtbf/PTt30/PTtbf	1	4.4	d	2	6.3	d	1	7.6	d	44	56	84	47	56	97	11	22	11	Axial Contraction?	NDAtbf - Strain
43	13	100	0.52	5.73	1	Inversion/NDAt30/ NDAtbf/PTt30/PTtbf	7	7.8	c	3	13.8	c	5	20.0	e	67	56	30	55	56	79	54	23	38	Axial Contraction?	NDAtbf - Strain
44	24	100	0.48	5.85	1	Inversion/NDAt30/ NDAtbf/PTt30/PTtbf	8	21.8	e	5	16.5	d	6	15.2	d	55	70	68	60	70	77	33	21	25	Conjugate fault sets?	NDAtbf - Strain
45	7	100	0.36	5.97	1	Inversion/NDAt30/ NDAtbf/PTt30/PTtbf	2	5.6	d	Insufficient data to calculate			Insufficient data to calculate			69	61	74	97	61	92	29	Not applic able	Not applic able	Conjugate fault sets?	PTtbf - Strain

Station	n	%Data	Confidence Number Average	Correction Error Average	Data Type	Tested fault-slip methods	DI			NDA t30			NDA tbf			PBT t30			PBT tbf			DI	NDA t30	NDA tbs	Estimated Faulting Scenario	Applied Fault-slip Method
							NEV	Average Misfit	Quality	NEV	Average Misfit	Quality	NEV	Average Misfit	Quality	P-Rpercent	B-Rpercent	T-Rpercent	P-Rpercent	B-Rpercent	T-Rpercent	%NEV	%NEV	%NEV		
46	5	100	0.50	2.18	1	Inversion/NDAt30/ NDAtbf/PTt30/PTtbf	2	0.4	e	2	19.0	e	1	17.4	d	56	78	62	89	78	88	40	40	20	Conjugate fault sets?	NDAtbf - Strain
47	17	100	0.63	2.81	1	Inversion/NDAt30/ NDAtbf/PTt30/PTtbf	8	14.4	c	1	18.0	d	2	18.0	d	65	75	69	75	75	81	47	6	12	Conjugate fault sets?	NDAt30 - Strain
48	9	100	0.67	2.12	1	Inversion/NDAt30/ NDAtbf/PTt30/PTtbf	2	15.8	d	2	11.2	d	3	13.4	d	75	77	69	85	77	78	22	22	33	Axial Contraction?	NDAt30 - Strain
49	18	100	0.49	6.03	1	Inversion/NDAt30/ NDAtbf/PTt30/PTtbf	5	11.8	c	1	13.5	c	Method not performed			68	54	60	Method not performed			28	6	Not applicable	unknown	NDAt30 - Strain
50	30	100	0.72	4.09	1	Inversion/NDAt30/ NDAtbf/PTt30/PTtbf	10	11.2	b	4	15.5	d	6	12.7	c	57	69	70	59	69	69	33	13	20	Conjugate fault sets	NDAtbf - Strain
51	12	100	0.60	3.64	1	Inversion/NDAt30/ NDAtbf/PTt30/PTtbf	3	21.3	e	2	15.3	d	1	25.3	e	43	60	48	66	60	78	25	17	8	Axial Extension	NDAtbf - Strain
52	12	100	0.50	6.13	1	Inversion/NDAt30/ NDAtbf/PTt30/PTtbf	4	10.5	c	2	22.6	e	2	20.6	e	71	73	68	75	73	71	33	17	17	Conjugate fault sets?	NDAtbf - Strain
53	18	100	0.46	4.59	1	Inversion/NDAt30/ NDAtbf/PTt30/PTtbf	12	11.4	c	2	18.8	e	5	17.5	d	60	76	47	60	76	55	67	11	28	Conjugate fault sets?	NDAtbf - Strain
54	17	100	0.60	6.65	1	Inversion/NDAt30/ NDAtbf/PTt30/PTtbf	8	32.5	e	6	34.7	e	6	34.7	e	60	76	47	60	76	55	47	35	35	unknown	NDAtbf - Strain
55	11	100	0.50	6.26	1	Inversion/NDAt30/ NDAtbf/PTt30/PTtbf	0	7.5	c	0	9.0	c	0	9.5	c	88	73	73	88	73	73	0	0	0	Axial Contraction	NDAtbf - Strain
56	7	100	0.68	2.41	1	Inversion/NDAt30/ NDAtbf/PTt30/PTtbf	3	13.4	d	1	27.4	e	2	27.4	e	58	39	24	62	39	26	43	14	29	unknown	NDAtbf - Strain
57	16	100	0.63	5.82	1	Inversion/NDAt30/ NDAtbf/PTt30/PTtbf	3	23.4	e	2	17.0	e	3	24.1	e	47	39	31	52	39	47	19	13	19	unknown	NDAt30 - Strain
58	8	100	0.47	6.39	1	Inversion/NDAt30/ NDAtbf/PTt30/PTtbf	1	1.6	d	1	20.9	e	1	21.7	e	60	52	56	63	52	55	13	13	13	Axial Contraction?	INV - Stress
59	21	100	0.67	9.98	1	Inversion/NDAt30/ NDAtbf/PTt30/PTtbf	8	19.0	e	6	24.7	e	7	24.1	e	28	43	55	66	43	61	38	29	33	Conjugate fault sets	NDAtbf - Strain
60	15	100	0.60	6.98	1	Inversion/NDAt30/ NDAtbf/PTt30/PTtbf	7	9.2	b	6	25.2	e	5	21.0	e	55	53	38	68	53	43	47	40	33	unknown	NDAtbf - Strain
61	15	100	0.63	7.12	1	Inversion/NDAt30/ NDAtbf/PTt30/PTtbf	5	12.5	c	5	35.3	e	8	30.3	e	35	30	20	60	30	35	33	33	53	unknown	NDAtbf - Strain
62	13	100	0.54	3.88	1	Inversion/NDAt30/ NDAtbf/PTt30/PTtbf	7	12.4	c	0	15.7	d	0	13.1	c	80	49	51	84	49	57	54	0	0	Axial Extension	NDAtbf - Strain
63	33	100	0.58	11.10	1	Inversion/NDAt30/ NDAtbf/PTt30/PTtbf	14	18.2	e	11	26.2	e	8	25.5	e	12	16	22	24	16	37	42	33	24	unknown	NDAtbf - Strain
64	16	100	0.47	5.00	1	Inversion/NDAt30/ NDAtbf/PTt30/PTtbf	9	13.9	c	1	12.4	c	3	15.0	c	82	58	53	93	58	63	56	6	19	Conjugate fault sets	NDAtbf - Strain
65	4	100	0.69	14.43	1	Inversion/NDAt30/ NDAtbf/PTt30/PTtbf	2	0.0	e	1	25.5	e	1	27.5	e	48	59	52	48	59	55	50	25	25	unknown	NDAtbf - Strain
66	9	100	0.67	11.82	1	Inversion/NDAt30/ NDAtbf/PTt30/PTtbf	3	5.6	d	0	8.4	d	1	11.6	d	85	74	80	83	74	82	33	0	11	Dominated by one orientation?	NDAtbf - Strain
67	7	100	0.57	3.94	1	Inversion/NDAt30/ NDAtbf/PTt30/PTtbf	1	19.0	e	0	15.3	d	0	17.1	d	82	57	69	84	57	69	14	0	0	Axial Extension	NDAtbf - Strain
68	21	100	0.60	10.62	1	Inversion/NDAt30/ NDAtbf/PTt30/PTtbf	1	14.0	c	2	20.2	e	3	22.1	e	42	25	73	61	25	71	5	10	14	Axial Contraction	NDAtbf - Strain
69	17	100	0.63	7.30	1	Inversion/NDAt30/ NDAtbf/PTt30/PTtbf	7	16.2	d	6	19.5	e	6	17.3	d	45	67	36	47	67	38	41	35	35	unknown	NDAtbf - Strain
70	15	100	0.70	6.98	1	Inversion/NDAt30/ NDAtbf/PTt30/PTtbf	3	20.3	e	4	22.1	e	4	22.2	e	46	54	52	48	54	52	20	27	27	unknown	NDAtbf - Strain

Station	n	%Data	Confidence Number Average	Correction Error Average	Data Type	Tested fault-slip methods	DI			NDA t30			NDA tbf			PBT t30			PBT tbf			DI	NDA t30	NDA tbs	Estimated Faulting Scenario	Applied Fault-slip Method
							NEV	Average Misfit	Quality	NEV	Average Misfit	Quality	NEV	Average Misfit	Quality	P-Rpercent	B-Rpercent	T-Rpercent	P-Rpercent	B-Rpercent	T-Rpercent	%NEV	%NEV	%NEV		
71	8	100	0.56	8.44	1	Inversion/NDAt30/ NDAtbf/PTt30/PTtbf	3	12.3	d	3	18.3	e	3	18.8	e	44	75	57	48	75	65	38	38	38	unknown	NDAtbf - Strain
72	8	100	0.59	3.08	1	Inversion/NDAt30/ NDAtbf/PTt30/PTtbf	1	11.3	d	0	16.0	d	0	16.3	d	86	73	67	86	73	67	13	0	0	Axial Contraction	NDAtbf - Strain
73	45	100	0.45	7.56	1	Inversion/NDAt30/ NDAtbf/PTt30/PTtbf	11	19.7	e	9	29.5	e	14	22.9	e	45	58	27	52	58	43	24	20	31	unknown	NDAtbf - Strain
74	10	100	0.43	9.71	1	Inversion/NDAt30/ NDAtbf/PTt30/PTtbf	4	10.0	c	2	40.7	e	2	28.5	e	31	60	39	48	60	48	40	20	20	unknown	INV - Stress
75	28	100	0.61	4.32	1	Inversion/NDAt30/ NDAtbf/PTt30/PTtbf	12	9.4	b	10	12.2	c	10	12.5	c	29	91	28	47	91	49	43	36	36	unknown	NDAt30 - Strain
76	57	100	0.68	3.68	1	Inversion/NDAt30/ NDAtbf/PTt30/PTtbf	18	35.8	e	12	21.2	e	18	21.6	e	24	54	30	44	54	48	32	21	32	Axial Contraction?	NDAtbf - Strain
77	25	100	0.49	5.72	1	Inversion/NDAt30/ NDAtbf/PTt30/PTtbf	14	21.7	e	6	25.4	e	7	25.2	e	52	24	32	68	24	35	56	24	28	unknown	NDAt30 - Strain
78	8	100	0.69	7.21	1	Inversion/NDAt30/ NDAtbf/PTt30/PTtbf	4	10.3	d	2	29.9	e	4	35.4	e	24	42	52	59	42	41	50	25	50	unknown	INV - Stress
79	27	100	0.75	6.06	1	Inversion/NDAt30/ NDAtbf/PTt30/PTtbf	7	13.6	c	5	12	b	13	33.5	e	64	17	16	37	17	47	26	19	48	Axial Contraction	NDAt30 - Strain
80	25	100	0.62	4.32	1	Inversion/NDAt30/ NDAtbf/PTt30/PTtbf	10	24.1	e	6	26.3	e	5	24.8	e	37	33	56	45	33	66	40	24	20	Axial Extension	NDAtbf - Strain
81	15	100	0.57	3.26	1	Inversion/NDAt30/ NDAtbf/PTt30/PTtbf	10	5.7	b	1	7.2	b	2	7.7	b	87	86	85	90	86	89	67	7	13	Axial Contraction but high R?	NDAt30 - Strain
82	28	100	0.68	7.03	1	Inversion/NDAt30/ NDAtbf/PTt30/PTtbf	15	12.5	c	8	17.8	d	9	19.2	e	60	51	44	69	51	53	54	29	32	Axial Extension	NDAt30 - Strain
83	13	100	0.73	5.02	1	Inversion/NDAt30/ NDAtbf/PTt30/PTtbf	5	7.5	c	3	18.6	e	7	15.7	d	51	67	18	56	67	75	38	23	54	Axial Extension	INV - Stress
84	37	100	0.74	7.24	1	Inversion/NDAt30/ NDAtbf/PTt30/PTtbf	17	27.5	e	11	32.4	e	16	29.3	e	8	44	22	33	44	32	46	30	43	unknown	NDAt30 - Strain
85	18	100	0.76	4.01	1	Inversion/NDAt30/ NDAtbf/PTt30/PTtbf	6	23.4	e	3	22.5	e	Method not performed			60	60	47	Method not performed			33	17	Not applicable	Axial Extension	NDAt30 - Strain
86	13	100	0.75	5.22	1	Inversion/NDAt30/ NDAtbf/PTt30/PTtbf	6	12.2	c	1	36.8	e	2	31.8	e	28	49	33	41	49	34	46	8	15	Conjugate fault sets	NDAt30 - Strain
87	20	100	0.89	4.09	1	Inversion/NDAt30/ NDAtbf/PTt30/PTtbf	7	7.7	b	6	21.6	e	8	12.0	b	47	69	32	59	69	75	35	30	40	Axial Contraction but high R?	INV - Stress
88	22	100	0.80	4.01	1	Inversion/NDAt30/ NDAtbf/PTt30/PTtbf	4	16.9	d	3	15.8	d	Method not performed			49	43	56	Method not performed			14	14	Not applicable	Axial Extension	NDAt30 - Strain
89	13	92	0.69	3.13	1	Inversion/NDAt30/ NDAtbf/PTt30/PTtbf	5	2.8	c	5	17.7	d	4	13.6	c	42	89	37	87	89	93	38	38	31	Conjugate	NDAtbf - Strain
90	15	100	0.55	11.58	1	Inversion/NDAt30/ NDAtbf/PTt30/PTtbf	8	11.1	b	4	18.3	e	3	22.5	e	33	59	29	50	59	54	27	27	20	Axial Extension	INV - Stress
91	17	100	0.59	5.66	1	Inversion/NDAt30/ NDAtbf/PTt30/PTtbf	4	24.1	e	1	23.8	e	0	25.4	e	55	29	44	69	29	54	6	6	0	Conjugate?	NDAtbf - Strain
92	11	100	0.82	5.89	1	Inversion/NDAt30/ NDAtbf/PTt30/PTtbf	4	12.4	c	3	32.5	e	0	25.5	e	43	64	41	71	64	68	27	27	0	unknown	INV - Stress

Appendix Table 3: Results of fault-slip inversions.

Inversion methods include the direct inversion method, the numerical dynamic analysis using a θ of 30° (NDA t30) and θ of best fit (NDA tbf), and the P-B-T method using θ of 30° (PBT t30) and θ of best fit (PBT tbf). The method chosen in the study is indicated in the last column. Column heading abbreviations are: n: number of measured fault sets per station, NEV: negative expected value, θ: angle between fault surface and the maximum principal stress or strain axis. σ1, σ2, σ3 correspond the maximum, intermediate, and minimum principal stress axes, respectively. λ1, λ2, λ3, correspond the maximum, intermediate, and minimum principal strain axes, respectively. P, B, T correspond to the maximum, intermediate, and minimum principal stress axes, respectively.

Station	n	Direct Inversion					NDA t30					NDA tbf						PBT t30			PBT tbf				Method Used
		σ1	σ2	σ3	R	NEV	λ1	λ2	λ3	R	NEV	λ1	λ2	λ3	R	NEV	θ	P	B	T	P	B	T	θ	
1	27	179/02	274/72	088/18	0.1785	12	134/07	039/38	233/51	0.5900	6	143/14	041/40	248/47	0.6341	6	12	141/01	057/46	225/45	148/08	057/46	244/46	12	NDAtbf
2	7	168/04	074/40	262/50	0.6512	2	138/16	311/74	048/02	0.2385	2	131/21	277/66	036/12	0.6288	2	12	303/08	153/74	047/01	300/06	153/74	044/02	12	NDAtbf
3	10	335/03	242/48	068/42	0.7428	3	007/18	124/53	266/31	0.2412	0	003/10	116/65	269/22	0.2462	0	40	002/18	139/68	274/27	359/12	139/68	275/24	40	NDAtbf
4	12	317/05	049/13	207/76	0.3575	4	259/29	162/13	051/58	0.8385	3	112/11	210/36	008/52	0.4612	3	70	335/06	183/62	079/37	123/02	183/62	012/56	70	INV
5	12	088/02	357/12	186/78	0.0512	3	300/10	042/50	202/38	0.1759	2	140/13	036/47	242/40	0.3457	1	58	290/18	127/64	193/17	143/01	127/64	236/26	58	INV
6	10	060/34	209/52	319/15	0.8430	5	010/23	115/31	249/50	0.4602	3	172/23	026/63	268/14	0.4411	3	60	307/06	119/76	139/25	162/04	119/76	295/23	60	NDAtbf
7	14	011/07	211/82	101/03	0.1247	5	069/21	212/65	334/14	0.4889	1	067/27	249/63	158/01	0.3250	1	12	065/26	109/77	157/11	067/29	109/77	159/12	12	NDAtbf
8	97	355/08	093/44	257/45	0.2434	31	325/04	234/06	090/83	0.8302	13	128/07	218/04	340/82	0.8245	13	46	180/08	028/08	109/77	121/03	028/08	021/83	46	NDAtbf
9	7	068/22	163/11	278/65	0.6925	3	237/26	342/29	113/49	0.2503	3	081/55	335/11	238/33	0.4863	3	84	258/17	356/16	099/66	094/57	356/16	255/28	84	INV
10	7	347/65	197/22	102/11	0.6607	4	261/41	142/29	028/35	0.4997	1	257/45	129/32	019/29	0.5336	1	38	268/36	125/67	004/14	263/37	125/67	360/15	38	NDAtbf
11	22	258/04	080/86	348/00	0.9335	6	232/25	005/56	132/22	0.4922	7	097/39	313/46	203/19	0.7575	10	84	326/24	009/84	143/05	116/11	009/84	201/14	84	PBTtbf
12	17	359/03	089/14	256/76	0.0833	9	315/03	218/69	046/21	0.5279	3	078/02	339/78	168/11	0.5958	5	84	307/02	277/87	052/11	077/03	277/87	168/08	84	NDAt30
13	15	171/15	032/70	265/13	0.5693	8	219/18	312/09	068/70	0.3209	3	221/29	312/01	044/61	0.5190	4	16	230/02	314/35	068/50	234/10	314/35	068/47	16	NDAtbf
14	7	328/03	059/22	231/68	0.6260	0	138/17	331/73	229/04	0.4610	0	134/21	317/69	224/01	0.4658	0	38	135/19	018/74	051/03	130/21	018/74	046/03	38	NDAt30
15	12	019/31	163/54	279/17	0.8221	7	035/25	271/50	140/29	0.8623	1	035/25	271/50	139/29	0.8457	1	28	350/40	099/70	129/09	237/14	099/70	129/09	28	NDAtbf
16	11	122/79	024/02	294/11	0.9408	7	280/28	184/10	077/60	0.3580	1	006/84	203/06	113/02	0.5011	3	84	290/21	210/15	083/63	018/83	210/15	114/03	84	NDAtbf
17	6	352/01	085/67	262/23	0.5964	2	048/03	141/51	316/39	0.7663	0	242/07	135/69	335/20	0.6333	0	56	052/11	117/63	322/34	062/00	117/63	339/24	56	NDAtbf
18	10	082/22	174/04	272/68	0.8430	2	Cannot be calculated					Cannot be calculated						062/79	181/03	274/10	088/36	181/03	280/54	74	PBTtbf
19	5	165/08	068/43	263/46	0.9835	3	Cannot be calculated					Cannot be calculated						308/47	129/34	231/11	324/54	129/34	229/24	50	PBTt30
20	5	140/01	050/09	234/81	0.2043	3	Cannot be calculated					Cannot be calculated						298/58	074/43	165/25	297/51	074/43	168/28	50	PBTtbf
21	4	313/20	063/42	204/41	0.3760	1	Cannot be calculated					Cannot be calculated						332/08	067/37	227/57	174/26	067/37	293/48	70	PBTt30
22	10	278/05	018/61	185/29	0.4951	1	283/17	039/55	183/29	0.5488	1	284/16	039/55	185/30	0.5429	1	34	285/20	056/58	184/25	287/19	056/58	186/26	34	INV
23	8	299/41	097/47	199/11	0.5732	2	298/30	048/30	173/45	0.5746	0	293/33	048/33	171/40	0.5850	0	24	279/28	043/47	178/37	284/27	043/47	182/41	24	INV
24	7	280/03	011/15	177/75	0.0895	2	260/01	350/39	169/51	0.5407	2	263/04	359/53	170/37	0.4896	3	10	264/08	017/54	165/38	267/08	017/54	170/35	10	NDAtbf
25	5	323/08	059/35	223/53	0.1295	1	307/14	052/47	205/40	0.3405	0	271/49	044/30	149/25	0.5351	1	76	308/15	066/56	211/28	277/48	066/56	149/18	76	NDAt30

Station	n	Direct Inversion					NDA t30					NDA tbf						PBT t30			PBT tbf				Method Used
		σ1	σ2	σ3	R	NEV	λ1	λ2	λ3	R	NEV	λ1	λ2	λ3	R	NEV	θ	P	B	T	P	B	T	θ	
26	9	139/14	043/22	259/64	0.7647	3	112/01	202/18	021/72	0.4890	3	097/42	194/08	292/47	0.4821	2	72	293/01	026/24	266/68	118/44	026/24	281/47	72	INV
27	9	036/14	139/42	292/45	0.9351	4	319/56	064/10	160/32	0.4703	4	125/44	017/18	271/41	0.6285	2	82	280/20	027/16	267/39	120/45	027/16	276/41	82	NDAtbf
28	14	338/06	072/37	241/53	0.1549	3	326/19	081/51	223/33	0.2636	3	326/28	086/43	215/34	0.2526	4	20	320/22	080/53	222/40	320/26	080/53	219/29	20	NDAtbf
30	47	356/29	151/58	259/11	0.5839	14	353/43	163/47	258/05	0.4949	6	354/44	166/46	260/04	0.4731	6	36	349/44	149/46	258/12	350/44	149/46	259/12	36	NDAt30
31	15	188/33	044/51	290/18	0.5228	7	227/14	359/69	133/15	0.4060	5	055/54	299/17	199/31	0.7187	6	84	262/33	029/07	133/10	102/29	029/07	197/37	84	NDAt30
32	9	002/20	234/59	100/23	0.8034	3	196/02	097/78	286/12	0.9318	0	050/38	173/35	290/33	0.7146	2	14	068/63	241/41	298/05	089/50	241/41	303/18	14	INV
33	30	239/07	331/11	116/76	0.4813	14	125/52	233/13	332/34	0.8988	9	310/51	054/12	153/37	0.3882	17	72	108/43	225/22	336/42	323/50	225/22	117/48	72	NDAtbf
34	24	110/70	201/00	291/20	0.0726	11	075/66	232/22	325/09	0.6499	7	322/38	054/03	147/51	0.5477	8	84	043/75	227/07	320/03	322/38	227/07	137/53	84	NDAtbf
35	10	122/23	017/31	243/49	0.1004	5	156/25	254/16	014/59	0.3628	4	327/53	230/05	136/37	0.6640	5	84	148/26	236/08	325/70	335/50	236/08	138/36	84	NDAtbf
36	20	153/10	250/33	049/55	0.5950	8	117/08	216/49	021/40	0.4468	6	018/47	221/41	121/12	0.5493	11	84	107/24	213/36	001/45	016/51	213/36	117/13	84	NDAtbf
37	12	307/83	185/04	094/06	0.6690	5	140/56	028/14	290/30	0.2405	4	294/55	027/02	119/35	0.4991	4	84	109/51	205/21	329/41	306/53	205/21	115/32	84	NDAtbf
38	24	143/61	042/06	309/29	0.1523	10	129/43	030/09	290/46	0.4490	11	140/38	034/19	282/45	0.5250	13	10	276/33	038/27	315/08	133/35	038/27	283/43	10	NDAtbf
39	13	079/03	169/06	327/83	0.5383	4	261/33	149/31	027/42	0.5421	1	262/31	152/29	028/45	0.5975	1	56	262/29	153/22	033/45	262/31	153/22	034/43	56	NDAtbf
40	10	089/01	179/19	356/71	0.3720	4	310/09	211/43	050/46	0.3846	1	285/42	169/26	058/37	0.4192	1	54	288/31	158/26	055/34	292/46	158/26	062/25	54	NDAtbf
41	7	167/85	338/04	069/01	0.8904	4	238/36	142/08	041/53	0.4804	0	252/61	153/05	060/28	0.5122	1	68	247/40	158/07	056/48	255/60	158/07	063/29	68	NDAtbf
42	9	261/13	351/01	084/77	0.6780	1	234/06	325/07	103/81	0.6651	2	235/13	328/12	100/73	0.7159	1	14	044/05	318/07	099/78	222/04	318/07	095/74	14	NDAtbf
43	13	058/62	184/17	281/21	0.9111	7	260/10	356/33	156/55	0.1588	3	020/45	152/34	260/26	0.6765	5	84	266/12	172/41	358/44	013/44	172/41	269/23	84	NDAtbf
44	24	169/15	267/28	054/57	0.1967	8	134/24	238/29	012/50	0.6580	5	137/26	239/22	004/54	0.6591	6	14	135/27	232/19	055/55	137/30	232/19	358/55	14	NDAtbf
45	7	313/13	045/11	174/73	0.1240	2	Cannot be calculated					Cannot be calculated						309/10	212/24	183/74	140/66	212/24	310/24	84	PTBtbf
46	5	109/03	357/83	199/07	0.0359	2	127/02	218/28	032/62	0.5578	2	351/78	187/12	096/03	0.4924	1	84	288/02	187/11	024/75	355/78	187/11	096/04	84	NDAtbf
47	17	014/05	119/71	283/18	0.7374	8	323/39	221/14	116/47	0.5247	1	002/77	217/11	126/07	0.5534	2	72	318/42	207/15	107/42	006/75	207/15	119/08	72	NDAt30
48	9	156/21	058/19	290/61	0.3242	2	282/09	188/26	030/62	0.3568	2	299/13	202/29	050/57	0.4082	3	12	292/12	203/30	033/65	301/15	203/30	047/60	12	NDAt30
49	18	266/61	068/27	162/07	0.3854	5	291/49	065/31	171/23	0.4159	1	Not performed: θ=30						290/46	061/32	159/27	Not performed: θ = 30				NDAt30
50	30	150/11	056/21	267/65	0.2976	10	155/35	048/22	292/47	0.5808	4	150/30	046/22	285/51	0.5263	6	22	148/36	042/23	291/45	146/31	042/23	286/49	22	NDAtbf
51	12	169/03	261/32	074/58	0.7291	3	284/25	184/20	060/57	0.6305	2	299/72	172/11	080/14	0.5800	1	78	272/08	173/16	052/57	309/72	173/16	078/17	78	NDAtbf
52	12	137/10	231/22	024/66	0.9213	4	082/38	191/22	304/44	0.4979	2	091/40	198/18	306/44	0.4969	2	22	088/42	215/25	315/41	092/42	215/25	317/43	22	NDAtbf
53	18	044/87	199/03	289/01	0.9339	12	097/19	211/50	354/33	0.3455	2	273/05	179/41	008/48	0.4565	5	10	101/24	202/30	355/55	282/02	202/30	023/60	10	NDAtbf
54	17	149/05	240/10	034/79	0.6135	8	300/11	037/31	193/56	0.4417	6	340/42	199/41	090/21	0.3281	6	76	101/24	202/30	355/55	282/02	202/30	023/60	76	NDAtbf
55	11	149/04	243/42	055/48	0.2022	0	326/07	230/40	063/49	0.3596	0	325/09	227/39	066/49	0.3624	0	34	324/04	233/35	068/51	324/06	233/35	070/50	34	NDAtbf
56	7	286/26	143/59	024/16	0.1774	3	326/33	056/01	147/57	0.3388	1	326/35	234/03	139/55	0.3152	2	20	324/29	083/53	182/53	321/31	083/53	178/49	20	NDAtbf

Station	n	Direct Inversion					NDA t30					NDA tbf						PBT t30			PBT tbf				Method Used
		σ1	σ2	σ3	R	NEV	λ1	λ2	λ3	R	NEV	λ1	λ2	λ3	R	NEV	θ	P	B	T	P	B	T	θ	
57	16	190/63	346/25	081/10	0.6518	3	301/63	169/19	072/18	0.5106	2	331/75	198/10	106/11	0.4887	3	52	301/56	161/26	059/17	338/67	161/26	098/10	52	NDAt30
58	8	148/11	053/21	264/66	0.1464	1	180/18	071/45	285/40	0.3433	1	183/24	071/40	296/41	0.3406	1	22	172/30	052/26	281/54	174/35	052/26	293/51	22	INV
59	21	182/04	089/44	276/45	0.7562	8	263/84	130/04	040/04	0.7240	6	022/17	142/59	284/25	0.4629	7	84	281/50	141/61	032/09	027/12	141/61	279/20	84	NDAtbf
60	15	163/70	355/20	263/04	0.8396	7	104/03	208/77	013/13	0.4967	6	094/09	201/62	360/26	0.4531	5	10	096/04	173/47	028/06	090/08	173/47	016/23	10	NDAtbf
61	15	081/04	348/32	177/58	0.2345	5	264/30	029/45	154/30	0.3627	5	246/10	351/56	149/32	0.3815	8	10	254/18	337/07	053/23	242/06	337/07	128/36	10	NDAtbf
62	13	208/07	116/17	320/71	0.4263	7	202/65	337/18	072/17	0.3364	0	211/61	336/17	073/22	0.2894	0	22	208/61	350/34	066/10	215/58	350/34	084/16	22	NDAtbf
63	33	066/10	334/09	203/77	0.7194	14	298/62	164/20	067/18	0.6266	11	331/12	070/37	225/51	0.5693	8	78	283/39	354/01	058/06	127/07	354/01	235/41	78	NDAtbf
64	16	009/05	102/34	272/55	0.8292	9	245/49	071/41	338/03	0.3352	1	266/48	081/42	173/02	0.2782	3	10	251/47	088/45	347/07	266/45	088/45	176/01	10	NDAtbf
65	4	243/52	131/16	030/33	0.2720	2	058/04	309/79	149/10	0.5322	1	057/06	258/83	148/02	0.5378	1	20	224/05	089/64	325/15	221/02	089/64	164/10	20	NDAtbf
66	9	092/04	198/78	001/12	0.1005	3	084/01	176/65	353/25	0.4760	0	315/18	178/66	050/15	0.4752	1	84	081/02	210/70	350/20	312/14	210/70	047/13	84	NDAtbf
67	7	217/68	002/18	095/12	0.4144	1	249/53	130/20	028/29	0.3958	0	247/49	129/22	024/32	0.3815	0	24	248/52	136/17	035/30	246/48	136/17	032/34	24	NDAtbf
68	21	160/01	250/07	058/83	0.6112	1	352/10	257/28	100/61	0.7068	2	356/12	258/30	104/57	0.6758	3	22	333/22	247/02	101/61	349/17	247/02	107/58	22	NDAtbf
69	17	084/27	284/62	179/08	0.6949	7	051/16	279/66	146/17	0.1282	6	047/21	283/55	148/26	0.2414	6	40	033/11	279/61	138/33	040/14	279/61	134/33	40	NDAtbf
70	15	173/16	079/12	312/70	0.3773	3	165/30	037/47	273/27	0.5614	4	164/33	037/43	275/29	0.5194	4	36	160/30	052/45	283/31	159/30	052/45	283/32	36	NDAtbf
71	8	146/87	270/01	360/02	0.6139	3	079/15	290/72	171/09	0.6331	3	077/06	308/80	168/07	0.7604	3	16	256/02	129/79	347/05	252/03	129/79	344/03	16	NDAtbf
72	8	132/07	222/01	317/83	0.3269	1	143/07	235/15	029/73	0.4058	0	144/06	236/15	033/74	0.3957	0	32	146/06	244/01	013/80	147/06	244/01	017/81	32	NDAtbf
73	45	281/04	013/25	182/65	0.2149	11	262/13	110/75	354/07	0.5106	9	333/07	075/59	239/30	0.3239	14	84	276/14	085/74	183/15	331/05	085/74	242/29	84	NDAtbf
74	10	349/15	089/32	238/54	0.3023	4	034/33	244/53	134/14	0.4111	2	325/52	124/36	222/10	0.5173	2	78	206/09	101/55	159/18	334/26	101/55	208/07	78	INV
75	28	070/69	235/20	327/05	0.7091	12	130/42	228/09	328/47	0.5379	10	021/70	218/19	126/06	0.6338	10	74	144/13	234/21	018/66	016/66	234/21	136/10	74	NDAt30
76	57	001/06	095/37	264/52	0.3438	18	276/03	006/08	165/81	0.6210	12	136/32	022/32	259/41	0.5836	18	78	120/09	021/22	239/70	133/35	021/22	262/39	78	NDAtbf
77	25	187/27	354/62	094/05	0.4175	14	254/41	134/30	021/34	0.3833	6	249/36	121/41	003/29	0.2957	7	12	262/31	023/40	007/30	249/34	023/40	015/24	12	NDAt30
78	8	341/08	076/33	239/56	0.1090	4	251/31	028/50	147/22	0.7795	2	126/13	353/72	219/13	0.2193	4	84	267/27	086/48	146/15	134/08	086/48	215/28	84	INV
79	27	109/02	200/06	004/84	0.2895	7	291/01	022/47	201/43	0.1593	5	232/20	348/50	128/32	0.5124	13	84	290/01	017/42	191/53	252/19	017/42	124/13	84	NDAt30
80	25	009/08	181/82	279/01	0.5908	10	336/43	185/43	081/15	0.5870	6	337/34	202/46	084/24	0.6826	5	12	331/42	195/23	088/12	327/40	195/23	88/25	12	NDAtbf
81	15	111/29	202/01	294/61	0.7961	10	297/46	201/05	106/43	0.4747	1	293/51	198/04	105/39	0.4813	2	20	291/47	016/03	105/43	290/51	016/03	105/39	20	NDAt30
82	28	016/10	108/12	248/74	0.8836	15	289/74	025/02	115/16	0.3082	8	268/71	026/09	119/17	0.3903	9	12	270/72	025/16	111/12	263/68	025/16	124/10	12	NDAt30
83	13	007/09	099/13	242/74	0.8964	5	055/77	176/07	268/11	0.4929	3	100/01	010/15	195/75	0.6562	7	84	261/87	020/10	236/53	288/08	020/10	200/73	84	INV
84	37	360/01	090/11	263/79	0.6669	17	299/58	040/07	134/31	0.4065	11	325/06	057/16	214/73	0.5856	16	84	215/28	035/54	177/26	315/02	035/54	216/53	84	NDAt30
85	18	009/34	211/54	106/10	0.3807	6	301/63	049/09	144/25	0.2996	3	Not performed: θ=30						330/65	257/02	162/20	Not performed: θ=30				NDAt30
86	13	100/12	191/02	290/77	0.6425	6	055/55	312/09	217/34	0.7764	1	107/42	341/33	229/30	0.7482	2	42	088/59	029/05	263/50	124/45	029/05	271/44	42	NDAt30

Station	n	Direct Inversion					NDA t30					NDA tbf						PBT t30			PBT tbf				Method Used
		σ1	σ2	σ3	R	NEV	λ1	λ2	λ3	R	NEV	λ1	λ2	λ3	R	NEV	θ	P	B	T	P	B	T	θ	
87	20	116/17	025/06	276/72	0.8632	7	343/48	195/37	092/16	0.1577	6	129/28	036/05	296/62	0.6970	8	84	308/59	033/22	147/46	132/29	033/22	280/62	84	INV
88	22	190/76	356/14	087/03	0.2798	4	290/59	157/22	059/20	0.5590	3	Not performed: θ=30						278/57	164/09	063/22	Not performed: θ=30				NDAt30
89	13	287/63	045/14	140/23	0.0172	5	316/58	175/25	077/18	0.5235	5	092/38	190/10	292/50	0.5438	4	84	303/45	190/10	082/40	092/39	190/10	292/50	84	NDAtbf
90	15	357/02	266/14	093/76	0.2368	8	198/71	310/07	042/17	0.9219	4	285/24	098/66	194/03	0.5599	3	78	129/01	313/84	030/11	279/12	313/84	182/02	78	INV
91	17	174/02	285/85	084/04	0.8282	4	345/31	163/59	254/01	0.2174	1	321/13	167/76	052/06	0.3240	0	60	334/23	075/70	249/11	320/10	075/70	055/12	60	NDAtbf
92	11	188/21	300/45	081/38	0.5100	4	348/43	187/46	087/09	0.4038	3	019/36	249/41	132/28	0.5050	0	68	006/44	236/39	116/33	024/43	236/39	125/25	68	INV